Fine Resolution Modelling of Ammonia Dry Deposition over Great Britain

Roderick John Singles

Doctor of Philosophy
The University of Edinburgh
1996

Declaration

This thesis has been composed by myself, and all work reported herein is my own except where otherwise stated.

Acknowledgements

I would like to thank my two brilliant supervisors, Dr. Keith Weston and Dr. Mark Sutton, who were extremely helpful with their advice and generous with their time. Many people from the Institute of Terrestrial Ecology, Edinburgh have aided me in my work and I would particularly like to thank Prof. David Fowler and Ron Smith for their useful discussions and kindly providing me with data to use in my work. The involvement of Dr. Helen ApSimon and Brian Barker at Imperial College in my project has been very useful, and I grately appreciate the use of the TERN code as a starting block for my work, and also the time they spared to answer my questions and help me get started in my PhD. The staff and students at the Department of Meteorology have given me much needed support, and life would not have been the same without that 11 am smell of freshly brewed coffee. My fellow student, Ulli Dragosits, has been a complete star in providing me with emissions data to use in my model, and I gratefully acknowledge her contribution to my work. The ongoing work in the UK Review Group on Acid Rain has enabled me to compare my model results with the latest available measurements, and I would like to thank all the people involved for their help, especially Dr. Sarah Metcalfe, Dr. Duncan Whyatt and Dr. Glenn Campbell. My parents have been very supportive throughout my studies, and their help and encouragement have helped me to keep going through the rough patches. The same can be said of my Aunt and Uncle in Canada, who helped me get back on track last summer and enabled me to have a wonderful time over there. Numerous thanks must go to my friends and flatmates who have put up with me through it all, especially Lee, John, Dean, Jo, Chris, Matthew, Anita and Linsay. And a final thanks must go to Mark, who was such a good aim with a snowball, even when his poor student had tripped over and was lying helpless on the ground.

Abstract

Deposition of atmospheric ammonia (NH_3) and ammonium (NH_4^+) form a significant contribution to the total nitrogen deposition to Great Britain, and can cause acidification of soils and may also lead to the replacement of one type of vegetation by another. Determination of the spatial distribution of deposition fluxes is an important requirement in locating areas where nitrogen deposition may be causing damage to the environment. Wet deposition fluxes have been estimated to an accepted level by using measurements in precipitation combined with adjustments for the effects of altitude. Of a more problematic nature is the determination of ammonia dry deposition fluxes on a national scale, which is due to the fact that almost all emissions of NH_3 are ground-based. Combined with the fact that there is a large spatial variability in NH_3 emissions, this means that NH_3 surface concentrations and dry deposition fluxes are extremely spatially variable, and existing measurement data are considered inadequate to be used to define dry deposition fluxes on a country-wide basis due to the relatively few monitoring sites.

In this study, an alternative approach has been taken, by applying an atmospheric transport model. Due to assumptions in the treatment of vertical dispersion, many current UK models are unable to describe the short-range dispersion of ammonia adequately, so a new statistical model has been created by extensively modifying an existing Lagrangian trajectory model. A number of atmospheric processes have been parameterised for inclusion in the model, and boundary data have been constructed to allow the inclusion of continental emissions. The wind speed data used to advect the model have been optimised for NH_3 dry deposition, and careful restructuring of the computer code has reduced computational time considerably. Initial testing of the model on a 20 km $\times$ 20 km grid has shown that modelled wet deposition fluxes of sulphate and nitrate

have a fair degree of success in reproducing measurement data. Comparisons of SO_2 and NO_2 surface concentrations with measured data have shown a variable degree of success, highlighting the uncertainties in emission heights. A number of sensitivity tests have been performed on various of the models processes, and have shown the degree of dependence of certain modelled species on the type of parameterisation used in the model.

Emissions data for NH_3 have been employed on a much finer horizontal scale of 5 km $\times$ 5 km grid squares than has been previously used in an atmospheric transport model over Great Britain. The use of a detailed description of vertical diffusion and dry deposition, together with a fine resolution emissions dataset, has produced the best yet agreement with measured NH_3 surface concentration estimates for Great Britain. Total annual fluxes of NH_3 dry deposition agree well with the official UK goverment estimates, but the spatial distribution of these data differ considerably, and highlight the possible over-estimation of the NH_3 samplers used in the monitoring network in areas of very low surface concentrations. A total annual budget for reduced nitrogen is given which shows the directional-dependence of both total deposition and export of reduced nitrogen. The model estimates that on average over half of the total dry deposition is the result of emissions being dry deposited in the same 5 km grid square. The spatial variation of this fraction is important information which can be used to guide emission reduction strategies.

Contents

List of symbols and other notation

Roman Alphabet

CLNlim the limiting critical load for nitrogen deposition, being the lower of the critical load for nitrogen eutrophication and the critical load for acidity assuming only nitrogen deposition.

CLnutN the critical load for nitrogen eutrophication.

C_f cloud reduction factors.

c_p specific heat capacity of air (1.01 J g$^-$ C^{-1}; approximately constant at useful environmental temperatures).

D diffusion coefficient of an entrained property in still air (m^2 s^{-1}).

DD_L modelled dry deposition of NH_3 emissions to the same grid square (μg m^{-2} s^{-1}).

DD_{NL} modelled dry deposition to a grid square, of ammonia emitted from other grid squares (μg m^{-2} s^{-1}).

DD_T total modelled dry deposition to a grid square from all sources (μg m^{-2} s^{-1}).

ΔE amount of energy absorbed by the modelled daytime boundary layer during a time period Δt (J m^{-2}).

ΔE_{sl} amount of energy absorbed by the modelled daytime boundary layer during a time period Δt due to entrainment of warmer air from above (J m^{-2}).

F the total net flux (flux density) with the atmosphere (positive value denotes emission) (μg m^{-2} s^{-1}).

F_d modelled dry deposition flux (μg m^{-2} s^{-1}).

F_{dTOT} total dry deposition during time Δt in RODMOD (μg m^{-2}).

F_e modelled emission flux used in RODMOD (μg m^{-2} s^{-1}).

g gravitational acceleration (9.81 m s^{-2}).

G geostrophic wind in the atmospheric boundary layer (m s^{-1}).

H sensible heat flux away from a ground surface (W m^{-2}).

H_{mix} depth of the atmospheric boundary layer. In a model, this represents the maximum height below which vertical mixing occurs.

H_z height above the surface at which the maximum value of

	K_z first occurs (m).
I	precipitation rate (mm s^{-1}).
k	von Karman's constant (approximately 0.41).
K_p	equilibrium constant for the formation of NH_4NO_3.
K_z	vertical diffusivity (m^2 s^{-1}).
K_{max}	maximum value of K_z. This occurs above height H_z (m^2 s^{-1}).
$\mathbf{L_d}$	the downwards flux of long wave radiation to a surface (W m^{-2}).
$\mathbf{L_u}$	the upwards flux of long wave radiation from a surface (W m^{-2}).
L	Monin-Obukhov stability length scale. Estimate of atmospheric stability above a surface. Independent of height within the constant flux layer (m).
Q_{NH_3}	emission flux of NH_3 in the EMEP model (μg m^{-2} s^{-1}).
$\mathbf{R_n}$	net radiation flux away from a surface (W m^{-2}).
Re_*	turbulent Reynolds number.
$R_a(z)$	turbulent atmospheric resistance from the surface to a height z above the surface (s m^{-1}).
R_b	quasi-laminar viscous sublayer resistance (s m^{-1}).
R_c	canopy (or surface) resistance. Defined as R_t-(R_a+R_b) (s m^{-1}).
R_s	resistance to transfer of material between the plant stomata and the plant canopy (s m^{-1}).
R_t	total resistance to dry deposition. Equals ${V_d}^{-1}$.
R_w	resistance to dry deposition on the leaf surface (s m^{-1}).
Sc	Schmidt number
$\mathbf{S_t}$	total solar irradiance (W m^{-2}).
$\mathbf{S_{tm}}$	maximum solar irradiance during a complete diurnal cycle (W m^{-2}).
T	temperature (°C or K)
T_*	turbulent fluctuations in heat (°C or K)
u(z)	mean horizontal wind speed at a height z above the surface (m s^{-1}) .
u_*	eddy (or friction) velocity (m s^{-1}).
V_d	the deposition velocity (defined as -$F/\chi(z)$) (m s^{-1}).
V_e	the exchange velocity to describe bi-directional fluxes of material (m s^{-1}).
X_i	position on the x-axis of the air column in the model domain
x	distance of the air column along the x-axis from the bottom-left corner

	of the model domain. (km)
Y_i	position on the y-axis of the air column in the model domain
y	distance of the air column along the y-axis from the bottom-left corner of the model domain. (km)
z	distance; height above the ground.
z_0	roughness length. Apparent height above the zero plane of predicted zero wind speed, from linearised logarithmic wind profile (m).

Greek Alphabet

γ	gradient of the potential temperature in the atmospheric boundary layer (K m^{-1}).
Δt	timestep used in RODMOD and FRAME models (s).
Δ_i	scavenging ratio for species 'i'.
λ	scavenging coefficient used to model wet deposition (s^{-1}).
χ_s	the concentration of the trace gas in the stomatal cavity (for ammonia stomatal compensation point) (μg m^{-3}, ppb).
χ_c	the canopy concentration point (μg m^{-3}, ppb).
$\chi(z)$	the concentration of the trace gas at a height z above the surface (μg m^{-3}, ppb).
$\Delta\chi$	change in concentrations over a period of time (μg m^{-3}, ppb)
ω_d	correction factor used to account for local dry deposition in the EMEP model.
ω_w	correction factor used to account for local wet deposition in the EMEP model.
ρ	density of air (g m^{-3}).
σ	the reflection coefficient of solar radiation for a surface.
θ	potential temperature in the atmospheric boundary layer (K).
ϕ_M,ϕ_H	gradient stability correction functions for momentum and heat.
Φ_M,Φ_H	integrated stability correction functions, with respect to height, for momentum and heat.
Φ	correction function used in the EMEP model to account for the non-uniformity of precipitation across a grid square.
ν	kinematic viscosity of air (m^2 s^{-1}).

Chapter 1

Introduction

During the last 2 decades there has been a major initiative to investigate the atmospheric behavior of sulphur and its oxidation products. Media attention has enhanced public awareness of the adverse ecological effect that deposition of these acidifying compounds can have on the natural ecology of the recipient areas. More recent interest has been on nitrogen oxides (NO_x) and their oxidation products which can also cause acidification. Deposition of these species can occur at distances of over 1000 km (Barrett and Seland, 1995) and so the transport of pollutants across national borders can cause political problems as well as ecological ones.

As a result of the research into transport and deposition of acidifying compounds, it has become apparent that ammonia (NH_3) plays an important role as an atmospheric pollutant. It can contribute to the acidification of ecosystems (Nihlgard, 1985), and can enhance the atmospheric life time of other primary pollutants thus leading to more long-range transport (Hov and Hjøllo, 1994).

The amount of ammonia emitted in Europe is estimated to be of the same order of magnitude as NO_x emissions. A large proportion of the emissions of ammonia are due to agricultural activity, with the majority arising from the volatilisation of livestock waste and the application of nitrogen-based fertilisers (Bujisman *et al.,* 1987). There is a very large spatial distribution of emission sources across Great Britain, with most of these sources being low-level or ground-based.

Because it is the most abundant gaseous base in the atmosphere, ammonia is extremely effective in neutralising the oxidation products of SO_2 and NO_x in the atmosphere. This process leads to the formation of ammonium (NH_4^+) aerosols,

such as ammonium sulphate ($(NH_4)_2SO_4$), ammonium nitrate (NH_4NO_3) and ammonium chloride (NH_4Cl).

Deposition of ammonia and ammonium aerosols to the earth's surface can have a varied effect on the recipient ecosystem, dependent on the magnitude of the flux and the type of vegetation present. Due to the use of ammonium nitrate as a fertiliser, any initial additional input of reduced nitrogen from the atmosphere, compared with background levels, might be considered beneficial to the local ecosystem. However, increased deposition may increase the level of fixed nitrogen in the soil which can lead to replacement of the original plants by more competitive, nitrogen-rich species (Hornung *et al.,* 1994). Also acidification of the soil can be caused by the ability of micro-organisms to oxidise NH_4^+ to NO_3^-.

Concentrations near the source will be large, since emission plumes are diluted slowly, and thus large dry deposition can take place, depending on the type of land. Further downwind of the source, the emissions will have become better mixed with the surrounding atmosphere, depending on the stability of the lower atmosphere. In consequence, the spatial variability of NH_3 concentrations is large, requiring a prohibitively high density of monitoring stations to define it adequately. Where detailed spatially-resolved emissions data are available, atmospheric transport models can provide a helpful complementary approach to estimate pollutant concentrations and deposition, especially to areas which may be susceptible to damage from increased ammonia deposition. This is particularly the case for NH_3, since concentrations are so spatially variable, and the atmospheric monitoring database limited.

1.1 Properties of ammonia

Ammonia is a colourless gas which has a distinctive and pungent smell at high concentration levels (> 50 ppm, NRC, 1979). It has a boiling point of -33.4°C which means that it is a gas at room temperature. It is an extremely reactive gas, and very soluble in water. Because of its alkaline nature, ammonia is an effective neutralising agent of acidic substances. This property is especially relevant in the atmosphere where ammonia is the predominant base present. The main atmospheric reactions are with the oxidation products of SO_2 and NO_x,

which lead to the formation of ammonium sulphate ($(NH_4)_2SO_4$) and ammonium nitrate (NH_4NO_3). Other reactions include the formation of ammonium chloride (NH_4Cl) and the oxidation of ammonia, though this is a slow reaction (McConnell, 1973; Levine *et al.,* 1980) and is not thought to be a significant process for regional-scale modelling in N.W. Europe.

1.2 Historical trends of ammonia in the environment

Most of the ammonia emission arises from agricultural sources. This includes the spreading of animal waste on fields, and the application of ammonia-based fertilisers, such as urea and ammonium nitrate.

Asman *et al.* (1988) estimated that between 1920 and 1980 emissions of ammonia from Europe have doubled. Another study by ApSimon *et al.* (1987), for the period between 1950 and 1980, gave the increase as being 50%, though in some countries emissions had doubled while in others the figure had slightly decreased. However, this study did not include the contributions from fertilisers which were expected to contribute an additional, though small, increase. Analysis of glacier ice cores in Greenland by Fuhrer *et al.* (1996) found that air transported from the European continent, reflected a doubling in concentrations of ammonium over the last 40 years. This is attributed to the rise in the number of livestock and the increase in application of fertiliser. In the UK, the use of nitrogen-based fertilisers has grown considerably over the last 50 years while the use of other types, such as phosphorus (P) and potassium (K) based products, have remained almost static (INDITE, 1994).

1.3 Main emissions sources of ammonia

Bujisman *et al.* (1987) estimated that emissions from the volatilisation of livestock waste were responsible for over 80% of European emissions, with much of the remaining emissions from the application of nitrogen fertiliser. A number of authors have attempted to estimate the annual emission from Great Britain (Kruse *et al.*, 1989; Jarvis and Pain, 1990; Asman, 1992; Eggleston, 1992a; Lee

Author	Cattle	Pigs	Sheep	Poultry	Fertiliser applic. & crops	Other animals	industry sources	Other emission	Total
Kruse *et al.* (1989) Great Britain	275 61%	25 6%	100 22%	34 8%	13 3%	2 0%	ni.	ni.	451
Jarvis and Pain (1990) UK	125 55%	53 23%	18 8%	19 9%	11 5%	ni.	ni.	ni.	226
Asman (1992) UK	274 59%	41 9%	50 10%	34 7%	67 14%	2 0%	(7) 1%	ni.	468
Eggleston (1992) UK (for 1988)	230 43%	34 6%	86 16%	inc. with pigs	116 21%	19 4%	15 3%	38 7%	538
Sutton *et al.* (1995a) UK (for 1988)	245.0 54.8%	41.7 9.3%	41.0 9.2%	35.0 7.8%	30.3 6.8%	7.1 1.6%	7.0 1.6%	40.1 9.0%	447
Dragosits *et al.* 1996 UK (for 1993)	160 50%	30 9.4%	20 6.3%	30 9.4%	40 12.5%	-	-	40 12.5%	320

Table 1.1: Example estimates of annual NH_3 emissions for Great Britain. ni. means not included. Adapted from Sutton *et al.* (1995a).

and Dollard, 1994; Sutton *et al.*, 1995a; Dragosits *et al.*, 1996), resulting in values ranging from 226 Gg year^{-1} to 538 Gg year^{-1}. There is obviously uncertainty in the above values, with the range of estimates being $\pm$ 54% around the mean value. In comparison, emissions of sulphur dioxide and nitrogen oxides are estimated to be known to be better than $\pm$ 20% (RGAR, 1990).

Emissions from cattle constitute the largest agricultural source. According to various authors (Table 1.1), the contribution from cattle to the agriculture emission total range from 43% (Eggleston, 1992a) to 61% (Kruse, 1989). Other livestock, such as poultry, sheep and pigs, are estimated to contribute smaller though still very significant amounts. Emissions from livestock can be categorised into three areas; losses arising from housing and storage of manure, from the spreading of manure on the land, and direct emissions that occur during grazing. The major uncertainty is from the land spreading of manure. To calculate this, the amount of N in the applied manure and the percentage of nitrogen (N) that is lost during volatilisation both need to be known. The uncertainties involved are very large, and the values given for cattle by various authors range from 3.4

to 12.7 kg N animal^{-1} year^{-1}.

Calculating the emissions that occur from fertilisers has the same inherent problem as the land spreading of animal wastes. Ammonium nitrate and urea form 60% of the total fertiliser applied, with others such as phosphorus and potassium based substances making up the remaining 40% (Asman, 1992). Of the combined total for urea and ammonium nitrate, 15% applied is urea, with ammonium nitrate making up the remaining 85%. The amount of volatilisation that occurs is dependent on a number of physical factors, which include the pH of the soil, temperature, wetness, humidity, and the concentration of ammonia in the atmosphere just above the surface. Urea is converted to ammonium by bacterial activity according to the equation;

$$CO(NH_2)_2 + 3H_2O \rightarrow 2NH_4^+ + HCO_3^- + OH^- \qquad (1.1)$$

This process is known as hydrolysis, and the rate of reaction is temperature dependent and will increase with increasing soil temperature over the range 10 to 40 °C. This process raises the local pH, which reduces the solubility of NH_x and favours emission. The solubility of NH_x is also temperature dependent and will decrease with increasing temperature (Sutton, 1990). Thus, in general, warm dry conditions will favour emission of NH_3 from fertilisers, whereas emission is generally low in wet conditions. An exception to this rule concerns the hydrolysis of urea, as discussed above, where wet conditions will actually favour this reaction and may promote emission.

Percentage losses from each type of fertiliser are different. Sommer and Jensen (1993) reported losses from the field of 25% for urea applied to crops on a non-calcerous soil, and Whitehead and Raistrick (1990) gave a value corrected to field conditions of 16.6% for the UK. In comparison, losses from ammonium nitrate are much lower with Whitehead and Raistrick (1990) suggesting a field loss for the UK of 2.5%.

Emissions from croplands present a more complicated situation than other emission sources that have been considered. This is because emissions from crops are a direct consequence of the nitrogen status of the plant. Application of fertiliser will affect this status, as reported by Harper *et al.* (1987) for an experiment in the US. They describe how, in the period of two weeks following the application

of fertiliser to a wheat crop, there was an estimated emission flux of 8 kg N ha^{-1}. In the subsequent period, defined as the growth phase, there was a net absorption by the crop of 1 kg N ha^{-1}, which was followed by a period of emission estimated as 7 kg N ha^{-1} during senescence. However theses values are much greater than would be expected for the cooler climates of the Europe (*e.g.* Schørring *et al.*, 1993; Sutton *et al.*, 1993c). The results do illustrate however the variable nature of the fluxes that can occur from a fertilised crop, and variations in the magnitude and direction of the flux may fluctuate daily and even hourly, dependent on many influencing factors, some of which have already been mentioned. This can present a problem for atmospheric transport models which require the magnitude and direction of the flux of ammonia to be defined.

1.4 Atmospheric behaviour of ammonia

1.4.1 Main meteorological factors affecting the dispersion of ammonia in the atmosphere

Most of the main emissions sources of ammonia discussed in this chapter are low-level sources. The exceptions are emissions from some types of anthropogenic sources, such as those arising from ammonia production and associated fertiliser manufacture, and biomass burning (Sutton *et al.*, 1995a). In these cases, emissions may be considered to have elevated sources, either due to the height of the industrial plant in the case of fertiliser production, or because biomass burning will cause elevated plume rise due to the heat content of the emission. These combined sources are estimated to contribute only 2.0% approximately to the total emissions for the UK (Sutton *et al.*, 1995a) and thus it is an acceptable approximation to assume that all emissions are ground-based.

The high density of livestock present in an animal house results in the existence of large sources, while other areas of ammonia emissions will be grazing fields, which may contain large numbers of small point sources, such as excrete patches, surrounded by areas of little or no emission. Once released into the atmosphere, the ammonia will be dispersed away from the source by the small- and large-scale motions of the surrounding atmosphere. Small-scale motions, such as turbulent eddies, result in the entrainment of less polluted air into the ammonia plume,

and thus dilution of the plume. Larger-scale motions, will result in the horizontal advection of the plume downwind from the source, and also possible vertical and crosswind motion of the plume by larger-scale eddies. The amount of entrainment that occurs is dependent on prevailing meteorological conditions. During nighttime, turbulence close to the ground is suppressed by surface cooling, and this can result in high ground-level concentrations of ammonia. During the hours of sunlight, mixing is usually more vigorous and concentrations of ammonia decrease rapidly downwind of the source, resulting in large horizontal gradients over a distance of just a few kilometres.

1.4.2 Important chemical reactions of atmospheric ammonia

Atmospheric ammonia occupies an important position in the many complex chemical reactions that occur in the lower troposphere. The main reactions involve the neutralisation of acidic species such as sulphuric acid (H_2SO_4), nitric acid (HNO_3) and hydrochloric acid (HCl) (Seinfeld, 1986). Ammonia and sulphuric acid react together to form ammonium hydrogen sulphate (NH_4HSO_4) and ammonium sulphate ($(NH_4)_2SO_4$).

The reactions of H_2SO_4 and HNO_3/HCl with NH_3 are competitive processes but NH_3 preferably reacts with H_2SO_4 (Seinfeld, 1986).

Any excess NH_3 remaining will then be available to react with HNO_3 and also HCl. These reactions are more complex than the reaction with H_2SO_4, as an equilibria exists between the reactants and the products. The equilibrium are described by

$$NH_3(g) + HNO_3(g) \rightleftharpoons NH_4NO_3(s) \tag{1.2}$$

$$NH_3(g) + HCl(g) \rightleftharpoons NH_4Cl(s) \tag{1.3}$$

The presence of ammonia in large quantities will also have an affect on other processes, such as in-cloud oxidation of SO_2. As NH_3 is highly soluble, it is readily taken up by cloud droplets. This leads to an increase in the pH of the droplets, allowing more SO_2 to be taken into the droplets, and influences the rate at which SO_2 is oxidised to SO_4^{2-}.

In areas where HNO_3 and, more importantly, H_2SO_4, are present in large con-

centrations, conversion of NH_3 to $(NH_4)_2SO_4$ and NH_4NO_3 will take place, and the concentration of NH_3 will decrease. An example of these processes is described in Kruse-Plass *et al.* (1993) where a study was made of an easterly air flow, first passing over the main SO_2 and NO_x emission regions of the industrial Midlands of England (see Figures 5.7 and 5.8 in Chapter 5) before reaching Wales, where there are areas of relatively large emissions of NH_3 (see Figure 2.5) and low values of SO_2 and NO_x emissions. Oxidation of SO_2 to H_2SO_4 was clearly observed, and formation of $(NH_4)_2SO_4$ led to a large proportion of the available SO_4^{2-} being neutralised. It is clearly important that any attempt to model the atmospheric transport of ammonia must at least describe the conversion to NH_4 aerosols and ideally be dependent on the availability of the appropriate acidic species necessary for this process.

1.5 Removal of ammonia and ammonium from the atmosphere

Removal of NH_3 and NH_4^+ from the atmosphere may occur by several different processes. These can generally be split into two categories: dry deposition and wet deposition. Dry deposition is defined as removal from the atmosphere at the surface by way of turbulence. Wet deposition occurs during periods of rainfall, and material can either be removed within the clouds or below the cloudbase.

1.5.1 Dry deposition

Strictly speaking, dry deposition is defined to be taking place if the net flux between the atmosphere and the surface is towards the surface. However, even if there is a net flux of ammonia away from the surface, dry deposition may still be occurring between various levels of the vegetation and underlying soil. Sutton *et al.* (1995b) presented a model of plant-atmosphere exchange where, although there may be a net flux from the plant canopy to the atmosphere, some of the emission from the plant will be dry deposited onto leaf cuticles. When defining whether dry deposition is occurring, it is important to define the scale over which the flux is to be considered.

If we consider dry deposition fluxes within the atmosphere, there are several

main factors which control the rate at which NH_3 is deposited. These include the concentration of NH_3 in the atmosphere, the type of surface onto which dry deposition is taking place, and the prevailing local meteorological conditions. Most of the NH_3 emissions are rural and are often situated close to areas which experience large rates of dry deposition. These areas are usually defined as semi-natural and unfertilised plant communities and include moorland, unfertilised grassland, and forests. In the case of moorland, Sutton *et al.* (1992) estimated that to some areas the annual input of nitrogen in the form of ammonia was of similar magnitude to that of NH_4^+-N in wet deposition. In areas close to NH_3 emission sources, dry deposition of NH_3 was expected to dominate inputs of atmospheric nitrogen.

It has been suggested by several authors that interaction with other pollutants, such as SO_2, may affect the rate of NH_3 dry deposition. Measurements using throughfall techniques have found NH_4^+ and SO_4^{2-} to be deposited in equivalent quantities (van Breeman *et al.,* 1982). One explanation is that deposition of one species alone can lead to saturation on the leaf surface due to pH limitation to solubility. Deposition of both SO_2 and NH_3 may limit this saturation effect and allow increased deposition. Erisman *et al.* (1993a) found enhanced deposition of NH_3 occurred in the presence of large SO_2 concentrations. However other studies (Sutton *et al.,* 1993d) postulated that the effect may be more complex. The authors observed that large concentrations of SO_2 were associated with NH_3 emission during some periods of the experiment. One explanation put forward for this is that the high SO_2 concentrations lead to the formation NH_4^+ aerosols, thus reducing the concentration of NH_3 to below the plant compensation point and so stimulating emission from the vegetation.

Average atmospheric residence times for NH_3 and NH_4^+ have been estimated as 1-4 days and 7-19 days respectively by Söderlund and Svensson (1976). Later estimates by Möller and Scheifdecker (1985) were less, with values of 0.8 and 7.7 days. The shorter estimated residence time of NH_3 is a direct consequence of the high rates of dry deposition and rapid conversion to NH_4^+ aerosols which are primarily removed by precipitation.

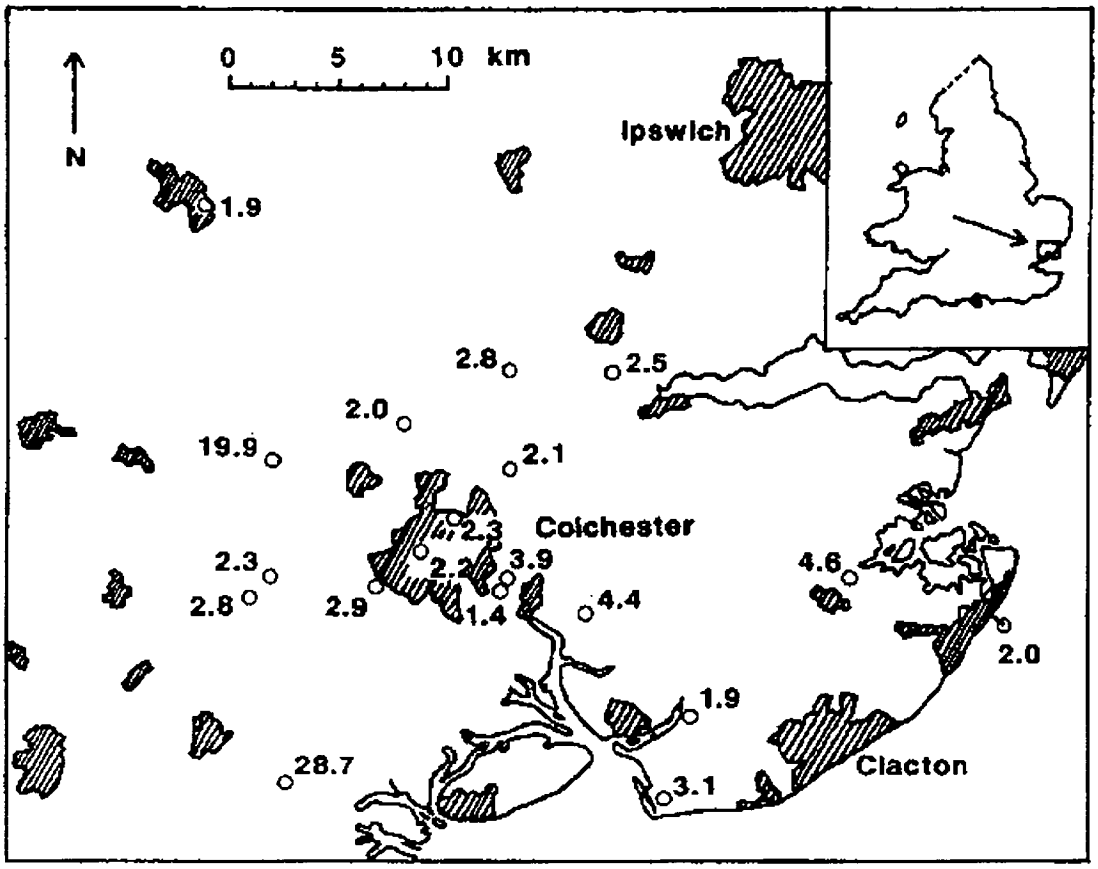

Figure 1.1: NH_3 concentrations in an area of S.E. England. Means from 8 months monitoring (μg NH_3 m^{-3}). Major urban areas are shown as shaded regions. Data taken from Allen *et al.* (1988). Plot from Sutton *et al.* (1994).

1.5.2 Problems in quantifying dry deposition fluxes of ammonia

Over the past few years, a number of experiments have been carried out to attempt to quantify the flux of NH_3 between surface and the atmosphere. Experiments over arable crops and fertilised grassland have shown that both emission and deposition can occur (Sutton *et al.*, 1993c; Schjørring *et al.*, 1993). In contrast, measurements made over semi-natural and unfertilised systems, such as moorlands and forests, have shown that these landtypes behave as sinks for NH_3 (van Breeman *et al.*, 1982; Duyer *et al.*, 1987, ; Sutton *et al.*, 1993b.). Sutton *et al.* (1993b) gave estimates of annual dry deposition fluxes for short vegetated

surfaces in the UK. These range from 2.1 kg $ha^{-1}year^{-1}$ for moorland through to 8.7 kg $ha^{-1}year^{-1}$ for unfertilised meadow. Annual fluxes for four forest sites considered in the study of Sutton *et al.* (1993b) range from 4.8 kg $ha^{-1}year^{-1}$ to 32.8 kg $ha^{-1}year^{-1}$, though it should be noted that the forest sites which experience the lower flux values are situated at heights of 300 m and 600 m and also experience much lower average concentrations than the low altitude sites. It is more difficult to estimate an average annual flux for arable crops and fertilised grassland because of the bi-directional nature of the fluxes, and also the variable timescale during which emission and deposition occurs. These measurements have only taken place in certain sites in Great Britain and thus it is very difficult to extrapolate these results to the entire country due to the extremely variable spatial distribution of ammonia emissions and surface concentrations. Allen *et al.* (1988) recorded concentrations at 19 sites in S.E. England, during an 8-month period. The majority of sites have concentrations in the range of 2-4 $\mu g\ m^{-3}$, but two sites, in livestock breeding areas, have values of 20-30 $\mu g\ m^{-3}$. The spatial distribution of mean concentrations for this period are shown in Figure 1.1. Sutton *et al.* (1994) commented that these data illustrate that while large-scale models may be be able to predict the background concentration reasonably well, they would not be able to capture the small-scale variability and large horizontal gradients as shown by these data.

Dry deposition can estimated from throughfall measurements, which are usually performed beneath forest canopies. The approach assumes that precipitation washes off all material dry deposited onto the canopy, and thus the collected solution should be a measure of the total deposition, i.e. the sum of the wet and dry deposition. If precipitation is also collected above or outside the forest, the difference between the two sets of measurements should equate to the total dry deposition. This difference is termed 'net throughfall'. (Draaijers, 1993; Sutton *et al.,* 1993e). A number of limitations exist for this method when applied to analysis of reduced nitrogen deposition. Absorption of nitrogen by the vegetation will render the method non-mass-consistent. Also this method is generally only applied to forests, and relatively few attempts have been made to apply this method to other smaller types of vegetation (e.g. Bobbink *et al.,* 1992).

To calculate country-wide deposition fluxes, a method has often been employed

which uses a combination of measured concentration fields and meteorological data. This technique is known as 'inferential modelling' since deposition fluxes are inferred from measured concentrations. It was employed by the Institute of Terrestrial Ecology, Edinburgh, to calculate the annual dry deposition flux of NH_3 over Great Britain (RGAR, 1996; section 2.2). The model calculated an annual dry deposition flux of 94.5 kg $ha^{-1}year^{-1}$, and assumed that dry deposition occurs only to semi-natural/forest land types. The concentration data used were from a network of passive diffusion tubes (1.5 m), operated between 1987 - 1990 (Atkins and Lee, 1992). There were only 40 sites used in the first year (June 1987 - May 1988) of the measurement study, and this number was reduced in the following year to 32 sites. Hence only broad-scale patterns of NH_3 concentrations in Great Britain could be inferred. To get clear overview of NH_3 surface concentrations, Asman (1994) recommends that many stations are required (up to 1 station per 25 km^2 in some areas of high emissions), due to the large spatial variability in the NH_3 concentrations. This was illustrated in the application of the TREND model to the Netherlands using 5 km $\times$ 5 km resolution emissions data (Asman and van Jaarsveld, 1992). The results clearly showed the spatial variability of NH_3 surface concentrations that occur when the spatial distribution of emission is so variable.

Obviously using 40 stations for the entire land area of the UK does not produce the expected spatial detail in the concentration map, and interpolation between stations will smooth out many features and lead to large errors in calculated deposition in some regions, especially those in areas of high emissions and in regions with a very low density of measurement stations. The advantage of atmospheric transport models is that they may be used to interpolate between measurement stations where necessary, and thus, depending on the success of them, can be used to create a more accurate representation of the spatial distribution of surface concentrations.

1.5.3 Wet deposition

Wet deposition is a term used to describe the general removal of material from the atmosphere by precipitation. Removal can take place in-cloud or below the cloudbase and occurs when moisture is falling from the cloud in the form of rain

or snow. In-cloud processes involve aerosol particles acting as condensation nuclei for cloud water droplets, with the process becoming more efficient at higher values of relative humidity. In-cloud scavenging is the main removal process for aerosols such as $(NH_4)_2SO_4$ and NH_4NO_3. The removal of material below the cloudbase is by way of falling raindrops or snowflakes. Smaller particles are not removed as efficiently as larger particles. In-cloud scavenging is the largest contributor to wet deposition of reduced nitrogen, according to the model of Asman (1994), with the different contributions being; in-cloud scavenging of NH_3 15%, in-cloud scavenging of NH_4^+ 77%, below-cloud scavenging of NH_3 6%, and below-cloud scavenging of NH_4^+ 2%. Most of the NH_3 removed by these processes will be converted to NH_4^+ by chemical reaction in the raindrops and thus it impossible to distinguish between NH_4^+ and NH_3 scavenging contributions to wet deposition without the use of a model.

There are a number of different samplers which can be user to monitor wet deposition of various species. The simplest sampler, known as a 'bulk sampler', is left open during the entire sampling period and collects rainfall through a funnel at the top of the device. A well known problem with this device is that material can be dry deposited to the open funnel, and thus analysis of ion concentration may lead to an over-estimation of the amount of material deposited during precipitation alone (Fowler and Cape, 1984).

The wet-only sampler is a more accurate device which is widely recommended for use. This device only opens its collector when precipitation occurs, and thus is much less prone to sample unwanted dry deposition.

In Great Britain, a network of measurement sites are used by the Department of the Environment (see the Review Group on Acid Rain, 1990) to monitor wet deposition of a number of species including sulphates, nitrates, chlorides and ammonium ions. There are a total of 37 sites (INDITE, 1994), with five of these locations employing wet-only samplers, and bulk-samplers being used in the remaining stations. To calculate the flux of material wet deposited, the samples are analysed for the relevant ion concentration, and then the results are combined with annual rainfall data. The data are subsequently adjusted for an altitude enhancement effect known as the 'seeder-feeder' process. High altitude sites can experience greater ion concentration in precipitation than surrounding

low altitude locations, due to orographic clouds forming in the air mass as it flows over the hills/mountains. As the collectors are located at low altitude, a correction factor must be applied to account for this effect at high elevated areas. Dore *et al.* (1992) applied this enhancement factor to create a map of ammonium wet deposition in Great Britain.

The latest figures for NH_4^+ deposition in precipitation, as reported in RGAR (1996), give the annual total for Great Britain as 131 NH_4^+-N Gg year^{-1}. This is a large fraction of the estimated emissions of NH_3-N for Great Britain of 335 Gg year^{-1} (Sutton *et al.* 1995a), of over 39%.

1.5.4 Ecological impacts of increased nitrogen deposition

Additional input of nitrogen to vegetation usually results in increased growth. This is because nitrogen is an essential nutrient, hence its universal use in fertilisers. However, for many ecosystems there is a limit above which any additional nitrogen input will cease to have beneficial effects and may adversely affect the health of the plant, or its competition with other plant species. In the case of increased ammonia deposition, there are a number of effects which may be separated into two categories.

In many semi-natural ecosystems, such as heathland and moorland, the vegetation are adapted to low levels of fixed nitrogen in the soil and are only able to function well in nitrogen-deficient conditions (Grime, 1979). It has been suggested that increased fixed nitrogen deposition over recent years will raise the level of available nitrogen (eutrophication) which may cause changes to the ecosystem (Pitcairn *et al.,* 1991). Such changes may involve the replacement of nitrogen-poor vegetation by grassland, and may also raise the nitrogen content of plant leaves which will favour attacks on the vegetation by insects such as the heather beetle in the case in heathlands. One such example was reported by Bobbink *et al.* (1992) who stated that 35% of the Dutch heathland had been transformed into grassland. Another effect of increased levels of fixed nitrogen in the soils was proposed by Sutton *et al.* (1992). Periods of emission from Dutch heathlands (Sutton *at al.,* 1992; Erisman and Wyers, 1993a) were suggested to have occurred because the large levels of measured nitrogen deposition resulted in 'nitrogen saturation' of the vegetation, which lead to some of this 'excess' nitrogen

being re-emitted to the atmosphere.

Nihlgard (1985) pointed out how increased uptake of nitrogen might also have adverse effects on forests. Excess nitrogen may be stored in leaves and needles which may shed during dry periods. This results in decreased root growth, making the trees more susceptible to frost damage and attacks by fungi, insects, bacteria and viruses.

Deposition of the acidic products of SO_2 and NO_x oxidation are well known to contribute to the acidification of ecosystems. In addition, acidification from NH_4^+ may also be considerable. This can be caused by the oxidation of NH_4^+ to NO_3^- by micro-organisms,

$$NH_4^+ + 2O_2 \rightarrow NO_3^- + H_2O + 2H^+ \tag{1.4}$$

which can lead to the production of H^+ and subsequent leaching of the NO_3^- by metal cations.

It is of great importance to assess the overall fluxes of ammonia to the locations that may be susceptible to damage from large deposition fluxes, and analyse whether damage is occurring with the present day conditions. Because ammonia is generally emitted from low-level sources, much of the deposition occurs close to the area of emission in the form of dry deposition. A detailed study was made for the Netherlands by Mass (1988) in order to determine where the NH_3 needed to be reduced in order to avoid damage. Asman and van Jaarsveld (1992) showed in a modelling exercise that at a distance greater than 300 km from the source, no NH_3 emitted from that source ought to be observed as it should have been either dry deposited or converted to NH_4^+ aerosols.

A policy tool used to assess environmental damage by pollutants is the 'critical load' concept (e.g. Bull, 1991b). The basis of this approach is to define the threshold pollutant load which causes harmful effects to a sensitive receptor and ensure that the actual pollutant load to the receptor is less than the critical value. In this way harmful effects are prevented. This concept has been used to assess acidifying damage by sulphur compounds, and the second stage of the UNECE sulphur protocol is based on emission reductions of SO_2 using the critical loads approach.

The definition of a critical load is 'the quantitative estimate of exposure to

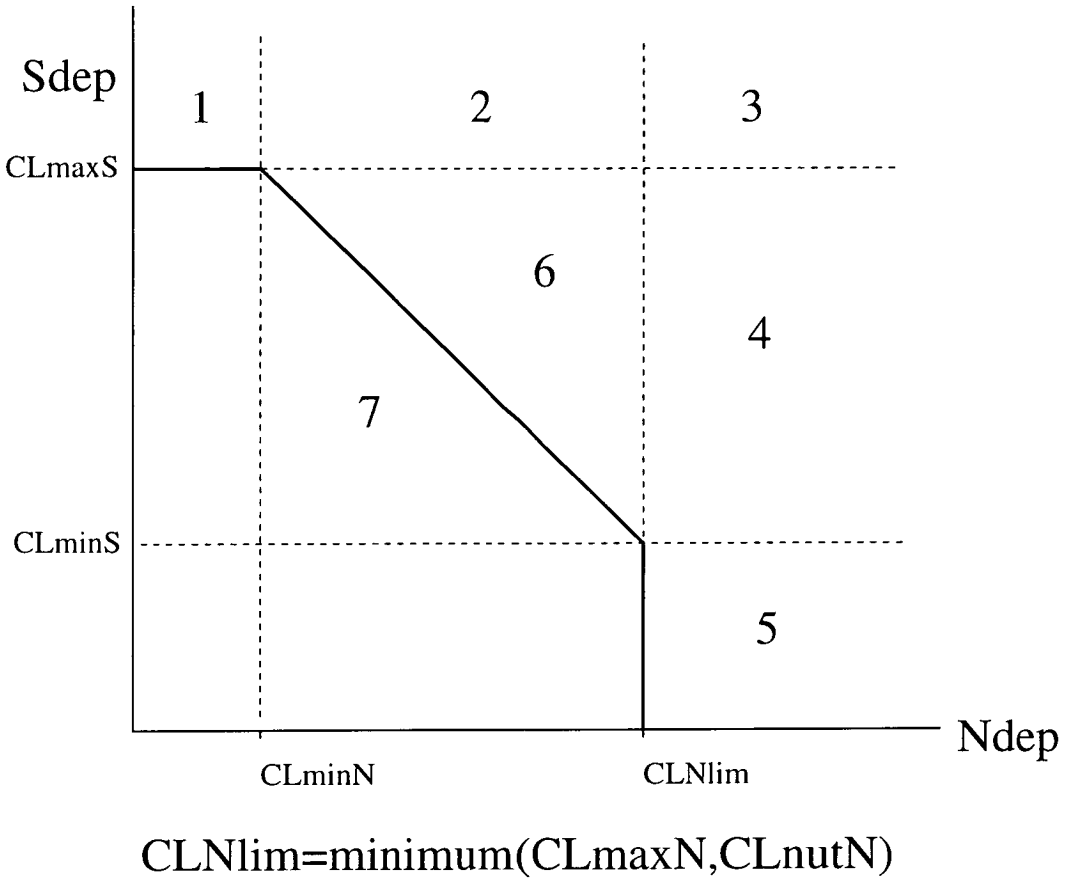

Figure 1.2: Regions of exceedance defined by a Critical Loads Function (CLF) (Bull *et al.*, 1994). The horizontal axis is the magnitude of the deposition flux of nitrogen, and the vertical axis is the magnitude of the deposition flux of sulphur. This plot shows 7 regions for a CLF. **7** Area of protection - critical loads not exceeded. **6** Area of 'options' - either sulphur or nitrogen reductions can offer protection. **5** Area where nitrogen deposition should be reduced - reduction of sulphur gives no benefits. **4** Area where nitrogen is a major contributor to exceedance - nitrogen must be reduced to provide the possibility of options available in area 6. **3** Area where sulphur and nitrogen are major contributors to exceedance - both must be reduced before there are options. **2** Area where sulphur is a major contributor to exceedance - sulphur must be reduced to provide the possibility of options. **1** Area where sulphur deposition should be reduced - reduction of nitrogen gives no benefits. **CLNLim** defines the maximum nitrogen deposition above which damage to the environment may occur. It is the lower of the two values of critical load for nitrogen eutrophication (**CLnutN**) and nitrogen acidity (**CLmaxN**), assuming only nitrogen deposition.

one or more pollutants below which significant harmful effects on specified sensitive elements of the environment do not occur according to present knowledge' (Nilsson and Grennfelt, 1988). The critical loads analysis for sulphur deposition concerns the acidifying effects of sulphur. In the UK, work for the DoE has produced critical load maps of sulphur and acidity for soils and freshwater (Bull *et al.,* 1991a).

Attention has turned more recently to critical load analysis for nitrogen deposition. Since nitrogen deposition can both acidify and eutrophicate ecosystems, it is more complicated to calculate critical loads for nitrogen deposition than for sulphur (Hornung *et al.,* 1995; Grennfelt and Thőrnelőf, 1992). One of the simplest methods is to calculate levels for both effects and take the lowest value, taking into account the various types of ecosystems (Gunderson, 1992; Bobbink *et al.,* 1992). This idea has been used to construct a function known as a critical loads function CLF (Figure 1.2, e.g. Bull *et al.,* 1994) which is used to define exceedance and protection levels for both sulphur and nitrogen deposition. By using information on the nitrogen and sulphur deposition at a certain location, it can be used to define a strategy in order to reduce the exceedance of the critical load. It contains information on the critical loads due to acidity (from both sulphur and nitrogen) and also critical loads for nitrogen eutrophication (CLnutN).

Maps can be prepared of critical loads on a regular grid, and these can be compared with deposition maps to calculate where the critical loads are exceeded and by how much.

1.6 Objectives of this study

It has been shown that it is important to quantify the fluxes of NH_3 and NH_4^+ deposition and to describe the spatial distribution of them as accurately as possible. This is due to the number of adverse effects that large fluxes of NH_3 and NH_4^+ deposition can cause to various types of vegetation, with some ecosystems being more susceptible to damage than others. The distribution of NH_x wet deposition is well understood and maps produced, with altitude correction factors, are a good estimation of the deposition produced by precipitation. In comparison, the calculation of a map of dry deposition fluxes to Great Britain is much

more problematic. Most of the dry deposition of reduced nitrogen that occurs is in the form of ammonia, and large amounts of material can be redeposited in the vicinity of the emission source. Asman (1994) recommended that a very large number of monitoring stations would be required to accurately reproduce the large spatial variability of ground levels concentrations, with a recommended density of 1 station per 25 km^2 in areas of large emissions. This would obviously be very expensive to setup and maintain. Also, it is possible that the equipment may have systematic errors in it, as has been suggested for diffusion tubes (Anderson, 1991; Singles *et al.,* 1995).

The aim of this project was to develop a statistical atmospheric transport model which would be able to describe the mean spatial distribution of NH_3 ground-level concentrations and dry deposition of reduced nitrogen over Great Britain on a fine spatial scale using 5 km $\times$ 5 km grid squares. To achieve this, the model would need to have emissions data on the same spatial scale which are necessary to clearly differentiate between areas of high and low emissions. Variability is also expected at the sub 5 km grid scale. However for the country-wide study here, the resolution in available emissions data is limited to 5 km $\times$ 5 km.

Since the magnitude of the dry deposition flux is both land-type dependent and diurnally-variable, it is important to parameterise the dry deposition process for NH_3 to an equal accuracy to allow the model to distinguish between major source and sink areas. The chemical scheme in the developed model must be able to describe the main reactions governing the conversion of NH_3 to NH_4^+ aerosol, since this will determine if the emitted NH_3 is dry deposited within the vicinity of the source or subject to long-range transport in the from of NH_4^+ aerosols. The parameterisation of vertical dispersion in the model plays a crucial role in determining the surface concentrations and dry deposition fluxes. The developed model should employ an appropriate mixing scheme which describes the diurnally-varying rates of vertical mixing, dependent on the stability of the atmosphere.

At the present time, there exist a number of models that are used for the purposes of modelling the transport of pollutants across Great Britain and determining the spatial scale of the deposition fluxes as a long-term average. However, some of the parameterisations used in these models, such as the type of vertical

dispersion scheme used and the description of NH_3 dry deposition, render them unsuitable to be used to model the dry deposition of NH_3 on the fine spatial scale intended in this study. There exists the need for a statistical atmospheric transport model which is able to both describe this short-range deposition of NH_3 explicitly, and also be applicable on a national scale to describe the behaviour of ammonium aerosols.

Many of the above requirements are fulfilled by the TERN model (Apsimon *at al.,* 1994), which is a Lagrangian model used to model the atmospheric behaviour of NH_3 along a predetermined trajectory across Europe. The TERN model described the changes that occur within an air column which has 33 layers, with a very detailed vertical resolution close to the surface. Eleven chemical species are used and formation of NH_4^+ aerosols is by way of dry- and aqueous-phase chemical reactions. The model is able to explicitly describe the ground-level nature of NH_3 emissions and predict the large surface concentrations that occurs around a high emissions source, which is an essential requirement for a statistical model using such a fine spatial resolution. The TERN model, however, is limited to single trajectory scenarios which require explicit information on meteorology, trajectory and atmospheric mixing depth. Substantive work is needed to use this as a basis for developing a statistical model of ammonia exchange in Great Britain.

In order to use TERN as a statistical model, a large number of modifications to the model structure were required. The main chemical and physical processes were retained since the aim of this project was to concentrate on the aspect of dry deposition, but the following changes were made.

- The meteorological data used by TERN had to be defined as a long-term average by the use of suitable statistics or by appropriate parameterisation.

- The dry deposition scheme for NH_3 was expanded and made both land-dependent and diurnally-variable.

- The project made use of existing databases for Great Britain, such as a 20 km $\times$ 20 km landuse database, annual rainfall data on a fine resolution grid, and also a dataset containing annually-averaged windspeed data for the entire country.

- A trajectory-scanning algorithm was written to allow the model to cover multiple trajectories originating from different wind directions.
- Concentrations were created for the edge of the model domain to include the effect of pollutants emitted from foreign sources.
- Optimisation of the computer code to reduce computational time to a minimum.

The use of an atmospheric transport model for a problem such as described in this chapter is a financially attractive method which can be used in conjunction with existing measurements to assess the accuracy of the model and be used at locations where measurements are not available.

The following chapters are presented as follows:

Chapter 2. General overview of previous modelling work to describe the atmospheric behavior of reduced nitrogen over Great Britain.

Chapter 3. Description of the main atmospheric processes that are relevant to ammonia and parameterisation of them for use in an atmospheric transport model.

Chapter 4. Analysis and evaluation of a multi-layer model (TERN), and a description of the methodology used to convert this into a regional model (FRAME) capable of producing concentration and deposition maps for Great Britain.

Chapter 5. Evaluation and testing of model results on a local scale and for Great Britain on a 20 km grid.

Chapter 6. Conversion of the FRAME model to a 5 km grid and introduction of a receptor model to describe concentrations at specified sites in Great Britain.

Chapter 7. Conclusions and recommendations.

Chapter 2

A Review of Previous Modelling Work to Describe the Deposition of Reduced Nitrogen over Great Britain.

2.1 Introduction

The concept of modelling is introduced in this chapter, and attention focuses on modelling the atmospheric behaviour of ammonia. Particular attention is paid to atmospheric transport modelling, and results from several of these models are reviewed and discussed.

Modelling the atmospheric behaviour of ammonia involves the application and solution of mathematical equations. Because the processes under consideration are extremely complex, such as the treatment of atmospheric turbulence, certain assumptions must be made. These assumptions can involve the parameterisation of certain key features by the use of simple equations or by assuming that the said feature has a negligible effect in comparison to other processes and thus should in fact be considered to have zero effect. The degree and number of assumptions made are crucial in determining the type of model created. A compromise has to be reached between the complexity of the equations used and the resources available to find solutions to the model. Any model created should be as accurate as possible but must ultimately be solvable in a reasonable amount of time.

Another factor which determines the accuracy of any model is the quality of the data used as input. In the case of an atmospheric transport model, the main

input data are emissions and meteorological data. The creation of the emission map itself can involve the use of a model, as is the case with Eager (1992) and Dragosits *et al.* (1996) who used a GIS framework to create maps of ammonia emission with a spatial resolution of 5×5 km^2 for Great Britain. Input data in this case included information on the spatial distribution of livestock and also the calculated emission factor of ammonia for each type of animal. Any error in the data supplied to the model will obviously affect the final results, and thus ensuring the accuracy of these data is as important as formulating the governing equations in the model.

Almost all mathematical models are solved by the use of computers. This may be due to the sheer number of calculations involved, or because complex numerical methods must be used due to the absence of any analytical solution. The rapid increase in computing power over the last decade has allowed the creation of more detailed and complex models which involve many orders of magnitude more calculations than would have been possible 10 years ago.

The application of atmospheric transport models (hereafter referred to as ATMs) are playing an increasingly important role in defining and implementing environmental policy, both on a national and international scale. On a national scale, ATMs have been used to calculate the spatial distribution of sulphur and nitrogen deposition (e.g. Metcalfe *et al.,* 1995; Asman and van Jaarsveld, 1992). Results from these models can show where deposition may be causing harm to the environment by the application of the critical loads concept (see section 1.5.4; Nilsson and Grennfelt, 1988). Another application of ATMs is the estimation of the effect of future policy and whether such policy will be effective. One such example is the second sulphur protocol signed in Oslo in 1994 by many countries, which commits the signatories to control emissions such that the long-term depositions does not exceed defined critical loads. States must thus be responsible, not only for the export of their pollutants, but also for the deposition and long-term effects that these substances have in areas outside their national boundaries. A description of the spatial distribution of critical loads is required to successfully implement this policy. Blanket reductions as defined by the Helsinki accord in 1985, which committed the signatories to a blanket reduction in sulphur emissions or their transboundary fluxes of at least 30% by 1993 as compared to 1980 levels,

could achieve this but a more feasible approach is to perform selective emission reduction. If one can identify the sources which are the main contributors to deposition in the area under consideration, then the application of a model could determine whether the proposed reduction will have the desired effect in the specified receptor area. This method of optimising the cost:deposition reduction ratio is a obviously a financially attractive one and can only be achieved by the use of models. Ongoing evaluation of the attainment of the protocol goals is being performed by the EMEP model (Barrett and Seland, 1995) which is discussed in section 2.4.1

Modelling is an important tool to use in analysing the atmospheric behaviour of pollutants. In the following sections several types of models employed to research the atmospheric behaviour of ammonia are examined, and the results are discussed and analysed.

2.2 Measurement-based models of reduced nitrogen deposition

A number of models make use of measurement data, which are recorded at sites situated across the country, to calculate deposition fluxes on a country-wide basis. To create maps of the required data, an interpolation procedure is performed on observations, which maps these data onto a regular grid. The measurements are used as input for a model which takes the data and calculates the required deposition fluxes. If there are sufficient measurements available, these models are a particularly attractive method of calculating the spatial distribution of deposition fluxes, since the use of observed data means that the overall set of results for the country should be a close fit to the actual conditions.

Two of these type of models are discussed in this section. They are used to create maps of annual dry and wet deposition fluxes of reduced nitrogen to Great Britain (INDITE, 1994; RGAR, 1996).

2.2.1 Inferential modelling

The first type of models to be considered are known as inferential models, since deposition fluxes are inferred from measured concentrations, as discussed in sec-

tion 1.5.2. Inferential models are used to specifically calculate fluxes of dry deposition. This is performed by using monitored concentration data together with sufficient meteorological measurements to calculate the magnitude of the flux. The relationship between the concentration data and the flux is given by

$$V_e = \frac{F}{\chi_s - \chi(z)} \tag{2.1}$$

where F is the dry deposition flux, $\chi(z)$ is the concentration of the material at a specified height (z) above the ground, and χ_s is the surface concentration. V_e can be viewed as the average velocity of the gases between the surface and the reference height. V_e has units of m s^{-1}, and is dependent on the particular species being removed, prevailing meteorological conditions and the nature of the surface itself. A simplification sometimes made in some types of inferential models (Hicks *et al.,* 1987, Erisman *et al.,* 1993b) is to assume that the surface concentration (χ_s) is zero. Equation 2.1 now becomes

$$V_d = -\frac{F}{\chi(z)} \tag{2.2}$$

where the flux is assumed to be towards the surface and V_d is defined as the deposition velocity. Hicks *et al.* (1987) considered this to be a satisfactory assumption for chemical species with no surface source.

This method of inferential modelling was used by the UK Review Group on Acid Rain (1990) to create a map of annual dry deposition fluxes of NO_2 and SO_2 for the UK. The authors made use of a landuse dataset for the UK which divided the land into 5 categories; arable cropland, permanent grassland, hill vegetation, forests and urban (RGAR, 1990).

An extension can be made to the argument, namely that this type of inferential model is only valid for chemical species with no surface source. If one has information on the spatial distribution of land-types, then for a particular location, one can say that it is also valid for a particular species if there exists one or more types of land on which no emission of this species occurs, and thus the flux of material is always towards the surface.

This is central to the reasoning behind the application of the inferential method of modelling to ammonia dry deposition. Ammonia is known to be emitted from arable croplands and fertilised grassland (Sutton *et al.,* 1993c). Thus the assumption that χ_s=0 in equation 2.1 seems inappropriate. Howvever, it is generally

considered that the net exchange for forests and hill vegetation are towards the surface and that general rates of dry deposition are large (Sutton *et al.,* 1993b, Erisman and Wyers, 1993b). It has been suggested that the process of dry deposition to land surfaces which experience bi-directional fluxes may also be modelled by the use of a 'compensation point' (Farquhar *et al.,* 1980). Erisman *et al.* (1993b) recommended a scheme which partitioned the direction of the flux according to wet and dry periods, distinguishing between daytime and night time. A dry period was defined to occur when the relative humidity was below 60%, otherwise a wet period was assumed.

The use of the UK land-use dataset, with detailed information of the surface area of different types of land in each 20 km grid square, means that calculations of dry deposition can be made land-type specific.

In constructing a map of annual NH_3 dry deposition fluxes to Great Britain on a 20 km $\times$ 20 km grid (INDITE, 1994; RGAR, 1996), it was assumed there was no net deposition to arable cropland and fertilised grassland. Deposition was limited to forest and moorland only. The rate of deposition was calculated from climatological wind speed data for each of the 20 km $\times$ 20 km grid squares and for each required landtype.

The concentration data of NH_3 were taken from measurements from a network of passive diffusion tubes, operated between 1987 - 1990 (Atkins and Lee, 1992). An interpolated map of the mean surface concentration data, from the entire monitoring period of 1987 to 1990, is shown in Figure 2.1, and these data were used as input for the inferential model. These data have been corrected by a factor 0f 0.45 (Anderson, 1991). The largest concentrations occur in the central area of the England/Wales border with values greater than 5 ppb. Most of central and southern England have concentrations greater than 4 ppb, and lower concentrations ($<$ 2 ppb) occur generally in northern England and Scotland, although southwest England and the western edge of Wales experience low values as well. Horizontal gradients are generally small, except for the area of highest concentrations, where fairly large gradients occur around this region.

The resultant map of the annual dry deposition flux to Great Britain is shown in Figure 2.2. The annual flux of NH_3 to Great Britain is 94.5 Gg year^{-1} of nitrogen in the form of ammonia (NH_3-N). The accuracy of this plot is dependent of the

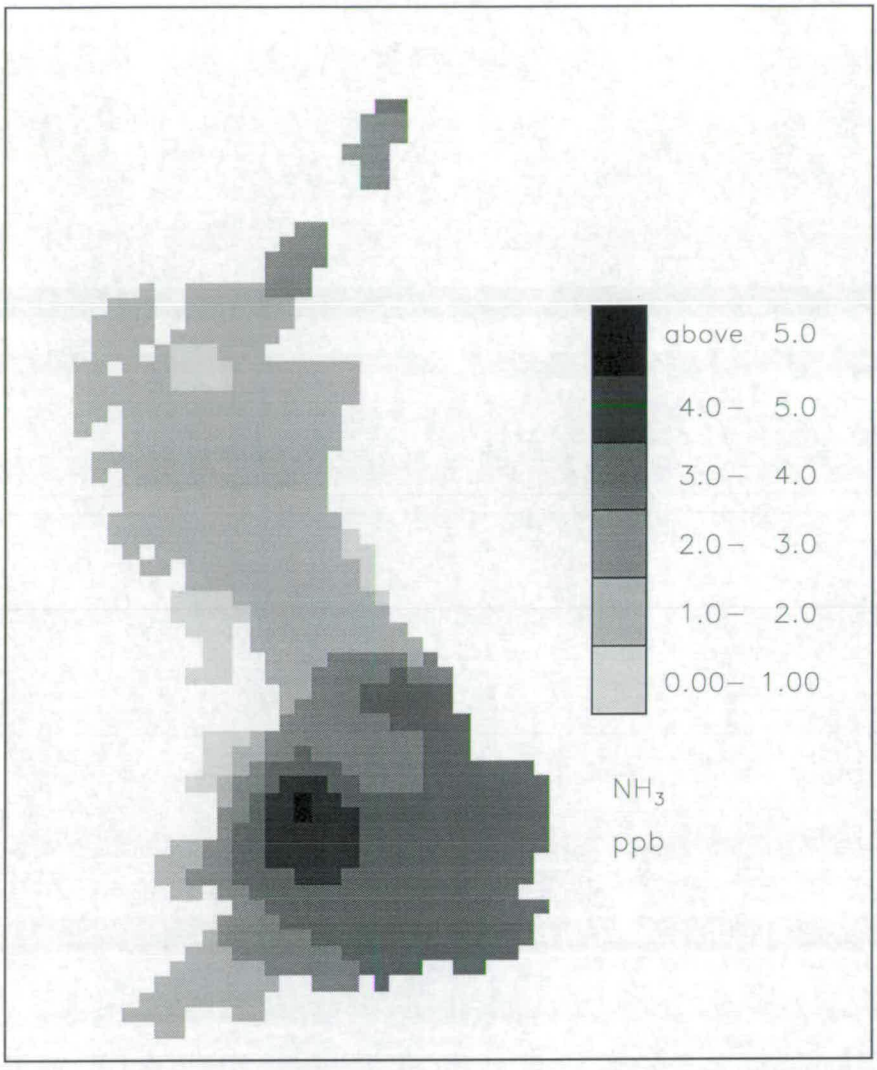

Figure 2.1: Measured ammonia concentration field for Great Britain (Mean values for 1987 to 1990) from a network of diffusion tubes (Atkins and Lee, 1992). Data are in ppb.

data supplied to the model. In this case the main input data are the NH_3 surface concentration data, and the data used to calculate the rate of dry deposition. It is also dependent on the assumptions used in the model, such as χ_s=0 for forest and moorland.

A problem with the diffusion tube was reported by Anderson (1991), who noted that the samplers appeared to give a value which is greater that the actual air concentrations present, and a scaling factor of 0.45 should be applied to all NH_3 diffusion tube data. This factor, though very uncertain, has been supported by further studies in the UK (Sutton *et al.*, 1995c).

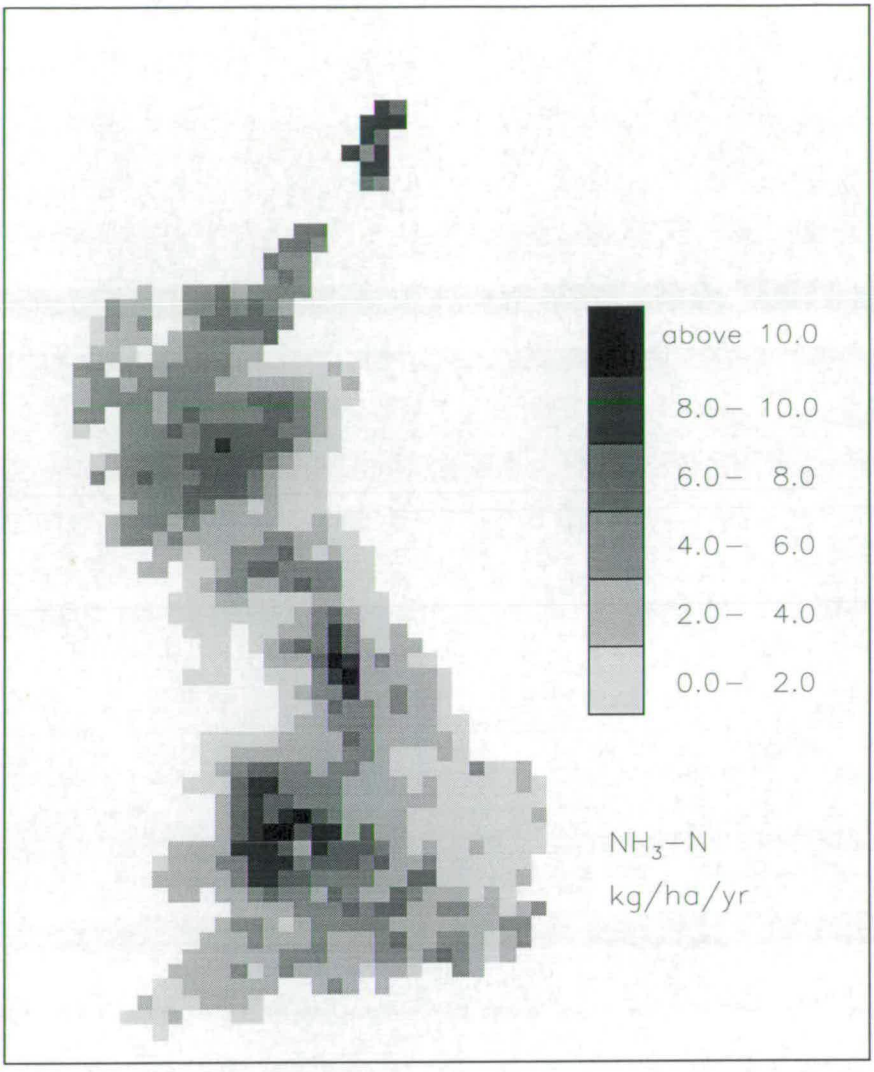

Figure 2.2: Average dry deposition of ammonia (1987-1990) (kg NH_3-N ha^{-1} $year^{-1}$) in the UK. INDITE (1994), RGAR (1996).

The total number of locations used for the network in the first year was 40. This results in an average station density of about 1 station per 6000 km^2 (assuming an approximate estimate of total GB land cover of 240000 km^2). Because of the large horizontal gradients that can occur, especially near emission areas, 40 stations is obviously too small a number to fully map the spatial distribution of NH_3 surface concentrations. This means that whilst concentrations close to the stations may be accurate (accepting the uncertainties on absolute values), interpolation of data between station locations may artificially smooth out the concentration gradients. This has the greatest implications for areas close to large emission sources, where the greatest dry deposition is liable to occur. Thus

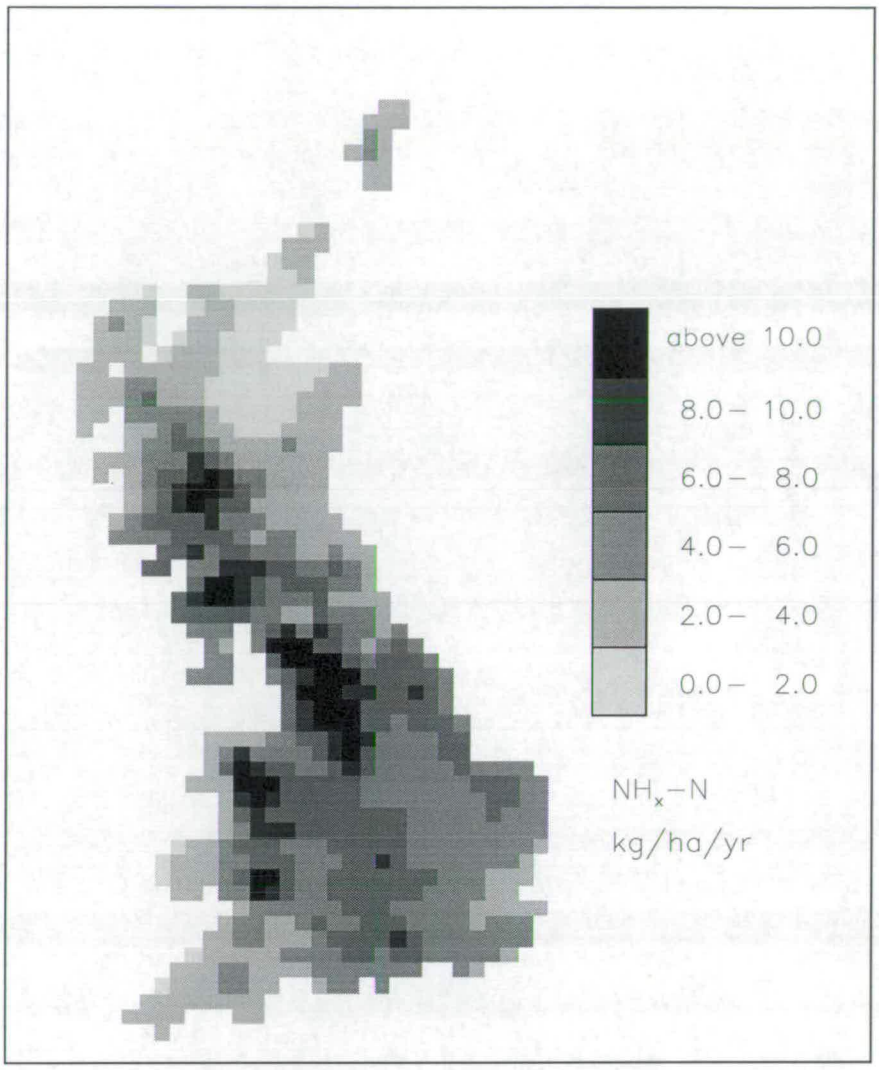

Figure 2.3: Wet deposition of ammonium (kg N ha^{-1} $year^{-1}$) in Great Britain (1992). Derived from measured data combined with an altitude enhancement factor to account for the seeder-feeder effect. INDITE (1994), RGAR (1996).

unless the stations are located both in areas of high and low emissions, and are of sufficient density, the concentration map will not be accurate in many areas, and this will lead to errors in the resultant dry deposition maps.

2.2.2 Calculation of the wet deposition of ammonium over Great Britain

As discussed in section 1.5.3, in the UK a network of measurement sites (UK Secondary Acid Deposition Network) is operated by the UK Department of the Environment. The network consists of a number of measurement sites situated

across Great Britain and Northern Ireland. The network collects data on the concentration in precipitation of a number of ions, including sulphate, nitrate, ammonium, sodium, magnesium, calcium, chloride and potassium. The wet deposition flux of a species is calculated using the concentration in precipitation data from this network, together with precipitation data from the UK Meteorological Office. Data for locations between the sites are calculated by interpolation. To account for the increased concentration of ions in rainfall at higher altitude sites (Fowler *et al.*, 1988; Dore *et al.*, 1990), a correction factor was applied to the relevant data (Dore *et al.*, 1992). This increase in ion concentration has been attributed to a mechanism known as the seeder-feeder effect (Carruthers *et al.*, 1983). This occurs when polluted air is lifted by orography, and a (feeder) cloud forms. The aerosol particles in the air mass act as condensation nuclei in the cloud, and are removed from the atmosphere by rain falling from a higher altitude cloud known as a seeder cloud. The aerosols in the water droplets in the cloud are more efficiently removed by precipitation than aerosol particles outside the cloud, and thus rainfall passing through the feeder cloud will contain a higher concentration of pollutants.

An analysis of rainfall data was performed to calculate the amount of rainfall due to non altitudinal factors. Any measured rainfall in excess of this value was assumed to have occurred due to the scavenging of precipitation from the feeder clouds formed on the hill caps. Ion concentrations in precipitation from these feeder clouds were assumed to be twice that of precipitation collected at nearby low-level sites.

This method of interpolation between measurement sites, and correcting for seeder-feeder enhancement has been used to create maps of annual wet deposition for a number of species. Figure 2.3 is such a map for ammonium wet deposition for 1992. The maximum deposition occurs in areas such as the Pennines in northern England, central Wales and western Scotland. All these areas contains mountainous and hilly regions, and experience large annual rainfall. The total wet deposition of reduced nitrogen for Great Britain calculated by this method amounts to a total of 131 Gg year^{-1} of nitrogen in the form of ammonium (NH_4^+-N) (INDITE, 1994; RGAR, 1996).

2.3 Modelling the spatial distribution of ammonia emissions

Annual totals of NH_3 emissions have been produced for a number of countries(the Netherlands (Bujisman *et al.,* 1984; Erisman, 1989), UK (ApSimon *et al.,* 1987; Kruse *et al.,* 1989; Eager, 1992; Sutton *et al.,* 1995a; Dragosits *et al.,* 1996), Denmark (Asman, 1990), Hungary (Fekete, 1992), continental areas (Europe, Asman, 1992; Asia, Wang and Zhao, 1993) and globally (Warneck, 1988; Schlesinger and Hartley, 1992; Dentener, 1994). Annual fluxes are calculated by first combining an emission flux for a particular emission source, with a quantitative estimate of the number of emission sources in the required region to calculate an annual flux. Emissions totals from each source category are then combined to give an estimate of total emission flux from the specified area. Sources of atmospheric ammonia are predominantly agricultural, and ECETOC (1994) estimated that agriculture accounted for 92% of the total emissions in western Europe. Emission data are an essential part of the input for ATMs. Such models require data on the spatial distribution of the emission fluxes. An emission total for a country is not sufficient for this purpose since the ATM grids generally are much smaller than states. Hence the emissions data must be spatially disaggregated. This process is a complicated procedure, and models have been created specifically for this task.

The spatial scale of the emission model may be determined by the purpose of its use, as well as a number of technical factors such as the availability of landuse data and the size of the entire region being considered. If these data are to be used in an ATM, then computational considerations may also restrict the spatial resolution of the emission map.

Annual ammonia emission maps for Europe have been complied by EMEP (Co-operative Programme for Monitoring and Evaluation of the Long-Range Transmission of Air Pollution In Europe) (e.g. Eliassen and Saltbones, 1983; Barrett and Seland, 1995). Countries participating in EMEP are required to submit emissions data for a number of species, including NH_3, in the form of annual emission fluxes using a 50 km square grid (Barrett and Seland, 1995). These data are used to create emissions maps with an average grid square size of 150 km (at 60°N)

for use in the EMEP long-range transport model (Barrett and Seland, 1995). The resulting EMEP emission grid for Europe consists of 39 × 37 grid squares of varying area, dependent on the latitude. A similar map for Europe, but on a 75 km grid, has been complied by Asman (1992), although this is an interpolation of the basic emissions data on the 150 km grid.

Fine spatial resolution emissions maps (grid size of 20 km or less), have been compiled for : the Netherlands (Bujisman *et al.,* 1984; Erisman, 1989), UK (ApSimon *et al.,* 1987; Kruse *et al.,* 1989; Eager, 1992; Sutton *et al.,*, 1995a; Dragosits *et al.,* 1996), Denmark (Asman, 1990), Hungary (Fekete and Gyenes, 1993).

2.3.1 An example of the methods used to create a fine resolution map of ammonia emissions

To illustrate the procedures involved in the creation of a fine resolution map of NH_3 emissions, the methods employed by Eager (1992), Sutton *et al.,* (1995a), and more recently by Dragosits *et al.* (1996), to create emissions data for Great Britain on a 5 km × 5 km grid are discussed.

The main tool used by these authors is the Geographical Information System (GIS) ARC/INFO. Emission factors were estimated for each major livestock class, and Table 2.1 lists several authors' estimates for different types of animal.

Another large source is the volatilisation of NH_3 from application of nitrogen-based fertilisers. The emission flux is estimated from the percentage of overall nitrogen content of the fertiliser which is lost to the atmosphere. Percentage losses vary for different types of fertiliser, but values have been calculated for average losses, taking into account the type of fertiliser and the relative use of it compared to total fertiliser application. Table 2.2 lists some recent estimates for average fertiliser loss for various regions.

Coupled to estimates of emission factors per source class, data are also needed about the spatial distribution and density of different emission sources. In the UK example discussed here, this information was derived from the June Agricultural Parish Census of MAFF (UK Ministry of Agriculture, Food and Fisheries) for 1988. The relevant information extracted from the census was (Eager, 1992):

Author	Region of application	Cattle	Pigs	Sheep	Poultry
Bujisman *et al.* (1987)	Europe	15.1	2.3	2.6	0.21
Bujisman *et al.* (1987)	UK	11.3	1.5	1.9	0.24
Kruse *et al.* (1989)	GB	19.3	2.9	2.7	0.23
Jarvis and Pain (1990)	UK	8.7	5.7	0.36	0.12
Asman (1992)	Europe	19.0	4.4	1.4	0.20
ECETOC (1994)	UK	20.2	2.3	1.2	0.22
Sutton *et al.* (1995a)	UK	17.0	4.3	0.8	0.22
Dragosits *et al.* (1996)	UK	11.2	3.2	0.4	0.2

Table 2.1: Comparison of average component NH_3 emission factor estimates for cattle, pigs, sheep and poultry. (kg N animal^{-1} year^{-1}). Updated from Sutton *et al.* (1995a).

1 Livestock populations for all of the livestock types enumerated by the census at a parish level.

2 Number of hectares of each arable and vegetable crop under cultivation at a parish level.

3 Number of hectares of grassland intended for mowing or cutting for silage/fodder at a parish level.

To maintain the confidentiality of the farmers, before 1988, the census data were aggregated up to the scale of civic parishes and redistributed before becoming publicly available. After 1988, the data were aggregated up to even larger areas, this time to the size of three or four English civil parishes. Hotson (1988) examined many of the problems encountered when trying to extract data from parish-size regions. Some farmers may be registered in one parish, but have some of their holdings in another, and this will lead to an artificially induced bias in the data towards the first parish. To distribute the parish data onto a regular

Author	Country of application	% loss of applied nitrogen			
		Urea	Ammonium nitrate	Other	Average fertiliser loss
Bujisman *et al.* (1987)	UK	10	10	1	5.8
Kruse *et al.* (1989)	GB	-	-	-	1
Jarvis and Pain (1990)	UK	15.5	0	0	0.6
Whitehead and Raistrick (1990)	UK	16.5	2.5	1.5 - 4.9	3.4
Asman (1992)	Europe	15	2	4	3.8
Eggleston (1992b)	UK	10	10	1	-
ECETOC (1994)	UK	15	3	8	4.4
Sutton *et al.* (1995a)	UK	10	1	2.5	2.4

Table 2.2: Comparison of average NH_3 emission factors from application of nitrogen fertilisers. Updated from Sutton *et al* (1995a).

grid, a 1 km landuse data-set was used by Hotson (1988). Each 1 km grid square was assigned one of three land classifications:

1 Land suitable for agriculture.

2 Land suitable for certain agricultural activities associated with rough 'pasture'.

3 Land quite unsuitable for the location of any agricultural activity e.g. urban, woodland and inland water areas.

The items of the census can then be treated one by one either for general distribution to both 'agricultural' squares and 'moorland' squares, or only to agricultural squares. Some items such as sheep, are suitable to be distributed over both 'agricultural' and 'moorland' squares. Census data were then distributed across the relevant 1 km squares contained in the parish area, with the total number for each item being divided evenly among the relevant 1 km squares.

Data were then aggregated onto a 5 km $\times$ 5 km grid format by the Data Library, University of Edinburgh (Hotson, 1988). The data for each grid square were then multiplied by the relevant emission factors to calculate the annual emission flux.

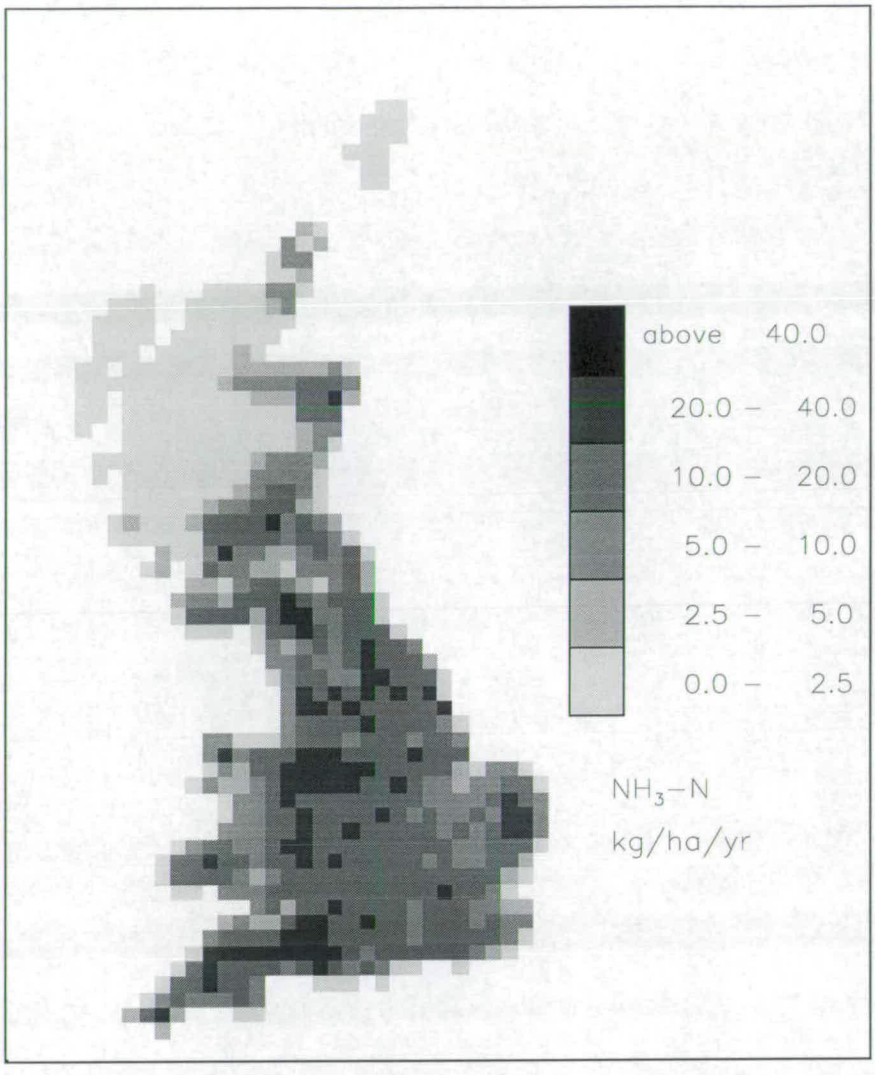

Figure 2.4: 20 km × 20 km NH_3-N emissions map for Great Britain for 1988 (kg ha^{-1} $year^{-1}$) (Dragosits *et al.*, 1996).

As with any model, the quality of the results depends on the supplied input data, in this case the spatial census data and the estimated emission factors. The data in Table 2.1 show the wide range of values that have been calculated for different livestock. Any errors in the data will not only affect the total emission for the country as a whole but also the spatial distribution. If an erroneous emission map is used as input for an ATM, the results of the model would be flawed even before the model was run.

Figure 2.4 is a map of total NH_3 emissions from agricultural and non-agricultural sources for 1988, as calculated by Dragosits *et al.*, (1996) for Great Britain on a 20 km × 20 km grid. The emission factors used are the official DoE values

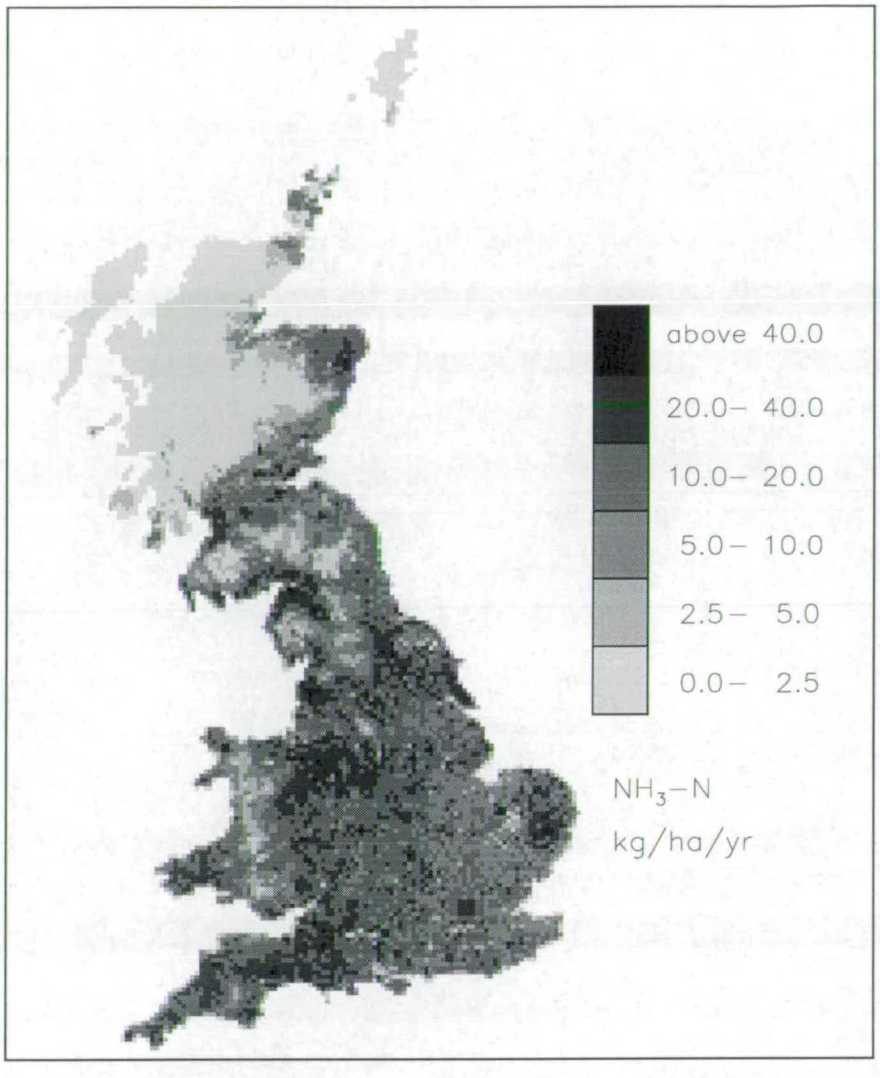

Figure 2.5: 5 km × 5 km NH_3-N emissions map for Great Britain for 1988 (kg ha^{-1} $year^{-1}$) (Dragosits *et al.*, 1996).

(Dragosits *et al.*, 1996) from Table 2.1. A large proportion of the emissions (Figure 2.4) are located in a broad band in the borders of England and Wales. This is consistent with mainly livestock, cattle and sheep farming in these areas, as well as more local high emissions areas in the northwest of England (west Lancashire, North Cumbria). A further high emission area in eastern England (East Anglia) is associated with large poultry and pig farming.

Figure 2.5 shows the same emissions data, but on a much finer spatial scale of 5 km × 5 km grid squares. With this plot, the large spatial variability of NH_3 is much more apparent, and more clearly shows the large horizontal gradients that occur within 20 km in areas such as East Anglia and north Wales.

2.4 Atmospheric transport models

This section examines the existing application of atmospheric transport models to the treatment of ammonia. Whilst there are many models available, the area of interest is deposition of ammonia over Great Britain, and thus example models which include treatment of Great Britain are examined, although reference is also made to other models.

Atmospheric transport models consider the emission, transport and deposition of material. These models usually require information on the spatial distribution of emission. This is usually is the form of an emission database, as described in the previous section. These models are mass conservstive, and thus can be used to calculate deposition budgets and import/export budgets for the region being modelled. The spatial scale of models can range from considering the entire globe, for example, with a resolution of a 10° × 10° grid (Dentener *et al.,* 1994), continental sizes such as Europe (Barrett and Seland, 1995), to the size of a small country such as Denmark, with 5 km × 5 km grid squares (Asman and van Jaarsveld, 1992) or even at much smaller and local scales such as the SLAM model (Boermans and van Pul, 1992) which has a horizontal resolution of 200 m grid squares. The model may be applied to describe specific episodes during a certain period of time, (Barrett and Seland, 1995; ApSimon *et al.,* 1994; Hertel *et al.,* 1995), or a statistical approach may be employed (Asman and van Jaarsveld, 1992; Metcalfe *et al.,* 1989, 1995; Fisher 1984, 1987) where the objective is only to model the the average behaviour over a long period of time.

Description of atmospheric transport and removal of material necessitates the parameterisation of the processes. The degree of parameterisation may range from a given empirical value to a function dependent on spatial and meteorological factors.

Two example models are reviewed in this section to highlight the approaches used to date. They have both been used to model the atmospheric behaviour of ammonia over Great Britain. Each are Lagrangian models, which means that the transport of material is performed by following an air parcel of defined size along a trajectory. In mathematical terms, a coordinate system is adopted which moves in space such that the flow is the same everywhere.

2.4.1 The EMEP atmospheric transport model

The EMEP atmospheric transport model is used as part of the Co-operative Programme for Monitoring and Evaluation of the long-range Transport of Air Pollutants in Europe (Barrett and Seland, 1995). The model describes the emission, transport and deposition of atmospheric pollutants across Europe The model can be described as being deterministic as data are calculated for specific periods in time, with a time resolution of 6 hours, and can use these data to calculate average annual values. The summarised description of the model given here is from the 1995 EMEP report (Barrett and Seland, 1995).

The horizontal resolution of the model is 150 km at 60° north, and the entire model domain is shown in Figure 2.6. A column of air is transported across the domain along predetermined trajectories. Each trajectory is calculated from the wind field at an altitude which can represent transport within the boundary layer, and is set to arrive at the receptor point every six hours. The calculated trajectories are 96 hours in length. The depth of the air column is determined from measured vertical soundings made at a number of stations across the domain. Measured precipitation data, supplied every 12 hours from 600-700 stations, are also used. Other meteorological data are supplied from the Numerical Weather Prediction model (NWP), which is run at the Norwegian Meteorological Institute (DNMI). These data includes the horizontal advection speed of the air column, which represents the mean flow of air at a pressure height of 0.925, corresponding to a vertical height of around 550 m.

The arrival points for these trajectories are the centre of each grid square, and monitoring sites, maintained by EMEP, are also used as arrival points for the model to assess the accuracy of the model results.

Emissions data of SO_2, NH_3 and NO_x ($NO + NO_2$) are used as input for the model. Ten chemical species are considered. These are nitric oxide (NO), nitrogen dioxide NO_2, nitric acid (HNO_3), peroxyacetyl nitrate (PAN), particulate nitrate (NO_3^-), sulphur dioxide (SO_2), particulate sulphate (SO_4^{2-}), ammonia (NH_3), ammonium nitrate (NH_4NO_3) and ammonium sulphate ($(NH_4)_2SO_4$). A detailed chemistry scheme is employed, as shown in Figure 3.4.

Emissions are assumed to be instantaneously mixed throughout this air col-

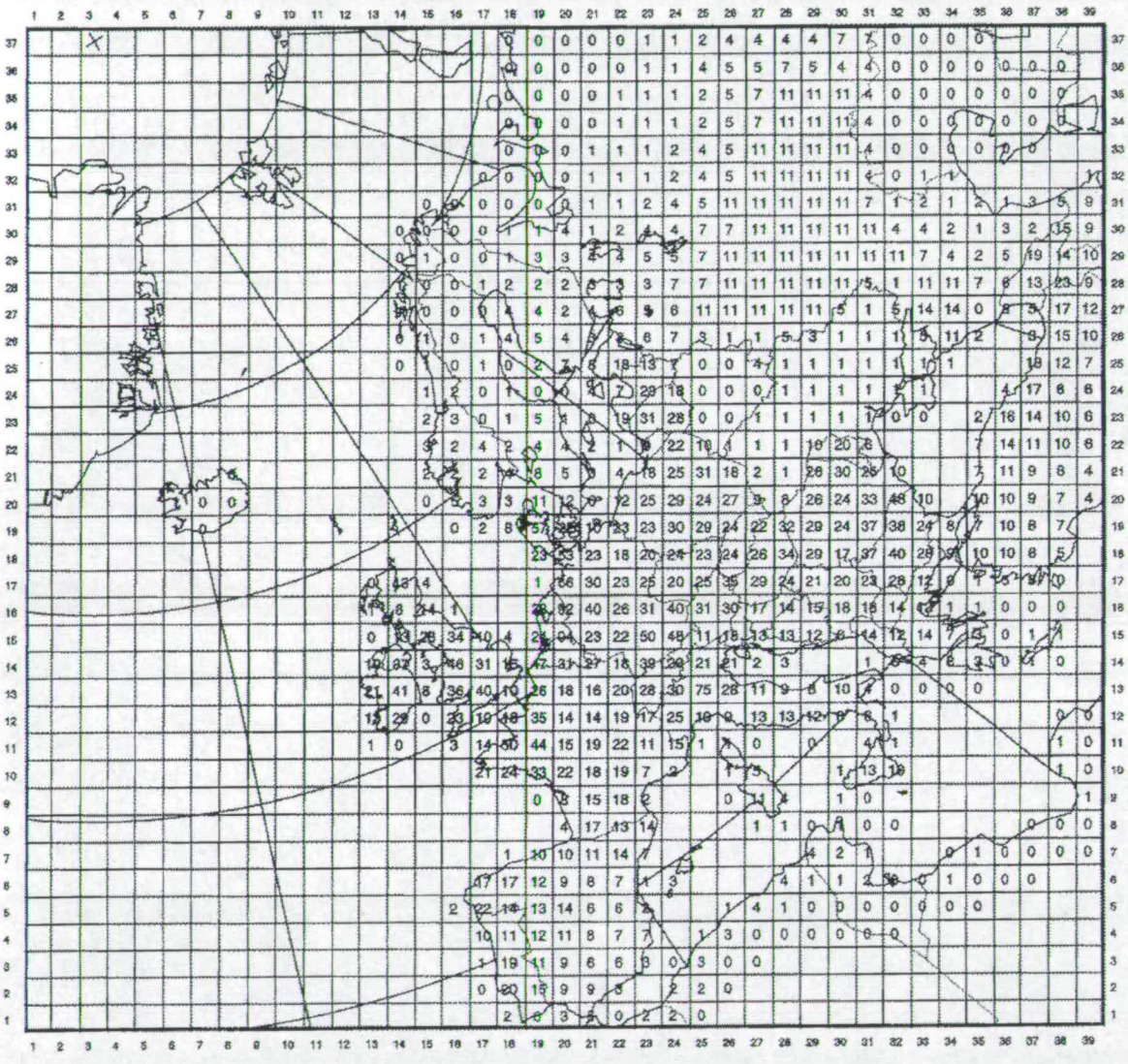

Figure 2.6: Estimated emissions of ammonia for 1993 (units of 1000 tonnes of NH_3). Used as input for the EMEP model (Barrett and Seland, 1995.)

Specie	Value of V_d(1m) over sea	Value of V_d(1m) over land	Value of V_d(50m)
NH_3	not pre-defined	not pre-defined	$(r_a + r_b + r_c)^{-1}$
NH_4^+ aerosols	1 mm s^{-1}	1 mm s^{-1}	1 mm s^{-1}

Table 2.3: Dry deposition velocities for the ammonia and ammonium aerosols in the EMEP model. From Barrett and Seland (1995).

umn, resulting in a uniform vertical concentration profile. This assumption of complete vertical mixing leads to the under-estimation of surface concentrations, and thus may (uncorrected) lead to the under-estimation of the dry deposition flux. A correction is made to this process in the model by assuming that an additional fraction of the emissions are dry deposited directly within the emitting grid square. The amount of material which is 'locally' dry deposited is dependent on the chemical species and meteorology. For NH_3, the correction factor for dry deposition (ω_d) is 0.19. There is also a correction factor for NH_3 local wet deposition (ω_w) which has a maximum value of 0.19, and is set to be dependent on the removal by precipitation. Thus the amount of NH_3 actually emitted into the air column is

$$(1 - \omega_d - \omega_w)Q_{NH_3} \tag{2.3}$$

where Q_{NH_3} is the emission of NH_3 per unit area and time. The treatment of SO_2 sub-grid deposition is more detailed, as a distinction is made between high- and low-level emission sources.

The normal treatment of dry deposition in the model involves the application of deposition velocities (V_d) combined with modelled concentrations, in order to calculate the dry deposition flux. Parameterisation of the value of V_d is dependent on the relevant species. Nitrate (NO_3^-) and sulphate (SO_4^{2-}) aerosol particles are assigned invariant values of V_d. The treatment for other chemical species, such as NH_3, is more detailed, involving the use of a resistance formulation (section 3.1), and a distinction is made between deposition to land and sea (Table 2.4.1).

Removal of material by precipitation is performed in the model by the use of scavenging ratios. The model uses a single value for each species to reflect the average effect of different schemes of removal by precipitation, such as in-cloud and below-cloud processes. Because of the coarse spatial resolution of the model

Species	Wet scavenging ratio
NH_3	1.4×10^6
NH_4^+ aerosols	1.0×10^6

Table 2.4: Wet scavenging ratios for ammonia and ammonium aerosols used by the EMEP model. From Barrett and Seland (1995).

(150 km grid squares), a correction is made to the calculations to account for the non uniformity of precipitation over such a large area (see section 3.2).

Results of the EMEP model

The mean annual concentration field of NH_3 produced by the EMEP model is shown in Figure 2.7. Over Great Britain, the maximum concentrations occur in a broad band across most of Wales and Western England, with values exceeding 1 μg m^{-3} in this area. This can be related to the emissions map in Figure 2.5, which shows the same area containing most of the large emission sources of NH_3. The large spatial variability of the emissions is not reflected in Figure 2.7. This is due to the large horizontal resolution of the EMEP model (150 km grid squares in comparison to the 5 km grid squares in Figure 2.5). In coastal regions there is a quite sharp decline in concentrations, as seas areas are assumed to have no emissions and act as an efficient sink of NH_3.

Figure 2.8 is a plot if the mean annual concentration field of NH_4^+ produced by the EMEP model. Ammonium aerosols are a secondary product of the reaction between ammonia and acidic species such as the oxidation products of SO_2 and NO_x. Average conversion rates from NH_3 to NH_4^+ have been estimated to be around 30% $hour^{-1}$ (Asman, 1994). Thus the concentration of NH_4^+ aerosols generally have smoother horizontal gradients over Great Britain than the field of NH_3 concentrations (Figure 2.7). This is apparent in Figure 2.8. The maximum concentrations over Great Britain are in an area containing central and southern England which also extends over much of central Europe. In comparison to Figure 2.7, concentrations of NH_4^+ over the sea areas surrounding Great Britain are much larger, and most of the reduced nitrogen in the atmosphere over the North Sea is in the form of NH_4^+ aerosol. In the EMEP model, much of the long-range

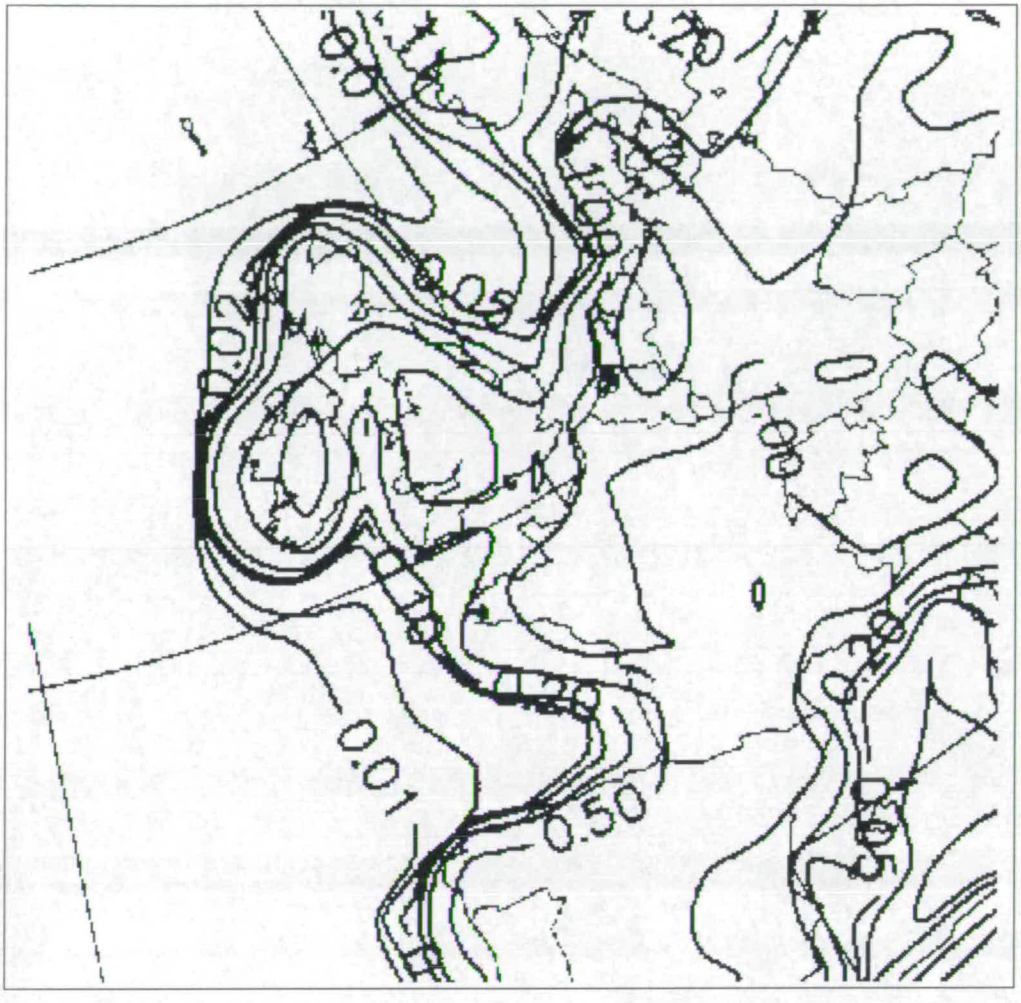

Figure 2.7: Mean concentration field of NH_3-N in $\mu g\ m^{-3}$. Isolines are 0.01, 0.02, 0.05, 0.1, 0.2, 0.5, 1.0 and 2.0. Calculated by the EMEP long-range transport model. From Barrett and Seland (1995). (Multiply by 1.72 to convert to ppb.)

transport of reduced nitrogen is in the form of NH_4^+ as opposed to NH_3.

The annual deposition of reduced nitrogen to Great Britain and the surrounding area is given in Figure 2.9. As with the plots of NH_3 concentration (Figure 2.7), the major area of deposition over Great Britain occurs over much of Wales and western England, with annual fluxes greater 10 kg ha^{-1} $year^{-1}$ of NH_x-N. It should be noted that this plot is a combination of both wet and dry deposition fluxes. Since the modelled dry deposition flux is dependent on the air concentration, it is not surprising that large deposition occurs in areas which experience the highest atmospheric concentrations of NH_3 (Figure 2.7). Dry deposition to this

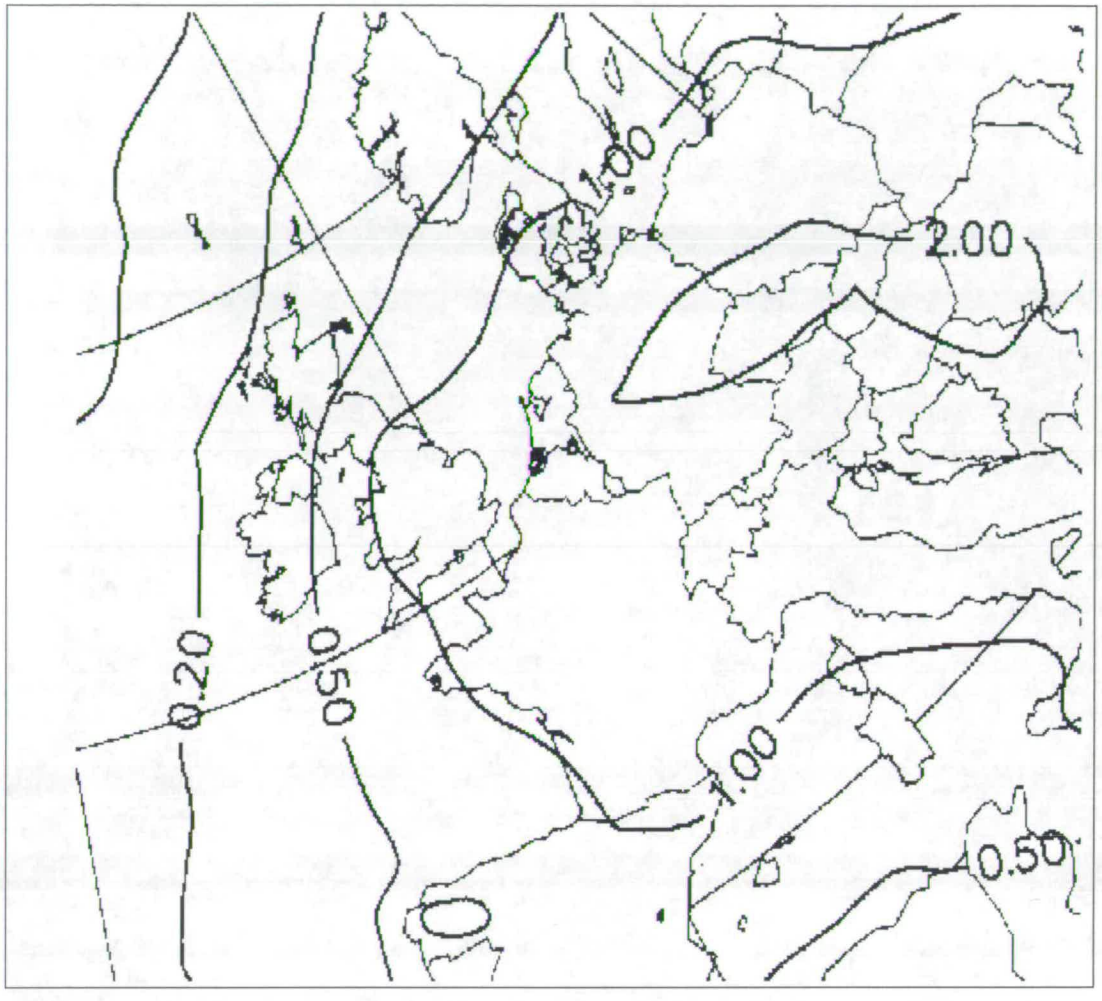

Figure 2.8: Mean concentration field of NH_4^+-N in μg m^{-3}. Calculated by the EMEP long-range transport model. From Barrett and Seland (1995).

area will also be enhanced by the local deposition factor employed by the model, since this area is also a large emission region. Dry deposition of NH_4^+ aerosol will not generally be an important contributor to the total deposition flux as the parameterised deposition velocity of NH_4^+ aerosol is smaller by an order of magnitude than that of NH_3. Dry deposition of NH_4^+ may only be an important fraction in areas where the concentration of NH_4^+ is much greater than NH_3, such as the coastal regions and northern Scotland.

The average annual budgets of reduced nitrogen for Great Britain, calculated by the EMEP model (Barrett and Seland, 1995), for the period 1985-1994, are given in Table 2.5. Over half of the reduced nitrogen emitted from Great Britain

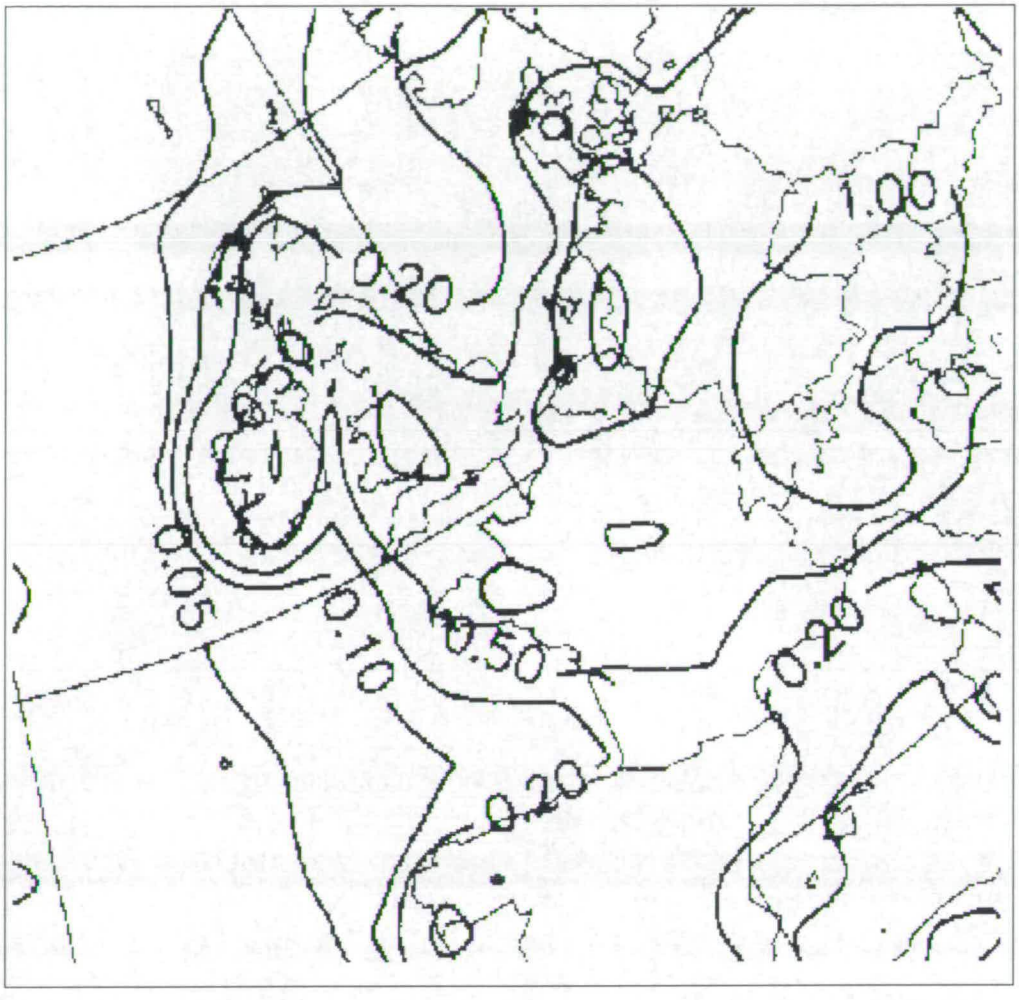

Figure 2.9: Annual deposition of reduced nitrogen in g(N) m^{-2}. Multiply by 10 to convert to kg ha^{-1} $year^{-1}$. Calculated by the EMEP long-range transport model. From Barrett and Seland (1995).

is redeposited. In fact, 84% (165.3/195.0) of the total deposition originates from British emissions. Thus it seems from the EMEP model results that the major proportion of NH_3 deposition to Great Britain are due to British emissions, as opposed to mainland Europe. However the fact that Britain is an island plays an important role in this, as the sea is a very good modelled sink of NH_3. Although British deposition may be a national concern, nearly half of the British emissions are exported. Examination of Figures 2.7 and 2.8 indicates that much of this export is in the form of NH_4^+ aerosol. These species have a longer atmospheric lifetime than NH_3 and can be transported over large distances and deposited in

Results form the EMEP model	Kilo tonnes year^{-1} of NH_3-N	% of emissions
Average emission of reduced nitrogen	314.5	100
Average import of reduced nitrogen	29.8	9.5
Average export of reduced nitrogen	149.2	47.4
Average total deposition of reduced nitrogen	195.0	62
Average deposition of reduced nitrogen arising from GB emissions	165.3	52.6

Table 2.5: Reduced nitrogen budget for Great Britain as predicted by the EMEP model. Average 1985-1994 (Barrett and Seland, 1995).

other countries, especially coastal regions of north-western Europe. This shows that British emissions of NH_3 are an international issue.

2.4.2 An example of a country-scale model for the UK: HARM

The Hull Acid Rain Model (HARM) is a regional model designed to calculate deposition budgets and air concentrations over the United Kingdom. It has been used to calculate deposition budgets of acidic species (Metcalfe *et al.*, 1989, 1995) and was developed from the Harwell Trajectory Model (HTM) (Derwent *et al.*, 1987, 1988). It was used to examine the source-receptor relationship, especially for sulphur compounds (Metcalfe *et al.*, 1995).

HARM is a Lagrangian statistical model with a horizontal resolution of 20 km grid squares for the UK, although this region is nested within the larger EMEP domain for the rest of Europe which has a coarser resolution of 150 km grid squares.

As with the EMEP model, HARM describes the atmospheric and chemical process in a column of air along a predetermined trajectory. Straight line trajectories are employed which have a length of 96 hours. Trajectories arrive at a receptor point from 24 equally-spaced wind directions, and the results are then weighted to reflect the frequency of the occurrence of wind from each direction.

A simplified treatment of meteorological processes is used, due to the statistical nature of the model. The depth of the air column is kept constant at a value of 800 m, and the advection speed is set at 10.4 m s^{-1}, independent of wind direction.

The model is driven by emission of sulphur dioxide (SO_2), nitrogen oxides (NO_x), ammonia (NH_3) and hydrogen chloride (HCl). Continental European emissions are from the EMEP dataset (Figure 2.6), while the UK emissions are from the UK Department of the Environment Review Group on Acid Rain (RGAR).

Vertical mixing is performed on the assumption of instantaneous mixing of the emissions. This assumption is acceptable for most of the species considered by HARM, especially the sulphur compounds (Metcalfe *et al.*, 1995). As much of the emitted sulphur comes from elevated sources, the plume will generally come into contact with the ground after it has traveled some distance from the source. In the EMEP model, the use of a coarse horizontal resolution (150 km grid squares), means that a correction factor is applied which accounts for this local deposition. Metcalfe *et al.* (1995) argued that for a more detailed resolution of 20 km grid squares, the under-representation of near-source SO_2 dry deposition is much less significant and approaches in magnitude the over-estimation of dry deposition because the plume is assumed always to be in contact with the ground. The good agreement between modelled values and measurements (Metcalfe *et al.*, 1995) shows that this assumption is valid for use with elevated sources and a fine resolution grid.

However, in the case of ammonia emissions, the assumption of instantaneous mixing is not as effective, as it creates the same problem as encountered with the EMEP model. Surface concentrations will be under-estimated and, without the use of appropriate correction factors, will lead to under-estimation of the dry deposition flux. In the present version of HARM, the correction factors used to account for local dry deposition are shown in Table 2.6. The normal treatment of dry deposition applies deposition velocities (Table 2.7) to calculated concentrations.

Annual rainfall data from 1990, on a 20 km $\times$ 20 km resolution, are used to calculate wet deposition of material in the model by using a constant drizzle approach and applying scavenging coefficients. This is discussed in more detail in section 3.2.

To account for the enhancement of wet deposition by orographic effects, the HARM model incorporates an enhanced oxidation of SO_2 to SO_4 and an increased

Emission species	Treatment over continental Europe with 150 km grid squares	Treatment over the UK with 20 km grid squares
SO_x	0.15	0
NH_3	0	0
NO_x	0	0

Table 2.6: Fraction of the emission directly redeposited to the emitting grid square to account for sub-grid dry deposition in HARM. (J. D. Whyatt, Pers Comms).

Species	Description of parameterisation.	Value of V_d (mm s^{-1})
SO_2	Land-dependent	1.95 - 4.7
NO_2	Land-dependent	0.8 - 2.3
Ammonia	Land-dependent	0.1 - 30.8
NO	Invariant	0
Nitric acid	Invariant	40.0
Aerosols	Invariant	1.0
Hydrogen chloride	Invariant	20.0
Ozone	Invariant	6

Table 2.7: Dry deposition velocities used in the version of HARM as reported in RGAR (1996).

rate of removal of aerosols by precipitation. Both these adjustments are step-wise proportional to the rainfall rate, and are set to increase in unit steps for each 250 mm and 500 mm of additional rainfall respectively.

Results from HARM

A map of the annual average concentrations of NH_3 is shown in Figure 2.10. The area of maximum concentration occurs along the Wales/England border, with values exceeding 0.4 ppb of NH_3. This is in broad agreement with the EMEP model results (Figure 2.7), though the results from HARM have an increased spatial resolution and concentrations are about a third the size of the corresponding EMEP values in this region. A large horizontal concentration gradient occurs in northwest Scotland, which is not produced in the EMEP results. This is due to the extremely low emissions density that occurs in the northwest, as opposed to

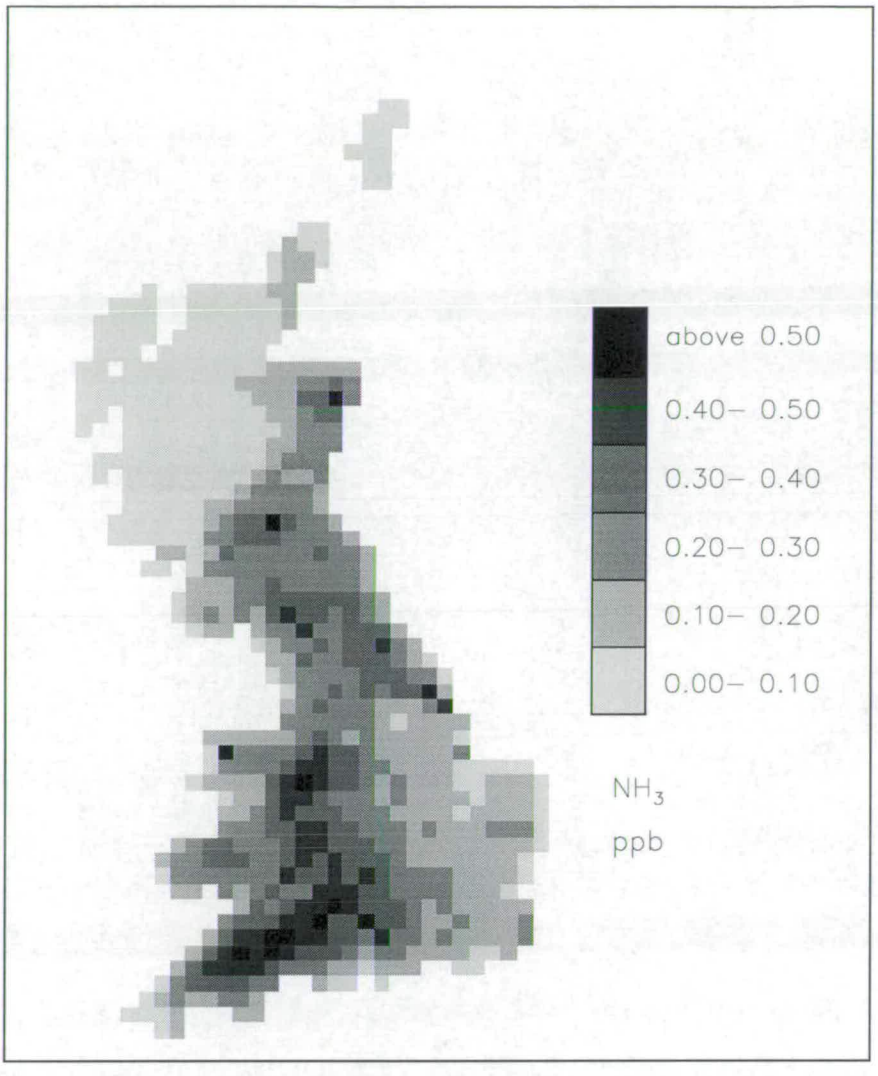

Figure 2.10: Map of ammonia surface concentration on 20 km grid squares as predicted by HARM. RGAR (1996). Units are ppb.

the large emissions in the southern and eastern areas of Scotland (Figure 2.4), which are not clearly resolved in the EMEP emissions. However, over much of England and Wales, the large gradients present in the UK emissions data (Figure 2.4) are somewhat reduced, as a result of instantaneous mixing.

Figure 2.11 is a plot of the concentration data against a set of (corrected) measured values. These data were recorded by a network of passive diffusion samplers during 1987-1988, and have already been discussed in section 2.2.1. These data are slightly different from the data presented in Figure 2.1 since these are the mean values for just one year, whereas the data in Figure 2.1 are the mean of the entire 3 year period. A correction factor of 0.45 (Anderson, 1991)

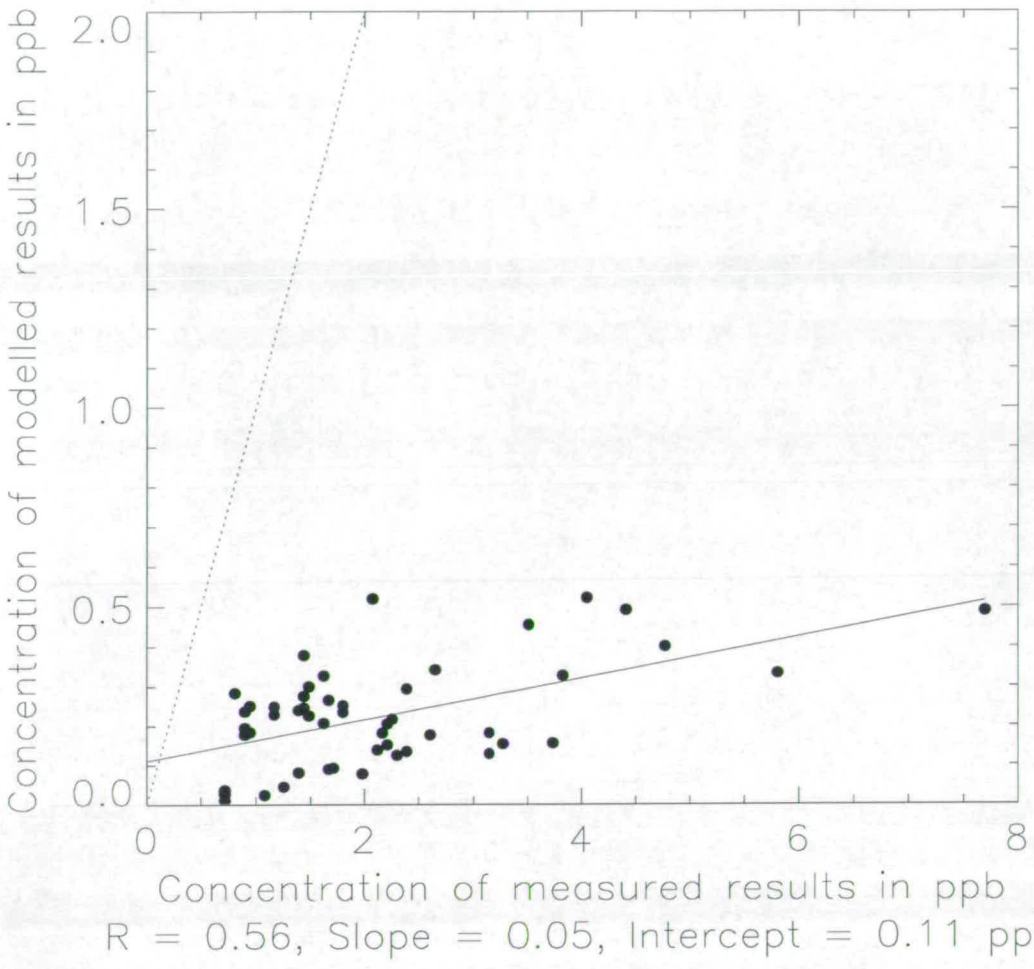

Figure 2.11: Correlation plot of modelled NH_3 concentrations from HARM versus adjusted observations ($\times 0.45$) from a network of passive diffusion tubes. The full line is the regression line and the dotted line is the one-to-one line.

has been applied to the measured data. One should be careful when performing a comparison of modelled and measured data of NH_3, since concentrations have been shown to vary greatly over the short-range of a few hundred metres (see Section 5.1). Thus a comparison with measurements should be treated with some caution and be viewed as giving an indication of the overall effective of the model performance, as opposed to accurately modelling concentrations at specific locations.

The solid line is the best fit line from the regression analysis and the dotted line is the one-to-one line. The value of the correlation coefficient (R) is 0.56. For the sample size of n = 51, this correlation is significant to $P<0.001$, (or $<0.1\%$), where P is the probability of the observed correlation having arisen by chance.

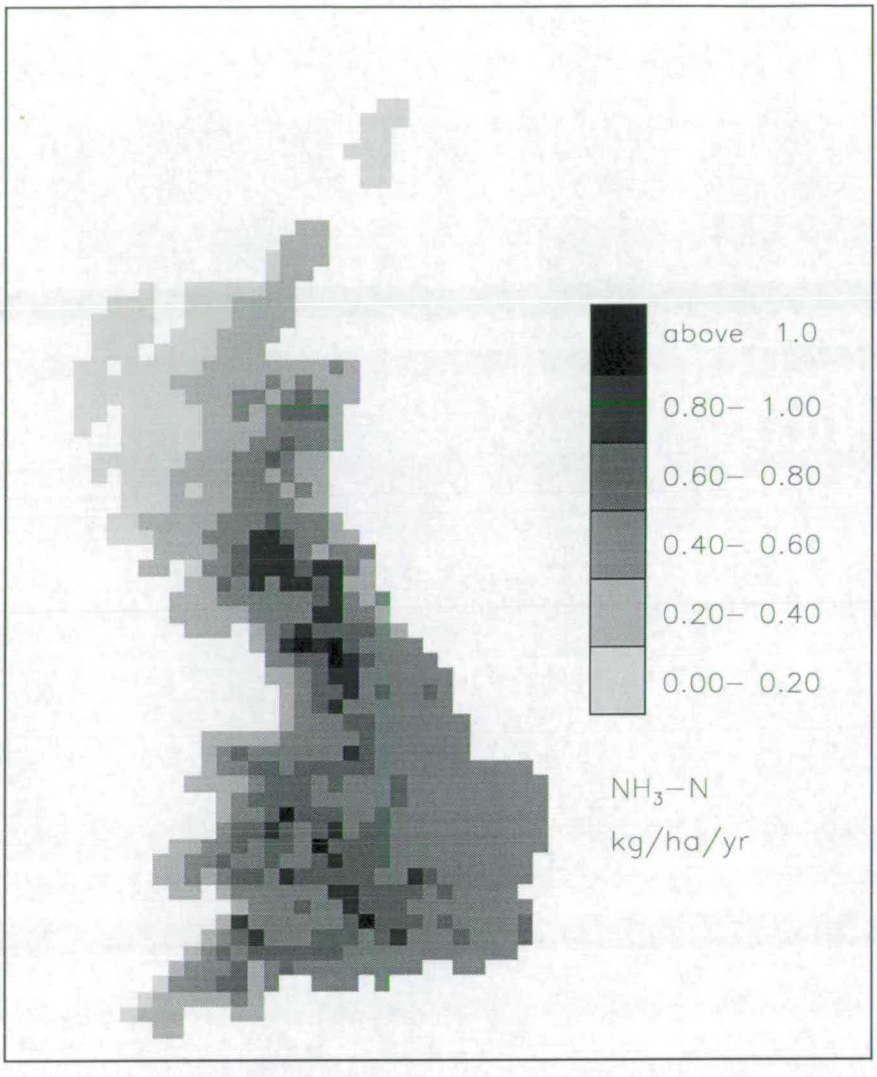

Figure 2.12: 20 km grid square map of dry deposition of ammonia over Great Britain from HARM (kg ha^{-1} $year^{-1}$). RGAR (1996).

The actual value of P is 2.21×10^{-5}. The slope of the regression line is 0.05 and the intercept is 0.11 ppb. This plot typifies the problem of modelling atmospheric NH_3. In general, model concentrations under-estimate the measurements by an order of magnitude, and this is a direct result of the assumption of instantaneous mixing.

The spatial distribution of NH_3 dry deposition is shown in Figure 2.12. The dry deposition field reflects the air concentration field (Figure 2.10) in that the same area around the Wales/England border experiences large dry deposition. This is not surprising since the modelled dry deposition is proportional to the air concentrations. However, the area which experiences the maximum flux of

dry deposition is in northern England, over the Pennines Hills. This is extremely interesting as much of the land in this area is semi-natural and the model uses large average deposition velocities per grid square in this area. Emission densities are low in this area (Figure 2.5), and thus most of the deposition will be due to material being transported from other regions.

Since the modelled mechanism of dry deposition is dependent on air concentrations, it is expected that the under-estimation in the surface concentration will lead to a subsequent under-estimation of dry deposition. The annual dry deposition total for the Great Britain predicted by HARM is 12.0 Gg year^{-1} NH_3-N. This is much less than the value estimated by the ITE inferential model of 94.5 Gg year^{-1} NH_3-N (RGAR, 1996).

Wet deposition is described very well by HARM. Comparison of Figures 2.3 and 2.13 show that the distributions are very similar. The maximum wet deposition occurs over the Pennines in both figures, with large deposition also occurring in Wales and western Scotland. The only major discrepancy between the two datasets is that HARM seems to under-estimate the wet deposition flux somewhat. The wet deposition total from HARM is 99 Gg year^{-1} NH_3-N, which is about 24% less than the calculated ITE value of 131 Gg year^{-1}. The increased spatial resolution of HARM, as compared to EMEP, shows a much more detailed picture of the pattern of deposition, and illustrates the advantages of using a regional model to describe deposition to a particular area.

A comparison of modelled data and measured data is shown in Figure 2.14. These data are taken from the measurement sites discussed in section 2.2.2, and are annual average data for 1994. These data are assumed to an approximation of measurements of NH_x wet deposition for 1992. The best fit line from the regression analysis is the solid line, and the dotted line is the one-to-one line.

The value of the correlation coefficient (R) is 0.78. For the sample size of n = 30, this correlation has a probability (P) of having arisen by chance of 1.7×10^{-8}, which is statistically significant at the P = 0.1% level. The slope of the regression line is 0.55 and the intercept is 2.23 ppb.

Analysing the HARM results overall, it is apparent that the parameterisation in HARM of atmospheric processes that occur throughout much of the mixing layer is quite good. Modelled fields of wet deposition agree well with measurements,

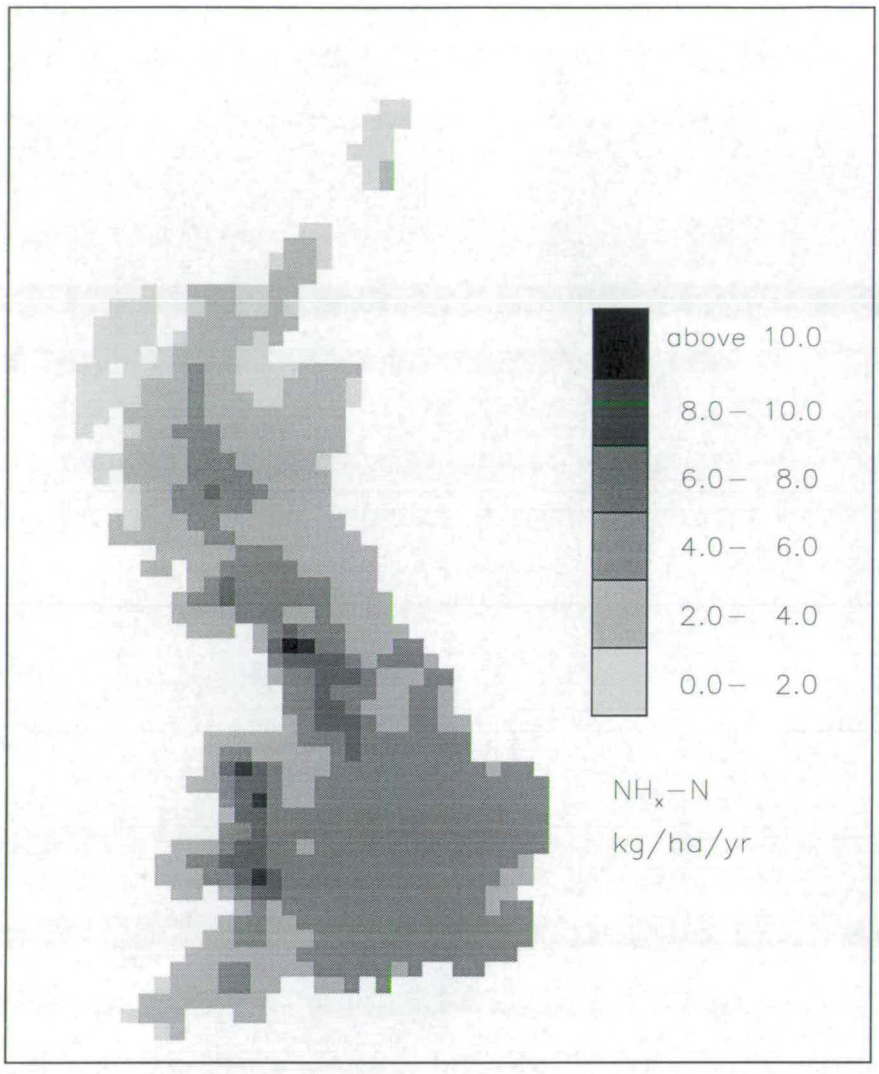

Figure 2.13: Wet deposition of reduced nitrogen over Great Britain from HARM (kg ha^{-1} $year^{-1}$). RGAR (1996).

since the process of removal by precipitation takes place both in-cloud and below the cloudbase (see sections 1.5.3 and 3.2). Thus the assumption of instantaneous mixing works well in this case and is also valid for modelling emissions from elevated sources. However it falls down when dealing with exclusively ground-based sources, and leads to under-estimation of both surface concentrations and dry deposition.

The increased spatial resolution of the model allows for greater knowledge of the distribution of the deposition and concentration fields. Even though the model under-estimates the NH_3 concentrations, it still gives a better description of the expected large spatial variability.

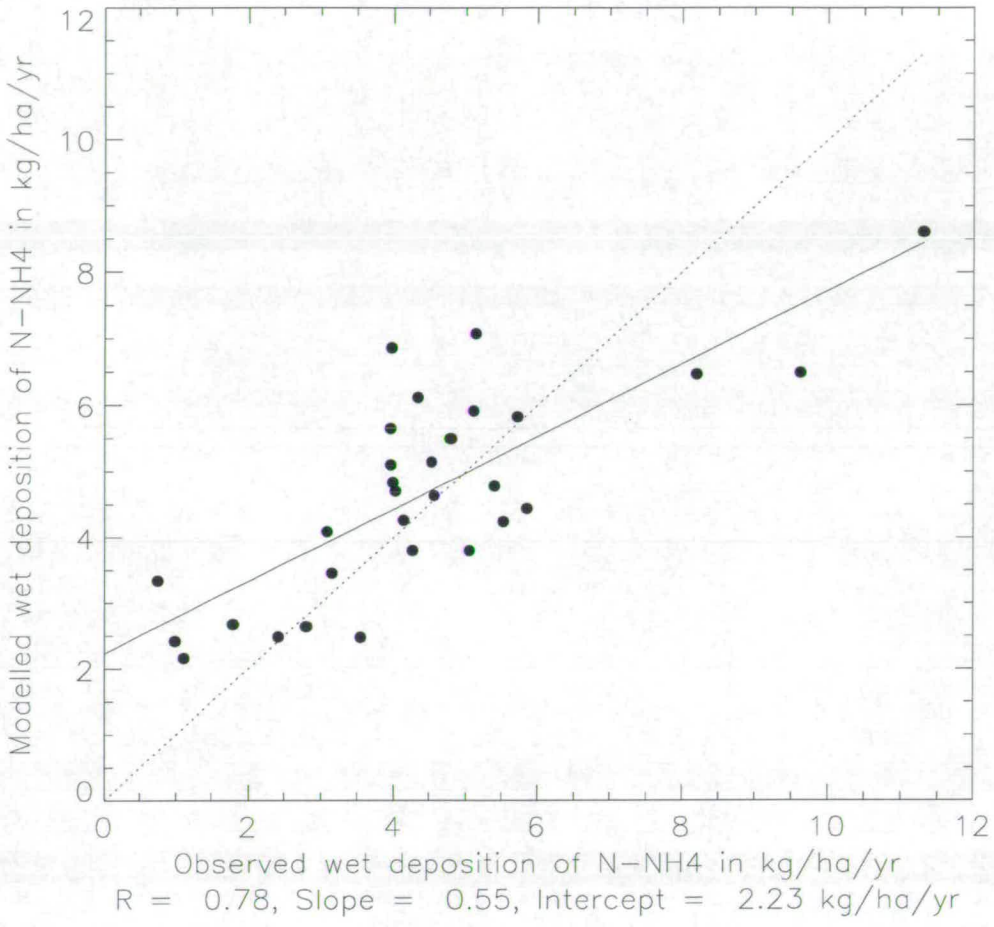

Figure 2.14: Correlation plot of modelled $NH_x - N$ wet deposition from HARM versus observations from a network of measurement sites. RGAR (1996). The full line is the regression line and the dotted line is the one-to-one line.

2.5 Discussion

A number of models have been reviewed in this chapter. The complexity of these models range from the simple interpolation of measured data, together with a scaling effect to account for the effect of altitude-enhanced concentrations of aerosols in precipitation, to detailed atmospheric transport models which perform millions of calculations per minute.

The creation of an emissions database relies heavily on recorded census information on animal numbers and locations. These data are combined with calculated emission fluxes for various types of animal in order to estimate annual emission fluxes for Great Britain. A difficulty arises in describing the spatial distribution

of the emissions, since the official census data are aggregated up to larger spatial regions in order to preserve confidentiality. In order to redistribute these data to smaller spatial scales, assumptions are made on what type of agricultural activity occurs on different land-types. The accuracy of these emissions data relies heavily on the census data, and thus the accuracy of the original information supplied to the the census bureau. It is extremely important, with respect to ATMs, that these data be as accurate as possible, since they form a major part of the model input data. Emissions data have been produced on a 5 km × 5 km grid for Great Britain (Eager, 1992; Sutton *et al.,* 1995a; Dragosits *et al.,* 1996). This is considered to be the most accurate resolution possible (for Great Britain) with the current data limitations, due to the uncertainties of disaggregation of agricultural data onto a finer scale.

The accuracy of these deposition models reviewed in this chapter depend on the input data, and the degree and number of assumptions used in order to make the model simpler to solve, but still accurate.

In the case of wet deposition of ammonium aerosols, the input data are measurements of concentration in precipitation, which were recorded at sites belonging to the UK Secondary Acid Deposition Network. For dry deposition of NH_3, the main input data were surface concentrations which were recorded at 40 sites, using diffusion tubes. In both of the above cases, observed data are interpolated between measurements sites to provide a spatial description of data on 20 km × 20 km grid squares over Great Britain, before being used as input for a deposition model. In the case of dry deposition, this is an inferential model, and for wet deposition it is the adjustment for the effects of altitude. Wet deposition of NH_x does not show a large spatial variation, since wet removal takes place over a large part of the mixing layer, and is therefore not influenced by local sources. Thus interpolated, and adjusted, data are deemed to be a good approximation of actual wet deposition fluxes. This is not the case with NH_3 concentrations, as they are strongly influenced by local sources. Since the estimated emissions data show a very large spatial variability in both the location and magnitude of the emissions, it is expected that this will be reflected in a map of surface concentrations. Thus an inferential model which employs these measured concentration data to model dry deposition fluxes will be dependent of the number of measurements and the

location of the measurements sites. Without an adequate number of stations, any interpolation of data will lead to the smoothing out of the expected large horizontal gradients, and this will cause errors in any estimation of dry deposition fluxes.

Atmospheric transport models are used on various spatial resolutions, dependent on the role they are expected to fulfill. In the case of the EMEP model, the main requirement is to assess the implementation of international protocols on emission reduction, and determine whether they are having the required effect on the transboundary fluxes of pollutants and deposition fluxes over Europe. To achieve this, the model is run on a spatial resolution of 150 km grid square (at 60° north), and thus the calculated deposition fluxes are an average for the entire grid square. This enables the model to calculate deposition fluxes for the country as a whole, but gives limited information on the spatial pattern of these fluxes. It is important to describe the spatial pattern of NH_3 dry deposition with as fine a resolution as possible, since a large fraction of the emissions may be re-deposited on a scale much finer than the 150 km × 150 km grid squares used by the EMEP model.

To address this problem of describing the spatial distribution of deposition fluxes on a UK national scale, the HARM model is employed over a 20 km × 20 km grid covering the UK, which is itself nested within the larger EMEP grid. A comparison of results from the EMEP model and HARM (Metcalfe *et al.* 1995) yielded some interesting differences. The EMEP model predicted that 25% of UK sulphur deposition was due to UK emissions, while the HARM estimate was 16%. The EMEP deposition total was dominated by dry deposition of sulphur, which accounted for 75% of the total, whereas in HARM dry deposition of sulphur accounts for only 45% of the total deposition flux. Metcalfe *et al.* (1995) surmised that the choice of V_d may be the cause of this difference. The finer horizontal resolution of HARM for Great Britain allowed the enhancement due to the seeder-feeder mechanisms to be included in the wet deposition processes. This meant that the wet deposition pattern predicted by HARM was much closer to the observed data than the EMEP model estimates. Thus, in terms of describing deposition patterns on a national scale, HARM is able to fulfill this requirement to a greater degree of accuracy than the EMEP model, which is employed to

describe pollutant transport on the international scale.

Whilst HARM is able to describe pollutant transport and deposition over a national scale, it is not able to model short-range regional transfer of material, as in the case of NH_3 dry deposition arising from surface emissions. This was illustrated by the under-prediction of NH_3 surface concentrations, which is a consequence of the parameterisation of vertical mixing used in HARM. Without the use of appropriate correction factors, which would account for the large local deposition of emissions within the same grid square, the use of this mixing scheme leads to an under-prediction of the dry deposition flux over much of the country. There exists the need for a model which is able to both describe this short-range deposition of NH_3 explicitly, and also be applicable on a national scale to describe the behaviour of ammonium aerosol. This implies that the model will need to have a fine resolution of emissions in order to distinguish clearly between source and sink areas, and be able to parameterise the exchange of NH_3 over different land-types. It should also have a detailed description of vertical dispersion to account for the high concentrations and large dry deposition fluxes which can occur in the vicinity of high emissions areas.

The NH_3 concentration data from HARM show that even if spatially-detailed emission data are used, the potential advantages are largely lost if the vertical mixing scheme is not suitable to cope with the problems of ground level emissions. Asman and van Jaarsveld (1992) applied the TREND model to the problem of modelling atmospheric NH_3. Vertical dispersion was described by a Gaussian plume formulation for a point source. The results from this model showed both the large spatial variability and high concentrations that are expected to occur in areas of high emissions density.

The computational cost of the proposed model to be used in this project could be extremely high, and thus will be applicable on a limited region, probably much smaller than the EMEP domain. The results from this work could be used alongside larger scale models to describe the spatial distribution of deposition patterns, and determine the location of areas where dry deposition of NH_3 may be causing damage to the environment.

Chapter 3

Parameterisation of Atmospheric Processes

Ammonia and ammonium are affected by a number of atmospheric processes in the tropospheric boundary layer. It is necessary to include a description of these processes in an Atmospheric Transport Model (ATM) if the model is required to produce results to a reasonable degree of accuracy.

In this chapter, attention will focus on the main atmospheric processes necessary to model the atmospheric transport of ammonia. The processes to be discussed are dry deposition, wet deposition, chemical reactions of reduced nitrogen oxidised nitrogen and sulphur, and vertical dispersion. A simple model to describe diurnal variations in the dry deposition of NH_3 is presented, and methods to parameterise the aforementioned atmospheric processes are reviewed.

3.1 Dry deposition

The process of dry deposition of NH_3 was introduced earlier (section 1.5.1). Here, a number of models which are currently used to parameterise NH_3 dry deposition are reviewed, and a scheme is proposed to implement one of these models in an ATM which will describe the diurnal variations of V_d, dependent on landuse and routine meteorological measurements.

3.1.1 Modelling the deposition velocity of ammonia

A parameterisation of the dry deposition of NH_3 was introduced in 2.2.1, where it had been used in an inferential model to describe the annual dry deposition

flux of NH_3 over Great Britain.

To recap, this model is based on the assumption that the concentration of material at the surface is zero ($\chi_s = 0$) in equation 2.1 (section 2.2.1), and thus the dry deposition velocity can be described by

$$V_d = -\frac{F}{\chi(z)} \tag{3.1}$$

where F is defined as the flux between the atmosphere and the surface, and $\chi(z)$ is the concentration of NH_3 at a height z above the surface. Rearrangement of this equation gives

$$F_d = V_d \cdot \chi(z) \tag{3.2}$$

where F_d is now defined as the dry deposition flux.

This assumption has been used in many atmospheric transport models (Barrett and Seland, 1995; Asman and van Jaarsveld, 1992; Metcalfe *et al.*, 1989, 1995; Fisher 1984, 1987; ApSimon *et al.*, 1994). The magnitude of V_d can either be a single invariant value, as used in one of the earliest NH_3 models (Asman *et al.*, 1987; 0.008 m s^{-1}), or a more detailed approach can be used to allow V_d to vary diurnally and spatially. The second option is a more realistic approach because the magnitude of the dry deposition flux is dependent on atmospheric turbulence to transport material to the surface. During a 24-hour period, the strength of the turbulent eddies can vary dependent on surface heating and wind speed. Plant physiology can also play an important role in determining the strength of the flux, due to the diurnal cycle of the stomata opening.

One way of describing V_d is to assume that transport between a specified reference height in the atmosphere and recipient surface takes place through three resistances in series (Figure 3.1). The first resistance, known as the aerodynamic resistance ($R_a(z)$), describes the resistance due to turbulent diffusion of material from the reference height (z) to the roughness elements of the surface. The second term, R_b, is known as the laminar boundary layer resistance, and it describes the transfer due to molecular diffusion through the quasi-laminar layer around roughness elements of the surface. The surface resistance (R_c) describes the ability of the surface itself to capture the airborne material, and is dependent on the nature of the surface. The three resistances are added together in series to create

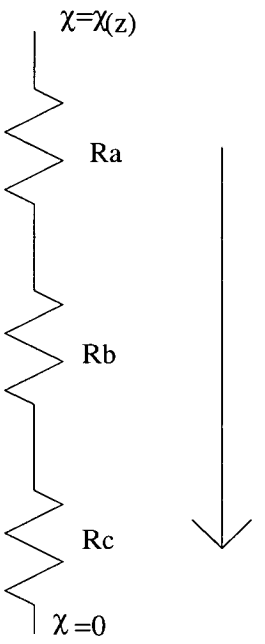

Figure 3.1: A representation of 'The Canopy Resistance Model' which describes the magnitude of V_d by the use of three resistances in series.

a total resistance to deposition $R_t(z)$. This is known as the 'Canopy Resistance Model' and is defined as

$$R_t(z) = (R_a(z) + R_b + R_c) \tag{3.3}$$

$R_t(z)$ and V_d are specified for a reference height (z), and the resistances related to V_d by:

$$V_d(z) = (R_a(z) + R_b + R_c)^{-1} \tag{3.4}$$

The one major draw back of the 'Canopy Resistance Model' is the inability to allow for any period of emission from the surfaces. As has already been mentioned in section 1.3, emissions can occur from arable crops due to favourable meteorological conditions and the application of fertiliser. Analysis of equation 3.1 shows that to achieve an emission flux, a negative value of V_d is required. This is due to the assumption that χ_s=0 in equation 2.1. The only way to describe this would be to alter the value of R_c in equation 3.4 to a negative number, yet this is clearly impractical as V_d would be then a non-continuous function and could be assigned impossibly large values if the wrong choice of R_c was chosen.

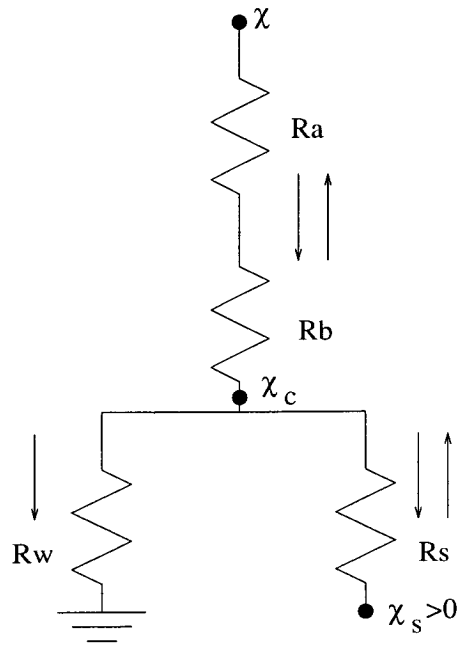

Figure 3.2: A resistance model to allow for bi-directional fluxes of NH_3. (Sutton and Fowler, 1993a).

An improved scheme to parameterise the plant-atmosphere exchange was formalised by Farquhar *et al.* (1980) who defined the NH_3 'Compensation Point' in plants, which is the gaseous NH_3 concentration in equilibrium with the concentration of NH_4^+ within the plant intercellular fluids. Experiments performed by the Farquhar *et al.* found that deposition would occur when air concentrations were greater than this value, and that emission was observed from the plant when air concentration were less than the compensation point.

This idea was used by Sutton and Fowler (1993a) and Sutton *et al.* (1993d, 1995b) to propose a new model, which allows for dry deposition onto a leaf surface, as in the canopy resistance model, and also allows for simultaneous bi-directional exchange with the plant stomata. A representation of this scheme is given in Figure 3.2. This models calculates a 'canopy compensation point' (χ_c), which is used to determine the direction and magnitude of the flux (F) between the plant and the overlaying atmosphere. Calculation of F and χ_c is given by

Sutton and Fowler (1993a):

$$F = (\chi_c - \chi(z))/(R_a\{z\} + R_b) \tag{3.5}$$

$$\chi_c = \frac{\chi(z)/(R_a\{z\} + R_b) + \chi_s/R_s}{(R_a\{z\} + R_b)^{-1} + R_s^{-1} + R_w^{-1}} \tag{3.6}$$

This model has been applied successfully to describe the diurnal exchange of NH_3 over a wheat crop (Sutton and Fowler, 1993a). Their study highlighted the fact that whilst emissions occurred from the plant stomata, dry deposition to the leaf surfaces recaptured much of the emission, and thus the value of the canopy compensation point (χ_c) was less than the stomatal compensation point (χ_s).

The major problem in applying the canopy compensation point approach is the determination of the value of χ_s and R_w that are to be used. Since they are both very uncertain, and dependent on temperature and humidity, at the present time much work is needed to be able to define these values in an statistical ATM on a country-wide basis, this formulation is not employed in the present study.

3.1.2 Formulation of a dry deposition model for inclusion in an atmospheric transport model

The magnitude and direction of the exchange of material between the surface and the atmosphere is a consequence of a number of influencing factors. These include the wind speed, the strength of the turbulence in the lower atmosphere, the stability of the atmosphere, the type of receptor surface and general prevailing meteorological conditions such as temperature and humidity.

The objective of this section is to create a simple but effective model description of NH_3 dry deposition that can be used in a statistical atmospheric transport model. As with any model, a number of assumptions must be made, based on the available scientific information, required complexity of the model and the computational time required to produce a solution. At the time of writing, the major problem in applying the canopy compensation point approach is the determination of the time- and space-varying values of χ_s and R_w that are to be used in a country-wide statistical ATM.

An approximate measure is to consider the long term fluxes of NH_3 and parameterise them accordingly. An example of this was given by Sutton *et al.* (1995a) in the calculation of the net flux of ammonia from arable crops. Measurements

allowed the net annual flux to be estimated as a net emission of 0.4 kg N ha^{-1}. This was composed of an emission flux of 1.2 kg ha^{-1} $year^{-1}$ following fertilisation, 0.3 kg N ha^{-1} $year^{-1}$ from hay drying and a net background deposition of 1.1 kg N ha^{-1} $year^{-1}$. Since the emissions from fertilisers are accounted for in the emissions data of Dragosits *et al.* (1996) (Figure 2.5), the surface represents a net sink of ammonia with an annual dry deposition flux of 0.8 kg N ha^{-1} $year^{-1}$. This value can be compared to annual deposition fluxes to semi-natural ecosystems of 3 to over 40 kg N $ha^{-1}year^{-1}$ estimated by Sutton *et al.* (1993c). Thus the long-term behaviour of an agricultural cropland surface, with relation to an ATM, can be represented by the use of a small deposition velocity, while the fertiliser related emissions that occur from this surface form part of the emissions input data.

The proposed scheme is to employ the canopy resistance model (Equations 3.3, 3.4), using determined values of R_a, R_b and R_c, to calculate diurnally varying values of V_d. In order to describe the effects of different types of land on the dry deposition process, it is necessary to be able to differentiate between the various surface types, and to assign a parameterisation of dry deposition which would describe more accurately the amount of material being deposited. To achieve this, a landuse database is employed, which has a spatial resolution of 20 km grid squares. The landuse database contains information on the classification of land into different categories for a specified grid square, and also the percentage land cover (section 2.2.1). There are five land categories; arable, forest, moorland, grassland and urban. Specific information for each surface type means that land-dependent deposition velocities can be calculated.

The following sections review the theory behind the proposed dry deposition model, and how it can be implemented into an atmospheric transport model.

Solar radiation and sensible heat flux

To describe the diurnal variations in the behaviour of V_d, the resistance model includes a simple description of the average daily cycle of solar radiation. This information can be used to determine the stability of the atmosphere and the amount of vertical turbulence.

Ground type	σ
Ocean	0.05
Tropical forest	0.10
Mixed agriculture	0.15
Grassland	0.20
Deserts	0.30
Snow	0.65

Table 3.1: Reflection coefficients for various surfaces. Smith (1975).

From Monteith (1973), the equation of radiation balance at the surface can be written as

$$\mathbf{R_n} = (1 - \sigma)\mathbf{S_t} + \mathbf{L_d} - \mathbf{L_u} \tag{3.7}$$

where $\mathbf{S_t}$ is the total solar irradiance, σ as the reflective coefficient of the surface, $\mathbf{L_d}$ is the downwards flux of longwave radiation from the atmosphere, and $\mathbf{L_u}$ is upwards flux of longwave radiation from the surface. Values of σ are given in Table 3.1 for various ground surfaces (Smith, 1975).

According to Montieth (1973), in the absence of cloud, the diurnal variation of total solar irradiance is approximately sinusoidal. To describe the behaviour of $\mathbf{S_t}$, it is necessary to take into account several factors which affect the angle of elevation of the sun and the day length. These factors include the latitude of the site, the Julian day of the summer solstice, and the hour of solar noon (when the angle of elevation is at a maximum). A value for the maximum possible solar irradiance ($\mathbf{S_{tm}}$) of 950.0 W m^{-2} was chosen to give a good fit to experimental data from Cambridge, UK. (Smith, 1975). Thus for a site of latitude λ with local noon at time n, the value of $\mathbf{S_t}$ at a time t hours, and on the of the year (d), is defined by the standard set of equations:

$$\mathbf{S_t} = 950.0(cos\phi\, cos\gamma\, cos\lambda + sin\phi\, sin\lambda) \tag{3.8}$$

where

$$\phi = tan^{-1}(0.4348 \times sin(d - 79)) \tag{3.9}$$

and

$$\gamma = 15(t - n) \tag{3.10}$$

Cloud amount (f)	C_f
0	1.00
1	0.89
2	0.81
3	0.76
4	0.72
5	0.67
6	0.59
7	0.45
8	0.23

Table 3.2: Reduction factors (C_f) for the incoming solar radiation, due to cloud cover (oktas). Smith (1975).

Equation 3.8 can be simplified by referring to the term in brackets as the *cosine of the zenith angle* or just simply $cos(zen)$. Thus an approximation for the total solar irradiance is

$$\mathbf{S_t} = 950.0\, cos(zen) \tag{3.11}$$

Cloud cover

With cloud present in the atmosphere, the amount of radiation received by a surface will be reduced in a complex way. An increase in cloud cover will mean that, in general, $\mathbf{S_t}$ will decrease.

A broad simplification of this problem was given by Smith (1975) with the use of cloud reduction factors (Table 3.2). These are used to adjust the solar irradiance equation (3.11) to give:

$$\mathbf{S_t} = 950.0\, cos(zen) C_f \tag{3.12}$$

where C_f is the cloud reduction factor, and f is the cloud cover in oktas.

Definition of the stability of the atmosphere

As discussed by Monteith (1973), turbulent eddies in the lower atmosphere can be affected by buoyancy forces arising from either heating or cooling of the earth's surface in relation to the overlaying atmosphere. Thom (1975) states that with fully forced convection, no significant amplification or damping of the basic,

frictionally-generated eddy structure occurs. The boundary layer can be said to be in a neutral stability state, and over an ideal site the wind profile near the surface is precisely logarithmic. In general this is not the case and there is usually some effect of the buoyancy forces, dependent on height. During the daytime, surface heating due to solar radiation will enhance both the turbulence eddies and the vertical transport of material. This is known as dynamic instability. Conversely at nighttime, cooling of the earth's surface will dampen the turbulence and thus the vertical transport of material will be reduced. In this case, the lower atmosphere would be said to be dynamically stable.

The surface layer was estimated by Stull (1988) to be the lowest part of the atmospheric boundary layer, where surface fluxes vary by less than 10% of their surface value. A measure of the stability of this lowest layer can be expressed in a parameter, known as the Monin-Obukhov length scale (L). If it is assumed that all fluxes in the surface layer are equal to their surface values, then it is possible to define L. The definition of L is given by

$$L = \frac{u_*^3 \rho c_p T}{kg\mathbf{H}} \tag{3.13}$$

where u_* is the friction velocity, ρ is the density of air, c_p is the specific heat capacity of air, T is the absolute temperature, k is the von Karman constant (about 0.41; Thom, 1975), $\mathbf{H}$ is the sensible heat flux from the surface, and g is the gravitational constant

The magnitude and sign of L can be used to define the stability of the surface layer.

$$\begin{array}{lll} L > 0 & & \text{stable} \\ L < 0 & & \text{unstable} \\ L = \infty & & \text{neutral} \end{array}$$

One interpretation of L is that when the atmosphere is classed as being unstable, the magnitude of L is proportional to the height below which frictionally driven turbulence dominates buoyantly generated turbulence, and above which the reverse is true. Because of its complexity however, the Monin-Obukhov length scale is not a parameter that is routinely measured. An alternative, and simpler, method of classifying atmospheric stability was introduced by Pasquill (1961)

Surface Wind Speed at 10 m ($m\ s^{-1}$)	Solar radiation (S_t) $W\ m^{-2}$			Night Time Cloud Cover	
	$S_t > 700$	$350 \leq S_t \leq 700$	$S_t < 350$	$\geq \frac{4}{8}$	$\leq \frac{3}{8}$
< 2	A	A - B	B		
2 - 3	A - B	B	C	E	F
3 - 5	B	B - C	C	D	E
5 - 6	C	C - D	D	D	D
> 6	C	D	D	D	D

A: extremely unstable
B: moderately unstable
C: slightly unstable
D: neutral
E: slight stable
F: moderately stable

Table 3.3: Determination of Pasquill stability classes. Adapted from Seinfeld (1986).

using the concept of stability classes. These classes have proved very useful in atmospheric diffusion calculations and are defined in Table 3.3. The solar radiation is calculated using equation 3.12.

A variable needed to calculate the Pasquill stability class is the 10 metre wind speed. For this study, an approximation to this value is made which uses the geostrophic wind speed. If the geostrophic wind speed (G) and the depth of the atmospheric boundary layer (H_{mix}) are known, then a power law approximation may be used, such that the wind speed attains its geostrophic value at the top of the boundary layer. Thus the wind speed at a height z above the surface ($u(z)$) can be given as a function of G as follows:

$$u(z) = G(\frac{z}{H_{mix}})^q \tag{3.14}$$

for $z < H_{mix}$. A simplification of this scheme was made by ApSimon *et al.* (1994) for use in the TERN model. The index q was constrained such that

$$u(10) = 0.5G \tag{3.15}$$

over land, and

$$u(10) = 0.85G \tag{3.16}$$

over the sea. This allowed values of $u(10)$ to be easily estimated.

	Pasquill stability class	Coefficients	
		a	b
extremely unstable	A	-0.096	0.029
moderately unstable	B	-0.037	0.029
slightly unstable	C	-0.002	0.018
neutral	D	0	0
slightly stable	E	+0.004	-0.018
moderately stable	F	+0.035	-0.036

Table 3.4: Coefficients for straight line approximation of the Pasquill stability class. Golder (1972).

Golder (1972) established a relation between the Pasquill stability classes, the Monin-Obukhov length and the roughness length (z_0). This relationship can be approximated using the parameters in Table 3.4, and the correlation

$$\frac{1}{L} = a + b\, log(z_0) \tag{3.17}$$

The value of z_0 describes smoothness of a surface. The larger the value of z_0, the greater the turbulence that is generated by wind passing over that surface. For a certain surface, z_0 can be determined from the neutral stability wind profile as the height at which the logarithmic wind speed is extrapolated to zero.

The determination of L, and hence the stability of the lower atmosphere is important is defining the wind profile, and is used to quantify the degree of turbulence in the atmosphere.

Wind profile in the lower boundary layer

The general form of the wind profile equation (Thom, 1975) is defined as

$$\frac{du}{dz} = \frac{u_*}{k\, z}\Phi_M \tag{3.18}$$

where z is the vertical height above the ground, u_* is known as the friction velocity, and k is the von-Karman constant. Φ_M is a dimensionless stability function, and is greater or less than unity in stable or unstable conditions respectively.

The friction velocity u_* is an important parameter as it describes the effectiveness of vertical turbulent exchange of momentum in the airflow over the surface.

It is assumed to have a constant value throughout the lower boundary layer.

An analogous stability function for heat exchange, Φ_H, can be defined by the generalised temperature gradient relationship

$$\frac{dT}{dz} = \frac{T_*}{k\,z}\Phi_H \tag{3.19}$$

where T_* quantifies the turbulent fluctuations in temperature within the boundary layer in much the same way that u_* describes the turbulent fluctuations in velocity.

The gradient stability correctors Φ_M and Φ_H can be calculated from semi-empirical correction factors derived by Webb (1970) and Dwyer and Hicks (1970) for stable and unstable conditions respectively. For stable conditions this gives

$$\Phi_M = \Phi_H = \{1 + 5.2\frac{z}{L}\} \;(L,\ positive) \tag{3.20}$$

and for unstable conditions,

$${\Phi_M}^2 = \Phi_H = \{1 - 16\frac{z}{L}\}^{-0.5} \;(L,\ negative) \tag{3.21}$$

For neutral conditions, Φ_M and Φ_H have a value of 1.00.

Using the above correction factors in 3.20 and 3.21, and then integrating 3.18 between $z = z_0$ and a reference height z, gives the windspeed at the specified height z to be

$$u(z) = (\frac{u_*}{k})[\,ln\{\frac{z}{z_0}\} - \psi_M\{\frac{z}{L}\}\,] \tag{3.22}$$

Values of ψ in stable conditions (Thom, 1975) and in unstable conditions (Paulson, 1970) are given as

$$\psi_M = \psi_H = -5.2\frac{z}{L} \tag{3.23}$$

for stable conditions, and

$$\psi_M = 2\,ln\{\frac{(1+x)}{2}\} + ln\{\frac{(1+x^2)}{2}\} - 2\,tan^{-1}(x) + \frac{\pi}{2} \tag{3.24}$$

$$\psi_H = 2ln\{\frac{(1+x^2)}{2}\} \tag{3.25}$$

for unstable conditions, where $x = \{1 - 16\frac{z}{L}\}^{0.25}$ and is in radians for the $\tan^{-1}$ term. For neutral conditions, ψ_M and ψ_H have a value of 0.

Parameter	Arable	Forest	Grass	Moorland	Urban	Sea
$z_0(m)$	0.05	1.00	0.03	0.03	1.00	0.01

Table 3.5: Land dependent values of z_0 used in the dry deposition model. (M.A. Sutton, Pers Comms).

3.1.3 Calculation of the dry deposition velocity

To calculate land-dependent deposition velocities for NH_3, certain data sets are necessary. One of the most important datasets contains information on the mean windspeed at a height of 3 m for all of Great Britain (Thompson *et al.*, 1982). These data are on a 20 km × 20 km grid. It has already been stated that the ITE landuse database (section 2.2.1) is employed in this model (section 3.1.2). To each of the land classes and also to the sea class, relevant land-dependent parameters are assigned. Values of z_0 for each land class applied here are listed in Table 3.5.

The calculation of the deposition velocity for each land class is as follows:

1. The first stage in the calculation of the values of V_d involves the use of the windspeed dataset. For a specified grid square, it is assumed that the windspeed represents average meteorological conditions, and an assumption is made that neutral stability is a reasonable approximation for average conditions.

2. The value of u_* is calculated by taking the estimated database windspeed at 3 m and applying the neutral formulation of equation 3.22, which assumes that $\psi_M\{\frac{(z)}{L}\} = 0$. The wind profile is then extended up to 60 m by again using the neutral form of 3.22. At a height of 60 m, the wind speed is unaffected by different surface roughness lengths (as used by Asman (1996)).

3. Using equation 3.12, Tables 3.3 and 3.4, together with equation 3.17 and Table 3.5, diurnally varying and land-dependent values of L are now calculated.

4. Equation 3.22 is now employed in its general form (using Ψ_M) to calculate

diurnal values of u_* and $u(z_{vd})$ for each land class , where z_{vd} is the reference height at which V_d is required for each land class.

5. The final stage of the model is to calculate values for the resistances (R_a, R_b and R_c) and use equation 3.4 to calculate V_d. The determination of R_a, R_b and R_c are given below.

The aerodynamic resistance R_a is calculated by using the formulation given by Garland (1977):

$$R_a(z) = \frac{u(z)}{u_*^2} - \frac{[\psi_H - \psi_M]}{u_* k} \tag{3.26}$$

The molecular diffusion resistance R_b expresses the transport of material across the laminar layer adjacent to the receptor surface. A widely accepted form (Garland, 1977) is given below, though a number of other formulations have been put forward.

$$R_b = 1.45\, Re_*^{0.24}\, Sc^{0.8}\, u_*^{-1} \tag{3.27}$$

Re_* is the turbulent Reynolds number given as $Re_*{=}u_* z_0/\nu$, Sc is the Schmidt number given as $Sc = \nu/D$, where ν is the kinematic viscosity of air and D is the diffusion coefficient of the entrained property in air. The value of $Sc^{0.8}$ is approximately 0.734 (M.A. Sutton, 1995. Pers Comms).

The surface resistance R_c is dependent on a number of conditions, the major one being the nature of the surface being deposited on. When measurements are conducted during field experiments, R_c is the quantity not able to be measured directly, and thus is calculated by

$$R_c = V_d^{-1} - R_a(z) - R_b \tag{3.28}$$

To describe the broad patterns of land-dependent dry deposition, a specific value of R_c is assigned to each land class, and these are combined with calculated values of R_a and R_b to create a set of land-dependent values of V_d. The values of R_c used are listed in Table 3.6. These values are chosen to provide a simple description consistent with the literature on surface atmosphere exchange of NH_3 with different surface types, e.g. Sutton *et al.* (1993e), Sutton *et al.* (1994). Since emissions from arable land (due to fertiliser application) are already included

Parameter	Arable	Forest	Grass	Moorland	Urban	Sea
R_c (s m^{-1})	1000	20	600	20	240	240

Table 3.6: Land-dependent values of R_c used in the dry deposition model to calculate diurnal values of V_d for NH_3. (M.A. Sutton, 1995. Pers Comms).

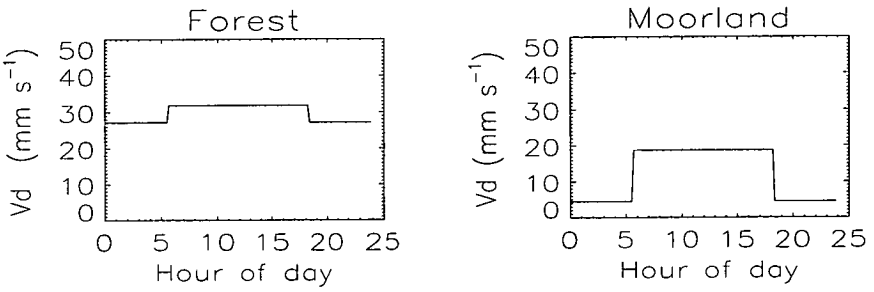

Figure 3.3: Modelled diurnal cycle of V_d for forest and moorland from the dry deposition proposed model.

in the emission inventory, and background exchange over this vegetation type suggests a balance between emission and deposition, a value of R_c is set to 1000 s m^{-1}. Rapid deposition is generally seen to forest/moorland vegetation, and for both these classes a value of 20 s m^{-1} is applied. Grassland represents a more problematic category. In the NH_3 emissions inventory to be used as input for the atmospheric transport model, (Dragosits *et al.*, 1996; Figure 2.5), the data for grazed grassland are defined as the *net* emission from this system. Sutton (1993e) recommended that surface atmosphere exchange should be set to zero over this surface. However grazing only takes place for part of the time, and exchange over ungrazed grassland is expected to show significant deposition. This effect has been accounted for in the present version of the resistance model by restricting the calculated V_d for grassland to very small values by use of a larger value of R_c than for moorland and forest.

Figure 3.3 is a plot of the diurnal cycle of V_d for forest and moorland. The windspeed at the surface (3 m) in this example is set at 4 m s^{-1} and there is no cloud cover.

3.2 Parameterisation of the wet deposition process

Removal of the atmospheric material by precipitation is a complex process. It has already been mentioned (section 1.5.3) that the two major mechanisms are in-cloud and below-cloud scavenging.

An overview by Asman (1994) gives a good description of the mechanisms of in-cloud removal. At relative humidities of greater than 40%, aerosol particles act as condensation nuclei for the water vapour in the atmosphere, allowing cloud droplet formation at high humidities (> 95%). Atmospheric NH_3 can be absorbed into these cloud droplets at a high rate. This means that most of the NH_x in clouds is found in cloud droplets, and that the gaseous NH_3 concentration in the surrounding air is much less than found in the air outside the cloud.

Below the cloudbase, falling rain drops can encounter high concentrations of NH_3. The large raindrops will not absorb much NH_3 on their descent, due to the short residence time and the low uptake rate, limited by aerodynamic transfer. Particles are absorbed even less efficiently than gaseous NH_3.

A widely accepted parameterisation of these processes in models takes the form of scavenging coefficients (s^{-1}). This is the fraction of the airborne concentration removed per unit time. The amount of material removed in a time period Δt is given by

$$\Delta\chi = \chi(1 - e^{-\lambda\Delta t}) \tag{3.29}$$

where $\Delta\chi$ is the decrease in concentration (χ) due to removal by precipitation, and λ is the scavenging coefficient. The calculation of the value of λ can be a simple process, or a very detailed one, depending on the assumptions one makes.

A number of ATMs make no differentiation between in-cloud and below-cloud processes (HARM, Metcalfe *et al.*, 1995; EMEP model, Barrett and Seland, 1995) and use an averaged value to describe the overall effect. The calculation of these scavenging coefficients is performed using the equation

$$\lambda = \frac{\Delta_i \cdot I}{H_{mix}} \tag{3.30}$$

where Δ_i is known as the scavenging ratio for species 'i', I is the precipitation rate (mm s^{-1}), and H_{mix} is the depth of the atmospheric boundary layer (m).

Symbol	Value for EMEP	Value for HARM
Δ_{HNO3}	$1.4 \cdot 10^6$	$1.3 \cdot 10^5$
Δ_{NH3}	$1.4 \cdot 10^6$	$1.3 \cdot 10^5$
Δ_{SO2}	varies seasonally to reflect variation in H_2O_2; $3 \cdot 10^5 + 1 \cdot 10^5 \sin(2\ \pi\ (T - T_o)/T_a)$	$1.3 \cdot 10^5$
Δ_{NO3}	$1.0 \cdot 10^6$	$1.3 \cdot 10^6$
Δ_{SO4}	$1.0 \cdot 10^6$	$1.3 \cdot 10^6$

Table 3.7: Scavenging ratios (Δ) from the EMEP model (Barrett and Seland, 1995) and HARM (Metcalfe *et al.*, 1995) models used to calculate the scavenging coefficients for wet deposition. T is the time of year, T_o=80 days and T_a=number of days in one year.

I (mm $(6h)^{-1}$)	0	3	6	9	12	20	50	90	150
Φ (%)	0	31	48	60	66	72	80	85	91

Table 3.8: Fraction of the grid square receiving precipitation as a function of grid averaged precipitation intensity in the EMEP model. Barrett and Seland (1995).

The scavenging ratios for both EMEP and HARM are listed in Table 3.7.

The EMEP model employs rainfall data for 6-hourly periods. These data are taken from observation stations situated across the large model domain. An additional term (Φ) is used in the EMEP model to account for the non-uniformity of precipitation throughout the 150 km $\times$ 150 km grid which cannot be explicitly described. This results in the modification of equation 3.30 to

$$\lambda = \frac{\Delta_i \cdot I}{\Phi \cdot H_{mix}} \tag{3.31}$$

The values of Φ are listed in Table 3.8.

In other models (TREND, Asman and van Jaarsveld 1992; ACDEP, Hertel *et al.* 1995) there are separate treatments of in-cloud and below-cloud processes, although this is only true in the TREND model when close to the source of the emission. Parameterisation of these in-cloud processes are performed using equation 3.30, but the scavenging ratios used are not empirical values and are determined using detailed formulations.

The present study involves the creation of an ATM that is statistical in nature. For that reason, the wet deposition parameterisation used in the HARM is ex-

Species	Scavenging coefficient
Nitrate aerosol	1.3×10^{-5} s^{-1}
Sulphate aerosol	1.3×10^{-5} s^{-1}
Ammonia	9.0×10^{-6} s^{-1}
Nitric acid	9.0×10^{-6} s^{-1}
Sulphur dioxide	1.0×10^{-6} s^{-1}

Table 3.9: Scavenging coefficients used by the HARM model based on an annual rainfall of 1000 mm. Metcalfe *et al.* (1995).

amined in more detail as this employs a statistical, or constant drizzle approach to wet deposition. The annual rainfall data for Great Britain is used on a 20 km $\times$ 20 km grid. Thus for a particular location, the rainfall intensity (I mm s^{-1}) is calculated as

$$I = \frac{I_T}{SEC_T} \tag{3.32}$$

where I_T is the total annual rainfall in mm for a specified location, and SEC_T is the total number of seconds in one year. For an annual rainfall of 1000 mm, the calculated scavenging coefficients used by HARM are listed in Table 3.9.

The calculation of these values were discussed in Derwent *et al.* (1988) and are summarised here. A simple model was set up and was subjected to alternating wet and dry periods. Wet scavenging was assumed to occur only during wet periods, with a first-order removal coefficient proportional to the rain rate. Distributions about the central values of rainfall rate (1 mm hr^{-1}), dry and wet periods lengths (40 and 8 hours respectively) were assumed. The constant drizzle coefficients were obtained by fitting a simple first-order loss coefficient to the time dependent average wet-scavenging rates over many thousands of samples.

3.3 Atmospheric chemistry

Figure 3.4 is a representation of the dry chemistry scheme employed by the EMEP model to represent the major reactions of oxidised nitrogen, oxidised sulphur and reduced nitrogen in the lower atmosphere. Whilst NH_3 is the main species under consideration, it is also important to represent accurately other species in the atmosphere as well. The conversion of NH_3 into NH_4^+ aerosols is dependent on

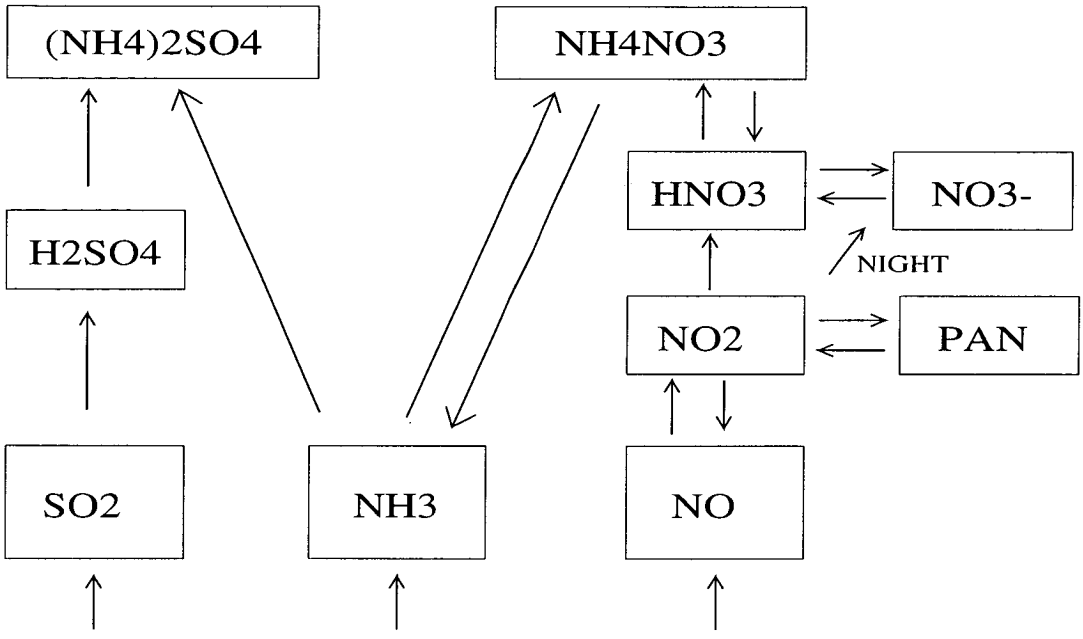

Figure 3.4: Overview of the dry chemistry scheme employed by the EMEP model. Barrett and Seland (1995).

the prevalence of certain acidic species, the main culprits being the oxidation products of SO_2 and NO_x. Thus it is necessary to include some representation of the interaction of NH_3 with these species, even if it is only a first order conversion of NH_3 to NH_4^+, as used in the TREND model (Asman and van Jaarsveld, 1992).

3.3.1 Gas phase reactions of oxidised nitrogen

In the EMEP model (Barrett and Seland, 1995) and the TERN model (ApSimon *et al.*, 1994) emissions of NO_x are in the form of nitric oxide (NO, 95% of emissions) and nitrogen dioxide (NO_2, 5% of emissions).

NO and NO_2 are in a semi-equilibrium state in the daytime. NO_2 is converted to NO by a photolytic reaction during the daytime through

$$NO_2 + h\nu \rightarrow NO + O \tag{3.33}$$

The rate of photolysis depends on the time of year, local time and the cloud cover, with 100% cloud cover (8 oktas) giving a 50% reduction in the reaction

Symbol	Definition	Value
J_{NO2}	Dissociation rate for the reaction. NO_2 + hv → NO + O function of latitude, time of year, local time and cloud cover.	J_{NO2} = a(1-C_f/2)exp(-b secθ) a=0.01 s^{-1}, b=0.39 C_f = fractional cloud cover θ = sun's zenith angle
k_{11}	Rate of the reaction NO + O_3 → NO_2 + O_2	$k_{11} = a_{11} \exp(-b_{11}/T)$ a_{11}= 2.1 · 10^{-12} cm^3 s^{-1} $molecule^{-1}$ b_{11} = 1450 K
k_{12}	Rate of net model reaction $2NO_2+O_3+H_2O \rightarrow 2NO_3^-+2H^++O_2$ which occurs in darkness according to $NO_2+O_3 \rightarrow NO_3+O_2$ $NO_3+NO_2 \leftrightarrow N_2O_5$ $N_2O_5+H_2O \rightarrow 2NO_3^-+2H^+$ The first step is rate determining	$k_{12}=a_{12} \exp(-b_{12}/T)$ a_{12} = 1.2·10^{-13} cm^{-3} s^{-1} $molecule^{-1}$ b_{12}= 2450 K
k_{21}	Rate of model reaction $NO_2+OH^{\cdot} \rightarrow HNO_3$	k_{21}=1.1·10^{-11} cm^{-3} s^{-1} $molecule^{-1}$
k_{77}	Rate of model reaction NO_2 + CH_3COO_2 → PAN	k_{77} = 3.2·10^{-12} cm^{-3} s^{-1} $molecule^{-1}$
k_Π	Rate of thermal decomposition of PAN	$k_\Pi = a_\Delta \exp(-b_\Delta/T)$ a_Δ = 7.94·10^{14} s^{-1}, b_Δ=12530K
q_a	Rate of gas-to-particle conversion $HNO_3 \rightarrow NO_3^-$ Rate of reverse conversion is $q_a/2$	q_a= 10^{-5} s^{-1}

Table 3.10: EMEP chemical conversion rates for oxides of nitrogen. T is the temperature in K. From Barrett and Seland (1995).

rate. NO reacts with ozone (O_3) to form NO_2

$$NO + O_3 \rightarrow NO_2 + O_2 \tag{3.34}$$

At nighttime, NO_2 will react with O_3 to create nitrate (NO_3^-) in the following set of reactions:

$$NO_2 + O_3 \rightarrow NO_3 + O_2 \tag{3.35}$$

$$NO_2 + NO_3 \leftrightarrow N_2O_5 \tag{3.36}$$

$$N_2O_5 + H_2O \rightarrow 2H^+ + 2NO_3^- \tag{3.37}$$

Reaction 3.35 is the rate determining reaction, and only occurs at night since NO_3 and N_2O_5 are rapidly photolysed to NO and NO_2.

Nitric acid is formed by the reaction of NO_2 and the hydroxyl radical ($OH^{\cdot}$) through

$$NO_2 + OH^{\cdot} \leftrightarrow HNO_3 \tag{3.38}$$

PAN (peroxyacetyl nitrate) is created through

$$NO_2 + CH_3COO_2 \rightarrow PAN \tag{3.39}$$

and is destroyed by thermal decomposition by way of the following reaction

$$PAN \rightarrow NO_2 + CH_3COO_2 \tag{3.40}$$

In the EMEP model (Barrett and Seland, 1995) and the TERN model (ApSimon *et al.,* 1994), there is a simple parameterisation to represent the formation of large nitrate particles on soil dust or marine aerosols. This is in the form of a first order decay coefficient

$$HNO_3 \rightarrow NO_3^- + H^+ \tag{3.41}$$

The reverse reaction

$$H^+ + NO_3^- \rightarrow HNO_3 \tag{3.42}$$

takes place at half the rate of equation 3.41.

The reactions that are important in this study are those that occur with NH_3 and NH_4^+. The main reaction of NH_3 and oxidised nitrogen is an equilibrium which occurs by way of

$$HNO_{3(g)} + NH_{3(g)} \leftrightarrow NH_4NO_{3(s)} \tag{3.43}$$

The production or destruction of NH_4NO_3 is determined by the equilibrium coefficient K_p. The calculation of K_p is given in Stelson and Sienfeld (1982) and is dependent on relative humidity and ambient temperature. To determine if any NH_4NO_3 is to formed, it is necessary to know the total nitrate (TN) and total ammonia (TA) available to form NH_4NO_3.

From Seinfeld (1986), TN and TA are defined as

$$[TN] = [HNO_3(g)]_m + [NO_3^-]_m \tag{3.44}$$

$$[TA] = [NH3_3(g)]_m + [NH_4^+]_m \tag{3.45}$$

where $[X]_m$ is the concentration of substance X. If [TN][TA] $\leq K_p$, no ammonium nitrate is predicted to be present. If [TN][TA] $\geq K_p$, then aerosol ammonium nitrate is predicted to be formed such that the product $[NH3_3(g)]_c[HNO_3(g)]_c = K_p$. The subscript c indicates a theoretically computed pollutant concentration. The reaction is assumed to occur instantaneously.

3.3.2 Gas phase reactions of oxidised sulphur

According to Seinfeld (1986), the most important gas phase reaction of SO_2 is with the hydroxyl radical ($OH^{\cdot}$). This is seen to be

$$OH^{\cdot} + SO_2 + M \rightarrow HOSO_2^{\cdot} + M \tag{3.46}$$

Subsequent reactions lead to the formation of sulphuric acid (H_2SO_4) by way of

$$HOSO_2^{\cdot} + O_2 \rightarrow HO_2^{\cdot} + SO_3 \tag{3.47}$$

$$SO_3 + H_2O \rightarrow H_2SO_4 \tag{3.48}$$

The rate determining step of $SO_2 \rightarrow H_2SO_4$ is equation 3.46. Calculation of this rate depends on the the concentration of $OH^{\cdot}$. Seinfeld estimated this rate, assuming $[OH^{\cdot}] = 1.7 \times 10^6$ which is representative of a typical cloudless summer day in relatively clean tropospheric air. He came up with a 24-hour averaged rate of SO_2 oxidation of 0.7% hr^{-1}. This is in fairly close agreement with the value given by RGAR (1990) and Asman (1994) of 1% hr^{-1}. Reactions of NH_3 and H_2SO_4 are assumed to be instantaneous and irreversible (Seinfeld, 1986).

3.3.3 Aqueous phase reactions of oxidised sulphur

As well as the gaseous reactions that occurs, many important reactions involve the presence of liquid water. In the atmospheric boundary layer this condition is usually satisfied inside clouds. The following section is a summary of the information given in Seinfeld (1986), and details some of the main reactions that can occur.

The absorption of SO_2 by water results in

$$SO_2(g) + H_2O \leftrightarrow SO_2 \cdot H_2O \tag{3.49}$$

$$SO_2 \cdot H_2O \leftrightarrow H^+ + HSO_3^- \tag{3.50}$$

$$HSO_3^- \leftrightarrow H^+ + SO_3^{2-} \tag{3.51}$$

The total dissolved sulphur in solution is given by

$$[S(IV)] = [SO_2 \cdot H_2O] + [HSO_3^-] + [SO_3^{2-}] \tag{3.52}$$

The amount of sulphur dissolved in solution is dependent on pH, with [S(IV)] increasing dramatically as pH increases. This is due to increased concentrations of HSO_3^- and SO_3^{2-}. The solubility of SO_2 is not dependent on pH. At higher values of pH, virtually all of the S(IV) is in the form of SO_3^{2-}, whereas at low pH S(IV) is in the form of $SO_2 \cdot H_2O$.

Oxidation of dissolved S(IV) to sulphate (SO_4^{2-}) is an important route for forming atmospheric sulphate, and thus can play an important role in the behaviour of atmospheric ammonia. The main species involved in the oxidation of dissolved S(IV) are ozone (O_3), hydrogen peroxide (H_2O_2), and oxygen (O_2). Also, some metal ions may act as catalysts for the oxidation process.

For O_3, there is a different rate of reaction for each of the sulphur species in S(IV). The largest rate of reaction occurs with SO_3^{2-}, followed by HSO_3^-, and with SO_2 having the lowest value. This means that oxidation by ozone will decrease with a reduction of the pH since this will force S(IV) to be dominated by SO_2 and concentrations of HSO_3^- and SO_3^{2-} will be reduced significantly. Conversely, increasing the pH will lead to a large increase in sulphate formation.

Hydrogen peroxide is generally accepted to react mainly with HSO_3^-. The rate of reaction is fairly constant for the pH range from 2 to 6, but will drop off at higher values due to decreased concentrations of HSO_3^-.

Metal cations, specifically Fe^{3+} and Mn^{2+}, will act as catalysts for the oxidation of S(IV) by O_2. These reactions also increase with higher pH.

The oxidation of SO_2 to SO_4^{2-}, is strongly dependent on pH, with an increased reaction at higher values. Thus inclusion of ammonia into the reactions will have such an effect, leading to an increase in the concentration of SO_4^{2-}, and thus an increase in the conversion of NH_3 to $(NH_4)_2SO_4$.

3.4 Vertical dispersion in the atmosphere

The vertical dispersion of atmospheric material is one of the most important processes that affects airborne pollutants. In the case of SO_2 emissions from a tall chimney stacks, the amount of vertical mixing that occurs is important in determining when the plume comes into contact with the ground. Contact with the surface is necessary for dry deposition to take place. If vertical mixing is

very weak, such as at nighttime, this may extend the average residence time of the material and enable it to be transported over a long distance. In the case of ammonia, the amount of vertical mixing that occurs is crucial is determining how much of the emissions are dry deposited locally, and how much are transported over long distances.

Parameterisation of this process in an ATM has been implemented using a number of different schemes. One such scheme used by the EMEP model (Barrett and Seland, 1995), HARM (Metcalfe *et al.,* 1995), which was discussed in section 2.4, is the assumption of instantaneous mixing. This treatment is computationally cheap as it assumes that there is just one vertical layer in the model and all material is distributed throughout this layer. Whilst this process works well for some chemical species, such as SO_2, it was shown (section 2.4) that it is inadequate to deal with the short-range transport of NH_3 due to the low-level nature of the emissions.

A more detailed description of vertical mixing is employed by the TREND model (Asman and van Jaarsveld, 1992). This is based on the Gaussian plume formulation for dispersion from a point source. This formulation assumes that close to the source, the distribution of material can be described by use the classic Gaussian distribution formula from statistical theory.

$$\eta = Cexp(-A\xi^2) \tag{3.53}$$

where A and C are constants.

This can be expanded to a two dimensional representation of the concentration field, at coordinates (x,y,z) downwind of a source, by adapting the above equation to

$$\chi = Cexp(-Ay^2)exp(-Bz^2) \tag{3.54}$$

where A, B and C are parameters which need to be determined from initial and boundary conditions.

The TREND model uses this parameterisation for vertical mixing, and assumes that the plume is reflected only once at the Earth's surface and the top of the mixing layer. At larger distances from the source, all material is assumed to have a homogeneous distribution throughout the mixing layer, apart from near the surface where depletion due to dry deposition takes place.

In some of the most recent acid deposition models created (TERN, ApSimon *et al.,* 1994; ACDEP, Hertel *et al.,* 1995), multiple vertical layers are used. Vertical dispersion is modelled by the transfer of material between adjacent layers, the rate of transfer being dependent on atmospheric stability. In both of these models, vertical mixing is described using K-theory eddy diffusivity, with the exchange of material between layers determined by the equation

$$\frac{\partial \chi}{\partial t} = \frac{\partial}{\partial z}\left(K_z \frac{\partial \chi}{\partial z}\right) \tag{3.55}$$

where χ is the concentration of the species under consideration. Determination of K_z is dependent on height and atmospheric stability. The ACDEP model has 10 vertical layers, with the bottom of the layers at 2 m, 25 m, 138 m, 343 m, 591 m, 858 m, 1136 m and 1420 m. The top of the model domain is 2 km. The vertical structure in the TERN model is even more detailed, with 33 vertical layers, of variable depth, with the bottoms at 1 m, 2 m, 4 m, 6 m, 10 m, 25 m, 50 m, 75 m, 100 m, 150 m, 200 m, and thereafter in 100 m steps up through the mixing layer. This is shown in Figure 4.1.

This detailed vertical structure in the TERN model is a result of it being created as an NH_3 specific model. It was used by ApSimon *et al.* (1994) to study the dependence of long-range transport of NH_3/NH_4^+ on diurnal variations in the boundary layer, emission and deposition processes. The authors compared measured data of vertical concentrations, which were recorded on the Cabauw mast in the Netherlands (Erisman *et al.,* 1988), with modelled concentrations for a nearby location. The modelled data showed similar characteristics to the averaged daytime profiles presented by Erisman *et al.* (1988).

The TERN model incorporates a detailed chemical scheme, both gas phase and aqueous (cloud) phase. As a starting tool for this project, TERN has many of the necessary physical and chemical parameterisation in place which can be used as a basis with which to create a statistical atmospheric transport model. The following chapter will outline the necessary work requires to adapt TERN for the required task of developing a statistical ATM of NH_3 for Great Britain, and will feature some testing and evaluation of the model to assess its accuracy.

Chapter 4

Construction of an Atmospheric Transport Model to Describe the Emission, Transport and Deposition of Ammonia over Great Britain

In this chapter, a description is given of the basic structure of the TERN model. The assumptions used by the model are analysed and any major areas of inaccuracy are discussed. A simple test model is presented, and the results from this model are assessed. Subsequent sections of this chapter discuss the major work involved in order to convert TERN into a statistical atmospheric transport model, and discuss any assumptions that are made.

The TERN (Transport over Europe of Reduced Nitrogen) (ApSimon *et al.*, 1994) model was chosen to form the basis for a statistical atmospheric transport model of NH_3 for Great Britain. TERN is a single trajectory Lagrangian model which describes the main atmospheric processes taking place in a column of air extending from ground to a maximum height of 2500 m. Much of the input data used by TERN was stored in an external data file which the model accessed while it was being used. The data file contained information on the trajectory coordinates, ground level temperature, relative humidity, rainfall, cloud cover, cloudbase height, wind speed, and depth of the atmospheric boundary layer. The main content of the model was concerned with solving the chemical and physical equations that describe the behaviour of the pollutants inside the modelled air

column.

The motivation for the creation of TERN was the need to investigate the main factors which determine the atmospheric behaviour of ammonia. These include vertical dispersion, chemical conversion to ammonium aerosol via dry or cloud processes, and removal from the atmosphere by dry and wet deposition. Previous modelling work (MARTA model, Kruse-Plass *et al.,* 1993) had shown how the uptake of NH_3 into clouds could greatly affect the rate of SO_2 oxidation and subsequent creation of NH_4^+ aerosol. Other such work (Hov *et al.,* 1994) describes how the the atmospheric lifetimes and transport distance of NH_3 and NH_4^+ in the atmosphere are dependent on the emissions of SO_2 and NO_x. Reduced emissions of SO_2 and NO_x meant that less NH_4^+ aerosol was formed and thus more NH_3 was dry deposited.

TERN was employed by ApSimon *et al.* (1994) to investigate the behaviour of ammonia in the atmosphere, and how this was affected by altering various parameters. These included the type of vertical mixing scheme used by the model, the rate of SO_2 oxidation to SO_4^{2-}, the assumption of a diurnal cycle in NH_3 emissions and the use of a diurnally varying deposition velocity versus a temporally-constant value. Results from this study showed how the residence time of NH_3 is strongly dependent on the type of vertical mixing scheme, with the assumption of instantaneous mixing resulting in much less dry deposition than occurred with the use of the multi-layered process using K-theory eddy diffusivity (section 3.4). Comparison of modelled NH_3 vertical concentration profiles (using multi-layer mixing) with measured data (Erisman *et al.,* 1988) gave a fairly good agreement. The study also reported how the long-range transport of reduced nitrogen is greatly dependent on rate of conversion to NH_4^+ aerosol, and thus the chemical scheme used by a model is also a major factor is determining its accuracy.

4.1 Description of the TERN model

The vertical structure of the model consists of 33 layers, of variable depth, with the bottoms at 1 m, 2 m, 4 m, 6 m, 10 m, 25 m, 50 m, 75 m, 100 m, 150 m, 200 m, and thereafter in 100 m steps up through the atmospheric boundary layer.

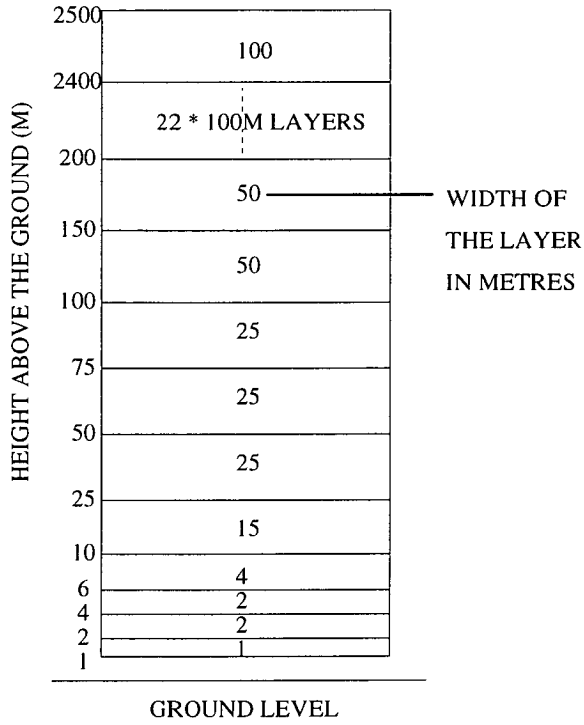

Figure 4.1: Vertical structure of the TERN atmospheric transport model.

This is illustrated in Figure 4.1. The bottom of the modelled air column 'floats' 1 m above the ground.

The method of vertical mixing, as mentioned in section 3.4, is by way of transfer of material between adjacent layers. The rate of transfer is determined by the diffusion equation

$$\frac{\partial \chi}{\partial t} = \frac{\partial}{\partial z}\left(K_z \frac{\partial \chi}{\partial z}\right) \tag{4.1}$$

where χ is the concentration of the species under consideration, and K_z is the vertical diffusivity. In the model, K_z has a linearly increasing value up a specified height H_z and then remain constant (K_{max}) up the top of the boundary layer (Figure 4.2). ApSimon *et al.* (1994) chose this profile to be consistent with a similar scheme used by Maul (1978). Although a more complex profile could have been used, it was not felt by ApSimon *et al.* to be justified, in view of the uncertainties in the diffusivity and the desire to keep the model simple in order to interpret the results.

The determination of K_z and H_z is reported by ApSimon *et al.* (1994) and is

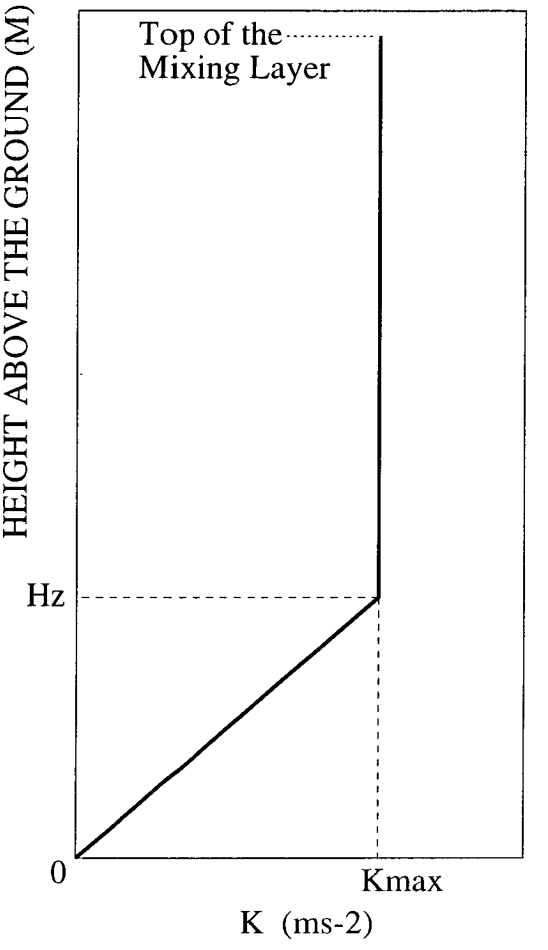

Figure 4.2: Vertical profile of the diffusion parameter K_z used by the TERN model to describe vertical mixing. H_z is the height at which K_z attains its maximum value.

reproduced here as follows:

During the Day:

Diffusivity depends on a combination of mechanical and convective mixing. The diffusivity adopted was chosen according to

$$K_{max} = max(A, B) \tag{4.2}$$

where A and B are prescribed below (subject to a maximum of 100 $m^2\ s^{-1}$), and H_z is taken as 200 m.

(i) A=0.55 $\times$ 10^{-3} $\times$ $\mathbf{H}^{\frac{1}{3}}$ $\times$ $H_{mix}^{\frac{4}{3}}$ corresponding to convective mixing, where H_{mix} is the modelled depth of the boundary layer (see section 4.3.3 for

Wind speed (ms^{-1})	Cloud cover	Pasquill class	H_z (m)	K_{max} (m^2s^{-1})
$G \leq 6$	{ cc $\leq \frac{3}{8}$	F	75 m	$0.09G$
	{ cc $> \frac{3}{8}$	E	100 m	$0.4G$
$6 < G < 10$	{ cc $\leq \frac{3}{8}$	E	100 m	$0.4G$
	{ cc $> \frac{3}{8}$	D	150 m	$0.016G^2$
$G \geq 10$		D	150 m	$0.016G^2$

Table 4.1: Nighttime diffusivity parameterisation based upon geostrophic wind speed and cloud cover. G is the geostrophic wind speed which is represented in the model by the advection speed of the modelled air column and cc is the cloud cover. K_{max} is the maximum value of K_z which occurs in the atmospheric boundary layer above the height H_z. The fractional cloud cover is represented by cc. ApSimon *et al.* (1994).

more detail), and **H** is the upwards heat flux into the atmosphere, using the incoming solar radiation $\mathbf{S_t}$ (section 3.1.2, equation 3.11) with a cloud factor value C_f (Table 3.2, section 3.1.2), to get

$$\mathbf{H} = 0.4(\mathbf{S_t} - 100)C_f \tag{4.3}$$

(ii) B= 0.16 G^2 (G is the geostrophic wind speed in the boundary layer) corresponding to mechanical mixing in stronger wind, thermally-neutral conditions. Over the sea, K_{max} is taken as proportional to the square of the depth of the boundary layer, this being proportional to geostrophic wind speed but corresponding to a reduced surface roughness (see ApSimon *et al.*, 1984).

The description of the nighttime diffusion profiles is given is Table 4.1.

Emissions of SO_2 and NO_x are uniformly distributed over the lowest 300 m to reflect emissions at different heights from domestic and low-level sources to tall stacks of power stations. In contrast, NH_3 emissions are introduced into the first layer, near the surface. Dry deposition is modelled by the use of species-specific deposition velocities (equation 3.2, Table 4.2), and material is removed from the lowest layer in the air column.

Species	V_d (1 m) (m s^{-1})
SO_2	0.008
SO_4 all forms	0.001
NH_3	0.01
NH_4^+ aerosol	0.001
PAN	0.01
NO	0.000
NO_2	0.001
NO_3^- aerosol	0.001
HNO_3	0.01

Table 4.2: The main dry deposition velocities used by the TERN model, though several other options are available for analysis purposes. ApSimon *et al.* (1994).

Wet deposition is calculated with a washout rate dependent on a specified rainfall rate, and material is washed out from all layers in the column at a rate dependent on concentration. The washout coefficients used are listed in Table 4.3. They are equal to the washout ratios used in the EMEP model (Barrett and Seland, 1995) with an air column 1000 metres deep and constant concentrations are assumed.

The dry chemistry scheme of the model is set up as described in Table 3.10. Creation of NH_4^+ occues due to reactions of NH_3 with H_2SO_4 and HNO_3. This chemical scheme is almost identical to that used by the EMEP model 3.3.1, which has been extensively tested and evaluated over the last decade, and is used to evaluate the effect of international treaties on emission reductions. In addition, TERN contains a detailed description of aqueous phase chemistry, as outlined is section 3.3.3. This scheme was first used in the MARTA model (Kruse-Plass *et al.,* 1993), to look at the processes of in-cloud oxidation of SO_2 to H_2SO_4 in a simulation of a measured pollution event. The results of this study showed how the rate of oxidation in clouds can be much higher than in just dry sunny conditions with no aqueous reactions, and that the more complex, aqueous reactions are just as important as the linear reactions of modelled gas phase chemistry.

A testing and evaluation of results produced by the TERN model, with an emphasis on the vertical dispersion scheme, is presented in section 5.1. Mod-

Species	λ (s^{-1})
SO_2	1.1×10^{-5}
SO_4 all forms	4×10^{-5}
NH_3	5.7×10^{-5}
NH_4^+ aerosol	4×10^{-5}
PAN	0.0
NO	0.0
NO_2	0.0
NO_3^- aerosol	4×10^{-5}
HNO_3	5.7×10^{-5}

Table 4.3: Scavenging coefficients (λ) used by the TERN model to calculate wet deposition, based on an annual rainfall of 1000 mm. ApSimon *et al.* (1994).

elled data are compared with measurements, and an assessment of the model's performance is given.

4.1.1 Discussion of the limitations of the TERN model

Whilst the TERN model contains detailed descriptions of vertical dispersion, atmospheric chemical reactions and deposition processes, it has a number of limitations which should be listed and discussed.

One of the main drawbacks is one that is inherent in most, if not all, Lagrangian-type models that are used for the study of atmospheric dispersion. This concerns the lack of vertical wind shear in the modelled air column, which is especially important close to the surface where large vertical gradients can occur. Since all model layers are advected with the same speed (in the case of TERN it is the geostrophic wind speed in the boundary layer), it means that the lowest layers of the model will actually spend a reduced amount of time over an emissions areas. Whilst this may not be important over a large emission area where some type of quasi-equilibrium may be reached, in the very short range this assumption may lead to some inaccuracies. This is especially important for ammonia since a significant proportion of it may be dry deposited in the close vicinity of the source.

Part of the problem of vertical shear was addressed in the dry deposition model

discussed in section 3.1. Values of V_d are calculated using surface wind data measured at a height of 3 m, and thus a much better approximation of the turbulence parameter u_* can be estimated than if the geostrophic wind speed had been used.

Another possible source of error is the lack of lateral horizontal dispersion. As material is advected away from a source, it is dispersed both vertically and laterally. The lack of explicit lateral dispersion in the air column could cause possible over-estimation of concentrations, and this inaccuracy will increase further downwind. The ACDEP model (Hertel *et al.*, 1995) attempted to address this problem by decreasing the horizontal area of the air column as it nears the receptor point. This accounts for the reduction in the area of emissions that will affect concentrations at a site as the distance between the air column and the site decreases. This problem is addressed later in this chapter by running the model with a wide spread of trajectories which originate from different wind directions to take some account of the horizontal dispersion problem. Since ammonia has a short residence time in the atmosphere, it is thought that this problem of horizontal dispersion will not be as important as it would be with the long-range transport of sulphur and its derivatives.

4.2 Construction of a simple atmospheric transport model

In this section, work is described on the creation of a simple model to simulate the atmosphere transport of ammonia over Great Britain. The motivation behind this work was to create a number of computer routines which would later enable the single trajectory model TERN to become a statistical atmospheric transport model which could produce maps of NH_3 concentration and dry deposition across Great Britain. To allow testing and evaluation of these routines, a model was created which describes the main atmospheric processes, but at the same time is not computationally intensive. This allowed the routines to be thoroughly tested, and make them ready for combination with the TERN model. This procedure is described in the final section of this chapter.

4.2.1 A description of the model

The test model, referred to as the Reduced nitrOgen Deposition MODel (RODMOD), is a simple atmospheric transport model which consists of a column of air, representing the atmospheric boundary layer, being transported across Great Britain. It deals with the emission, transport, and dry deposition of NH_3 in the atmosphere. The main setup of the model is similar to HARM (Metcalfe *et al.,* 1995), with a constant boundary layer depth of 800 m and a constant uniform wind speed of 10.4 m s^{-1} throughout the air column, so there is no vertical wind shear. Emissions from the ground are assumed to be instantaneously well mixed throughout the air column, which results in a uniform vertical concentration profile throughout the mixing layer. The emissions data used is the official NH_3 data for Great Britain (RGAR, 1996; Dragosits *et al.,* 1996), applied on a resolution of 20 km grid squares, as shown in Figure 2.4.

Removal from the atmosphere is by way of dry deposition only, with the use of deposition velocities. NH_3 is the only chemical species in the model, and thus there are no chemical reactions.

The modelled column of air is horizontally advected cross Great Britain from 24 equally-spaced wind directions. The concentration of NH_3 is assumed to be zero at the start of a trajectory. An overall average map of air concentrations and dry deposition are produced by statistically combining the results from each wind direction with the probability of a wind originating from a certain direction. The wind data are taken from a study of wind trajectories (Jones, 1981), which are representative of wind data measured at a height of 400 m. These data were originally extracted from a database used by the MESOS model (ApSimon *et al.,* 1984) to look at the transport of radioactive debris over long distances. Unclassified wind trajectories, such as cyclonic and anti-cyclonic winds, are ignored by Jones (1981).

The landuse database, described in section 2.2.1, is used, and each landuse category has a specific deposition velocity assigned to it. The six velocities (for the five land-surface classes and sea) are listed in Table 4.4 (M.A. Sutton, 1995. Pers Comms; Sutton *et al.,* 1994). The values of V_d represent the overall 'effectiveness' of the specified surface class to be a recipient for NH_3 dry deposition, and are

LandClass	V_d (m s^{-1})
Arable	0.003
Grassland	0.01
Moorland	0.02
Forest	0.03
Urban	0.004
Sea	0.004

Table 4.4: Land-dependent values of V_d used by RODMOD. (M.A. Sutton, Pers Comms).

meant to be preliminary values for use in testing of the model. To calculate the dry deposition in a square consisting of several surface classes, each surface class is initially considered independently. The deposition flux is calculated for a grid square assumed to consist of 100% of a specific surface class. This is done for each of the five land-surface classes and the same procedure is also performed for dry deposition to sea areas. The calculated dry deposition flux for each surface class are then combined using the following equation to work out the total deposition flux ($\{F_d\}_T$) to the grid square,

$$\{F_d\}_T = \sum_{i=1}^{6} \{\{F_d\}_i \cdot \mathbf{R}_i\} \tag{4.4}$$

where $\{F_d\}_i$ is the deposition flux for each surface class i, and $\mathbf{R}_i$ is the fraction of the grid square which is occupied by surface type i.

The governing differential equation for the model is

$$\frac{d\chi}{dt} = \frac{F_e}{H_{mix}} - \frac{\chi \cdot V_d}{H_{mix}} \tag{4.5}$$

where χ is the concentration of NH_3, H_{mix} is the depth of the modelled boundary layer (m) and F_e is the emission flux of NH_3. The solution of equation 4.5 for a time period Δt is

$$\chi_{(T_0+\Delta t)} = \chi_{(T_0)} \cdot exp\{-\frac{V_d \cdot \Delta t}{H_{mix}}\} + \{1 - exp\{-\frac{V_d \cdot \Delta t}{H_{mix}}\}\} \cdot \frac{F_e}{V_d} \tag{4.6}$$

where $\chi_{(T_0)}$ and $\chi_{(T_0+\Delta t)}$ are the concentrations at times T_0 and $T_0 + \Delta t$ respectively. If the air column enters the grid square at time T_0 and exits at a later

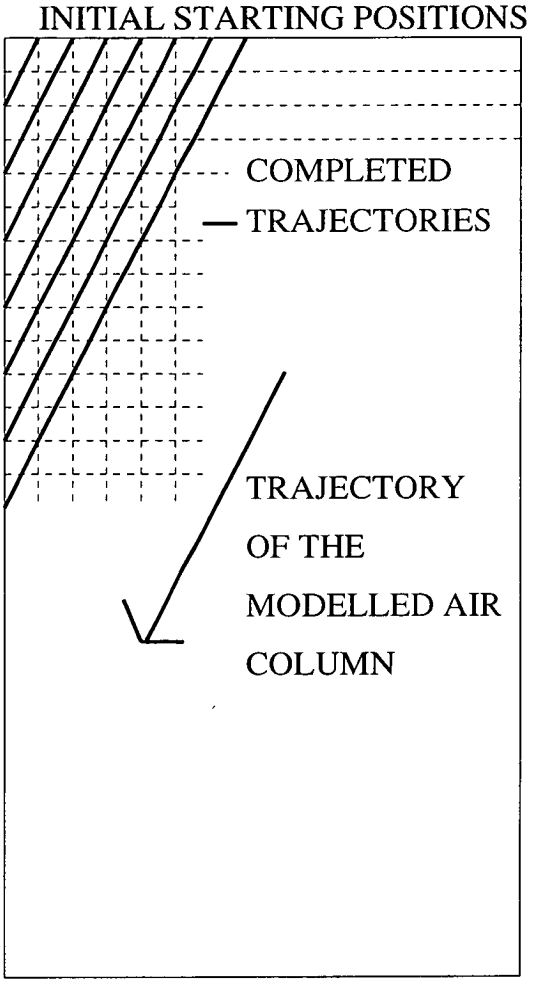

Figure 4.3: Diagram of the straight line trajectories used to model the horizontal advection of the air column across the model domain.

time $T_0 + \Delta t$, then equation 4.6 can be used to calculate the dry deposition to the grid square. Since the model is mass consistent, the change in concentration over a time period Δt is equal to the change due to emissions minus the change due to dry deposition (F_{dTOT}).

$$\Delta\chi = \frac{F_e \cdot \Delta t}{H_{mix}} - \frac{F_{dTOT}}{H_{mix}} \tag{4.7}$$

Assuming that the model takes a time period of Δt to traverse a grid square, the resultant dry deposition to that grid square is given by equation

$$F_{dTOT} = F_e \cdot \Delta t - \Delta\chi \cdot H_{mix} \tag{4.8}$$

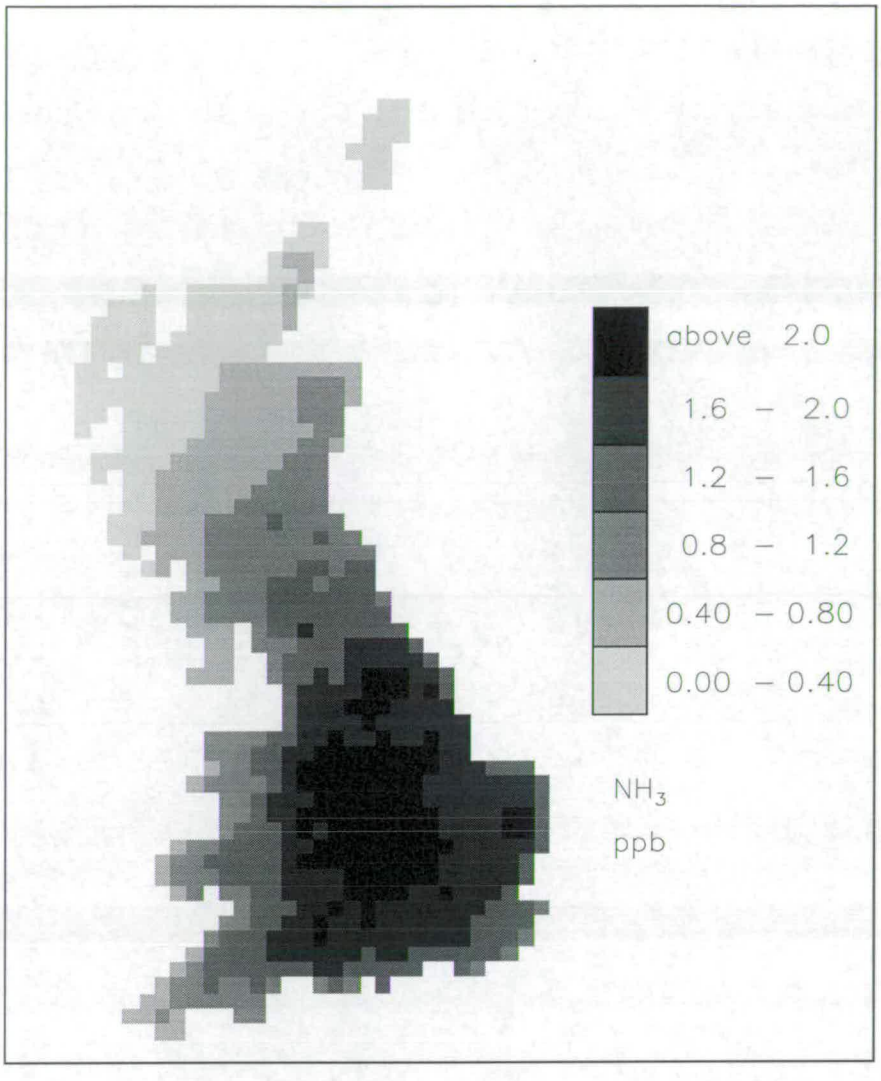

Figure 4.4: Annual average concentration field of NH_3 for Great Britain from ROD-MOD. Units are ppb.

The simulated air column is transported across the Great Britain along a series of straight line trajectories. Each trajectory has an initial position which is changed as a trajectory is completed. This enables the model to cover the entire map of Great Britain with a set of adjacent and parallel trajectories such that each grid square on the map is crossed only once by any one trajectory for a particular wind direction (Figure 4.3). A detailed description of the trajectory scanning routines is given in Appendix A.

The time spent in each grid square is determined by the advection speed, the trajectory angle with respect to the grid and the dimension of the grid square. When the entire grid is covered with trajectories, the angle is incremented by 15°

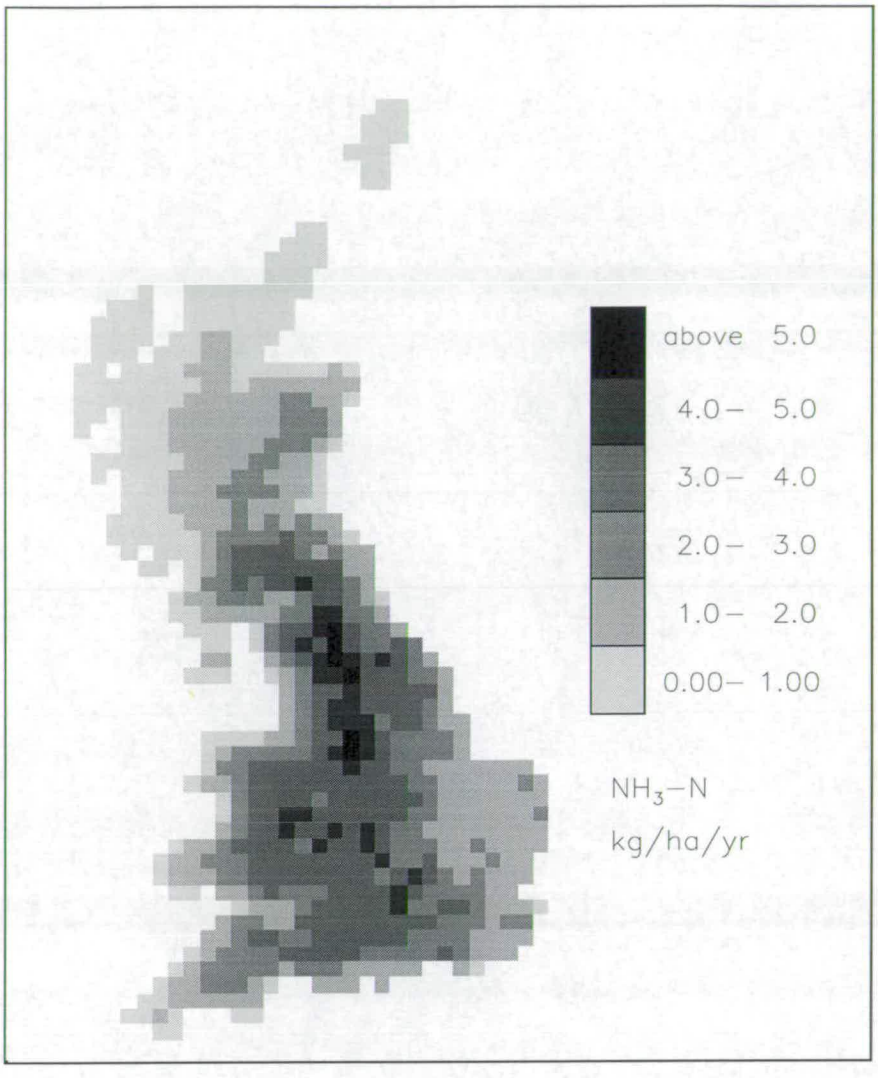

Figure 4.5: Annual dry deposition field of NH_3-N for Great Britain from RODMOD. Units are kg ha^{-1} $year^{-1}$.

so that the model domain is eventually crossed by trajectories originating from 24 equally-spaced directions on the compass. The deposition to a grid square for each trajectory angle is multiplied by the wind frequency probability, to give an overall average deposition map. This process is also done for the concentration calculations to give an average concentration field for Great Britain.

4.2.2 Results and discussion

The concentration field of NH_3 produced by RODMOD is shown in Figure 4.4. The area of maximum concentrations occurs over central England, with values exceeding 2.0 ppb. Horizontal concentration gradients are very low across all

of Britain, due to the assumption of instantaneous mixing. The absence of any chemical reactions will affect regional air concentrations, since the conversion of NH_3 to NH_4^+ aerosols would have led to a substantial reduction of NH_3 concentrations.

The spatial distribution of dry deposition of NH_3-N predicted by RODMOD is shown in Figure 4.5. The maximum dry deposition occurs in northern England (Pennines), where modelled deposition velocities are relatively large. The assumption of instantaneous mixing, no chemical conversion and no wet deposition also increases the atmospheric lifetime of NH_3, allowing large deposition fluxes to occur in remote areas far from areas of large emissions, such as northern Scotland.

The annual dry deposition for the country is 56.6 Gg NH_3-N $year^{-1}$. This means that out of the annual emission flux of 281.4 Gg of NH_3-N $year^{-1}$, nearly 225 Gg of NH_3-N $year^{-1}$ is exported from Great Britain.

Creation and testing of RODMOD allowed a number of computer routines to be written and tested. These routines were created in order to fulfill the following requirements. The simulated column of air must be advected along straight line trajectories which would traverse a model domain containing the entire land area of Great Britain. This domain would be covered by an overlaying grid containing squares of defined dimensions. The entire grid must be covered by adjacent and parallel trajectories such that each grid square is covered by only one trajectory, for a certain wind direction. The routines must allow the trajectories to originate from various directions on the compass, and be able to combine the results accordingly, dependent on wind frequency data. These routines would be combined with the core code of the TERN model to create a new statistical atmospheric transport model. The initial resolution of the model would be on 20 km grid squares, to allow testing and evaluation of the model (Chapter 5). Further work would enhance this resolution to a 5 km $\times$ 5 km grid, allowing detailed data maps to be produced (Chapter 6).

4.3 Conversion of TERN to a statistical multi-trajectory model

Once the computer code for the trajectory scanning technique used by RODMOD had been written and tested, the next major step was to insert the TERN model into these routines. Thus the simple atmospheric process described in equation 4.5 were replaced by the much more complex descriptions of vertical mixing and chemical reactions. This new statistical atmospheric transport model was named FRAME (Fine Resolution AMmonia Exchange) to reflect the application of the model to a 5 km $\times$ 5 km grid resolution, which is much finer than has previously been done for Great Britain.

In addition to the emissions of NH_3 (RGAR, 1996; Dragosits *et al.,* 1996), emissions were required for sulphur dioxide and nitrogen oxides. These data were taken from the UK national emissions inventory (Eggleston, 1992b; see Figures 5.7 and 5.8).

Once integration of the TERN code had been achieved, there remained a number of major problems which needed to be solved, and these are listed below.

- Meteorological data: All of the required data used by the TERN model were contained in an external parameter file. The main data consisted of the ground level temperature, rainfall, cloud cover, cloudbase height, wind speed, and depth of the boundary layer. These data were very specific for a definite period of time and space, and thus were not applicable for use in the FRAME model, which is intended to describe long-term average behaviour. Thus it was necessary to define some type of long-term average description for these data.

- Initialisation of trajectory concentrations: The model domain is confined to cover an area containing Great Britain. This is due to the restriction on computing time imposed by the detailed vertical diffusion process. Results from the EMEP model (Barrett and Seland, 1995) show how a significant proportion of the deposition over Great Britain is due to material emitted in other countries. For oxidised nitrogen, an estimated 41% of the deposition is due to imported material. Imported sulphur accounts for 19% of the total

deposition, and for reduced nitrogen, this figure is 15%. Thus it is important to include the import of material from outside the British mainland in order to describe the spatial distribution of deposition as accurately as possible.

- Determination of the horizontal advection speed for the model: This is an important parameter for the model as it defines the amount of time that the air column spends over an emissions area. Detailed wind frequency data are available for a number of wind ranges, and it is important to assess how sensitive the model results are for various wind speeds.

- Depth of the modelled boundary layer: The depth of the boundary layer defines the maximum height below which vertical mixing will take place within the air column. Above this height, the atmosphere is assumed to be stable and no vertical transfer of material takes place. This depth will usually be below the maximum height of the modelled air column (2500 m), and thus there will almost always be some redundant vertical layers in the model above this height in which no vertical exchange will occur. It is important to describe this phenomenon well since the time taken to traverse an average trajectory of 600 km in length, with a wind speed of 7.5 m s^{-1}, is 22 hours. Thus the diurnal cycle plays an important role is determining the behaviour of pollutants in FRAME.

- Computing time: The detailed treatment of vertical dispersion in the TERN model requires a very small timestep to be used. In the application of TERN to study trajectories over Europe (ApSimon *et al.,* 1994), the timestep used was 6 seconds. In comparison HARM employs a timestep of 2 minutes and the EMEP model uses a value of 15 minutes. In order to make the calculation time of FRAME as small as possible, various time saving measures were incorporated. These include the optimisation of the trajectory length, and allowing the timestep to vary, adjusting continuously to minimise computational error to a defined degree.

The following sections describe how these problems were dealt with and the improvements to the FRAME model that were brought about by these changes.

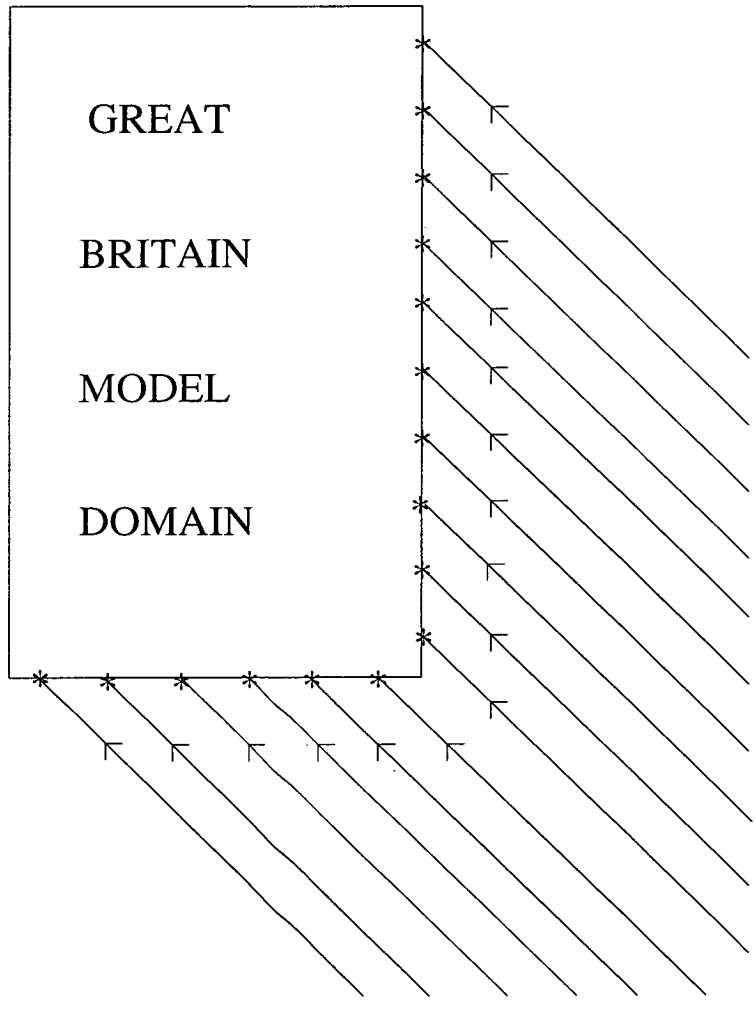

Figure 4.6: Diagram of the straight line trajectories used to model the horizontal advection of the air column across the model domain.

4.3.1 Initialisation of boundary concentrations

One way to implement the import of non-British pollutants would be to expand the domain of FRAME to include large areas of Europe, as has been done with other models such as HARM model for the UK (Metcalfe *et al.,* 1995) and the TREND model for the Netherlands (Asman and van Jaarsveld, 1992). In these models, runs are performed by moving trajectories across this expanded domain to designated receptor points. Thus, when the modelled air column arrives inside the required model domain, it will contain pollutants which originated from foreign sources.

Although this method would seem to be the most logical way to model the

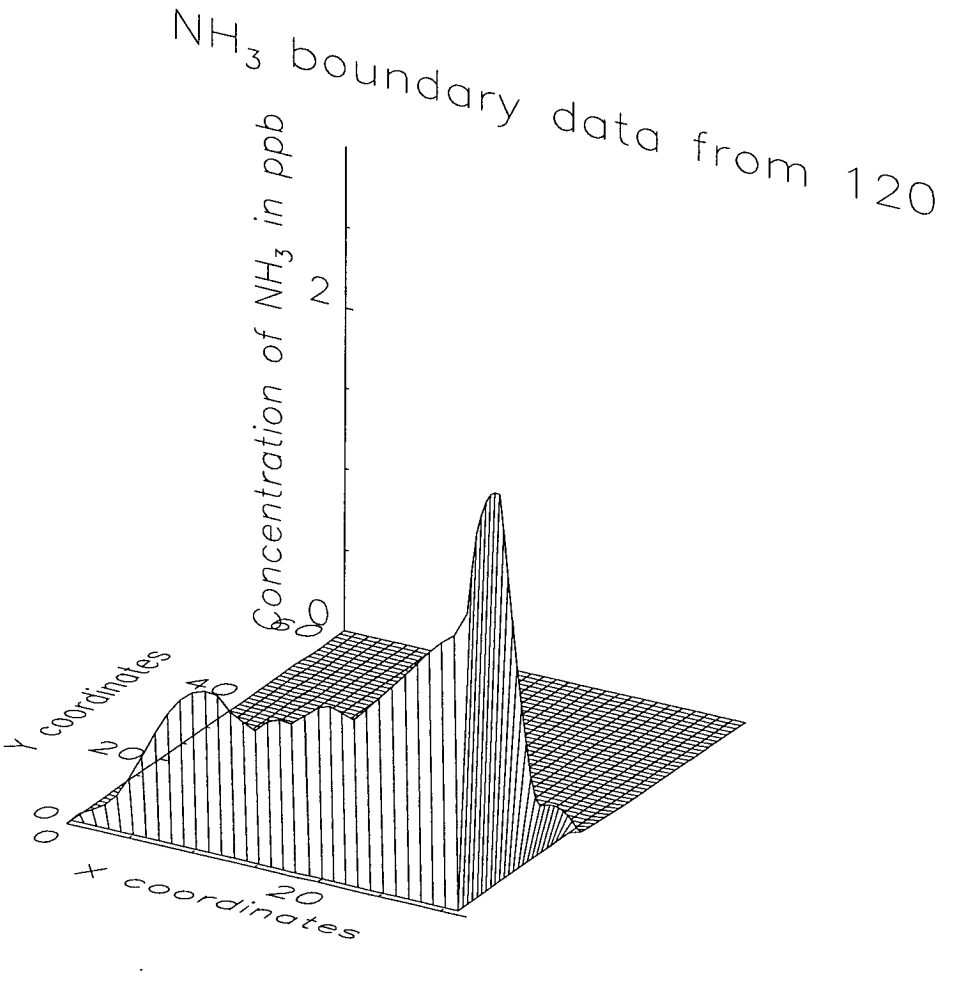

Figure 4.7: An example of the concentration boundary data used to initialise the trajectories in the FRAME model. These data represent NH_3 surface concentrations arriving from an angle of 120°. Units are ppb.

import of non-British pollutants, it was not feasible to implement it directly into FRAME in the same way. The problem was due to the excessive computational time which would result if the model domain was expanded to the European scale. One of the main reason for this is the multi-layer vertical diffusion scheme, which is solved by a computationally intensive fourth-order Runga-Kutta method.

A simpler way to model the transboundary import of foreign material was to create a set of vertical concentration profiles for the edge of the model domain, which would then be used to initialise the trajectories. To achieve this, the TERN model was adapted to traverse a series of 96 hour long trajectories which were set to terminate at the edge of the model domain (Figure 4.6). The multi-layer diffusion scheme was employed and a timestep of 6 seconds was used.

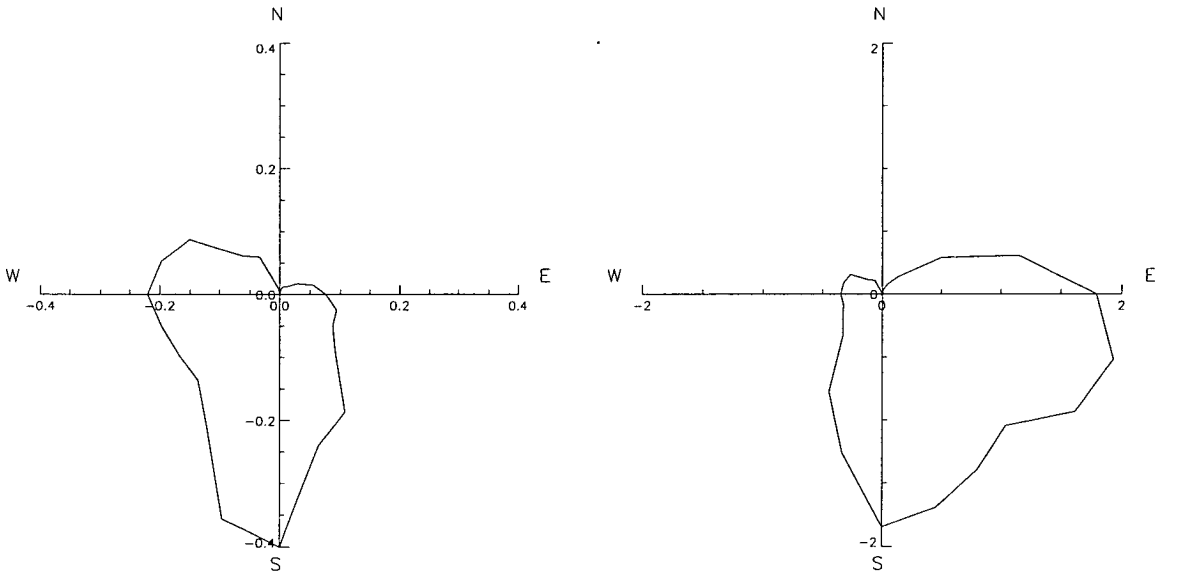

Figure 4.8: A summarised plot of the directionally-averaged imported mass of nitrogen below 2500 m (Gg trajectory^{-1} year^{-1}), in the form of (a) NH_3-N and (b) NH_4^+-N aerosol. This figure is representative for the entire model domain. The boundary data are used to initialise the trajectories of the FRAME model.

The receptor points for the trajectories were evenly spaced in 20 km intervals along the boundary. EMEP emissions data were employed on a 150 km × 150 km grid, and the advection speed was set at 10.4 m s^{-1}. This value was used in HARM to model the advection of pollutants over Europe, and thus would seem to be an appropriate choice.

The diurnal depth of the atmospheric boundary layer was determined by the method which is outlined in section 4.3.3. Rainfall was set at an average value of 1000 mm year^{-1}. Trajectories were set to arrive from 24 wind directions, 15° apart, and each trajectory was run for 4 separate times, 6 hours apart, and combined accordingly to get the 24-hour averaged concentration values. Boundary data were constructed for 4 equally spaced months of the year to reflect seasonal variability. All other parameterisation were set up as given in the description of TERN (section 4.1). Data files were created for every one of the 24 wind directions, and for each wind direction there was a separate datafile for each of the 11

chemical species in FRAME.

The simplicity of this scheme is that the program need only be run once to create these values, which can then to used any number of times to initialise the necessary model runs. However, the steady state conditions of the boundary data mean that running the model for very different conditions could not be incorporated in the boundary data, and this may prove to be a restriction on the model results. Figure 4.7 is an example plot of the spatial distribution of NH_3 surface concentrations along the domain boundary. The trajectories in this plot arrive at the boundary from 120°. The x and y coordinates refer to the spatial coordinates of the 20 km grid squares contained in the model domain. Even though the European emissions have a resolution of 150 km grid squares, the plot shows the maximum concentrations occurring in the south-eastern corner of the domain, due to high emissions areas occurring in the Netherlands.

A summarised plot of the boundary data is shown in Figure 4.8. This plot shows the average mass of NH_3-N and NH_4^+-N (Gg trajectory^{-1} year^{-1}) below 2500 m, which is imported by the model, and is representative for the entire model domain. A large amount of the imported NH_3 is from the south and west. Southern imports correspond to material being transported from mainland France and the Benelux countries, whereas the western fluxes are NH_3 originating from Ireland. Both of these areas are relatively close to Great Britain, and thus a large proportion of the emissions from these sources are still in the from of NH_3. In comparison, most of the imported NH_4^+ aerosol is from the east, southeast and south. This distribution reflects more the areas of both high NH_3 emissions and high SO_2 and NO_x emissions in continental Europe.

4.3.2 Determination of the horizontal advection speed for the model

The horizontal advection speed of the model is a very important parameter. It determines the length of time that the air column will take to traverse an emission area, and thus how much NH_3 is emitted into the air column. As was discussed earlier in this chapter (section 4.1.1), one of the main deficiencies of a multi-layer Lagrangian model is the lack of vertical wind shear. Other Lagrangian models (Barrett and Seland, 1995; ApSimon *et al.,* 1994; Metcalfe *et al.,* 1995) have used

Wind Sector	0-5 m s^{-1} (2.5)	5-10 m s^{-1} (7.5)	10-15 m s^{-1} (12.5)	> 15 m s^{-1} (20.0)	total
0-45	2.556	3.567	2.7	2.073	10.896
45-90	2.895	2.387	1.437	1.16	7.879
90-135	2.73	2.818	0.8571	0.23	6.6351
135-180	2.98	2.88	1.094	1.64	8.594
180-225	2.61	3.602	1.85	3.51	11.572
225-270	2.61	6.785	4.26	5.655	19.31
270-315	3.089	4.773	4	5.972	17.834
315-360	2.99	5.937	4.242	4.09	17.259
total	22.46	32.75	20.44	24.33	100.00

Table 4.5: A representative windrose for use in long-range dispersion calculations. The wind data are grouped into four categories and the units are m s^{-1}. The value in brackets in the representative value for each wind category. The data are the % wind frequencies of occurrence. Adapted from Jones (1981).

some form of the mean wind speed throughout the modelled boundary layer to advect the air column. The wind data for HARM are taken from a study of wind trajectories (Jones, 1981), which contains wind frequency data for wind speed categories and wind directions. These data comprise a representative windrose for the UK, and were measured at a height of 400 m. A summarised version of the dataset is shown in Table 4.5.

This table contains wind frequencies for a number of sectors and also for a range of wind speeds. Ideally the model should be used with all these data, and thus be run for a number of different wind speeds as well as directions. However this would be computationally expensive. A more convenient option would be to run the model for just a single speed for each direction. The most obvious choice would be to use the calculated mean wind speed values for each sector. These are shown in Table 4.6.

Due to the non-linearity of the model, it was necessary to perform first some sensitivity tests on the chosen wind speeds. This involved running the model for the four separate wind speeds groups shown in Table 4.5 and combining these results using the wind frequency data to create weighted-averaged results, hereafter known as the combined results. The model was then run using the mean wind speed and a comparison was made to see if the combined results were similar

Wind Sector	0-45	45-90	90-135	135-180	180-225	225-270	270-315	315-360
Mean speed	9.94	8.42	6.52	8.79	10.96	11.6	11.94	10.83

Table 4.6: Mean wind speed rose (m s^{-1}) calculated from the data of Jones (1981).

to the results produced using a mean speed. Twenty four sample trajectories were run. Each trajectory angle was separated by 15°, and the trajectories commence at various points along the boundary of the model domain, and were spread evenly around the perimeter. This was done to try and get as representative spread of trajectories as possible while minimising the number of trajectories due to computational time. There were 8 wind sectors, and each wind sector was given three trajectories so as to assess the results of individual trajectories and see whether there were any large variations between individual trajectories belonging to the same wind sector. Thus if results produced by each of the three trajectories, belonging to a certain wind sector, produced similar results, one could assume that the results could be extended to all trajectories run for that wind sector.

The results for ground-level concentration of NH_3 and dry deposition of NH_3-N from a sample of three of the trajectories are shown in Figures 4.9 and 4.10. These plots refer to trajectories being run across the British landmass on a 20 km × 20 km grid. The first trajectory was run from the north-east, across northern England. The second trajectory was across the east of England, with wind originating from the south-southeast. The third trajectory followed a path across western Scotland, northern England and East Anglia.

Analysis of these data showed that using a mean wind speed leads to an underestimation of both the surface concentration and dry deposition flux in comparison with the combined results. For each trajectory, the combined results were calculated by running the model for the 4 different wind speeds and combining them using the weighting coefficients. These coefficients are the wind frequency data for each wind sector (Table 4.5) divided by the sum of the wind frequencies

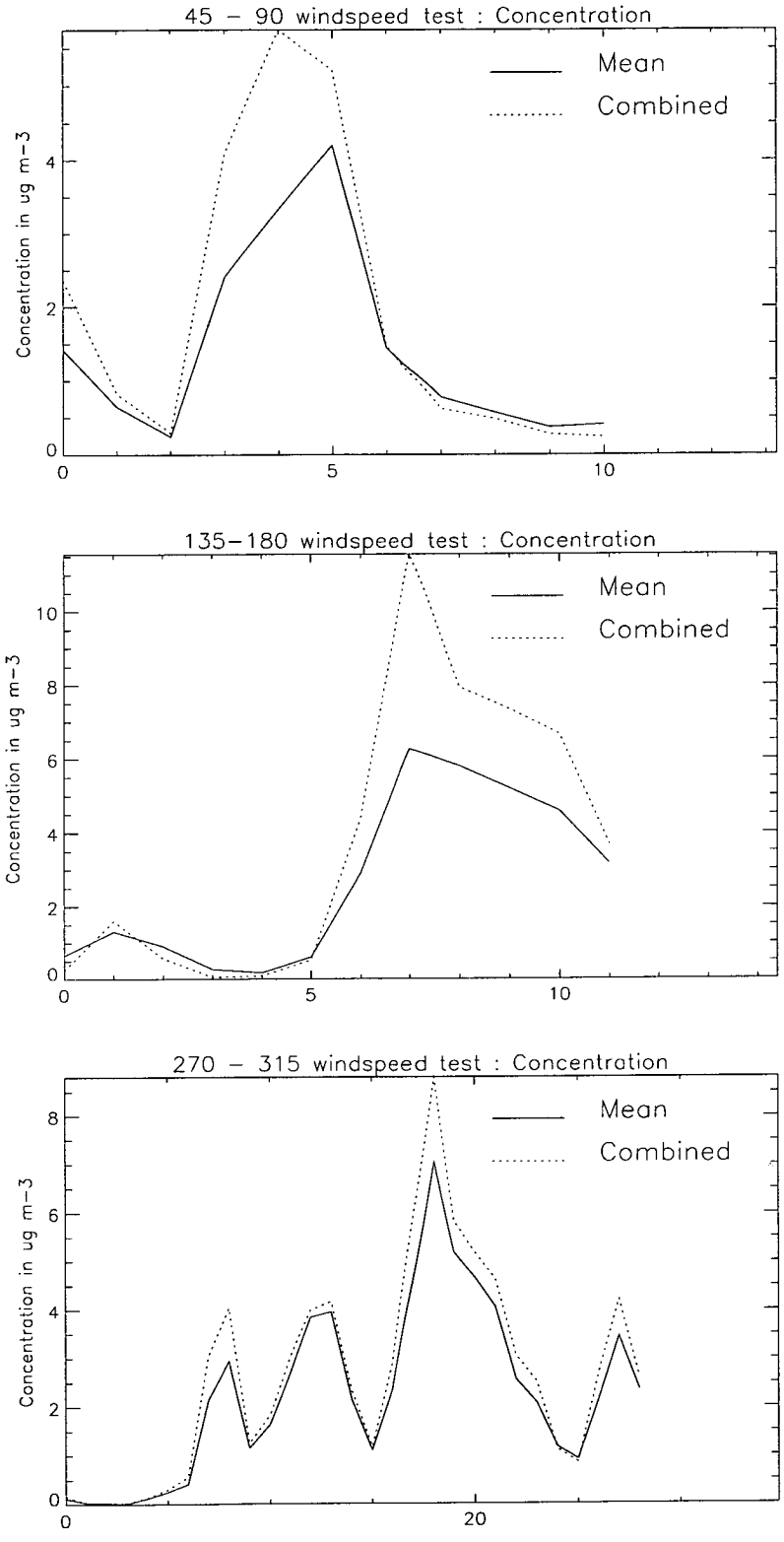

Figure 4.9: Comparison of NH_3 concentrations for the sample trajectories, using mean wind speeds, against the combined concentrations. The values on the x-axis for each plot represent the number of 20 km grid squares that the air column has traversed on the defined trajectory.

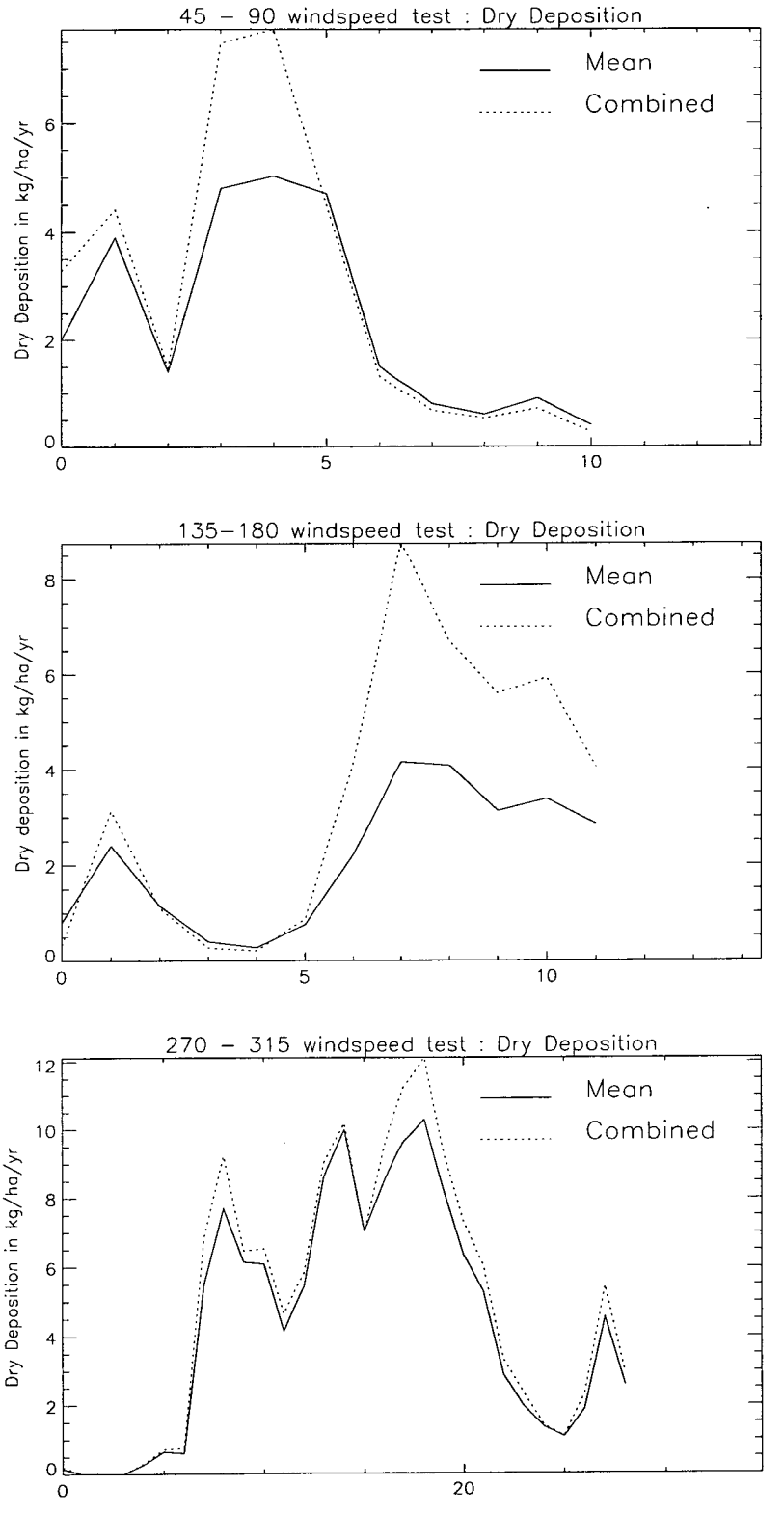

Figure 4.10: Comparison of NH_3-N dry deposition for the sample trajectories, using mean wind speeds, against the combined concentrations. The values on the x-axis for each plot represent the number of 20 km grid squares that the air column has traversed on the defined trajectory.

for the same wind sector. The differences in the results were large enough that it was considered unacceptable to use the mean wind speed as input data for the model.

A solution to this problem was to use the data from all of the sample trajectories and calculate a new wind speed for each wind sector which would give the best fit to the combined results. Since the sum of the weighted coefficients for each wind sector is 1.0, each combined result must lie somewhere in the range of results produced for each separate wind speed. It should be possible to find two wind speeds whose results bracket the combined result. Linear interpolation between these two wind speeds may be used to produce an optimised wind speed which in theory would produce results approximately close to that of the combined result.

As a hypothetical example, if we assume that the four weighting coefficients are α, β, γ and δ, then

$$\alpha + \beta + \gamma + \delta = 1.0 \tag{4.9}$$

There are four wind speeds a, b,c and d, which each respectively produce results A, B, C and D. Thus the mean wind speed is

$$\alpha a + \beta b + \gamma c + \delta d \tag{4.10}$$

and the combined result (W) is

$$\alpha A + \beta B + \gamma C + \delta D \tag{4.11}$$

The combined result lies somewhere within the range of the results A, B, C and D. If we assume that it actually lies between result A and result B then we can say that

$$W = \theta A + \lambda B \tag{4.12}$$

where

$$\theta = \left| \frac{W - B}{A - B} \right| \tag{4.13}$$

$$\lambda = \left| \frac{W - A}{A - B} \right| \tag{4.14}$$

and

$$\theta + \lambda = 1.0 \tag{4.15}$$

Thus the new optimised wind speed (o) was determined by linear interpolating between wind speeds a and b, resulting in

$$o = \theta a + \lambda b \tag{4.16}$$

To determine these new optimised wind speeds, interpolation procedures were carried out using concentration and dry deposition data from all the sample trajectories. For the concentration data, an optimised wind speed was calculated for each 20 km grid square along the trajectory, and then a mean value for the optimised wind speed was determined by dividing the sum of the optimised wind speeds by the total number of trajectory points.

The procedure for the dry deposition data was slightly different. In this case, a total integrated dry deposition flux was calculated for the entire trajectory. Thus the optimised wind speed would produce the same integrated dry deposition flux as the combined result.

For each trajectory, two optimised wind speeds were produced, one for dry deposition and one for concentration. These data were grouped into wind sectors and are shown in Table 4.7. Both sets of optimised values for dry deposition and concentration are less than their corresponding mean values. This is extremely interesting as it illustrates that low wind speeds have a greater effect on model results than high values. Using a low wind speed means that the air column spends more time over an emission area, and thus more NH_3 will be emitted into the atmosphere. Low wind speeds will reduce V_d (section 3.1), since the value of R_a and R_b (section 3.1.3) are dependent on the wind speed, and also the rate of vertical diffusion will be reduced. The consequence of all these effects is that air concentrations will be very large.

Since the ultimate aim of the project is to map dry deposition, it was decided that the optimised wind speeds calculated for dry deposition would be used in the model. The optimised wind speeds for concentration in Table 4.7 are generally slightly less than the corresponding values for dry deposition. This implies that the use of optimised wind speeds for dry deposition will predict lower concentrations than if optimised wind speeds for concentrations were used.

To assess the accuracy of the new wind data, the sample trajectories were run again using the new optimised wind speeds for dry deposition. The results from

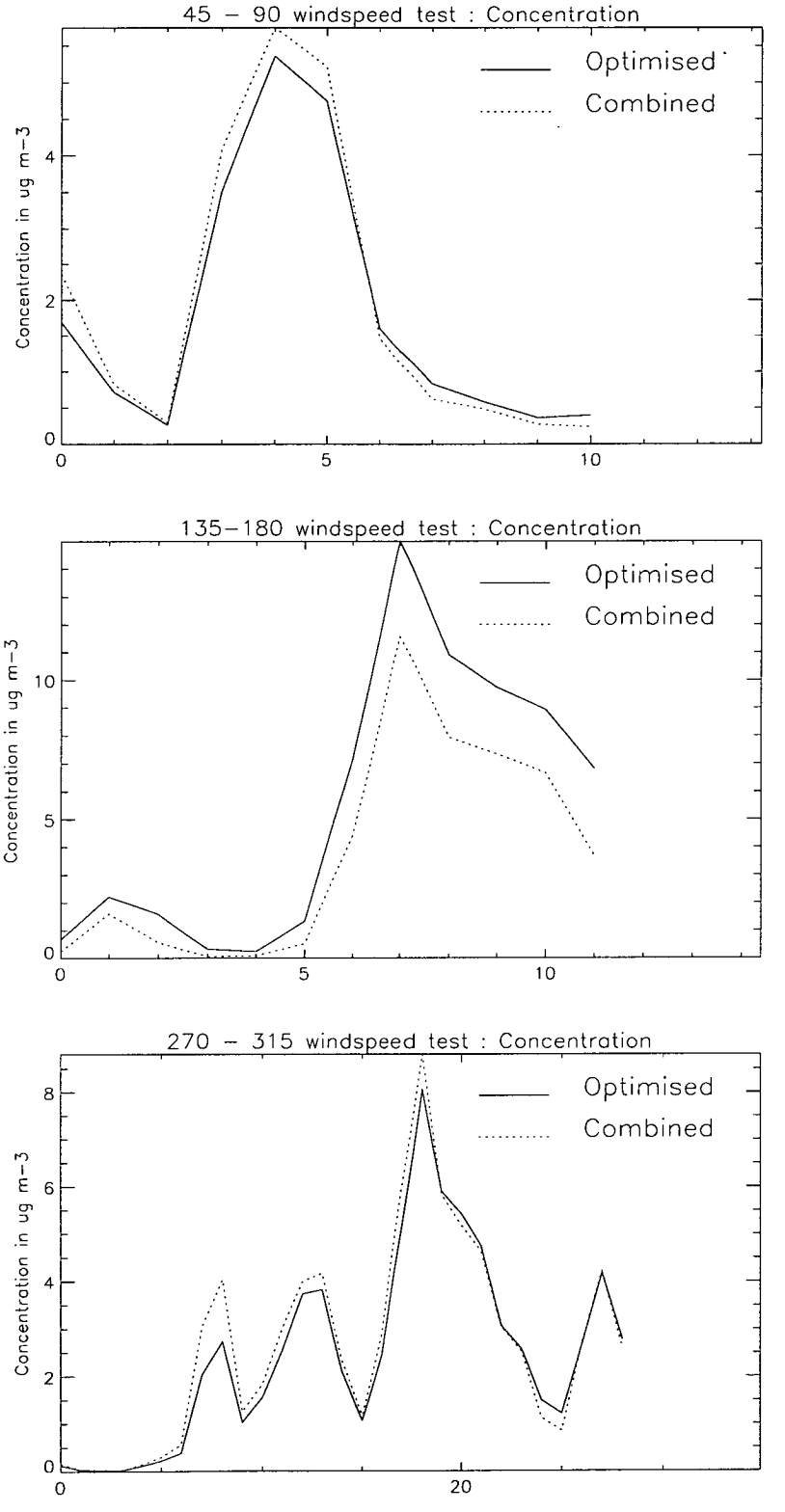

Figure 4.11: Comparison of concentrations using optimised wind speeds for dry deposition, against the combined results. The values on the x-axis for each plot represent the number of 20 km grid squares that the air column has traversed on the defined trajectory.

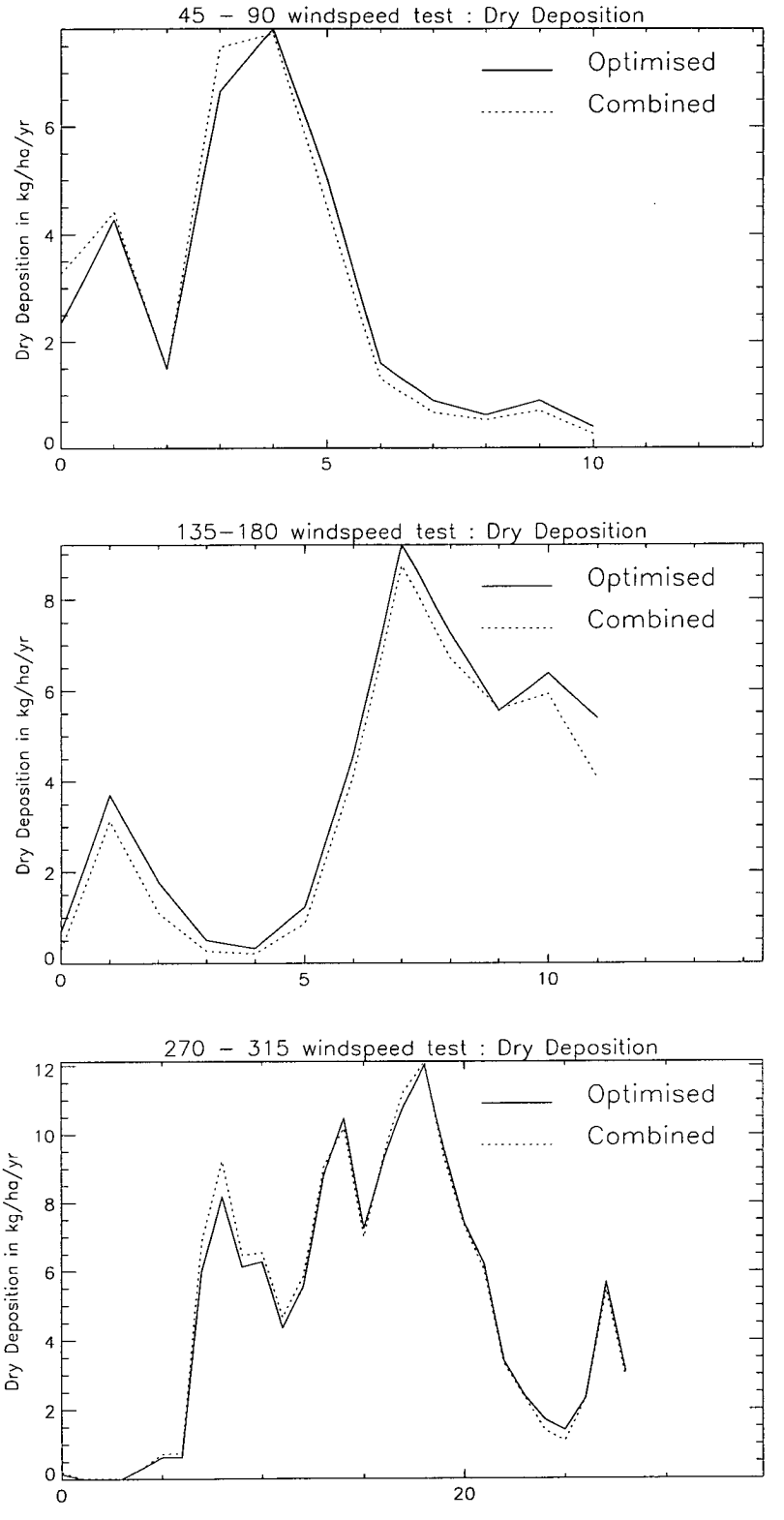

Figure 4.12: Comparison of dry deposition using optimised wind speeds for dry deposition against the combined results. The values on the x-axis for each plot represent the number of 20 km grid squares that the air column has traversed on the defined trajectory.

Wind Sectors	Optimised wind speed for Dry Deposition	Optimised wind speed for Concentration	Mean wind speed
0 - 45	7.5 (0.69)	6.91	9.94
45 - 90	6.26 (0.31)	6.29	8.42
90 - 135	5.79 (0.15)	5.67	6.52
135 - 180	5.95 (0.52)	5.62	8.79
180 - 225	7.71 (0.21)	7.4	10.96
225 - 270	7.9 (0.88)	7.98	11.6
270 - 315	8.61 (0.14)	7.27	11.94
315 - 360	8.0 (0.075)	7.43	10.83

Table 4.7: Calculated optimised wind speeds for concentration and integrated dry deposition for each wind sector. Units are m s^{-1}. The values in brackets are the standard deviations for the dry deposition wind speeds. These values were calculated by using 3 sample trajectories for each wind sector.

these runs were compared with the combined results and are shown in Figures 4.11 and 4.12.

The concentration data, using the optimised wind speeds for dry depositions, show a great deal of improvement, with all the plots showing that the use of the optimised wind speed produced a closer agreement with the combined result than the use of a mean wind speed. The best improvement is with the dry deposition data, as expected, since the wind speeds were optimised for dry deposition. For all of the three sample trajectories illustrated, the use of the optimised wind speed has greatly decreased the difference between those plots and the plots of the combined results. Some of the trajectory data are virtually identical.

4.3.3 Depth of the diurnally-varying atmospheric boundary layer

The values for the depth of the boundary layer (H_{mix}), employed in the TERN model, were in the form of data which were read in from an external data file, and represent the depth of the atmospheric boundary layer. Thus the TERN model contained no explicit description of the evolution of the H_{mix} in its internal code. In order to convert the TERN model into to a statistical atmospheric transport model (FRAME), it was necessary to build into the model some description of the diurnal variation of H_{mix}.

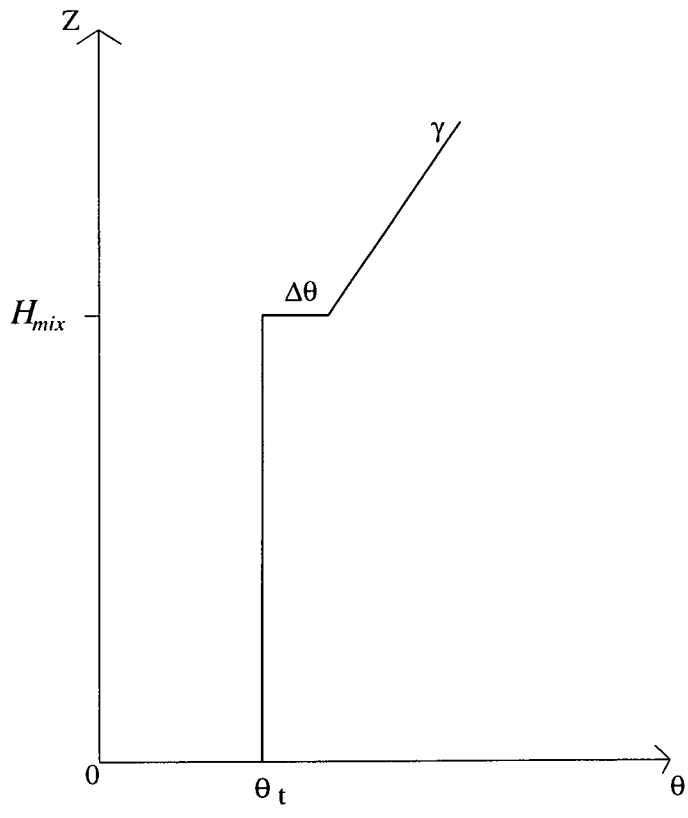

Figure 4.13: Idealised slab model of the atmospheric boundary layer, with discontinuous jumps of variables at the top of the atmospheric boundary layer. H_{mix} is the defined depth of the boundary layer, θ_t is the current potential temperature of the boundary layer, and $\Delta\theta$ is the discontinuous jump of potential temperature across the top of the boundary layer.

The daytime depth of H_{mix} in the TERN parameter file was calculated using an adapted version of the model proposed by Carson (1973). Nighttime values were assigned using Pasquill stability classes. It was decided to implement both the day and nighttime schemes directly into the new model. The following sections give an overview of these methods and the procedures used to adapt them to the intended use in a statistical atmospheric transport model.

The daytime boundary layer model

The model of Carson (1973) was earlier implemented in the MESOS model (Ap-Simon *et al.*, 1984). It depends on the sensible heat flux from the surface and the

entrainment of warmer air from above. The basic setup of the model is a bulk or slab model in which the atmospheric boundary layer (ABL) is represented by a uniform slab of air. There is a uniform potential temperature (θ_t) throughout the layer which is due to assumed infinite turbulent mixing (Figure 4.13). At the surface there is a layer of the order of a few tens of metres with relatively large vertical shears of wind, where heat is transported mainly by mechanically induced motion; this shallow layer was ignored by Carson (1973) since it is relatively thin. It is also assumed that at the top of the ABL there is a sharp discontinuity in the potential temperature, with an increase of $\Delta\theta$ across a thin layer, known as the entrainment zone. This zone is assumed to be infinitesimally thin. Above this zone, the air is assumed to be stable with a linearly increasing potential temperature profile with a gradient γ (K m^{-1}).

During a time interval Δt, heat energy is added to the boundary layer by surface heating and also by entrainment of warmer air from just above the ABL. Following Carson (1973), the amount of energy absorbed due to entrainment is assumed to be proportional to the surface heating. This means that if the integrated surface energy flux ($\mathbf{H}$), over a time period Δt, is $\mathbf{H}\Delta t$, then the total energy content of the mixing layer will increase by ΔE where

$$\Delta E = (1 + A)\mathbf{H}\Delta t \tag{4.17}$$

where A is the constant of proportionality for the entrainment of heat energy.

The stable layers just above the entrainment zone lose an amount of energy ΔE_{sl}

$$\Delta E_{sl} = -A\mathbf{H}\Delta t \tag{4.18}$$

due to mixing with cooler air exchanged during entrainment.

In the MESOS model (ApSimon *et al.,* 1984), a value of 0.15 was adapted for A since it was found to be the best value for use in the model which produced good comparison with measurements, and this value of A is used in this study.

The parameterisation of the surface heat flux $\mathbf{H}$ was taken from Smith (1979) with the approximation

$$\mathbf{H} = 0.4(\mathbf{S_t} - 100.0)C_f \tag{4.19}$$

where $\mathbf{S_t}$ is the incoming solar irradiance from equation 3.11, and C_f is the appropriate cloud reduction factor from Table 3.2 in section 3.1.2.

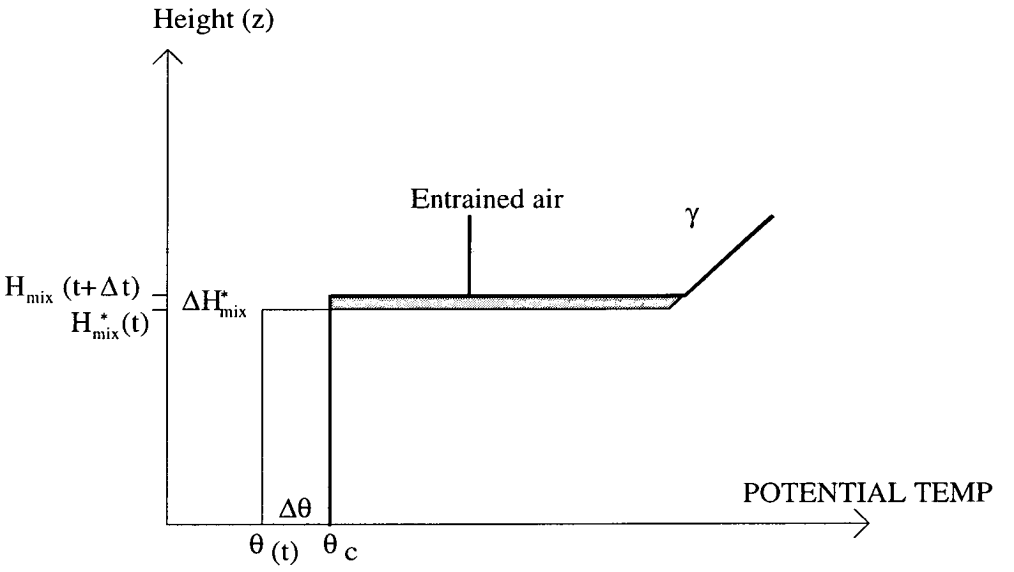

Figure 4.14: Growth of the atmospheric boundary layer in a time period Δt by surface heating and entrainment. Adapted from the model of Carson (1973).

To translate the model into computer code, it was assumed that equation 4.17 would be integrated numerically, using the previous timestep (time = t) depth of the ABL ($H_{mix}(t)$) and potential temperature θ_t.

A time step (Δt) of 10 minutes is used. The structure of the model is as follows:

1. The ABL is defined to have a heat energy content of E_t (this value is carried over from the previous timestep). The amount of energy added to the ABL (ΔE) over the timestep Δt is determined using equation 4.17.

2. A new value of θ is determined so that the increase in area under the profile of θ in Figure 4.13 that is equal to ΔE. This new value of θ (θ_c) on the profile (Figure 4.14) has a corresponding depth of the ABL $H^*_{mix}(t)$ (Figure 4.14).

3. To determine the amount of air that is entrained from above the ABL, one can assume that the entrained energy in equation 4.18, is equal to the energy lost by increasing the depth of the column of air by a further amount $\Delta H^*_{mix}(t)$. This is equal to the shaded area in Figure 4.14.

4. The final value of H_{mix} at time $t + \Delta t$ is thus

$$H_{mix}(t + \Delta t) = H^*_{mix}(t) + \Delta H^*_{mix}(t) \qquad (4.20)$$

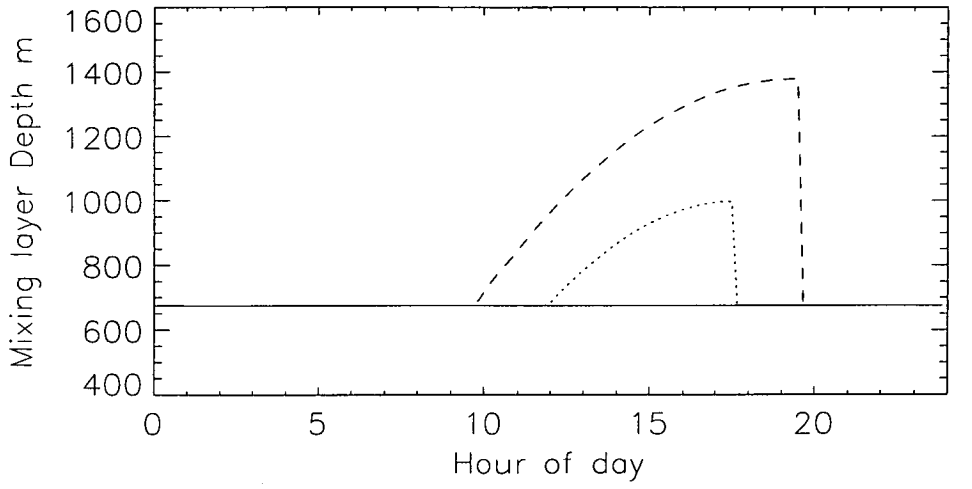

Figure 4.15: Diurnal variation in the boundary layer depth with a cloud cover of 6 oktas. These values were calculated for the Winter (full line), Spring (dotted line) and Summer (dashed line), and are assumed to be representative for the whole of Great Britain.

and the new potential temperature throughout this layer is θ_c.

The potential temperature gradients γ were taken from the parameterisation used in the MESOS model (ApSimon *et al.,* 1984). A two-stage temperature profile was employed, with a gradient of 6×10^{-3} K m^{-1} above 300 m, and more stable air with a gradient of 12 $\times10^{-3}$ K m^{-1} below 300 m for the uneroded layer above the ABL at dawn.

The calculation of the depth of the daytime boundary layer is performed until the modelled day finishes, at which point the model switches to a different scheme described in the next section to calculate the depth of the nocturnal boundary layer.

The nighttime boundary layer model

During the night a statistical approach is employed to calculate H_{mix}. The MESOS model adopted an approach of assigning values to H_{mix} which were typical of different wind and cloud cover conditions. These values depended on the Pasquill stability class and the wind speed (see Table 3.3, section 3.1.2). Table 4.8 gives details of these values.

Figure 4.15 is a plot of a typical 24-hour evolution of the ABL over Great Britain

Stability Category	Mixing Layer Depth m
F	$H_{mix} = \max(25 \times G\ ,\ 100)$
E	$H_{mix} = \max(50 \times G\ ,\ 200)$
D	$H_{mix} = 90 \times G$

Table 4.8: Following ApSimon *et al.,* (1984), nighttime values of the boundary layer depth dependent on the Pasquill stability class. H_{mix} is the depth of the ABL, and G is the model wind speed used to advect the air column.

Month	Maximum temperature (°C)	Minimum temperature (°C)	Time of maximum temperature (°C)
Jan	7	2	14.30
Feb	7	2	15.00
Mar	9	2	15.00
Apr	12	4	15.30
May	16	7	15.30
Jun	18	9	16.00
Jul	21	11	16.00
Aug	20	12	16.00
Sept	17	9	15.30
Oct	14	7	15.30
Nov	9	3	15.00
Dec	7	2	15.00

Table 4.9: Data used to parameterise the diurnal variations in surface temperature. These values are assumed to be representative of Great Britain. (K.J. Weston, Pers Comms).

with a cloud cover of 6 oktas, for three different times of the year: Winter, Spring and Summer. Values are low at night due to surface cooling, but become large during daytime due to large surface heating and entrainment of warmer air from above.

4.3.4 Parameterisation of the diurnal change in surface temperature

To parameterise the diurnal variation in surface temperature, statistical data were used which are representative of temperatures in central Great Britain (K.J.Weston, 1996. Pers Comms). These data consist of monthly mean values

for maximum temperature, minimum temperature, and time of day at which the maximum value occurs (Table 4.9). A sinusoidal wave was fitted to these data in order to interpolate across the required 24-hour period.

The vertical temperature profile in the model is calculated using the ground-level temperature and an assumed lapse rate. Below the cloudbase, a lapse rate of 9.8×10^{-3} K m^{-1} is assumed, and above the cloudbase, the lapse rate is 6.3×10^{-3} K m^{-1}. This is unchanged from the TERN model (ApSimon *et al.*, 1994).

4.3.5 Optimisation of the TERN code

In order to reduce computational time, many of the diurnally-varying parameters were assumed to remain constant while the air column traversed a particular grid square (20 km or 5 km). Thus certain processes, such as the calculation of the vertical diffusion coefficients and some chemical conversion rates, would only be calculated once for each new grid square. Assuming a horizontal advection speed of 7.5 m s^{-1} across a 20 km grid square, the maximum time it would take for the air column to traverse the square is

$20000 \times\sqrt{2}$ / $(7.5\times3600.0) = 1.05$ hours

For a 5 km grid square, the time reduces to just over a quarter of an hour. This assumption reduces computational time considerably as calculation of these variables for each timestep would be computationally expensive.

4.3.6 Optimisation of the model trajectories

The model domain comprises not only the landmass of Great Britain but also the surrounding sea areas. Since the model is concerned only with modelling fluxes of NH_3 over land and in-land water bodies, many of the non-land squares on a trajectory are surplus to requirements. This is illustrated in Figure 4.16 which shows a sample trajectory as a dashed line, but the solid line is the segment of the trajectory which covers just the the land grid squares and the intervening non-land grid squares. To implement this in the model, a new subroutine was written, which is employed at the start of each new trajectory. This routine scans along the trajectory path and determines the initial and final land squares which will be encountered by the air column. If no land squares are found, a new adjacent,

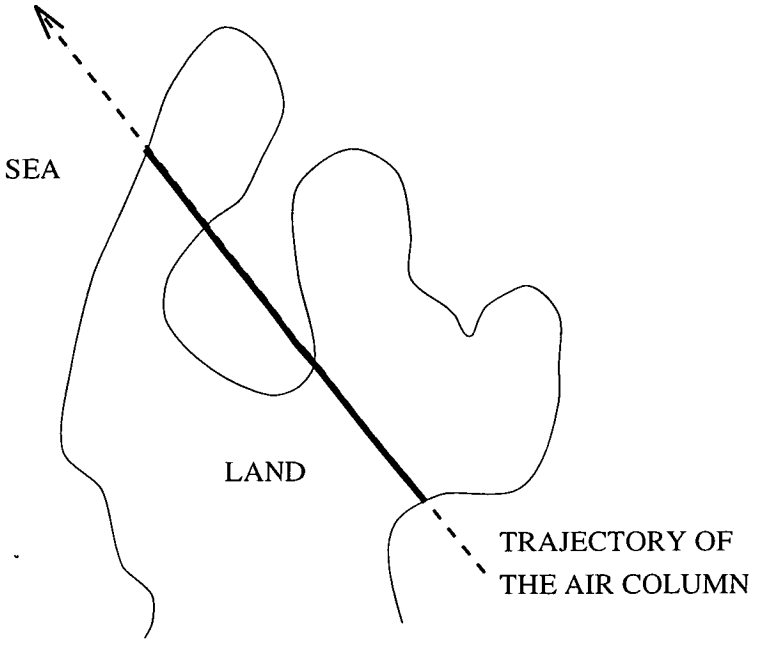

Figure 4.16: Dashed line is the entire model trajectory, while the bold line is the segment of the trajectory which contains all the land squares.

and parallel, trajectory is initiated and the routine repeated until a land square is found. The model is then constrained to travel between the first and the last land grid squares along the trajectory and thus will miss out a number of surplus (non-land) grid squares. The application of this routine in the model was found to reduce running times by upwards of 30%.

One might argue that by removing the trajectory path over the sea before it reaches the first land square, important deposition over the sea is being neglected, which might cause over-estimation of concentrations and dry deposition fluxes in coastal regions. However, since most of the regions of high deposition are inland, any inconsistencies incurred by this assumption will not be important as mainland emissions and dry deposition will be the main factor in determining the concentration profiles over the land area.

4.3.7 Adaptive timestep control for the vertical diffusion

The vertical transport of material between adjacent layers is described by K-theory diffusion using equation 4.1. Numerical solution of this equation for each timestep is done by the use of a *fourth-order Runge-Kutta* formula. In this section, a scheme is described which allows the timestep in the model to vary, dependent on the prevailing rates of vertical diffusion.

In the TERN model, the timestep (Δt), was set at a fixed value of about 6 seconds to force the computational scheme to remain stable. The main reason for this is the large vertical transfer of material that takes place in the lower layers, and also the complex scheme of aqueous chemistry used.

A more flexible method can be employed in FRAME, due to the large spatial variability of emissions and deposition that may occur using such a high resolution grid. This involves the use of a scheme which adjusts the size of the timestep to give a defined degree of accuracy, dependent on the current status of the model. This method should allow the model to proceed with small timesteps in areas where large vertical exchanges of material occurs, and then let the model take much larger timesteps when the vertical exchange is more muted.

Mathematically, the *fourth-order Runge-Kutta* formula scheme works by the following theory. On the x-y plane, assume that there is a function y=f(x). For an initial position of (x_n,y_n), where y_n = f(x_n), the determination of a new position (x_n+ h, y_{n+1}), where $y_{n+1} = f(x_n + h)$ and h is the increment in the x-direction, is as follows:

$$
\begin{aligned}
k_1 &= hf'(x_n, y_n) \\
k_2 &= hf'(x_n + \tfrac{h}{2}, y_n + \tfrac{k_1}{2}) \\
k_3 &= hf'(x_n + \tfrac{h}{2}, y_n + \tfrac{k_2}{2}) \\
k_4 &= hf'(x_n + h, y_n + k_3) \\
y_{n+1} &= y_n + \tfrac{k_1}{6} + \tfrac{k_2}{3} + \tfrac{k_3}{3} + \tfrac{k_4}{6} + O(h^5)
\end{aligned}
\qquad (4.21)
$$

This method has an error of order h^5 ($O(h^5)$).

A scheme for an adaptive stepsize control for a fourth-order Runge-Kutta

scheme is given in Numerical Recipes in Fortran (1988). This scheme is based on minimising the difference produced by performing calculations for one whole incremental step, and for two half steps.

In the implementation of the above scheme, if one assumes that the full step has value 2h, then to calculate the value f(x_n+ 2h), one can either take a larger step of size 2h (y_1), or two smaller steps of size h (y_2). Since the basic method is fourth-order, the true solution and the two numerical approximations are related by

$$\begin{aligned} y(x+2h) &= y_1 + (2h)^5\Psi + O(h^6) + .. \\ y(x+2h) &= y_2 + 2h^5\Psi + O(h^6) + .. \end{aligned} \tag{4.22}$$

where to order h^5 the value Ψ remains constant over the step 2h. The difference between the two numerical estimates is a convenient indicator of the truncation error

$$\Delta \equiv y_2 - y_1 \tag{4.23}$$

The main objective of this scheme is to keep the truncation error sufficiently small by adjusting the timestep. By specifying this required degree of accuracy, it is possible to adjust the current timestep such that the truncation error for the next step will remain within the defined bounds.

In terms of implementing the above theory into the FRAME model, y_n is the concentration (χ) of a certain chemical species, x_n is the time (t), and $2h$ is the timestep Δt. The process is used in FRAME by first taking two half timesteps ($\frac{\Delta t}{2}$), and then one full timestep (Δt). Although 3 steps must be taken to calculate the new timestep, optimising the code can mean that in practice, the overall cost is only 1.375 (Numerical Recipes in Fortran 1988, page 708) since calculation of $\chi(t+\Delta t)$ is done using the two half timesteps ($\frac{\Delta t}{2}$), and thus greater accuracy is achieved than with the use of the full timestep (Δt).

By defining the degree of accuracy, a number of options are available

- One can allow the model to take the same run time as before (using the constant timestep), and thus improve the accuracy of the results.
- The model can be allowed to have a certain degree of inaccuracy and thus greatly decrease the run time.

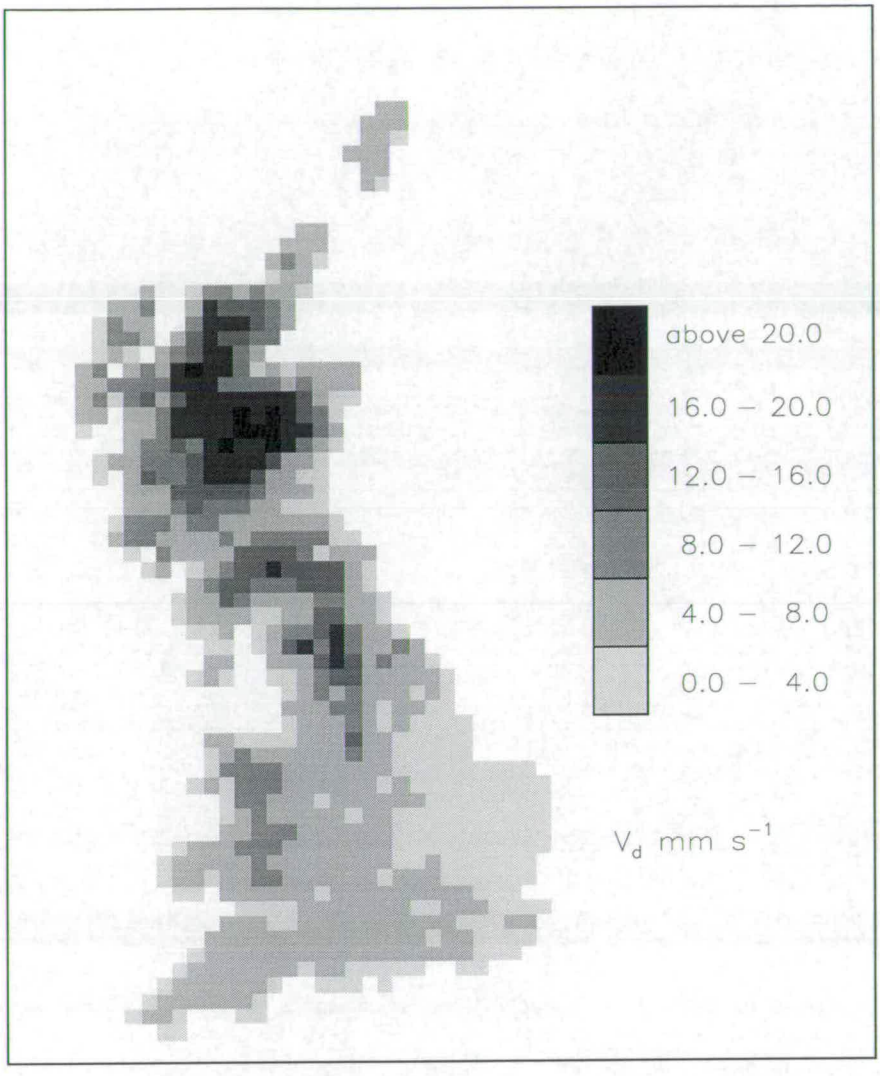

Figure 4.17: Average values of V_d used by the FRAME model to describe NH_3 dry deposition.

- A combination of the above can be used where the model is still more accurate than before, but computational time is still decreased. This is the option that has been used in FRAME.

4.3.8 Inclusion of land-dependent rates of dry deposition

The basic structure of TERN used a single invariant value of V_d for each chemical species (Table 4.2), though several other options were considered for analytical purposes. For NH_3, the value used was 0.01 m s^{-1}. Conversion to the FRAME model allowed a more detailed approach to be used, dependent on landuse. A

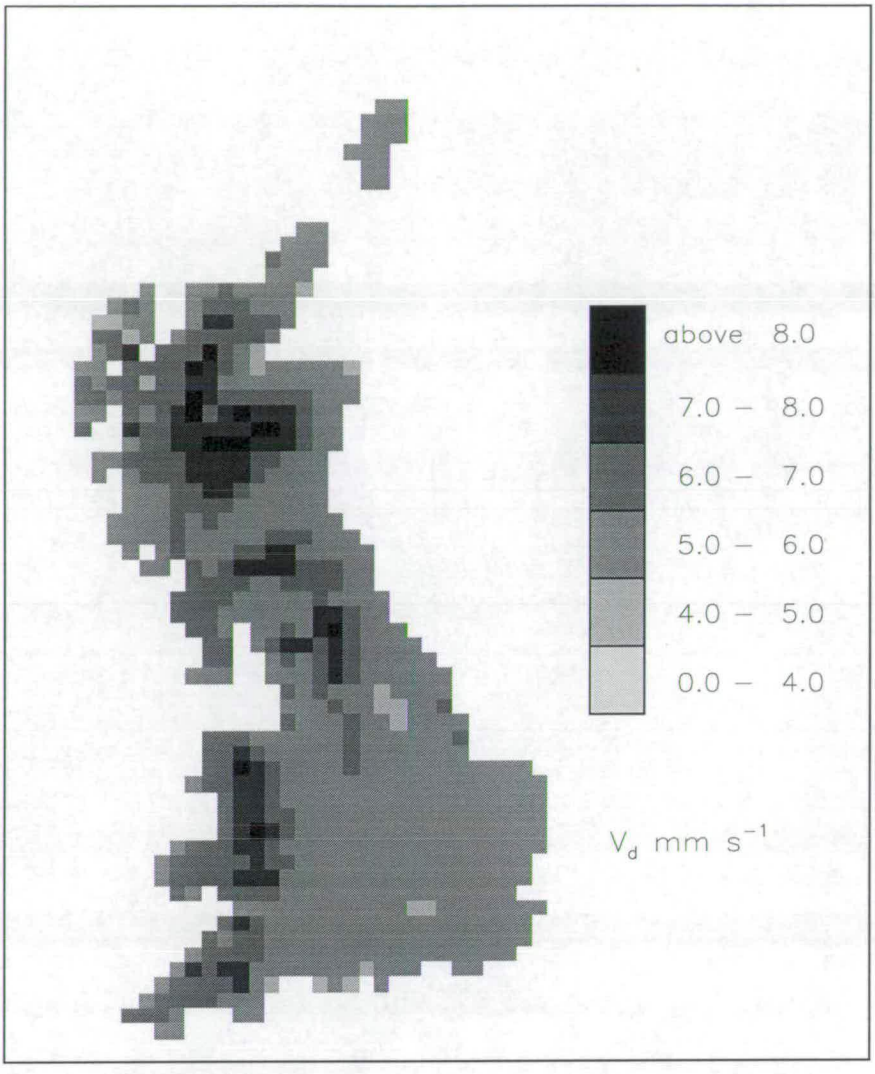

Figure 4.18: Diurnally-averaged values of V_d for SO_2 on a 20 km grid.

similar scheme to the one used in RODMOD (section 4.2.1) was employed. This involved the use of the ITE landuse database (section 2.2.1), combined with the dry deposition scheme developed in section 3.1.2, to provide diurnally varying and land-dependent values of V_d for NH_3. A dataset was also used which contains spatial information on mean monthly values for the surface (3 m) wind speed, on a 20 km $\times$ 20 km grid. These data were used to parameterise the degree of atmospheric turbulence and hence calculate the land-dependent values of R_a and R_b (section 3.1.3, equations 3.26 and 3.27).

A map of the annually-average and diurnally-averaged values is shown in Figure 4.17. This shows the greatest dry deposition velocities in northern Scotland, with values of V_d exceeding 20 mm s^{-1}, which are due to the large surface winds in this

area and also the land areas of moorland (which has a low value of R_c assigned to it in the deposition model; Table 3.6). In comparison, eastern England has values of less than 5 mm s^{-1}, since wind speeds are fairly low in this region and there are also large areas of arable land in this region, which is assigned a very high value of R_c in the model. The average value of V_d for Great Britain is 8 mm s^{-1}.

For SO_2 and NO_2, a land-dependent scheme of dry deposition is also employed in FRAME. These data are in the form of an annually-averaged map of deposition velocities on a 20 km grid, and were created by the Institute of Terrestrial Ecology (RGAR, 1990) using the same wind data used in the V_d model for NH_3 discussed in section 3.1.3. A map of the annually-averaged values of V_d for SO_2 is shown in Figure 4.18.

4.3.9 Parameterisation of the wet deposition process in FRAME

The choice of washout coefficients in FRAME, using a constant average scavenging approach, has been discussed in section 3.2. These values are combined with rainfall data to calculate appropriate scavenging coefficients. The rainfall data used are averages for the period 1989-1992 and are in the form of an annual rainfall field for Great Britain on a 20 km $\times$ 20 km grid (Figure 4.19). These data are converted into constant drizzle values by the use of equation 3.32.

A parameterisation of the seeder-feeder effect is included in the model by application of the method proposed by Dore *et al.* (1992) (section 2.2.2). For areas with rainfall less than an assumed sea-level value of 700 mm, the scavenging coefficient (λ_i) is calculated by

$$\lambda_i = \frac{\Delta_i \cdot I_T}{H_{mix} \cdot SEC_T} \tag{4.24}$$

where I_T is the annual rainfall (mm) for a specified location, and SEC_T is the total number of second in one year.

Over areas where rainfall exceeds 700 mm, it is assumed that this excess rainfall is due to altitudinal effects, and thus some material is removed by the seeder-feeder mechanism. In this case, λ_i is calculated by assuming that this excess rainfall will remove twice as much material as normal, and thus:

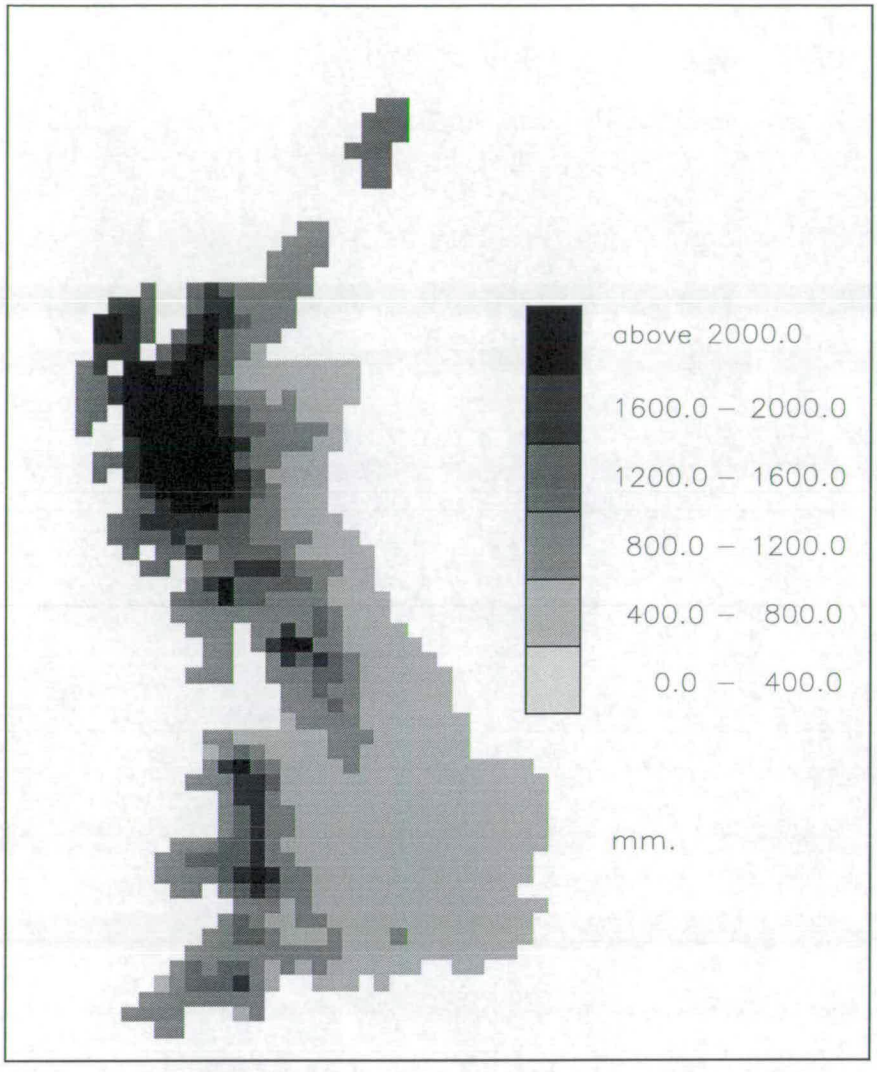

Figure 4.19: Average annual rainfall map for Great Britain (1989-1992).

$$\lambda_i = \frac{\Delta_i \cdot 700}{H_{mix} \cdot SEC_T} + 2 \cdot \frac{\Delta_i \cdot (I_T - 700)}{H_{mix} \cdot SEC_T} \tag{4.25}$$

Over areas not included in the rainfall map (i.e. the surrounding ocean), rainfall is set at an annual rate of 700 mm.

4.4 Structure of FRAME

A flowchart showing the overall structure of the FRAME model is given in Appendix B. It illustrates how the model works, and how the various routines and methods described in this chapter fit together in the overall framework of the model.

4.5 Numerical tesing of the model

To assess the accuracy of the model, a number of numerical tests were performed throughout the development process. These were done to continuously assess the model performance and determine the effect of upgrading the model with additional features.

A detailed assessment of the TERN model was performed by ApSimon *et al.* (1994), which included a large number of sensitivity tests. These results were reproduced as part of this project, and were in agreement with the data presented by ApSimon *et al.* (1994).

The TERN model contains certain routines in the numerical schemes which assess their performance and decide whether any errors have occured. In the vertical diffusion scheme, any negative concentrations would immediately cause the program to stop with an error message, in order to prevent possible instabilities occuring. The numerical scheme used to model the cloud chemistry contains a routine which determines whether the solution to the cubic equation in the code is converging to a stable solution, and it terminates the program with an appropriate error message if this is not the case.

One of the most important aspects of the numerical testing involved the property of mass conservation. In relation to the FRAME model, this means that

$$IMP + EMIT = DRYDEP + WETDEP + EXP \tag{4.26}$$

where IMP is the amount of material in the air column at the start of the trajectory, $EMIT$ is the amount of material emitted into the air column, $DRYDEP$ and $WETDEP$ are the amounts of material deposited from the air column while traversing the trajectory, and EXP is the amount of material in the air column at the end of the trajectory. Any numerical error in the model may have an effect on the mass consistency, and thus it was very important to ensure that the budget balanced correctly.

Sensitivity tests were performed on the adaptive timestep scheme in order to ensure stability of the numerical scheme. The focus of these tests was the choice of the allowed truncation error ($O(h^5)$), since a relaxation of this would allow a greater timestep, but would increase the numerical errors and thus affect the

mass balance to an unacceptable degree. On the other hand, using too small a value may cause the model to run unacceptably slow and would defeat the entire purpose of the scheme. As an example, an increase in the computational time of about 30%, gave a error in the mass balance analysis of 0.1% of the emission total of NH_3.

4.6 Discussion

This chapter has discussed the various problems and processes that needed to be addressed in order to convert a deterministic model (TERN) which used a single trajectory into a statistical atmospheric transport model capable of producing data on concentration and deposition fields for Great Britain as a whole (FRAME). One of the many areas of investigation was the problem of reducing the computational time of the model, while still retaining an essential level of accuracy. It is estimated that the combined effectiveness of the routines described in the later sections of this chapter have reduced the overall processing time of the model by a factor of at least 4.

The overall purpose has been to create a model which is capable of describing the short- and long-range behaviour of ammonia in the atmosphere over Great Britain. The optimisation of the directionally-dependent wind speeds means that it is possible to run the model for a single wind velocity and obtain results which, if not identical to, then should be much more similar to results using a range of wind speeds, than would have have been possible using a mean wind speed. This exercise also highlighted the non-linearity of the model by the fact that the use of the full range of winds speeds together with weighted coefficients produced results greatly different to the results using just the mean wind speeds. The results show that running the model with lower wind speeds has a greater influence on the model results than the use of higher values.

In the following chapters, results from the FRAME model are analysed and discussed. A number of sensitivity tests are performed to assess some of the assumptions used. Attention will focus on the short-range behaviour of ammonia, and the model will attempt to provide estimates of the proportions of emissions that are deposited in the same grid square, as well as budgets for the country as

a whole.

Chapter 5

Testing and Evaluation of Model Results on local scale and for Great Britain on a 20 km grid.

In this chapter, a number of model results are presented and discussed. In the first section, a test is performed on the TERN model, which was described in the previous chapter (section 4.1). The test focuses on the effectiveness of the vertical dispersion scheme used in both TERN and FRAME, and how modelled results compare with measurements.

The following sections contain the main results from the FRAME model on a 20 km $\times$ 20 km grid. In the second section of this chapter, there is a general analysis of the model results, examining how the modelled surface concentrations and deposition fluxes compare with measured data. Subsequent sections contain the results of a number of model sensitivity studies to analyse the significance of many of the assumptions in the model, and what effect they have on the results. They focus on the choice of vertical dispersion scheme, and the assumption of certain values to describe the behaviour of modelled cloud.

5.1 Testing and evaluation of the TERN model : The ADEPT experiment

The motivation for this section was to test the TERN model to see if it could reproduce actual measurements that were recorded in an experiment that took place during May 1995 (Sutton *et al.,* 1996). This experiment, forming part of

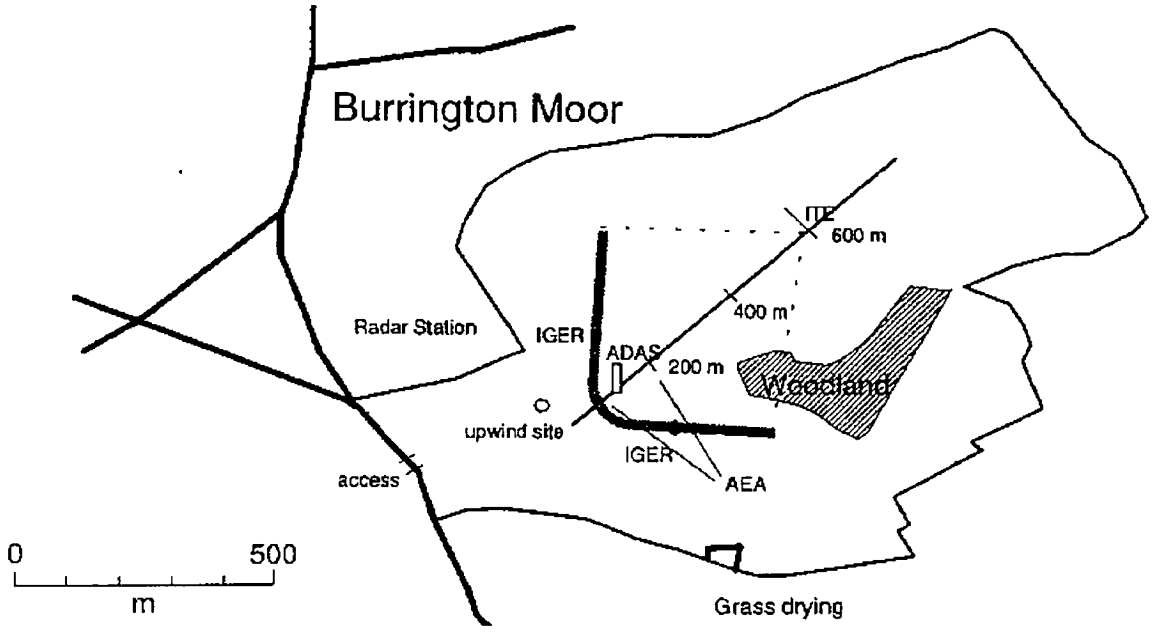

Figure 5.1: Simplified map of the field site of the Burlington Moor experiment, showing the slurry strip and principle locations of the different measuring equipment.

the ADEPT project (Ammonia Deposition and Effects ProjecT), took place on Burlington Moor, Devon, UK. The basic setup of the experiment consisted of a strip of slurry which was laid out in an arc of about 20 m width and greater than 400 m in length (Figure 5.1), surrounded by a field of short grassland. Measurement equipment were set up downwind of the strip in order to record concentrations and calculate surface fluxes. The aim of the experiment was to see how rapidly the large emissions of NH_3 would disperse in the atmosphere, and how much of the emissions would be dry deposited in the vicinity of the slurry strip. Measurements were taken during a number of time periods after the slurry had been laid, each period or 'run' lasting two hours. Four different groups of instruments were used, which all measured the concentration at certain distances downwind of the slurry strip. The measurement techniques have been discussed in more detail elsewhere (Sutton *et al.,* 1996), and the focus here is on the model comparison with a range of independent measurement methods.

The basic setup of the TERN model was altered slightly in order to be used for this exercise. All chemical options were switched off, and only emissions of

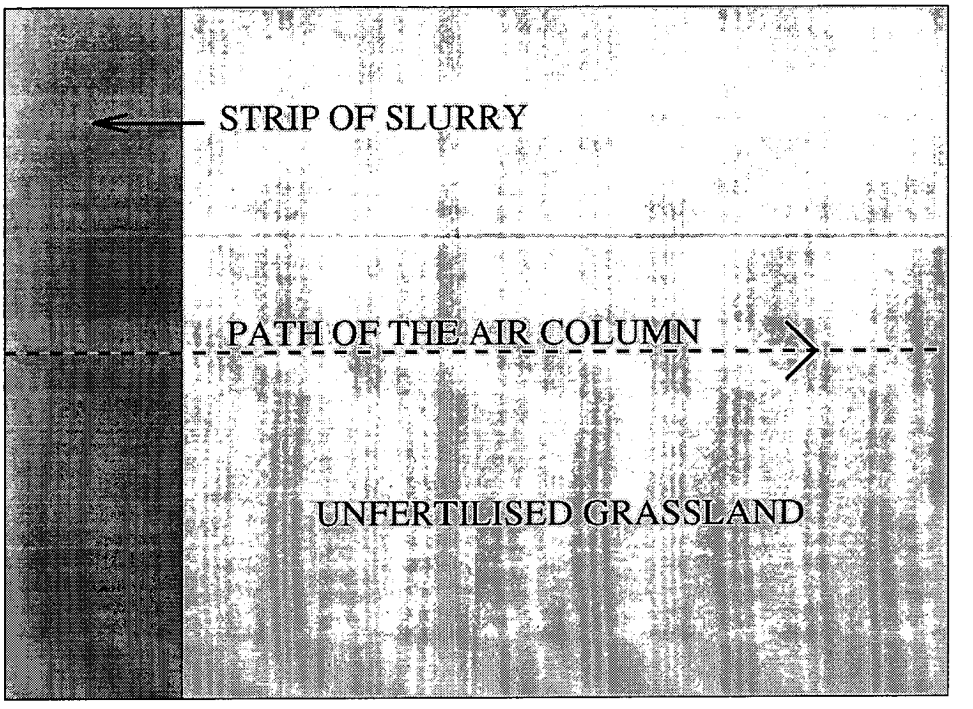

Figure 5.2: Diagram of the model domain used in the simulation of the ADEPT experiment. The modelled slurry strip is the dark grey ban, and the lighter grey area represents unfertilised grassland.

NH_3 were considered. Thus the only processes that would affect the atmospheric concentration were vertical dispersion and dry deposition. Chemical reactions were not considered as the time period taken to traverse the site would be small, and it was assumed that air coming from the southwest would be relatively clean. Figure 5.2 is a plot of the model domain, with the determined trajectory of the air column shown as a dashed line. As with the actual field experiment, the model emissions were assumed to be a strip of slurry of predetermined width with the length of the strip much greater then the width. This assumption allows the crosswind advection of material to be neglected. The column of air would first traverse the strip of slurry, where ammonia would be emitted into the atmosphere, and after the slurry strip has been passed, the air column would then be assumed to be passing over uniform unfertilised grassland. Whilst the air column was transported across the simulated slurry strip, no dry deposition would take place. Conversely when the air column passed over the unfertilised grassland, no emissions would occur and dry deposition would take place using

Run number	Emission flux from the strip (μg m^{-2} s^{-1})	Width of the strip (m)	Horizontal advection speed at 3 m (m s^{-1})	Time of the midpoint of the run (GMT)
1	30	20	4.7	1500 hrs
6	20	20	4.4	1700 hrs
10	53	16	6.1	1120 hrs
12	21	18	7.3	1220 hrs

Table 5.1: Main values from the ADEPT runs which were used as input to the adapted TERN model.

a specified deposition velocity (V_d) of 0.01 m s^{-1}. Since the model would be run for only a very short horizontal distance of less than 1 km, it was assumed that the depth of the mixing layer would have little effect on the rate of vertical dispersion, and so the mixing height was set at 1000 m for every run.

5.1.1 Results

To compare measured and modelled results, 4 sample runs were selected from the measurement data. Table 5.1 contains all the main data for the 4 runs which were used as input data for the adapted TERN model.

The results of the four runs are shown in Figures 5.3 to 5.6. The model data from Run 1 (Figure 5.3) seem to compare well with the measurements and fits the general trend of the horizontal concentration gradient, though model data are at the maximum range of the measurements.

For Run 6 (Figure 5.4), the model performs better than for Run 1, with the model results remaining within the range of the measurements for most of the trajectory. The only large discrepancy is in the first 100 metres when most of the measurements are much lower that the modelled values, apart from the AMANDA measuring equipment.

The data from Run 10 (Figure 5.5) do not have such good agreement. Modelled concentrations almost consistently over-estimate the measurements, with the differences becoming much greater further downwind of the source. After 500 metres, measured concentrations are virtually zero, while the model predicts values of between 10 and 20 μg m^{-3}. Analysis of Run 12 (Figure 5.6) results suggest that the model is again over-estimating the measurements, though by

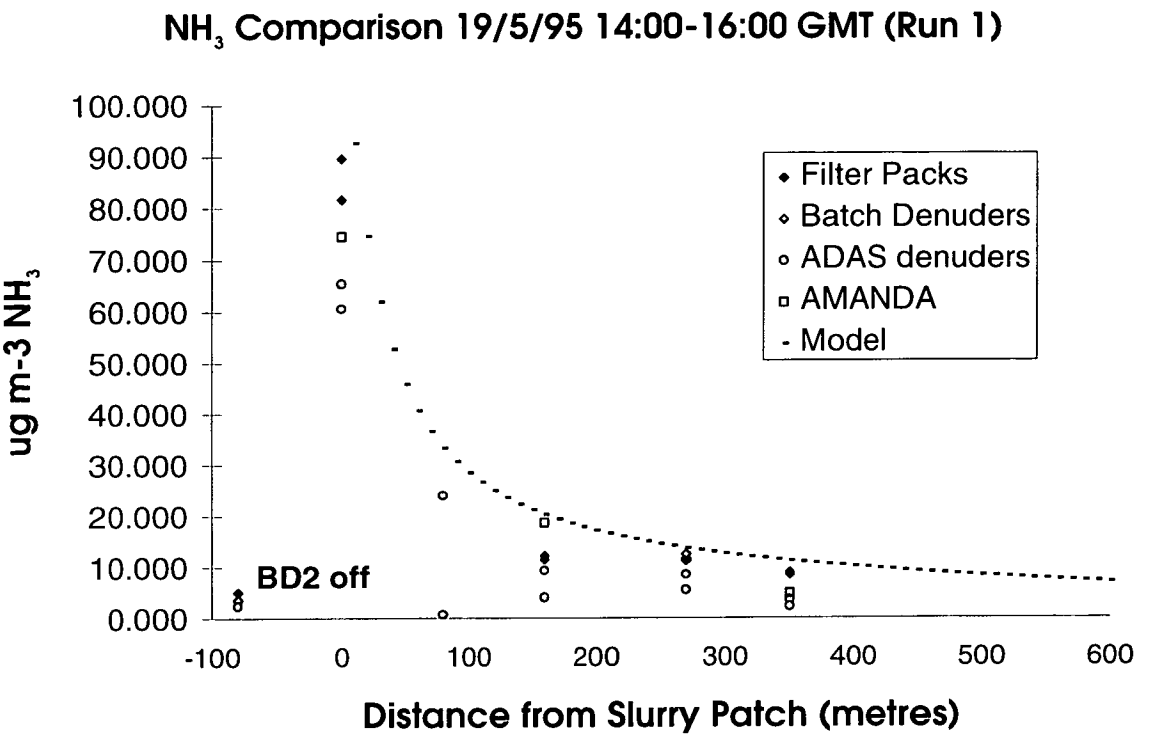

Figure 5.3: A comparison of measured data and modelled concentrations for Run 1 of the ADEPT experiment.

not as much as in Run 10 (Figure 5.5).

Overall the model seems to describe the horizontal distribution of concentration downwind of the slurry strip relatively well. The model results agree better with the runs performed in the afternoon (Run 1 and Run 6), as opposed to those which took place around midday (Run 10 and Run 12). One possible explanation for this is that strong convective mixing took place during the midday runs, causing increased turbulent mixing. This type of vertical dispersion, which can cause enhanced vertical movement of material by the plume rise above that described by the vertical diffusion process, is not accounted for in the TERN model.

However, if one considers how the model would have performed if vertical dispersion had been by way of instantaneous mixing, it becomes apparent that the multi-layer mixing scheme has reproduced measurements remarkably well. A quick calculation for Run 1 shows that the amount of NH_3 emitted into the air column was 127 μg m^{-2}. Dividing this number by the mixing height of 1000 m gives an average concentration of just 0.127 μg m^{-3}. This is a gross underestimation of the actual concentrations and clearly shows the inadequacy of the

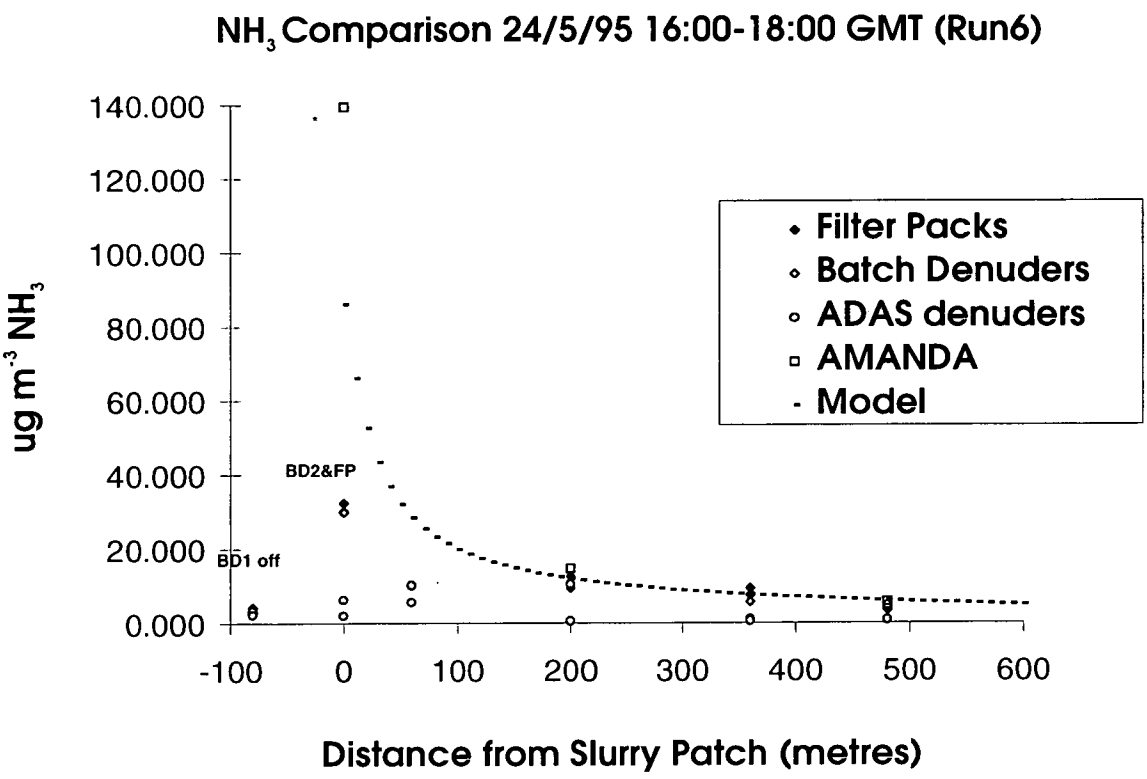

Figure 5.4: A comparison of measured data and modelled concentrations for Run 6 of the ADEPT experiment.

instantaneous mixing scheme for use with short-range dispersion calculations.

In this experiment, the parameterisation of vertical dispersion used by TERN has reproduced measured data to a good degree of accuracy. The high concentration near the slurry patch illustrate clearly how large fluxes of dry deposition can occur near to an emission area, and thus how important it is to get a good parameterisation of the process of vertical dispersion.

5.2 Testing and evaluation of the FRAME model results on a 20 km square grid

The structure of the FRAME model was setup as described in the previous chapter. The aim of the FRAME model is to create annually-averaged data fields for surface concentration and deposition fluxes.

To recreate average data values for the year, the model was set to run on the spring equinox, when the lengths of the day and night are equal. The height of the cloudbase was assigned a value of 250 m. This value was taken from the ACDEP

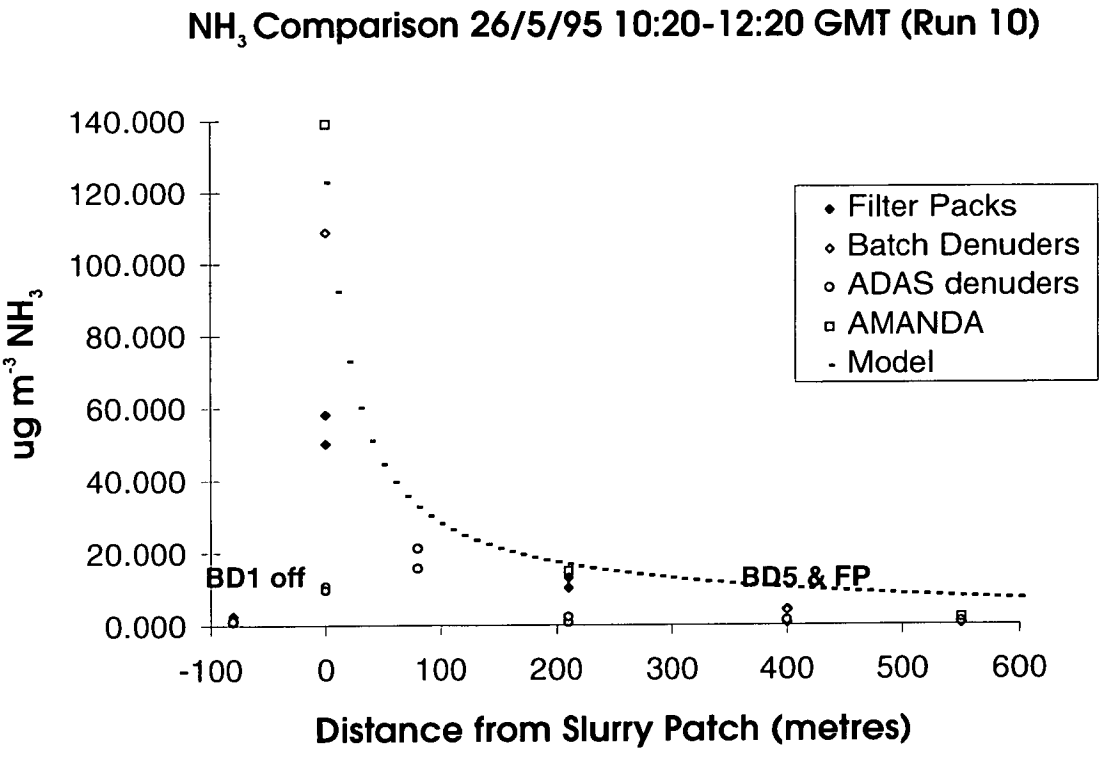

Figure 5.5: A comparison of measured data and modelled concentrations for Run 10 of the ADEPT experiment.

model (Hertel *et al.*, 1995) as the assumed height above which the model defines all vertical layers to be cloud layers during precipitation events. The FRAME model uses a continuous rate of precipitation, due to the assumption of constant drizzle. In the atmosphere the average height of the cloudbase is much greater than this, but aqueous chemical reactions may occur at lower levels in mist and fog, so the height of 250 m assumed in the model takes account of this. The sensitivity of the model to this parameter is examined later in section 5.9.

The cloud cover was set at 6 oktas. This was based on data in World Survey of Climatology Volume 5 (1970), which contained 10-year averages of cloud cover for a number of stations across Great Britain. This assumption is examined later in this chapter and sensitivity tests are performed and evaluated.

To reduce the effect that occurs due to the lack of lateral dispersion (as discussed in section 4.1.1), the model was run using trajectories from 72 wind directions on the 20 km × 20 km grid.

FRAME is a multi-pollutant model, dealing with a number of chemical species, not just NH_x. The chemical species considered by FRAME include SO_2, $(NH_4)_2SO_4$,

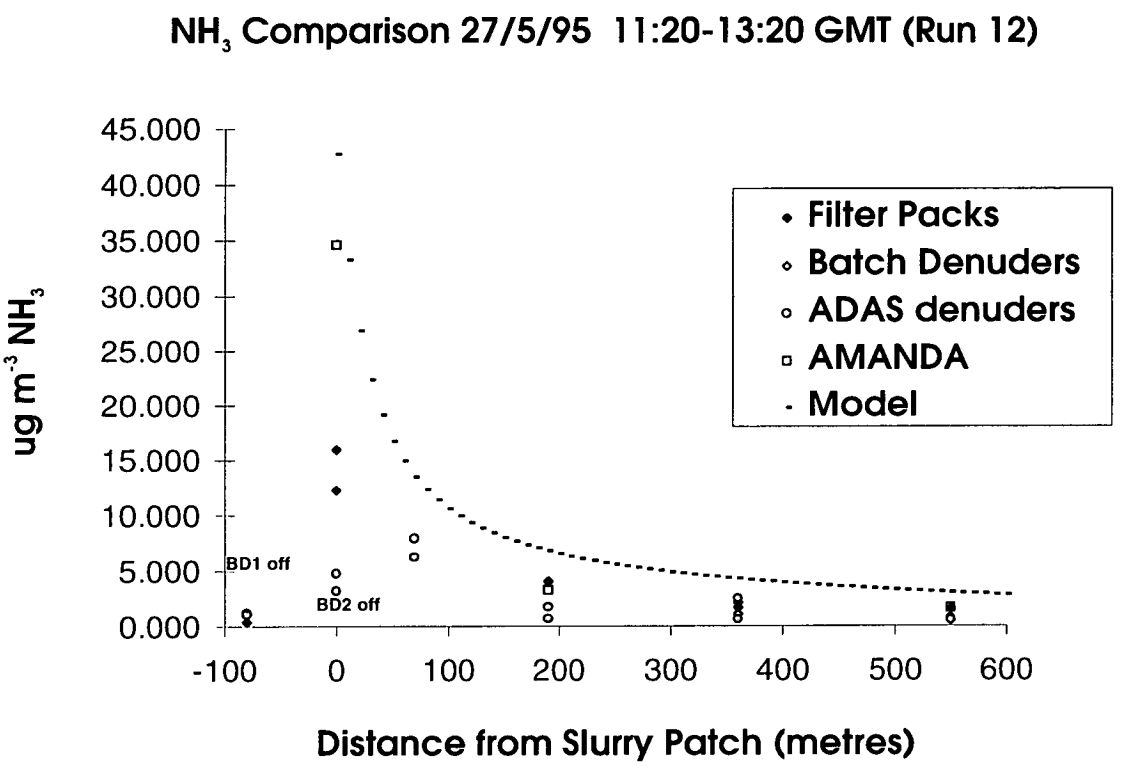

Figure 5.6: A comparison of measured data and modelled concentrations for Run 12 of the ADEPT experiment.

H_2SO_4, NH_3, NO, NO_2, HNO_3, NH_4NO_3, NO_3, PAN, and H_2O_2. The atmospheric behaviour of NH_x is affected by the presence of other species, such as the oxidation products of SO_2 and NO_x. Thus while the primary concern of this study is to describe the behaviour of NH_3 and NH_4^+ as accurately as possible, it is also important to describe the behaviour of other chemical species.

The emissions data used for sulphur and oxidised nitrogen are shown in Figures 5.7 and 5.8. These data are taken from the UK National Atmospheric Emissions Inventory (Eggleston, 1992b).

Results are presented for oxidised sulphur, oxidised nitrogen, and reduced nitrogen. Where possible, comparisons are made with measured data.

5.3 FRAME model results : Oxidised sulphur

5.3.1 Surface concentrations of sulphur dioxide

The modelled field of SO_2 surface (1-2 m layer) concentrations is shown in Figure 5.9. To a large extent, these concentrations reflect the distribution of emissions

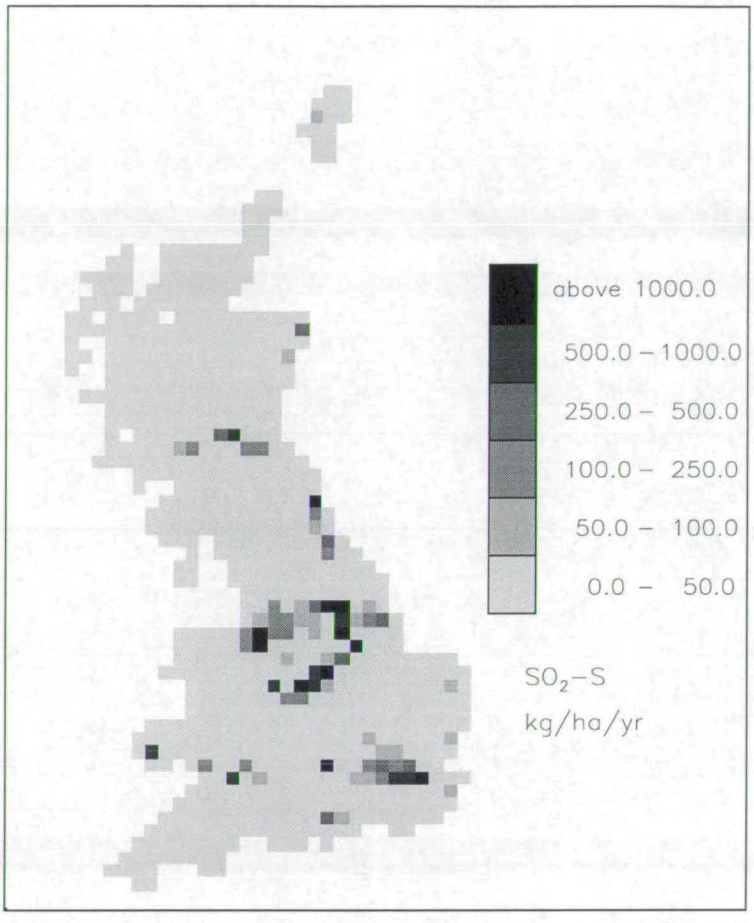

Figure 5.7: Annual emissions of SO_2-S for Great Britain (Eggleston, 1992b). Units are kg ha^{-1} $year^{-1}$.

(Figure 5.7), with the largest concentrations occurring in the north Midlands and South Yorkshire. This large area contains concentrations of SO_2 well in excess of 8 ppb. Away from this area, concentrations decrease fairly smoothly with values of less than 1 ppb over much of northern and western Scotland, and the tip of southwest England. There are some 'hotspots' of large concentrations surrounded by much lower values, which all contains very large emission sources.

Modelled data have been compared with measured data recorded at 34 sites during 1992 across Great Britain. One should note that a measurement is recorded at a single site, while modelled values represent an average for a 20 km grid square. A plot of measured values versus modelled data is shown in Figure 5.10. The

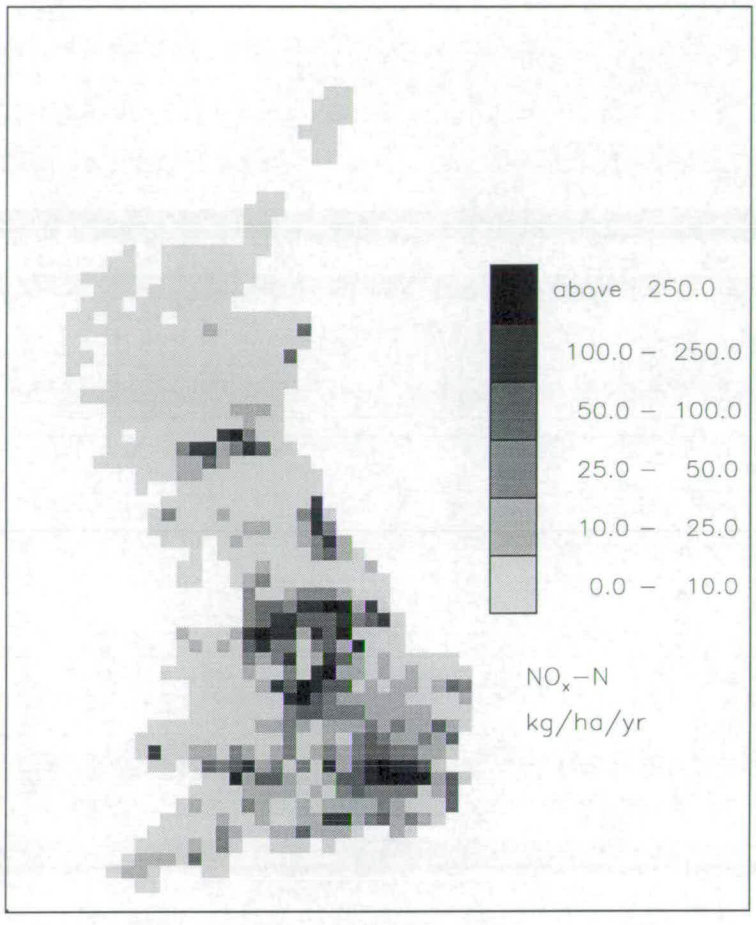

Figure 5.8: Annual emissions of NO_x-N for Great Britain (Eggleston, 1992b). Units are kg ha^{-1} $year^{-1}$.

dotted line represents a theoretical one-to-one agreement while the full line is the best straight line calculated by regression analysis. The most obvious feature is that the vast majority of the modelled values over-predict measurements, with the the regression line having a gradient of 2.44. The correlation coefficient R has a value of 0.86. For the sample size of n = 34, this correlation has a probability (P) of having arisen by chance of 4.16×10^{-10}, which is statistically significant at the P = 0.1% level. The regression analysis was calculated using Microsoft Excel 5.0. This over-estimation of the model could be due to a number of factors. One possibility is the assumption that all emissions are uniformly distributed throughout the lowest 300 m of the air column. With the appropriate parameterisation

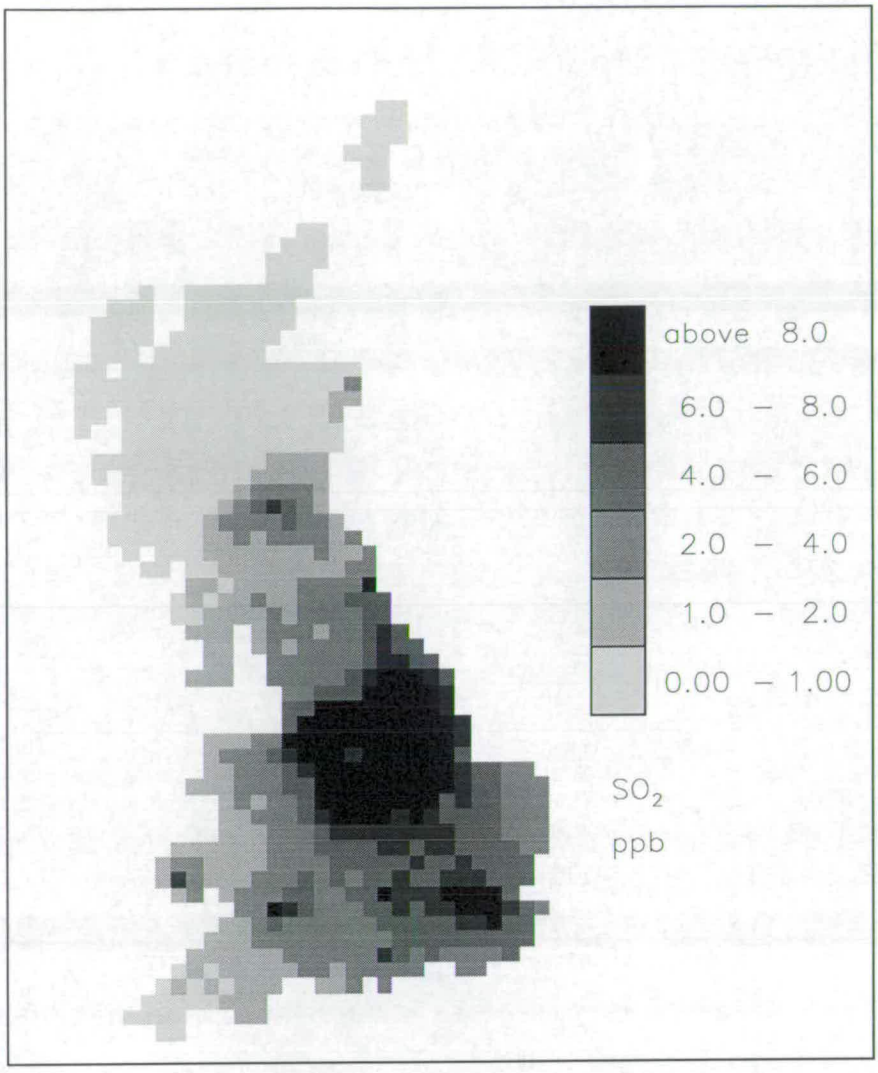

Figure 5.9: Modelled surface concentrations of SO_2 for Great Britain. Data represent an annual average. Units are ppb.

to account for plume rise, SO_2 could be emitted into only certain layers of the model, dependent on the height of the source.

Another point which may affect the results is that the optimised wind speeds (section 4.3.2) were calculated to accurately model the behaviour of ammonia. The fact that ammonia is a ground-based source, whereas SO_2 is released throughout the lower part of the air column, might mean that an optimised wind speed for SO_2 should be much higher. This illustrates one of the problems that can occur in modelling, in that as one tries to increase the accuracy of one area of the model, it may have an adverse effect on another part of the model.

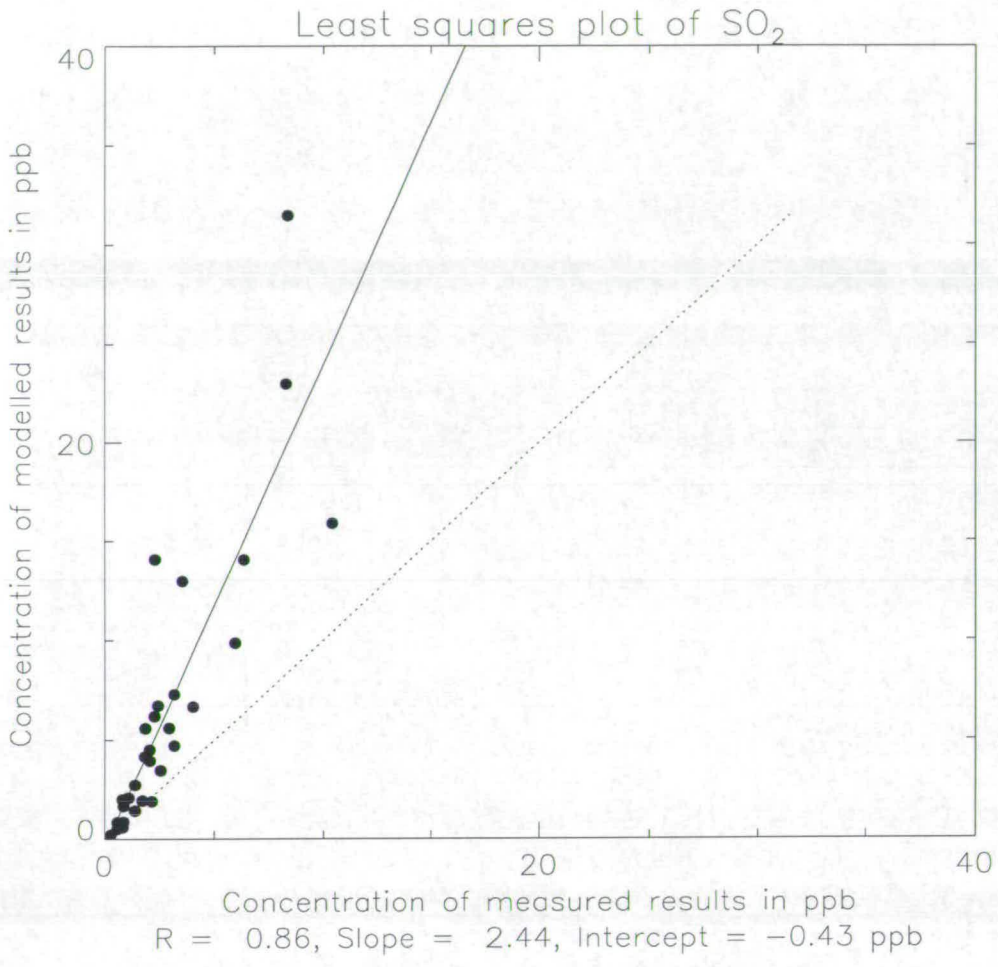

Figure 5.10: Correlation plot of modelled SO_2 concentrations from the FRAME model versus observations from a network of measurements sites. RGAR (1996). The full line is the regression line and the dotted line is the one-to-one line.

5.3.2 Wet deposition of sulphate

The modelled distribution of (non-marine) sulphur wet deposition is shown in Figure 5.11. These data represent the total sulphur removed from the modelled air column by precipitation. The model results represent an average value for a 20 km grid square. The areas of greatest deposition are located in Wales and northern England, which corresponds to areas of high rainfall and also, in the case of northern England, an area of very high SO_2 concentration. In areas of large rainfall, the large deposition will be partly due to the modelled seeder-feeder effect (section 4.3.9; Dore *et al.*, 1992), which increases the effective washout coefficients above a certain rainfall level. Much of England has a deposition flux of greater

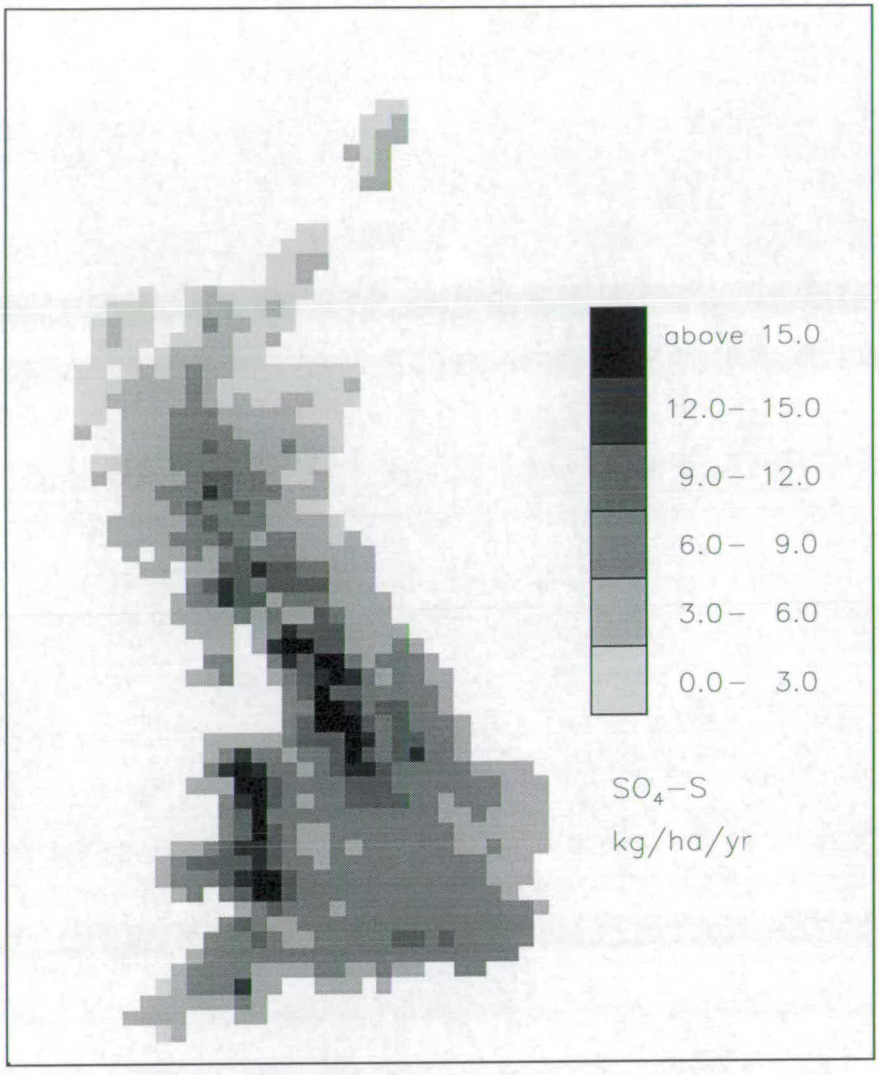

Figure 5.11: Modelled wet deposition of sulphate over Great Britain. Data represent an annual flux. Units are kg S ha^{-1} $year^{-1}$.

than 6 kg S ha^{-1} $year^{-1}$, and the areas of lowest modelled wet deposition are located in the far north of Scotland.

Measurements of sulphate in precipitation have been recorded at locations belonging to the UK Secondary Acid Deposition Network (section 2.2.2; RGAR, 1996). These data have been used in conjunction with recorded rainfall, and then interpolated across the country to create a map of the annual wet deposition flux to Great Britain. Adjustments were made to the data to account for the increased concentration in precipitation due to the seeder-feeder effect, similar to the parameterisation in FRAME (Dore *et al.*, 1992; section 4.3.9). The interpolated map for 1992 is shown in Figure 5.12.

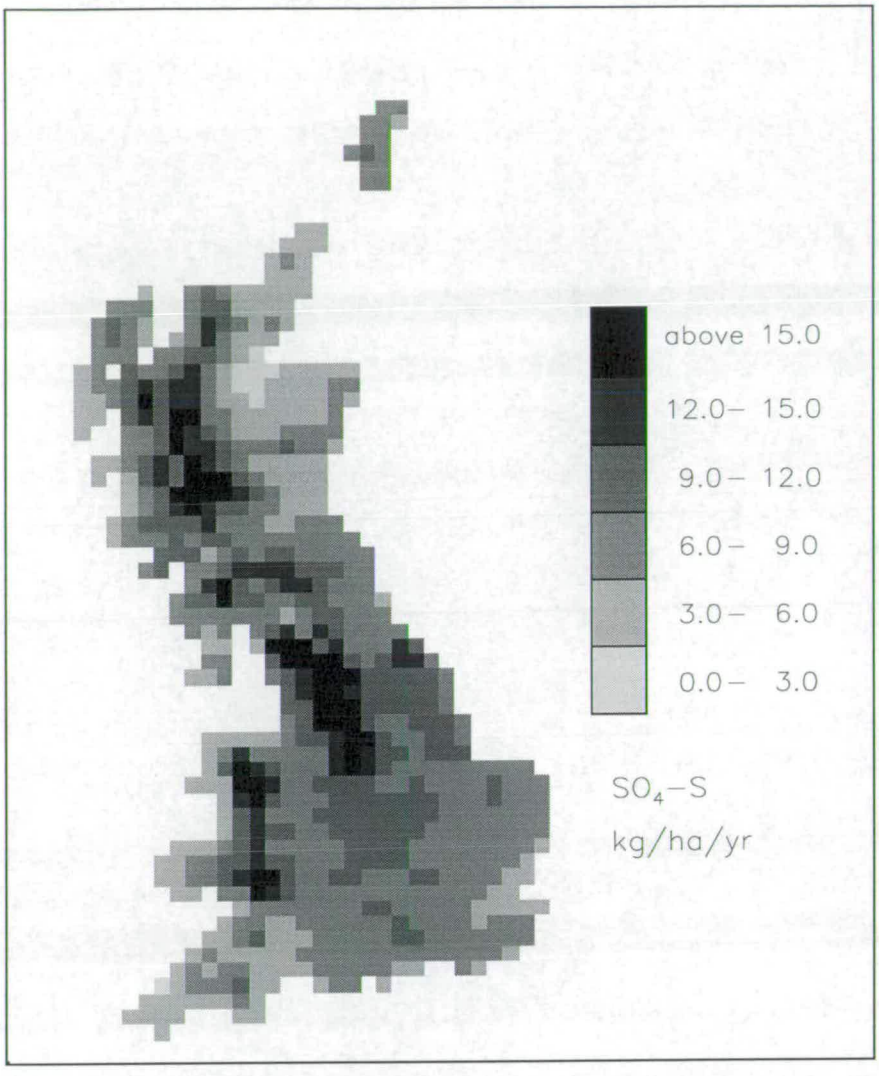

Figure 5.12: Recorded and adjusted measurements of wet deposition of sulphate over Great Britain. Data represent an annual flux for 1992. Units are kg S ha^{-1} $year^{-1}$. RGAR (1996).

The model data agree well with the observed values over much of England and Wales, with the areas of largest deposition occurring roughly in the same areas. However in Scotland the modelled results under-predict the large fluxes that occur in the northern and western areas.

These modelled data have been used to perform a comparison of wet deposition fluxes with measured data, which were recorded at 33 measurement sites. The regression plot is shown in Figure 5.13. The value of R is 0.78. For the sample size of n = 33, this correlation has a probability (P) of having arisen by chance of 4.37×10^{-7}, which is statistically significant at the P = 0.1% level. The regression

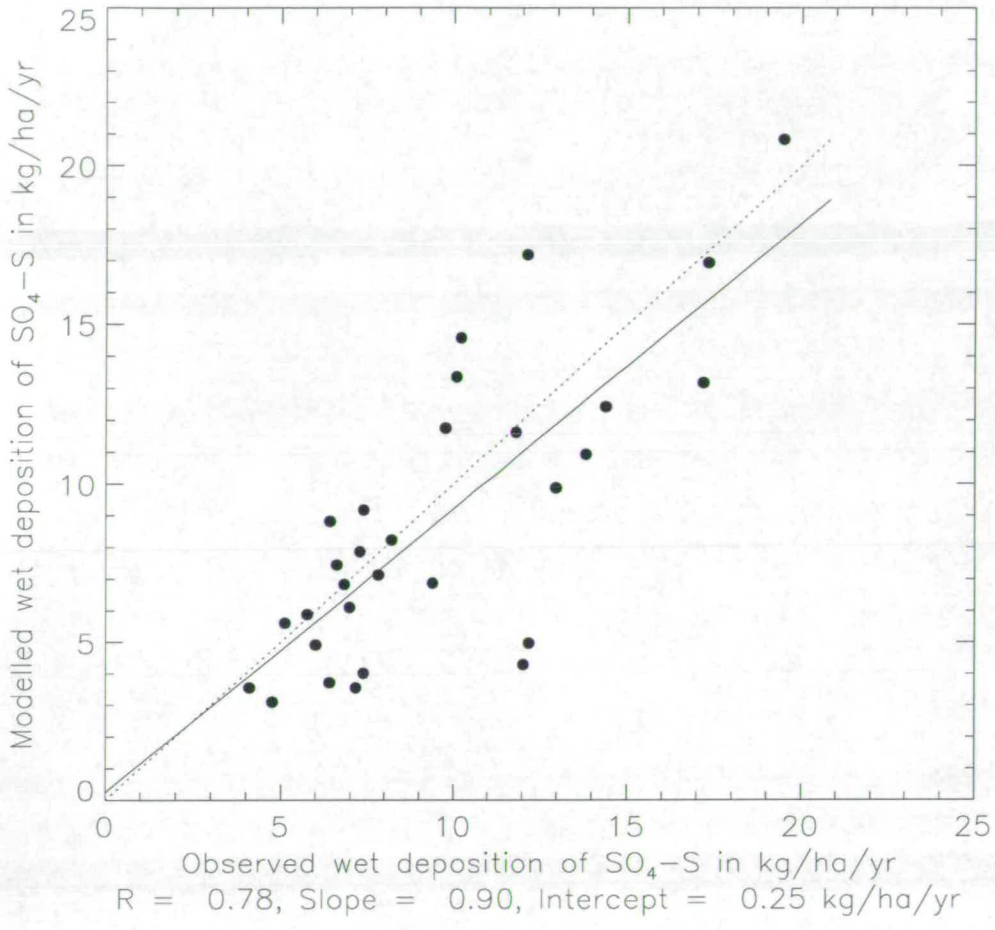

Figure 5.13: Correlation plot of modelled SO_4-S wet deposition fluxes from the FRAME model versus observations from a network of measurements sites. RGAR (1996). The full line is the regression line and the dotted line is the one-to-one line.

line (full line) is close to the one-to-one line (dotted line) , showing that the model is estimating the magnitude of the wet deposition fluxes without too much scatter.

5.3.3 A comparison of annual budgets of sulphur for Great Britain

The annual budget of sulphur for Great Britain predicted by the FRAME model is shown in Table 5.2. The total modelled annual flux of dry deposition is 255.8 Gg S year^{-1}, and the wet deposition flux is 170.2 Gg S year^{-1}. The annual import of sulphur is 101.2 Gg S $^{-1}$ and the annual export is 1370.4 Gg S year^{-1}. In comparison with interpolated and adjusted measurements (Table

Wind sector origin of trajectories	Emissions of S	Import of S	Dry deposition of S	Wet deposition of S	Export of S
0 - 45	1695	19.7 (2.1)	281.3 (30.7)	199.9 (21.8)	1233.7 (134.5)
45 - 90	1695	133.7 (10.6)	295.8 (23.4)	231.1 (18.3)	1301.9 (102.6)
90 - 135	1695	597.7 (39.5)	325.3 (21.5)	362.2 (23.9)	1605.5 (106.0)
135 - 180	1695	228.8 (19.7)	409.9 (35.2)	436.7 (37.6)	1077.4 (92.7)
180- 225	1695	101.3 (11.8)	210.8 (24.5)	142.0 (16.5)	1443.6 (167.5)
225 - 270	1695	47.2 (9.1)	159.9 (30.9)	77.3 (14.9)	1505.2 (290.5)
270 - 315	1695	37.9 (6.7)	182.6 (32.5)	73.8 (13.1)	1476.7 (262.8)
315 - 360	1695	10.0 (1.7)	330.7 (57.2)	139.6 (24.1)	1234.9 (213.6)
Averaged annual modelled budget of S	1695	101.2	255.8	170.2	1370.4

Table 5.2: Modelled annual budget of sulphur for eight wind sectors and an averaged annual budget for the country. Data in brackets are the frequency weighted total for each wind sector. The units are Gg S $year^{-1}$.

Dry Deposition		
% SO_2	% $(NH_4)_2SO_4$	% H_2SO_4
95	3	2

Table 5.3: A comparison of annual modelled dry deposition of sulphur.

Wet Deposition		
% SO_2	% $(NH_4)_2SO_4$	% H_2SO_4
19	30	51

Table 5.4: A comparison of annual modelled wet deposition of sulphur.

Source of data	Emissions of S	Import of S	Dry deposition of S	Wet deposition of S	Export of S
EMEP model data for 1992	1750	84.2	Combined total of 475		1360
ITE interpolated data	-	-	148.4	216.8	-

Table 5.5: Annual sulphur budgets from the EMEP model for 1992 (Barrett and Seland, 1995) and ITE interpolated data from an inferential model (dry deposition) and a seeder-feeder model (wet deposition) (RGAR, 1996).

5.5), the FRAME model has a variable degree of success. The observed annual flux of SO_2-S dry deposition was calculated by the use of an inferential model, as described in section 2.2.1.

Since this inferential model employs an interpolated field of measured surface concentration as the main input, any disagreement between the FRAME results and the observed surface concentartions will also occur when comparing the dry deposition totals. In fact the FRAME dry deposition total of 255.8 Gg S $year^{-1}$ is a factor of 1.7 times greater than the observed value, which is less than the gradient of the regression plot for SO_2 surface concentrations (Figure 5.10) of 2.44, but still very large.

The modelled and measured data for the annual wet deposition flux are in better agreement, with an annual modelled total of 170.2 Gg S $year^{-1}$ and the observed value being 216.8 Gg S $year^{-1}$.

Table 5.3 gives a breakdown of the contribution of each sulphur species to the annual dry deposition flux of sulphur to Great Britain, according to the FRAME model. The main contributor is SO_2, which accounts for 95% of the sulphur dry deposition. Table 5.4 gives a similar breakdown for the total annual wet deposition flux of sulphur. Wet deposition of H_2SO_4 contributes to over half of the total flux, while $(NH_4)_2SO_4$ makes up 30%. The remaining 19% is from wet deposition of SO_2.

The EMEP model results for 1992 predicts the annual import of sulphur to be 84.2 Gg S $year^{-1}$. This is about 16% less than the FRAME value of 101.2 Gg S $year^{-1}$. The export totals are in better agreement, with the EMEP value of 1360 Gg S $year^{-1}$ only slightly less than the value of 1370.4 Gg S $year^{-1}$ predicted by FRAME. The combined dry and wet deposition flux from EMEP has a value of 475 Gg S $year^{-1}$. This can be compared to the ITE value of 365.2 Gg S $year^{-1}$ and the FRAME value of 426 Gg S $year^{-1}$.

5.4 FRAME model results : Oxidised nitrogen

5.4.1 Surface concentrations of nitrogen dioxide

The modelled field of NO_2 surface concentrations is shown in Figure 5.14. Like the SO_2 field (Figure 5.9), the spatial distribution is heavily influenced by the large

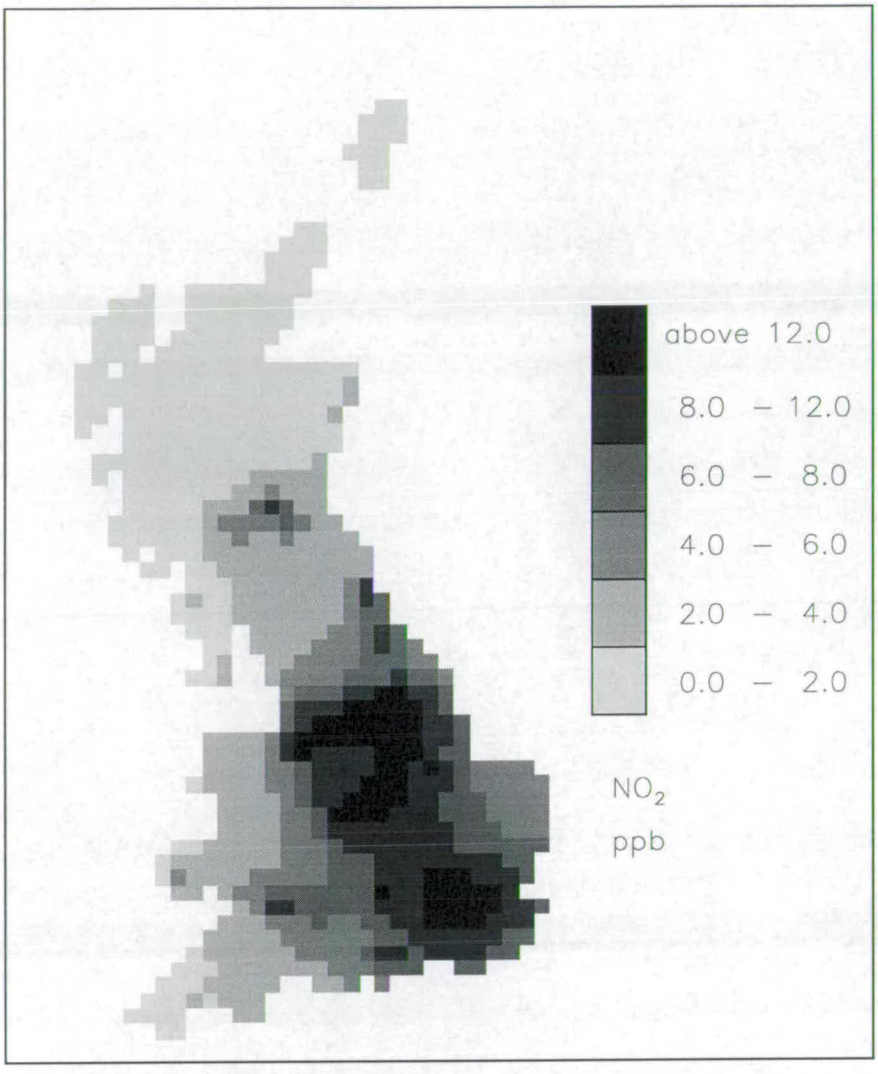

Figure 5.14: Modelled surface concentrations of NO_2 for Great Britain. Data represent an annual average. Units are ppb. RGAR (1996).

sources located in the area between the Midlands and south Yorkshire/Lancashire, and also the area encompassing the Greater London region and the southeast of England (Figure 5.8). These emissions reflect the large urban conurbations, and the fact that population density, road traffic and industrial activity are closely related (INDITE, 1994). A large proportion of these emissions are ground-based, with over half of the total annual emissions for the UK due to motor vehicles (Gillham, *et al.,* 1992).

The grid squares containing power stations are also evident as large 'point source' emissions. Concentrations in these areas are greater than 12 ppb, and fairly large horizontal gradients also occur in these regions. Concentrations in

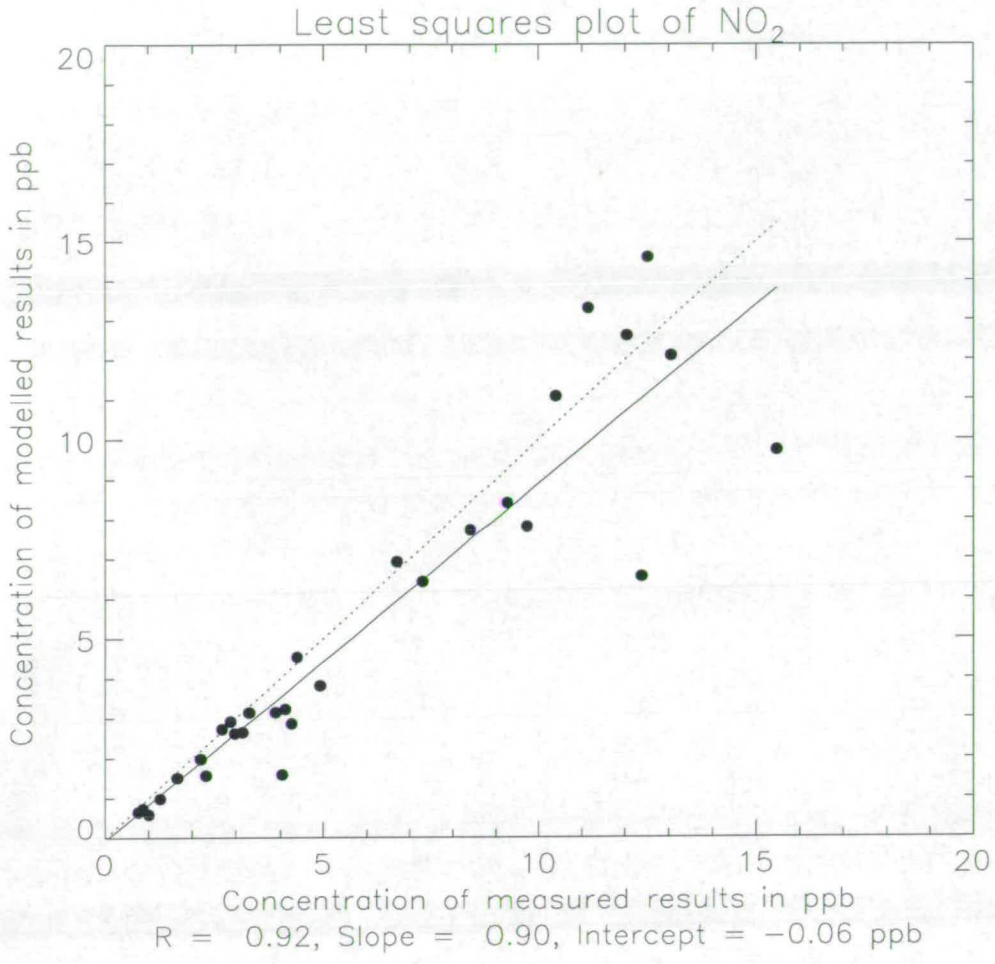

Figure 5.15: Correlation plot of modelled NO_2 concentrations from the FRAME model versus observations from a network of measurements sites. RGAR (1996). The full line is the regression line and the dotted line is the one-to-one line.

more rural areas of Britain, such as northern Scotland and southwest England, have modelled concentrations of less than 2 ppb.

Nitrogen dioxide concentrations are measured at locations belonging to the UK Secondary Acid Deposition Network (section 2.2.2). A comparison was performed between annually-averaged measured data at 32 sites for 1992 and modelled concentrations for grid squares containing these sites. Modelled values represent an averaged value for the grid square as a whole. Figure 5.15 is a regression plot of these modelled and measured data. The correlation between these two sets of data is very good, with a R value of 0.92. For the sample size of n = 32, this correlation has a probability (P) of having arisen by chance of 3.04×10^{-13}, which is statistically significant at the P = 0.1% level. The regression line (full

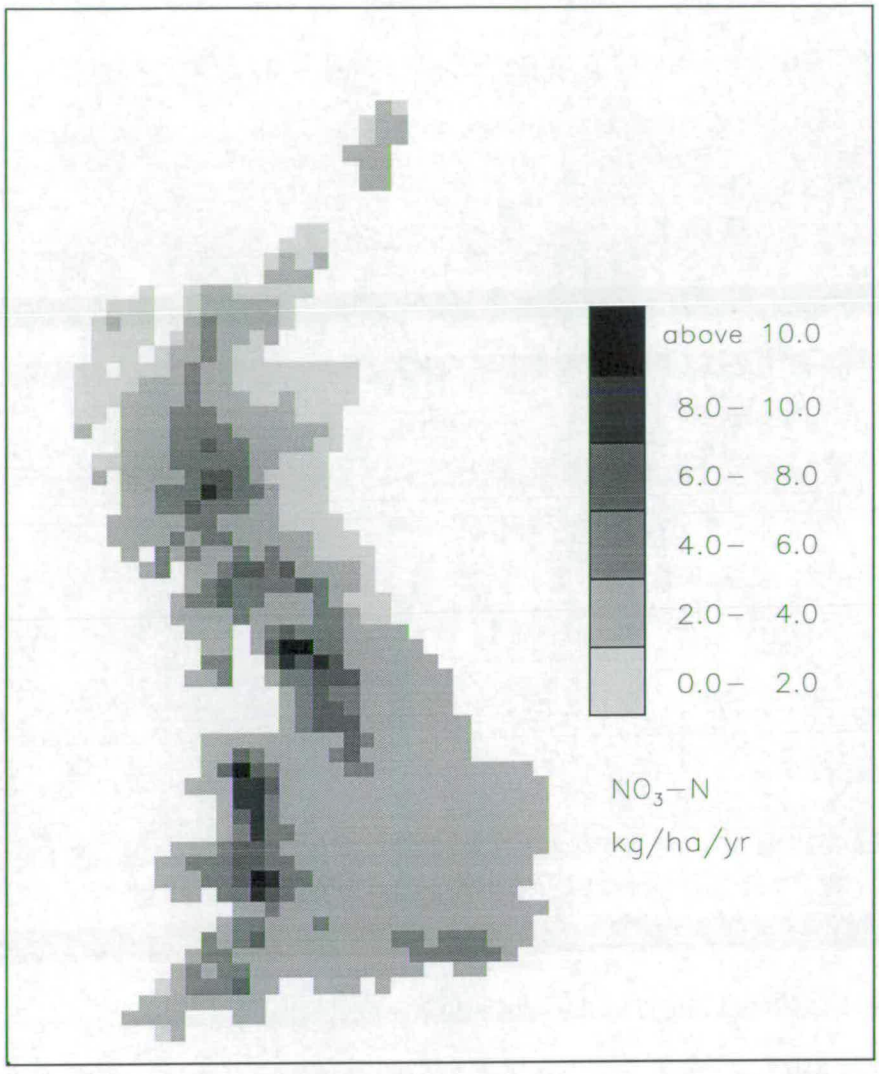

Figure 5.16: Modelled wet deposition of nitrate over Great Britain. Data represent an annual flux. Units are kg N ha^{-1} $year^{-1}$.

line) is very close to the one-to-one line (dotted line), with a slope of 0.90 and an intercept of -0.06 ppb.

5.4.2 Wet deposition of nitrate

A map of the modelled annual flux of nitrate wet deposition is shown in Figure 5.16. The areas which experience large deposition fluxes have a similar pattern to that of the modelled sulphate (Figure 5.11). These locations include central Wales, Northern England around the Pennines hills, and areas of north and west Scotland. These are all areas of high rainfall and fluxes in these areas exceed 8 kg N ha^{-1} $year^{-1}$. There is also a region of high deposition in the south of England,

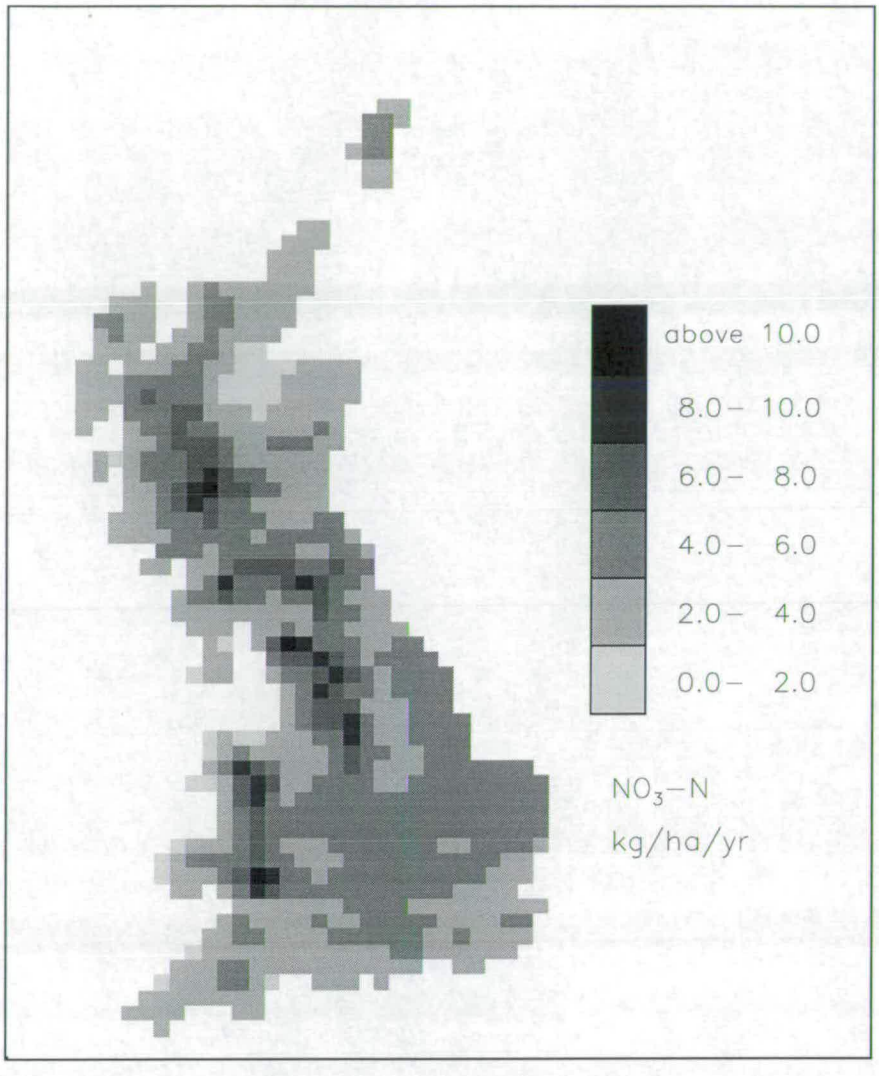

Figure 5.17: Recorded and adjusted measurements of wet deposition of nitrate over Great Britain. Data represent an average annual flux for 1992. Units are kg-N ha^{-1} $year^{-1}$. RGAR (1996).

which may be due to large amounts of material imported from the continent, being removed by the modelled wet deposition process.

A corresponding map of annual fluxes of wet deposition for Great Britain (1992) is shown in Figure 5.17. This was created by using measurements of nitrate in precipitation (section 2.2.2) combined with precipitation data. Like the map of observed sulphate fluxes (Figure 5.12), an interpolation procedure has been employed for locations between the measurements. The same adjustment was used to account for the seeder-feeder effect (Dore *et al.*, 1992).

The one major difference between this figure and the modelled data (Figure

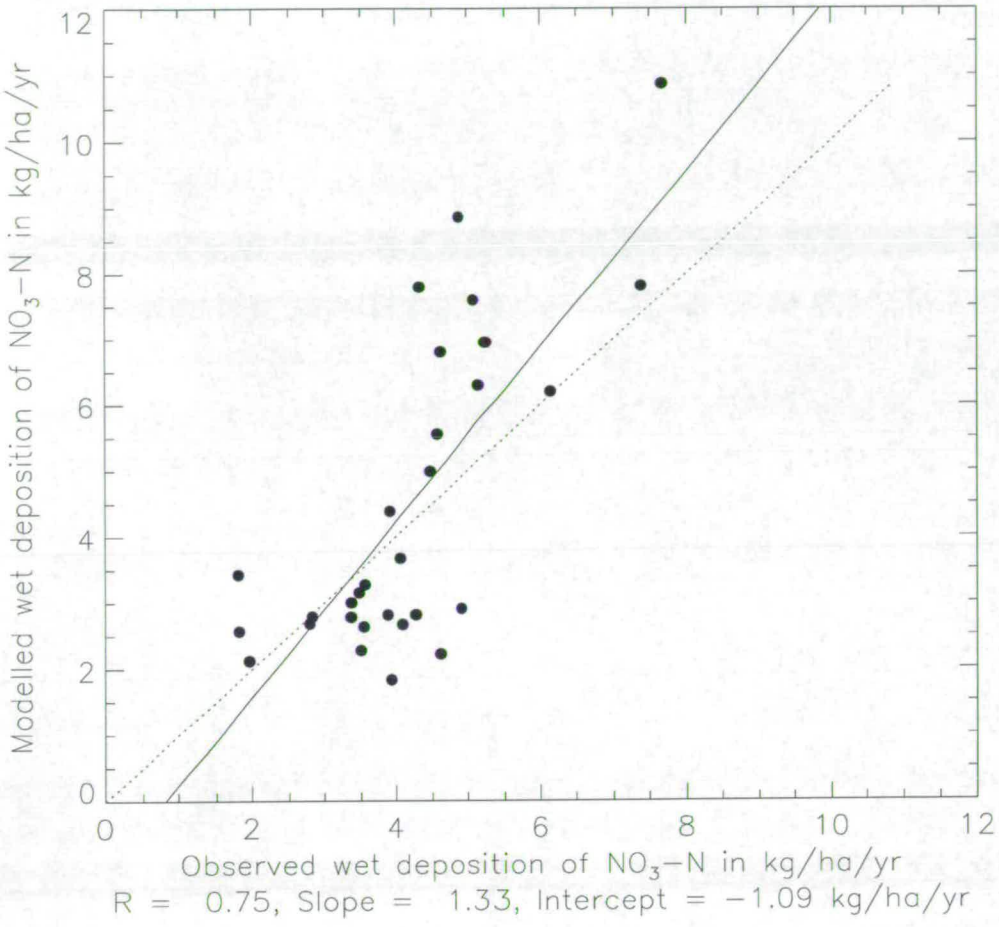

Figure 5.18: Correlation plot of modelled NO_3-N wet deposition fluxes from the FRAME model versus observations from a network of measurement sites. RGAR (1996). The full line is the regression line and the dotted line is the one-to-one line.

5.16) is that central and eastern England experience larger fluxes, between 4-6 kg N ha^{-1} $year^{-1}$ compared to modelled values of 2-4 kg N ha^{-1} $year^{-1}$. Areas in central Wales have slightly less observed deposition, compared to the modelled data, while recorded deposition to Scotland as a whole seems to be greater than the modelled fluxes.

A regression plot of measured and modelled data is shown in Figure 5.18. The value of R is 0.75. For the sample size of n = 32, this correlation has a probability (P) of having arisen by chance of 1.55×10^{-6}, which is statistically significant at the P = 0.1% level.

5.4.3 A comparison of annual budgets of oxidised nitrogen for Great Britain

The annual budget of oxidised nitrogen for Great Britain, calculated by the FRAME model, is given in Table 5.6. The annual import of material is 126.0 Gg N year^{-1} and the annual export of nitrogen oxides from FRAME is 768.5 Gg N year^{-1}. The model predicts the annual flux of dry deposition to be 53.8 Gg N year^{-1} and the wet deposition flux to be 87.6 Gg N year^{-1}. The official UK Department of the Environment estimate of dry deposition (INDITE, 1994; RGAR, 1996) is 70.0 Gg N year^{-1}. This figure is a combined total for NO_2 and HNO_3. The calculation of the ITE NO_2 total is identical to the procedure used for SO_2 described earlier, being an inferential model (2.2.1) using an interpolated field of NO_2 surface concentrations. The ITE value of 70.0 Gg N year^{-1} is larger than the FRAME estimate of 53.8 Gg N year^{-1}, which comprises not just NO_2 but other NO_x species as well. The model concentration field reflects the measured data very well (Figure 5.15), but the ITE dry deposition total is under-estimated by about 23%.

Table 5.7 gives a breakdown of the contribution of each oxidised nitrogen species to the total dry deposition flux to Great Britain. The majority of the dry deposition is in the form of NO_2, but dry deposition of NO_3^- also contributes a significant amount.

The modelled wet deposition data is 18% less than the ITE values. The FRAME estimate for annual wet deposition of oxidised nitrogen to Great Britain is 87.6 Gg N year^{-1} compared to the value in RGAR (1996) of 106.7 Gg N year^{-1}.

The EMEP model predict an annual import of oxidised nitrogen for 1992 of 46.6 Gg N year^{-1} which is around 37% of the FRAME estimate of 125.8 Gg N year^{-1}. The annual export value of 703.6 Gg N year^{-1} from EMEP is closer to the FRAME value of 768.5 Gg N year^{-1}. The total deposition flux as predicted by EMEP is 117 Gg N year^{-1}, which is less than both the FRAME estimate of 141.4 Gg N year^{-1} and the ITE value of 176.7 Gg N year^{-1}.

Wind sector origin of trajectories	Emissions of NO_x-N	Import of NO_x-N	Dry deposition of NO_x-N	Wet deposition of NO_x-N	Export of
0 - 45	784.1	23.1 (2.5)	48.5 (5.3)	62.5 (6.8)	696.2 (75.9)
45 - 90	784.1	247.7 (19.6)	62.8 (5.0)	123.2 (9.7)	845.9 (66.8)
90 - 135	784.1	705.7 (46.6)	90.3 (6.0)	283.9 (18.7)	1115.6 (73.6)
135 - 180	784.1	385.3 (33.1)	99.9 (8.6)	333.3 (28.7)	736.2 (63.3)
180- 225	784.1	122.8 (14.2)	49.6 (5.8)	59.2 (6.9)	798.1 (92.6)
225 - 270	784.1	30.9 (6.0)	34.3 (6.6)	18.0 (3.5)	762.7 (147.2)
270 - 315	784.1	17.7 (3.2)	33.7 (6.0)	16.7 (3.0)	751.4 (133.8)
315 - 360	784.1	3.6 (0.6)	61.4 (10.6)	59.5 (10.3)	666.8 (115.4)
Averaged annual modelled budget of NO_x-N	784.1	125.8	53.8	87.6	768.5

Table 5.6: Modelled annual budget of oxidised nitrogen for eight wind sectors and an averaged annual budget for the country. Data in brackets are the frequency weighted total for each wind sector. The units are Gg N $year^{-1}$.

Dry deposition			
% NO	% NO_2	% NO_3	% PAN
0	72	20	8

Table 5.7: A comparison of annual modelled dry deposition of oxidised nitrogen.

Source of data	Emissions of N	Import of N	Dry deposition of N	Wet deposition of N	Export of N
EMEP model data for 1992	774	46.6	Combined total of 117		703.6
ITE interpolated measurements	-	-	70	106.7	-

Table 5.8: Annual oxidised nitrogen budgets from the EMEP model for 1992 (Barrett and Seland, 1995) and ITE interpolated data from an inferential model (dry deposition) and a seeder-feeder model (wet deposition) (RGAR, 1996).

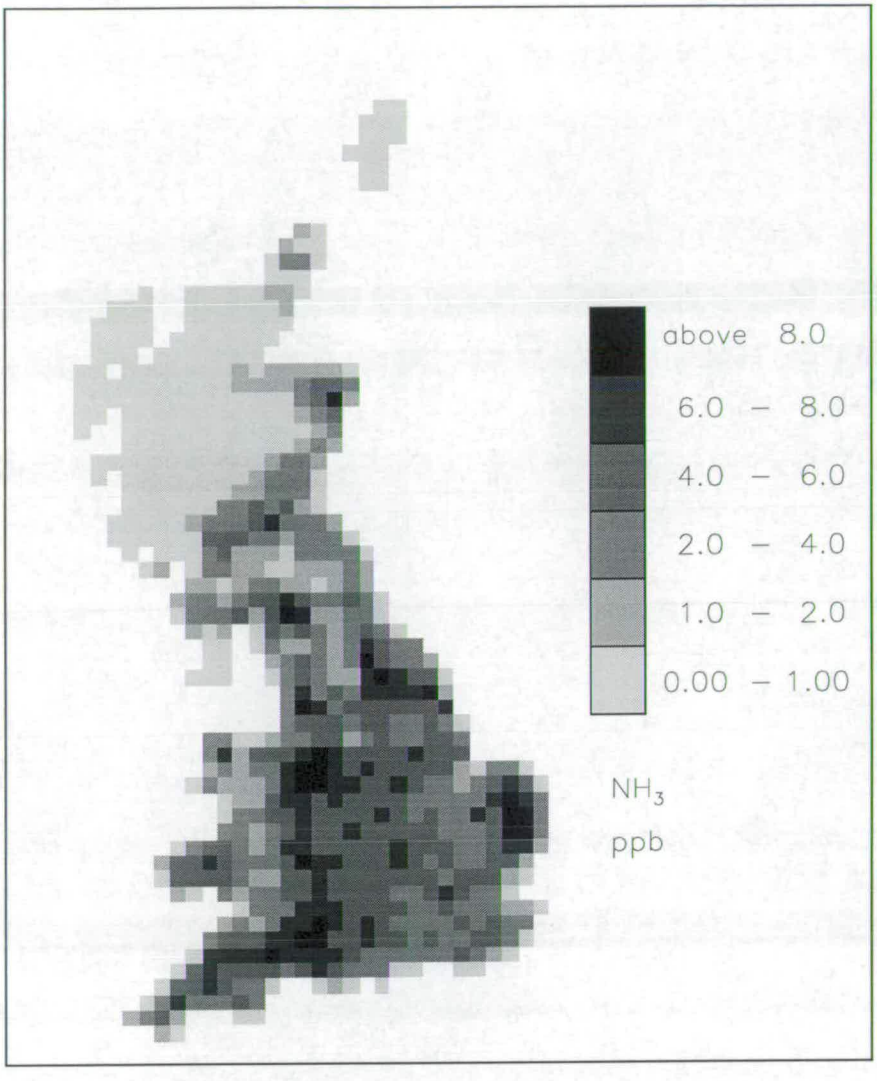

Figure 5.19: Modelled surface concentrations of NH_3 for Great Britain. Data represents an annual average. Units are ppb.

5.5 FRAME model results : Reduced nitrogen

5.5.1 Surface concentrations of ammonia

A plot of the modelled surface (1-2 m layer) concentrations of NH_3 is shown in Figure 5.19. The air concentration field shows the very large predicted spatial variability in NH_3 ground level air concentrations. The distribution of air concentrations is very similar to the distribution of emissions (Figure 2.4), showing the highest air concentrations in a broad band in the borders of England and Wales. This is consistent with large concentrations of livestock, cattle and sheep farming in these areas, as well as more local high emissions areas in north-

west England (west Lancashire, north Cumbria). A further high emission area in eastern England (East Anglia) is associated with large concentrations of poultry and pig farming. A significant feature of this map is the model estimation of extremely low air concentrations over the whole of the Scottish Highlands, reflecting an extremely low density of the known sources in this area.

This plot is very different to the interpolated map of surface concentrations measured by the diffusion tubes (Figure 2.1). There is much greater spatial variation in the modelled concentrations and much larger horizontal gradients are observed in the modelled results. The diffusion tube map does not have a concentration peak over East Anglia and modelled concentrations in northern and western Scotland are much less than the diffusion tube data.

To test the accuracy of the model results, a comparison was performed with measured data of ground level ammonia air concentrations at a height of 1.5 m. The network of passive diffusion tubes, operated between 1987 - 1990 (Atkins and Lee, 1992), provides the most extensive set of measurements available in the United Kingdom at the present time. The greatest number of monitoring sites were operational in the period of 1987 - 1988 with a total of 40 sites, and these are the data that are used to compare with the model results. These data are slighlty different from the data presented in Figure 2.1 since these are the mean values for just one year, whereas the data in Figure 2.1 are the mean of the entire 3 year period.

Anderson (1991) reported that the samplers were thought to give a value which is greater that the actual air concentrations present, and a scaling factor of 0.45 should be applied to all diffusion data. This factor, though very uncertain, has been supported by further studies in the UK (Sutton *et al.*, 1994, unpublished data), and was also used in a previous comparison of model results with the UK measurements by Lee and Johnson (1993). It should also be noted that, as with the concentration data for SO_2 and NO_2, the model results represent a grid square average. It has already been mentioned in section 2.4.2 that concentrations can vary greatly over the range of a few hundred metres (section 5.1), and thus over a range of 20 km, there may be a great deal of variation. Any comparison with measurement data should be treated with some caution and be viewed as giving an indication of the overall effectiveness of the model performance, as opposed

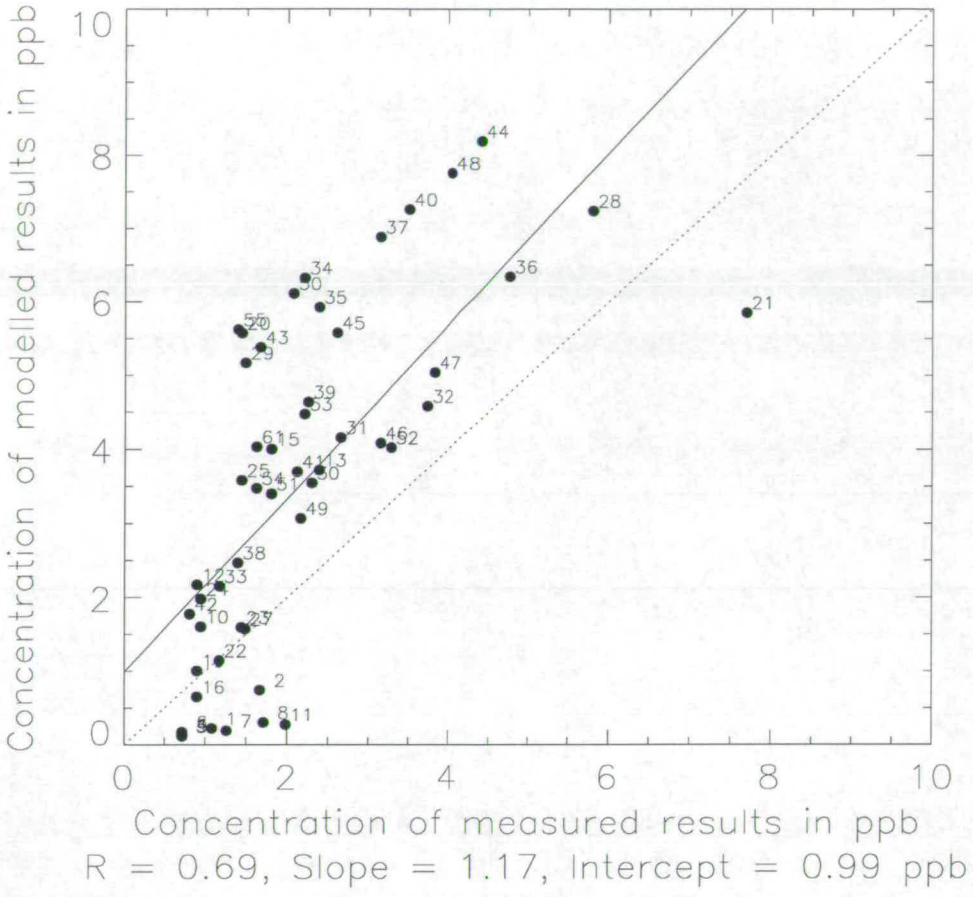

Figure 5.20: Correlation plot of modelled NH_3 surface concentrations from the FRAME model versus observations from a network of measurements sites (Atkins and Lee, 1992; multiplied by a correction factor of 0.45; Anderson, 1991). Each point has number assigned, which corresponds to the location of the measurement site shown in Figure 5.21. The full line is the regression line and the dotted line is the one-to-one line.

to accurately modelling concentrations at specific locations.

Figure 5.20 is a regression plot of modelled values against measured data (corrected by 0.45), and can be compared with a similar plot using data from the HARM model (section 2.4.2, Figure 2.11). The dotted line is the one-to-one agreement, and the solid line is the best fit line produced by regression analysis. The correlation coefficient (R) has a value of 0.69. For the sample size of n =51, this correlation has a probability (P) of having arisen by chance of 1.53 $\times 10^{-8}$, which is statistically significant at the P = 0.1% level. Although there are significant divergences between the model predictions and the corrected measurements, Figure 5.20 shows that the slope of the regression line is close to a value

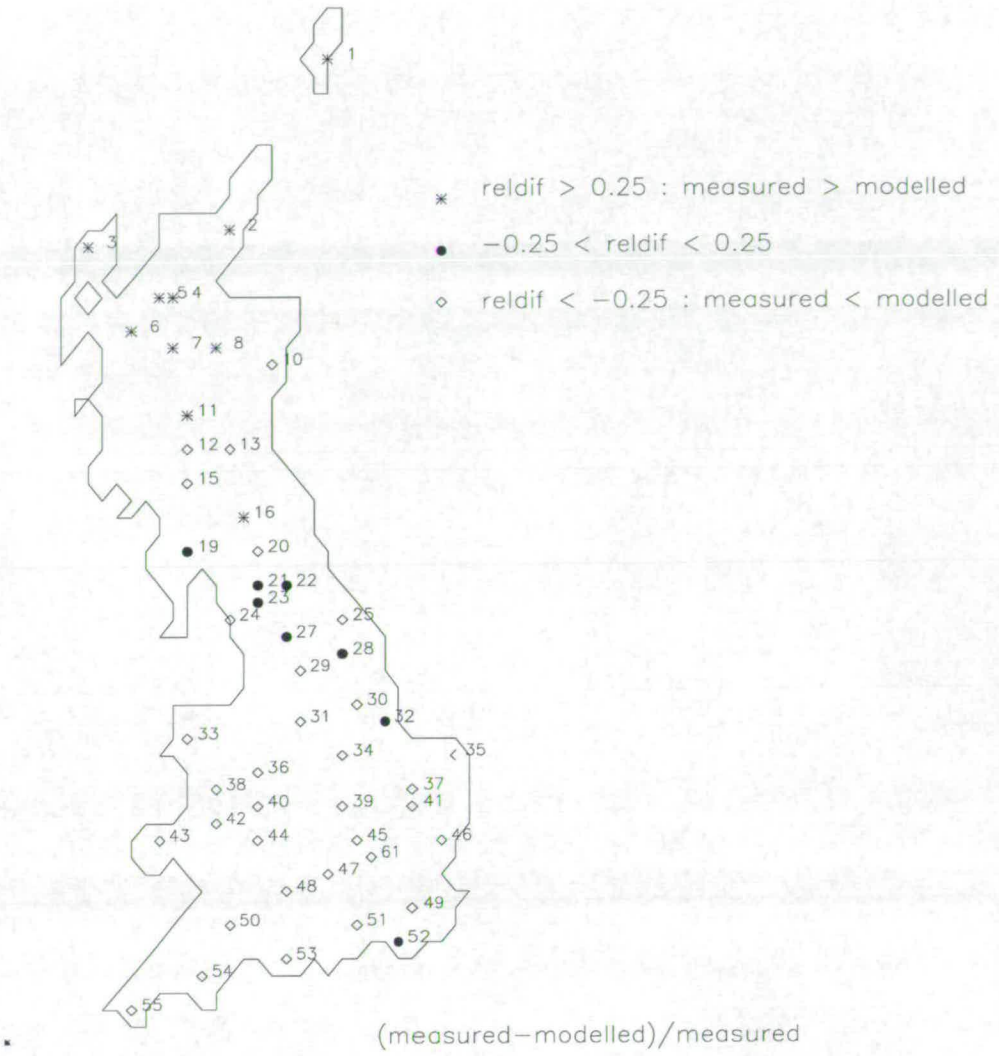

Figure 5.21: A map of categorised relative differences (reldif) ($\frac{\text{measured}-\text{modelled}}{\text{measured}}$) of NH_3 surface concentrations. Modelled data are from the 20 km version of FRAME.

of 1. The model generally seems to over-estimate the corrected measurements, with the intercept value of 0.96 ppb giving an indication of the magnitude of this over-prediction. A group of measurements from northern Scotland seems to be at odds with the general trend of the data (Figure 5.21; station numbers 1, 2, 3, 4, 5, 6, 7, 8 and 11). The fact that all of these stations are in the same area, and form a cluster, suggests that there is a general disagreement between model data and measurements for this region. Whilst diffusion tubes may over-estimate concentrations at low levels, recent measurements form the Netherlands suggest that at large concentrations of NH_3 (typically 5-20 μg m^{-3}) diffusion tubes may perform satisfactory (Thijsse *et al.*, 1996).

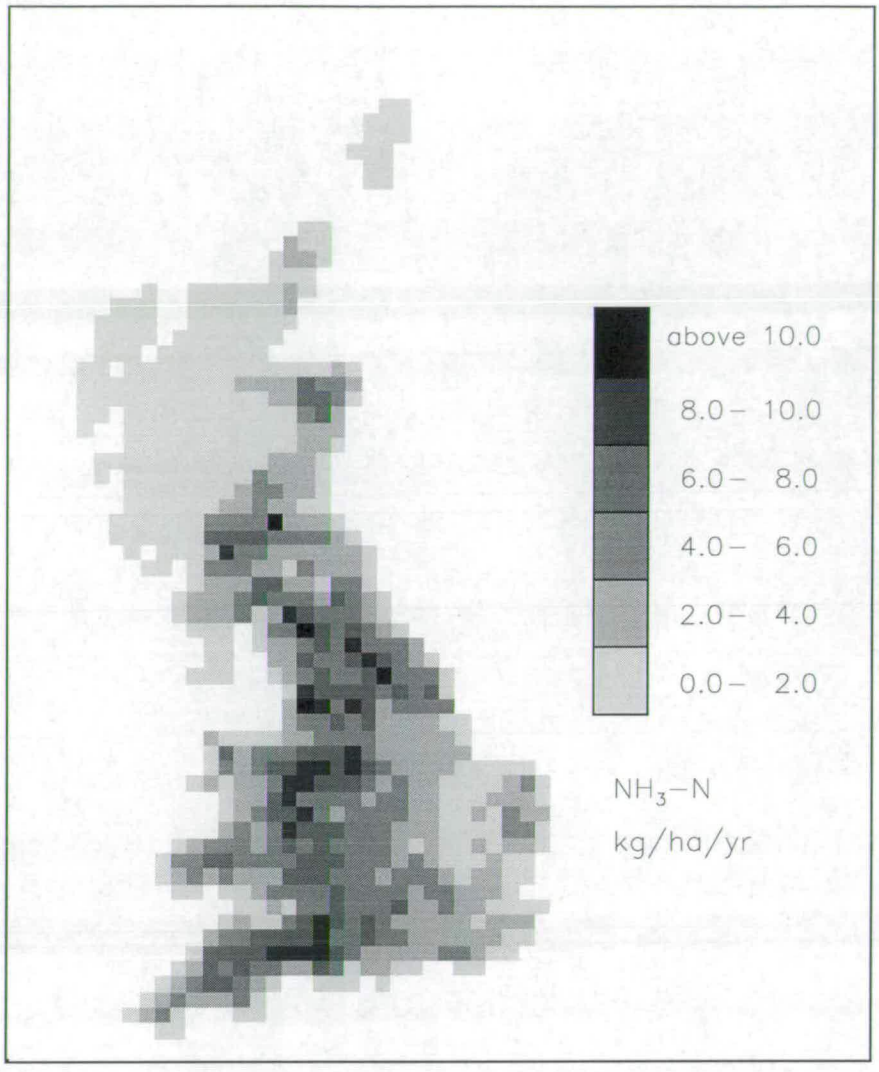

Figure 5.22: Modelled annual flux of ammonia dry deposition to Great Britain. Units are kg ha^{-1} $year^{-1}$.

5.5.2 Dry deposition of ammonia

A plot of annual dry deposition of NH_3-N, as calculated by the FRAME model, is shown in Figure 5.22. The total annual flux of NH_3-N dry deposition to Great Britain as a whole is 87.9 Gg N $year^{-1}$. As with the map of air concentrations of NH_3, the areas of large deposition are generally associated with areas of high emission. These areas include south-west England, the Wales/England border region and areas in northern England. The largest deposition occurs in areas where there are both high emissions and large areas of semi-natural ecosystems, such as forest and moorland, generally in the west. This is due to the relatively large values of V_d assigned to these regions by the model (section 4.3.8, Figure

4.17). Consequently, in areas where emission is large, but the modelled deposition velocity is small, such as in East Anglia, dry deposition will be smaller than similar emission areas in the west, but the air concentrations will be greater. A comparison can be made of modelled data and the INDITE (1994) data, which were produced using an interpolated concentration field and an inferential model (Figure 2.2). The two plots seem quite similar over areas of England and Wales, but differ significantly over Scotland. This is a consequence of the difference in air concentration fields shown in Figures 5.20 and 5.21. Because of the large modelled deposition velocities used by both FRAME (Figure 4.17) and the inferential model in this area, any error in the air concentrations will lead to a large error in the calculated dry deposition flux.

5.5.3 Surface concentrations of ammonium aerosol

A plot of surface concentrations of ammonium aerosol over Great Britain is shown in Figure 5.23. The largest concentrations occur in a broad band stretching from the Greater London region up to the north Midlands and Yorkshire, with the maximum values occurring in the same area of large SO_2 and NO_2 emissions (Figures 5.7 and 5.8). East Anglia also has large concentrations, due to the area of very large NH_3 emissions that occur there (Figure 2.4) and NH_4^+ aerosol formation will be enhanced in that region due to polluted air being advected over from the continent. Horizontal concentration gradients are very small over all of the country, and values in northern and western Scotland are very low, less than 0.4 μg m^{-3}.

5.5.4 Dry deposition of ammonium aerosol

Figure 5.24 is a plot of NH_4^+-N dry deposition to Great Britain. The data in this plot are directly proportional to the surface concentration data of NH_4^+, shown in Figure 5.23, since a spatially and temporally-invariant deposition velocity of 0.001 m s^{-1} is used in FRAME to model NH_4^+-N dry deposition. The total annual dry deposition flux to Great Britain as a whole is 6.7 Gg N $year^{-1}$, which is 7.1% of the total annual flux of NH_x-N dry deposition.

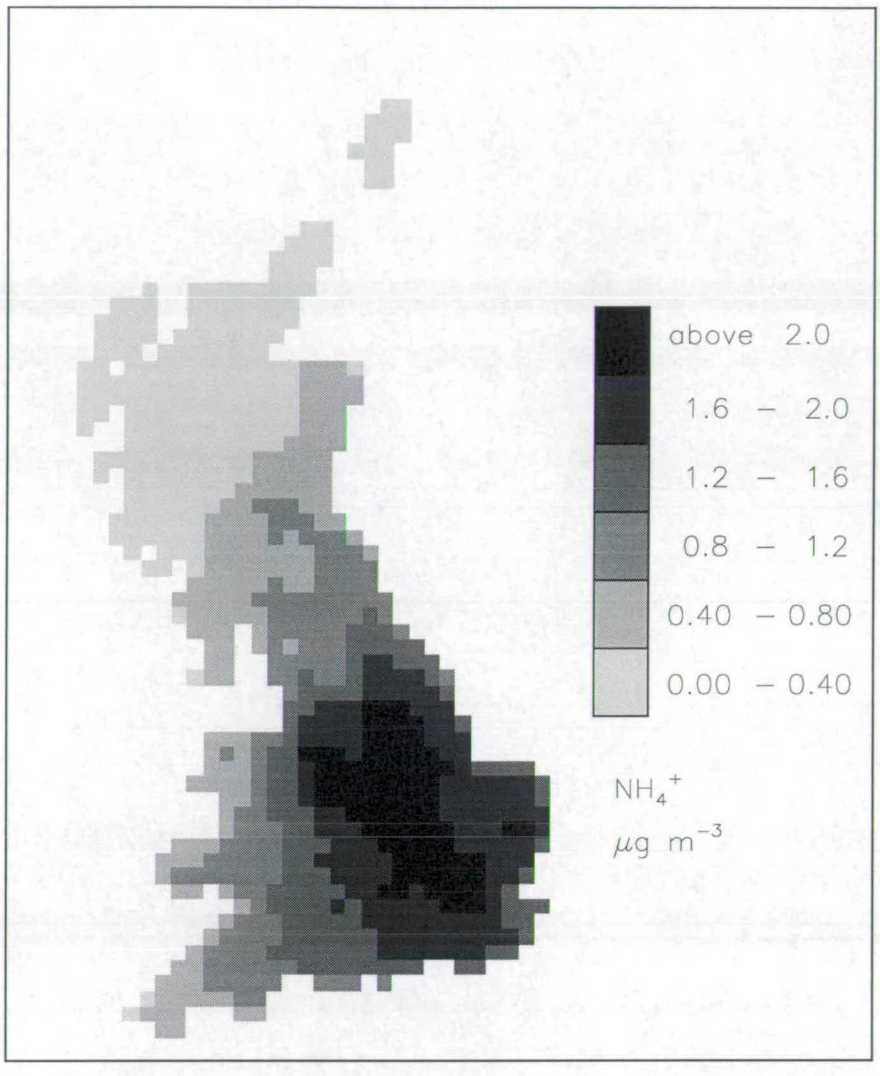

Figure 5.23: Modelled surface concentrations of NH_4^+ for Great Britain. Data represents an annual average. Units are $\mu g\ m^{-3}$.

5.5.5 Wet deposition of reduced nitrogen

A map of the annual wet deposition flux of reduced nitrogen to Great Britain is shown in Figure 5.25. Wet deposition is modelled by the use of washout coefficients (section 3.2), together with an annual rainfall map (Figure 4.19). NH_3 and NH_4^+ are treated separately by the model, and the results are combined to create the map in Figure 5.25. The total wet deposition flux of NH_3-N is 6.8 Gg N $year^{-1}$ and the total wet deposition flux of NH_4^+-N is 51.9 Gg N $year^{-1}$. This gives a ratio of NH_4^+-N to NH_3-N of 7.54:1. The spatial distribution of this plot is very similar to both the modelled sulphate (Figure 5.11) and nitrate (Figure 5.16) wet deposition data. This is not surprising since the main form of NH_3 and

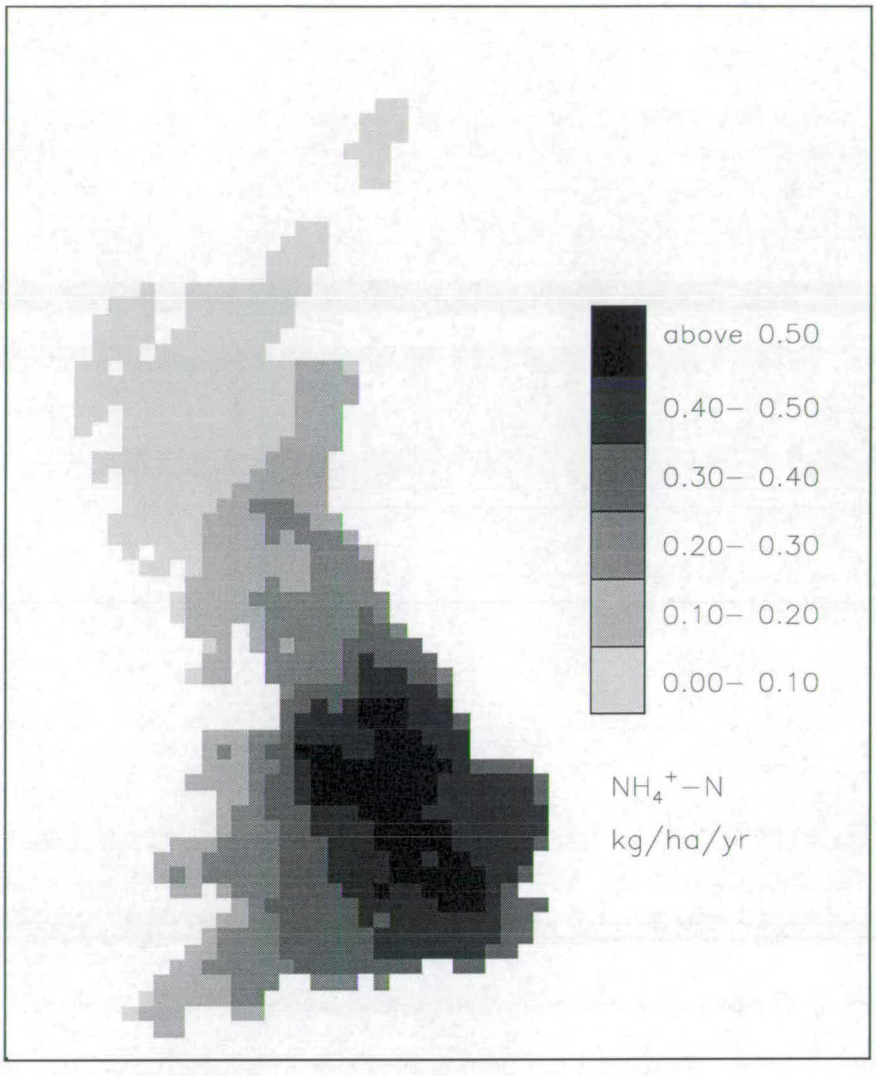

Figure 5.24: Modelled annual flux of ammonium aerosol dry deposition to Great Britain. Units are kg ha^{-1} $year^{-1}$.

NH_4^+ wet deposition is in the form of $(NH_4)_2SO_4$ and NH_4NO_3. Measured data were recorded at locations which belong to the UK Secondary Acid Deposition Network (section 2.2.2), and have been interpolated across the country to create a map of the annual wet deposition flux to Great Britain. Adjustment were made to the data to account for the increased concentration in precipitation due to the seeder-feeder effect (Dore *et al.*, 1992). The interpolated map is an annual average for 1992 and is shown in Figure 2.3. Whilst the spatial patterns are similar, the FRAME data seems to under-estimate the observed data by a factor of 2.2.

A correlation plot of the measured data and modelled data is shown in Fig-

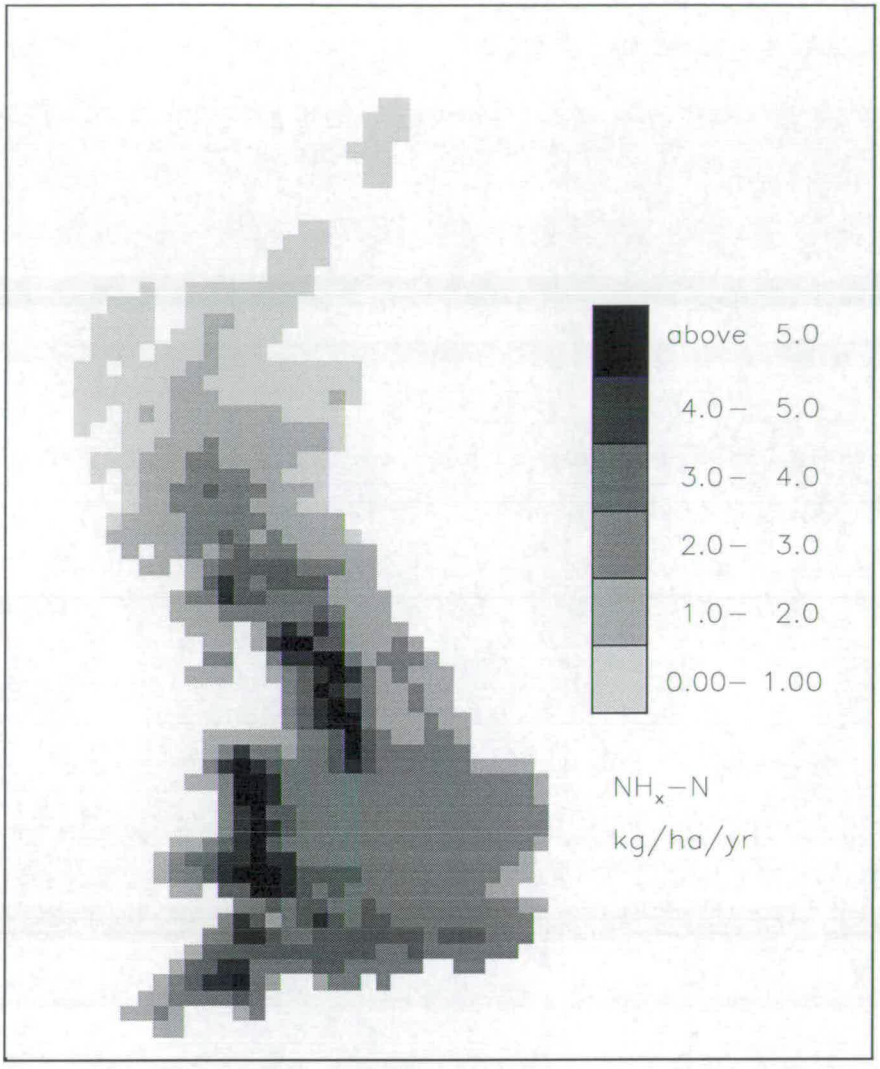

Figure 5.25: Modelled annual flux of N-NH_x wet deposition to Great Britain. Units are kg ha^{-1} $year^{-1}$.

ure 5.26. The correlation coefficient R has a value of 0.71. For the sample size of n =30, this correlation has a probability (P) of having arisen by chance of 9.88×10^{-6}, which is statistically significant at the P = 0.1% level. The gradient of the regression line (full line) is 0.54, which shows that the model is under-estimating measurements by nearly a factor of 2. The locations of the measurement stations are shown in Figure 5.27, which is a plot of the relative differences of (modelled - measurements)/measurements. With the majority of the stations, the model is consistently under-estimating measurements by more than 25%, and it is only at 7 stations where the magnitude of the relative difference is less than 0.25. At two stations, 31 and 8, the model over-estimates the measured data by

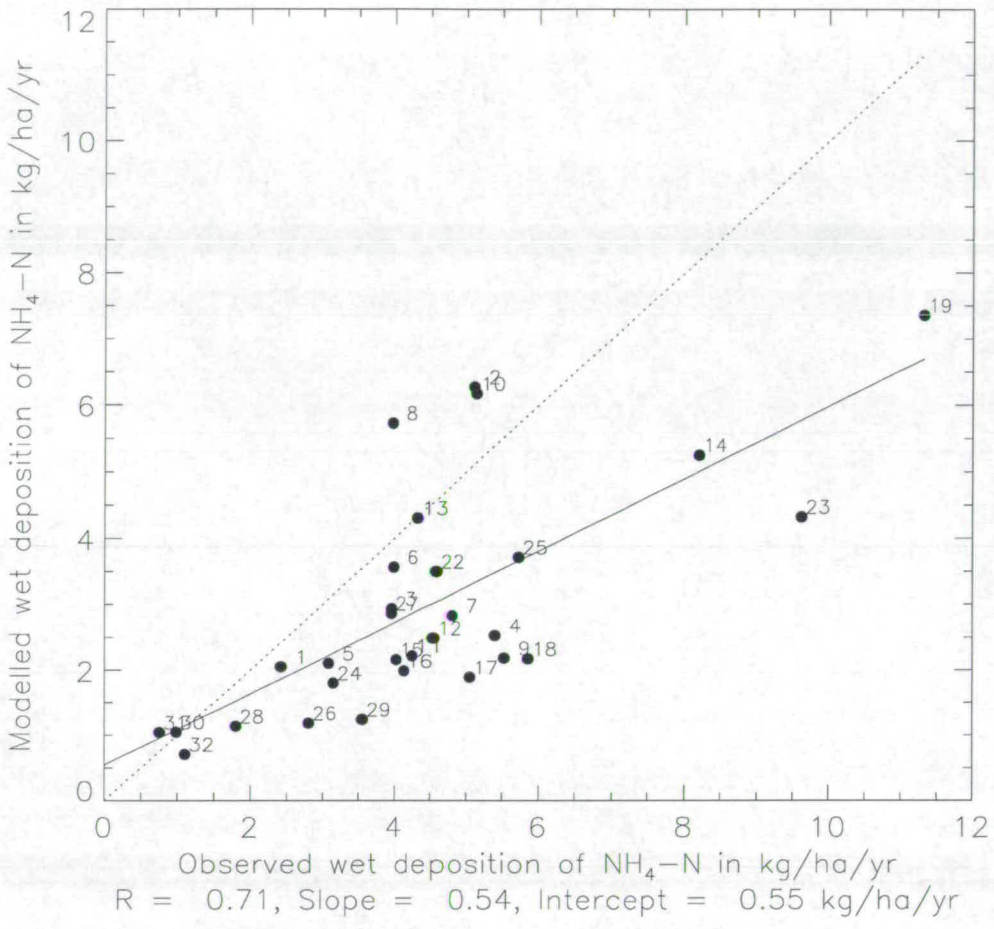

Figure 5.26: Correlation plot of modelled N-NH_x wet deposition fluxes from the FRAME model versus observations from a network of measurements sites. Each point has number assigned, which corresponds to the location of the measurement site shown in Figure 5.27. RGAR (1996). The full line is the regression line and the dotted line is the one-to-one line.

more than 25%.

5.5.6 A Comparison of annual budgets of reduced nitrogen for Great Britain

The modelled annual budget of reduced nitrogen to Great Britain, as predicted by the the FRAME model, is given in Table 5.9. The annual dry deposition flux of reduced nitrogen is 94.6 Gg N $year^{-1}$ and the wet deposition total is 58.7 Gg N $year^{-1}$. The model calculates that 35.7 Gg NH_x-N are imported annually and 163.8 Gg NH_x-N are exported annually. The results from each wind sector show

Wind sector origin of trajectories	Emissions of NH_x-N	Import of NH_x-N	Dry deposition of NH_x-N	Wet deposition of NH_x-N	Export of NH_x-N
0 - 45	281.4	2.5 (0.3)	82.5 (9.0)	55.1 (6.0)	146.4 (16.0)
45 - 90	281.4	39.9 (3.2)	97.2 (7.7)	74.5 (5.9)	149.5 (11.8)
90 - 135	281.4	105.5 (7.0)	133.0 (8.8)	103.0 (6.8)	150.8 (10.0)
135 - 180	281.4	73.4 (6.3)	132.3 (11.4)	106.9 (9.2)	115.5 (9.9)
180- 225	281.4	55.8 (6.5)	85.3 (9.9)	68.2 (7.9)	183.6 (21.3)
225 - 270	281.4	32.6 (6.3)	84.1 (16.2)	41.8 (8.1)	188.1 (36.3)
270 - 315	281.4	28.7 (5.1)	81.0 (14.4)	36.7 (6.5)	192.3 (34.2)
315 - 360	281.4	6.4 (1.1)	99.6 (17.2)	47.4 (8.2)	140.7 (24.3)
Averaged annual modelled budget of NH_x-N	281.4	35.7	94.6	58.7	163.8

Table 5.9: Modelled annual budget of reduced nitrogen for the eight wind sectors and an averaged annual budget for the country. Data in brackets are the frequency weighted total for each wind sector. The units are Gg of NH_x-N $year^{-1}$.

Source of data	Emissions of NH_x-N	Import of NH_x-N	Dry deposition of NH_x-N	Wet deposition of NH_x-N	Export of NH_x-N
EMEP model data for 1992	314.6	29.6	Combined total of 205.7		138.4
ITE interpolated measurements	-	-	94.5 (only NH_3-N)	131	-

Table 5.10: Annual reduced nitrogen budgets from the EMEP model for 1992 (Barrett and Seland, 1995) and ITE interpolated data from an inferential model (dry deposition) and a seeder-feeder model (wet deposition) (INDITE, 1994; RGAR, 1996).

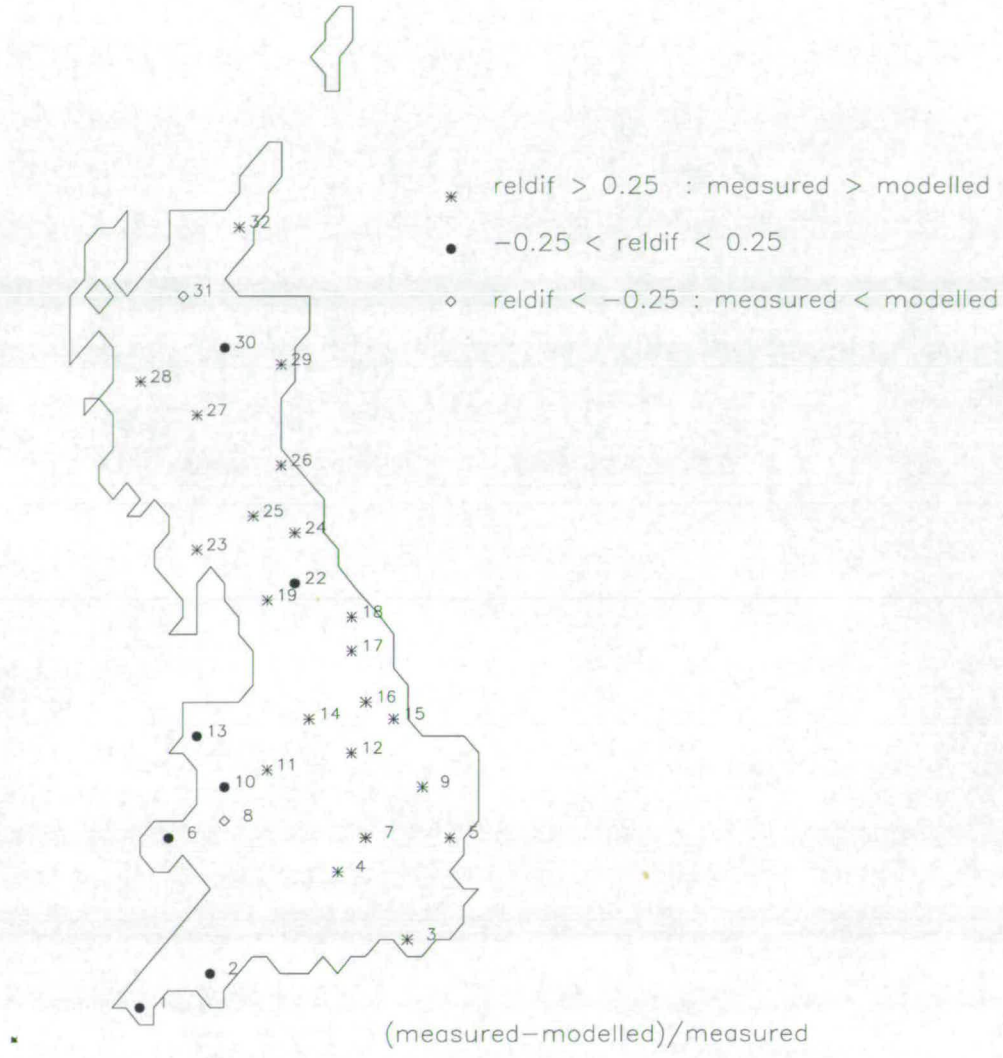

Figure 5.27: A map of categorised relative differences ($\frac{\text{measured}-\text{modelled}}{\text{measured}}$) of NH_x wet deposition flux. Modelled data are from the 20 km version of FRAME.

some interesting differences. The greatest export of reduced nitrogen occurs when wind comes from the west-northwest direction. The amount exported from this wind sector is equivalent to 68.3% of the annual emissions. In comparison, wind from the south-southeast shows the least export of NH_x-N, equivalent to just 41% of the annual emissions. This low export rate is accompanied by the largest total for wet deposition, nearly 38% of the emissions. This is due to polluted air being advected over northwest Scotland, where the greatest rainfall occurs (Figure 4.19), and thus a large proportion of the material in the air column is washed out. The directional-dependence of the annual dry deposition flux shows an inverse relationship to the optimised wind speeds calculated in section 4.3.2, Table 4.7. With a lower wind speed, the air column will spend more time over

land and thus will have a longer period of time during which dry deposition can take place. This appears to have a greater effect than the reduced magnitude of V_d with low wind speeds, which would tend to decrease the rate of dry deposition.

The modelled (FRAME) dry deposition total for NH_3 of 87.9 Gg NH_3-N year^{-1} is slightly less than the ITE calculated figure of 94.5 Gg NH_3-N year^{-1}. However, the spatial distribution of the two sets of data are very different in some areas. The observed wet deposition total is 131 Gg NH_x-N year^{-1} and is over twice the value of the FRAME estimate of 58.7 Gg NH_x-N year^{-1}.

The FRAME data compares better with the EMEP model results. The EMEP estimate for annual import of NH_x-N is 29.6 Gg year^{-1}, which is 83% of the FRAME value of 35.7 Gg year^{-1}. The annual export of NH_x-N from the EMEP model is 138.4 Gg year^{-1} which is close to the FRAME estimate of 163.8 Gg year^{-1}. The combined deposition total estimated by the EMEP model is 205.7 Gg year^{-1} and the comparable FRAME value is 153.3 Gg year^{-1}.

5.6 Spatial variation of the model timestep

The adaptive timestep scheme presented in section 4.3.7 allows FRAME to have a variable timestep, dependent on the maximum rate of vertical diffusion occurring in the air column. In practice, the main factors influencing the size of the timestep are the large gradients of NH_3 occurring near the surface, which require the smallest timestep. However, large gradients may also occur across the cloud base as material, such as SO_2, is removed by oxidation. The map of the average timestep employed by the model is shown in Figure 5.28. Large timesteps are taken across north-western Scotland, due to the low emissions in this area resulting in small gradients of material even though modelled values of V_d for NH_3 are relatively large (Figure 4.17). The areas of smallest timestep occurs in a region of north-eastern England and southern Scotland.

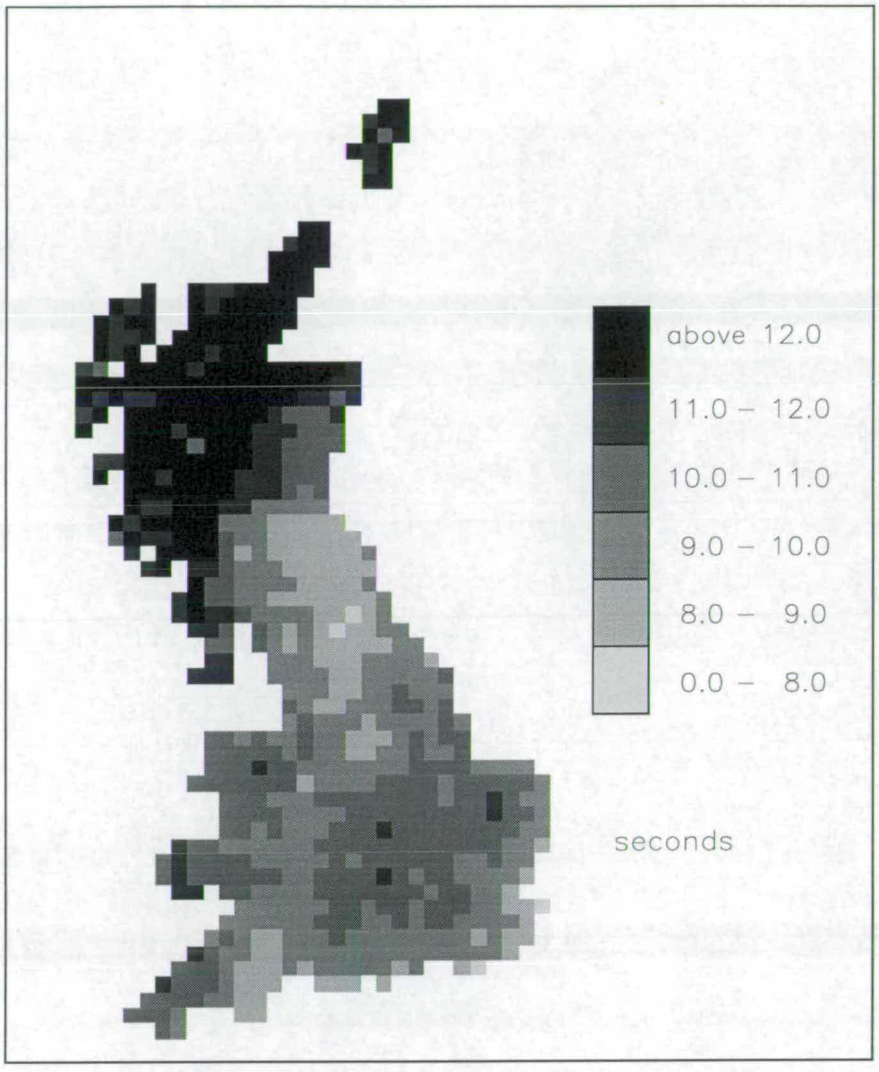

Figure 5.28: Spatial variation in the model timestep using the adaptive timestep method. Units are seconds.

5.7 Assessment of model results using a simpler vertical mixing scheme

The main feature of FRAME, which is different from many other models (section 2.4), is the use of a multi-layer method of describing vertical dispersion. This is especially important for ammonia, as it allows the model to determine the surface concentrations with a much greater degree of accuracy than has been possible with the use of simpler methods, specifically those using the assumption of instantaneous and thorough mixing of emissions throughout the boundary layer. However, it is not so clear how much the use of a multi-layer scheme benefits

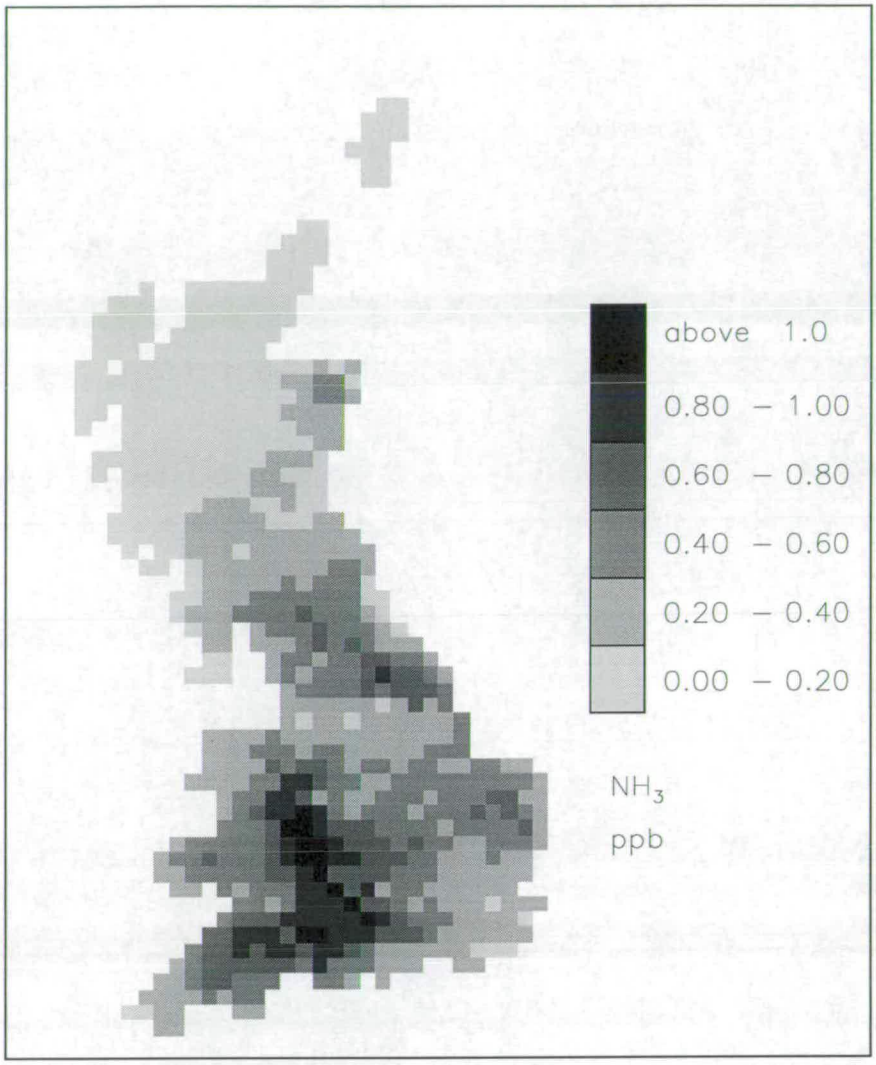

Figure 5.29: Modelled surface concentrations of NH_3 for Great Britain using the vertical dispersion scheme of instantaneous mixing. Data represent an annual average. Units are ppb.

other chemical species in the model, if indeed at all. In this section, the results produced by FRAME using the instantaneous mixing scheme are examined and discussed, and comparisons are performed with relevant model results produced using the multi-layer mixing scheme.

5.7.1 Surface concentrations of ammonia

A plot of surface concentrations of NH_3, produced by FRAME using the method of instantaneous mixing, is shown in Figure 5.29. The concentrations in this plot are very much reduced over much of Great Britain, especially in areas of high

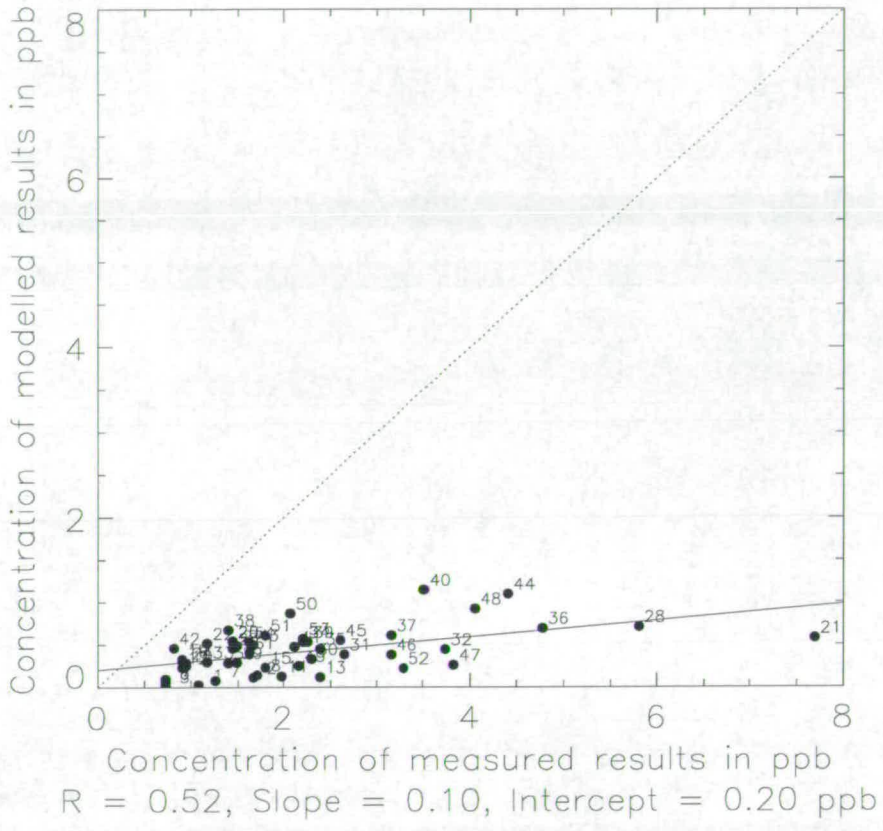

Figure 5.30: Correlation plot of modelled NH_3 surface concentrations from the FRAME model versus observations from a network of measurements sites (Atkins and Lee, 1992). These data were produced using the vertical dispersion scheme of instantaneous mixing. Each point has number assigned, which corresponds to the location of the measurement site shown in Figure 5.21. The full line is the regression line and the dotted line is the one-to-one line.

emissions, in comparison with the concentration data produced by FRAME using the multi-layer mixing scheme. There is less spatial variability and horizontal gradients are greatly reduced. Maximum concentrations are just over 1 ppb, which occur around the England/Wales border.

A correlation plot of this modelled data versus measured data is shown in Figure 5.30. These are the same measurements as described in section 5.5.1. The correlation coefficient R has a value of 0.52. For the sample size of n=51, this correlation has a probability (P) of having arisen by chance of 7.39×10^{-5}, which is statistically significant at the P = 0.1% level. The gradient of the regression line (full line) is 0.10, illustrating the degree of under-estimation produced by the

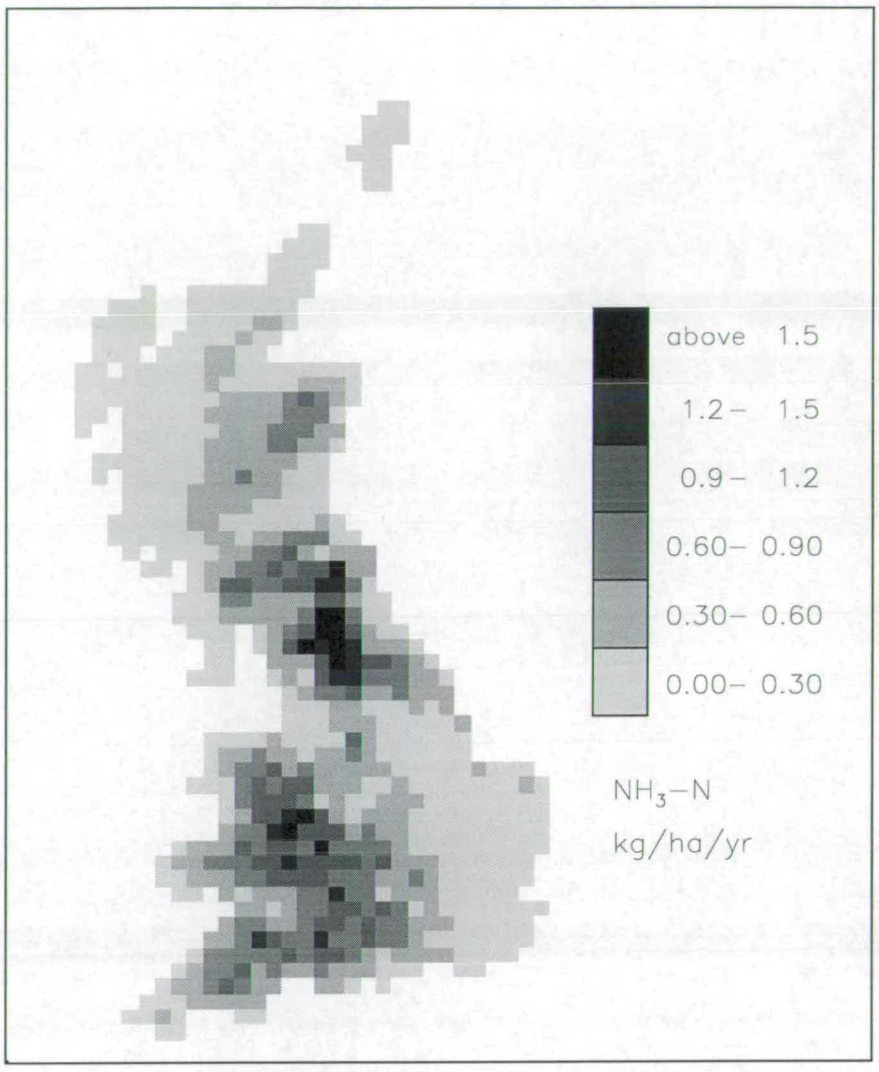

Figure 5.31: Modelled annual flux of ammonia dry deposition to Great Britain using the vertical dispersion scheme of instantaneous mixing. Units are kg ha^{-1} $year^{-1}$.

FRAME model using the instantaneous mixing scheme.

5.7.2 Dry deposition of ammonia

The under-estimation of surface concentrations strongly suggests that dry deposition will also be less than that produced using the multi-layer mixing scheme. A map of annual dry deposition of NH_3-N to Great Britain is shown in Figure 5.31. The largest dry deposition occurs in areas of high emissions (Figure 2.4) such as Wales and the southwest of England. It also occurs in areas which have large modelled deposition velocities assigned to them (Figure 4.17), such as the Pennines in northern England, and northern Scotland. The maximum dry depo-

sition flux is just over 1.5 kg N ha^{-1} $year^{-1}$, and large dry deposition fluxes occur in the area of northern England around the Pennines hills. The corresponding dry deposition field, produced using the multi-layer mixing (Figure 5.19), does not have this maximum deposition in the same location, and in fact most of the dry deposition occurs around the large emission areas (Figure 2.4). This point illustrates how the use of instantaneous mixing has increased the atmospheric residence time of NH_3, so that a greater proportion can be transported longer distances to regions of high modelled deposition velocity which are located at some distance from the main emissions areas. In some areas (eastern England and western Scotland) the flux is less than 0.3 kg N ha^{-1} $year^{-1}$. The total annual flux of NH_3-N to Great Britain is 11.7 Gg N $year^{-1}$, and the corresponding contribution from NH_4^+-N aerosols is 7.3 Gg N $year^{-1}$, providing a total dry deposition flux of 19.0 Gg NH_x-N $year^{-1}$.

5.7.3 Wet deposition of reduced nitrogen

The reduced flux of dry deposition that occurs with the use of the instantaneous mixing implies that more ammonia and ammonium are present in the modelled atmosphere that can be removed by wet deposition. The map of annual wet deposition to Great Britain, shown in Figure 5.32 confirms this hypothesis, with the total flux of reduced nitrogen being 83.6 Gg N $year^{-1}$. This comprises 75.3 Gg N $year^{-1}$ of NH_4^+ aerosol and 8.3 Gg N $year^{-1}$ of NH_3. The spatial distribution of this plot is very similar to Figure 5.25, but with the magnitude of the fluxes increased.

A correlation plot of the data displayed in Figure 5.32, and the same measurements discussed in section 5.5.5 is shown in Figure 5.33. The correlation coeficient R has a value of 0.74. For the sample size of n =30, this correlation has a probability (P) of having arisen by chance of 2.56×10^{-6}, which is statistically significant at the P = 0.1% level. Whilst the slight improvement in the value of R from 0.71 (Figure 5.26) may not be statistically significant, the fact that the gradient of the regression line has a value of 0.83 compared to the previous value of 0.54, indicates that the use of instantaneous mixing actually gives an closer agreement with measurements than with the use of the multi-layer diffusion scheme.

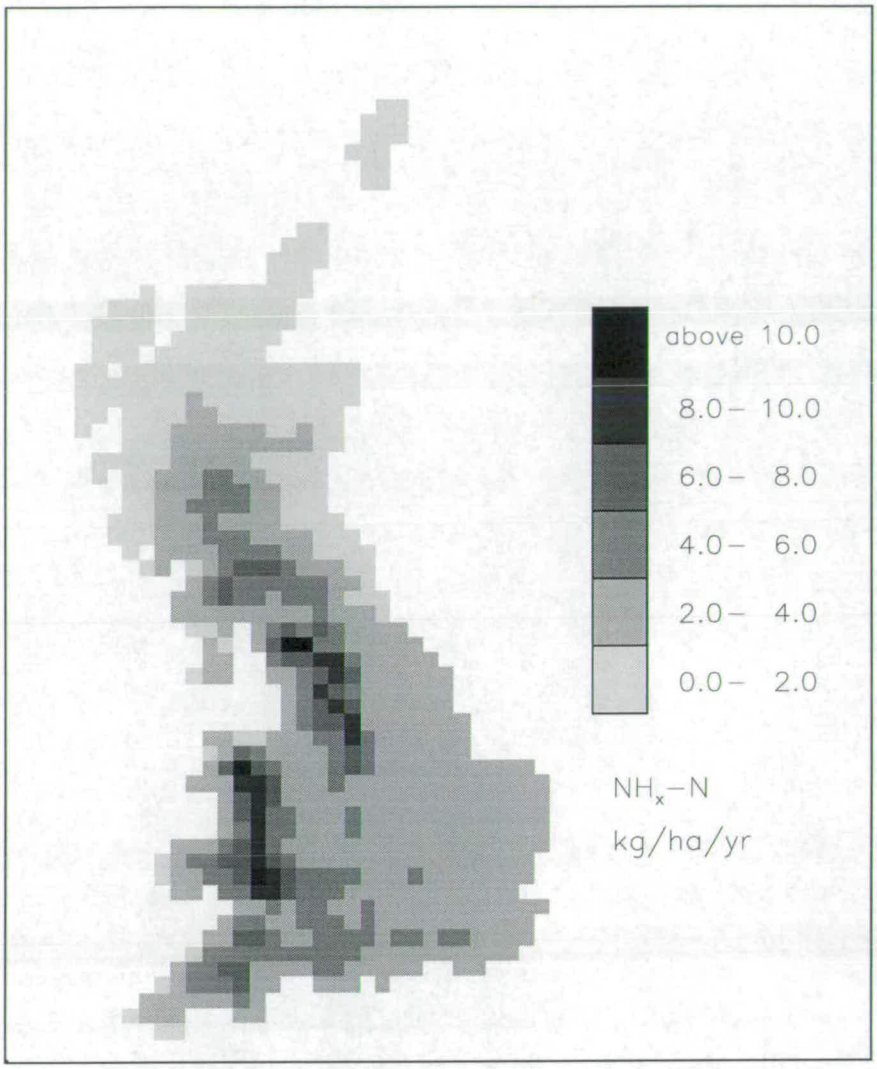

Figure 5.32: Modelled annual flux of wet deposition of reduced nitrogen to Great Britain using the vertical dispersion scheme of instantaneous mixing. Units are kg NH_x-N ha^{-1} $year^{-1}$.

These results show that FRAME is not able to model the spatial distribution and magnitude of both NH_3 and NH_4^+ deposition simultaneously using the present set of modelled atmospheric processes and input data. One reason for this is that there may not be enough NH_x emitted into the modelled atmosphere to reproduce both sets of deposition fields well, and that it may be the emissions data which are under-estimated.

Another explanation is that the wet deposition process used by FRAME are inadequately described. This may be due to the use of a constant drizzle rainfall as opposed to having rainfall split into wet and dry periods as suggested by

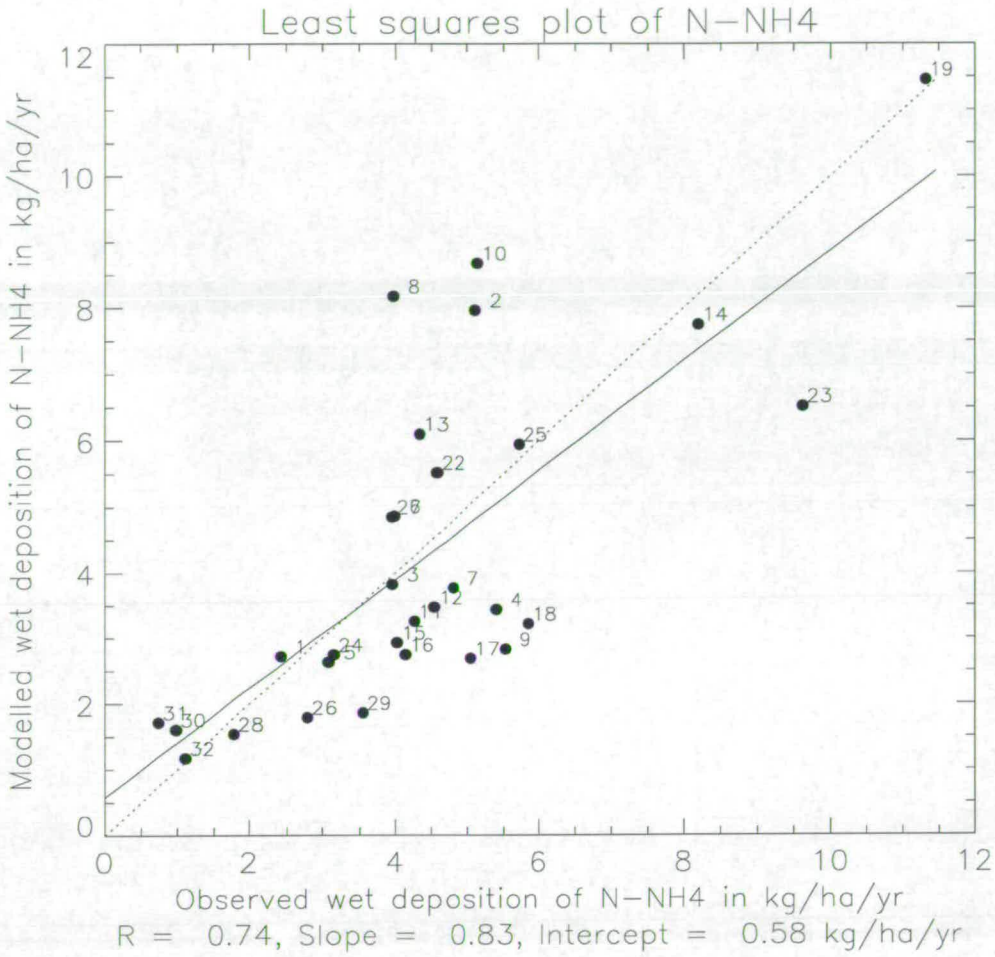

Figure 5.33: Correlation plot of modelled NH_x-N wet deposition fluxes from the FRAME model versus observations from a network of measurements sites. Vertical dispersion is by way of the scheme of instantaneous mixing. Each point has number assigned, which corresponds to the location of the measurement site shown in Figure 5.27. The full line is the regression line and the dotted line is the one-to-one line.

Smith (1980), or by the omission of the directional-dependence of the rainfall which would alter the spatial distribution of rainfall patterns, dependent on the direction of the wind origin and orography (Weston and Roy, 1994). The size of the washout coefficients may also be incorrect, and may in fact need to be greater for aerosol. There may also be incorrect assumptions in the chemical structure of FRAME which inhibits the creation of more ammonium aerosols.

5.7.4 Modelled annual budgets

Table 5.11 gives data on the annual budgets of reduced nitrogen, sulphur and

Species	Emissions	Import	Dry deposition	Wet deposition	Export
Reduced Nitrogen (N)	281.4	35.7	19.0	83.6	214.5
Sulphur (S)	1695.2	101.2	268.9	186.6	1340.9
Nitrogen Oxides (N)	784.1	125.8	58.1	85.9	765.9

Table 5.11: Modelled budget of reduced nitrogen, sulphur and nitrogen oxides for Great Britain produced by the FRAME model using the vertical dispersion scheme of instantaneous mixing. These data represent an averaged annual budget for the country. The units are Gg year^{-1}.

Species	R	Gradient of regression line	Intercept of regression line	P value
S-SO_4 (Inst)	0.7	0.95	0.32	1.09×10^{-5}
S-SO_4 (Multi-Layer)	0.78	0.90	0.25	5.24×10^{-9}
N-NO_3 (Inst)	0.73	1.37	-1.33	3.27×10^{-6}
N-NO_3 (Multi-Layer)	0.75	1.33	-1.09	1.67×10^{-6}
SO_2 (Inst)	0.9	2.12	-0.13	4.45×10^{-12}
SO_2 (Multi-Layer)	0.86	2.44	-0.43	1.67×10^{-9}
NO_2 (Inst)	0.94	0.75	0.38	6.44×10^{-15}
NO_2 (Multi-Layer)	0.92	0.90	-0.06	2.63×10^{-13}

Table 5.12: A comparison of modelled results using multi-layer mixing (Multi-Layer) and the scheme of instantaneous mixing (Inst).

nitrogen oxides for Great Britain using the vertical dispersion scheme of instantaneous mixing. These data can be compared with Tables 5.9, 5.6 and 5.2 to assess the effect that the choice of vertical dispersion scheme has on the annual deposition budgets. The reduced nitrogen budget has already been discussed. The two budgets for sulphur are very similar with the multi-layer wet deposition total (170.2 Gg S year^{-1}) being about 9% less than the instantaneous mixing total (186.6 Gg S year^{-1}). Dry deposition totals differ by about than 13 Gg S year^{-1}. Oxidised nitrogen budgets agree very well, with a difference of 4.3 Gg N year^{-1} between the dry deposition totals, and less than 1.7 Gg N year^{-1} difference between the wet deposition budgets.

Table 5.12 contains correlation data of modelled results produced using instantaneous mixing, and also contains multi-layer mixing results to allow assessment of the effect of using different schemes of vertical dispersion.

The correlation data for wet deposition of SO_4-S has a value of R of 0.7. For the sample size of n=33, this correlation has a probability (P) of having arisen by chance of 1.09×10^{-5}, which is statistically significant at the P = 0.1% level. These data are extremely similar to those in Figure 5.13 which is the correlation plot of the model results using the multi-layer mixing scheme. The reduction in the value of the correlation coefficient (R), is offset by the increase in the gradient of the regression line from 0.90 to 0.95. Thus it seems that effect of using instantaneous mixing instead of the multi-layer scheme has had a varied effect on the spatial distribution and magnitude of sulphate wet deposition.

The results for SO_2 concentrations show a slight improvement from the data presented in Figure 5.10 The value of R has improved slightly to 0.9, though this may not be significant, and the gradient of the regression line, though still very large, has decreased from 2.44 to 2.12. The use of instantaneous mixing has had no adverse effect on SO_2 concentrations, and could actually have improved the agreement with measurements.

There is little change in the value of R for nitrate wet deposition (0.75 to 0.73) The gradient of the regression line has slightly increased from 1.33 to 1.37. The data comparison now has a P value of 3.27×10^{-6}, which is statistically significant at the P = 0.1% level.

For surface concentrations of NO_2, the value of R^2 has increased slightly to 0.89 (from 0.85). The gradient of the regression line is 0.75 which is lower than the results produced using the multi-layer scheme (0.90). The correlation analysis has a P value of 6.44×10^{-15}, which is statistically significant at the P = 0.1% level.

5.7.5 Discussion

The one major advantage of using this simpler scheme of vertical dispersion over the more detailed multi-layer mixing is the large saving of computational time. At present, running the model on a 20 km square grid takes around 8 hours to finish while running on a Sun Sparc 10 workstation. Any decrease in the computational time, while still retaining a good degree of accuracy, is obviously advantageous. For instantaneous mixing, the computational time is approximately 1 hour. The results in Table 5.11 show that that sulphur and oxidised nitrogen deposition bud-

gets show little variation between the two dispersion schemes. Reduced nitrogen, however, is extremely sensitive to the modelled parameterisation of vertical mixing, with almost a factor of 5 difference between the two dry deposition budgets. This fact, coupled with the corresponding under-estimation of NH_3 surface concentrations, illustrate the need to use a more detailed scheme of vertical mixing with NH_3 emissions.

The surface concentrations of NO_2 also show a slight reduction in their overall magnitude with the instantaneous mixing scheme, though this is only very small when compared with the NH_3 under-estimation. Whilst emissions of NO_2 and NO are not exclusively ground-based, over half of the total annual emissions for the UK are due to motor vehicles (Gillham *et al.*, 1992). Thus while concentrations of NO_2 are not as sensitive as those of NH_3 to the choice of vertical mixing scheme, there is enough of an effect for the multi-layer mixing scheme to be recommended for use with both NO_2 and NO, and further studies should be performed to allow the model to determine the initial vertical distribution of emissions dependent on the source height.

The same argument can be applied to emissions of SO_2, though in this case, the emphasis is more on determining the vertical distribution from elevated sources such as power stations, as these are the sources which determine the very large concentrations that occur over much of the country. Thus it is also recommended that vertical dispersion of SO_2 be performed using the multi-layer mixing scheme.

In comparison with the primary model species of SO_2, NO_x and NH_3, the data from Tables 5.11 and 5.12 show that the behaviour of the secondary species of SO_4^{2-} and NO_3^- is less affected by the choice of mixing scheme. The results for nitrate data show very little dependence on the choice of vertical mixing scheme, while the discrepancies for sulphate may be reduced if a height-dependent scheme for sulphur emissions were introduced into the model. These species are removed from the modelled air column mainly by the process of wet deposition. The washout coefficients used by FRAME are height independent, and thus the wet deposition flux is not very sensitive to vertical gradients of material if there is little variation in the total integrated mass of the air column. The data for NH_4^+ show a pronounced variation with mixing schemes. This is due to the large variation of the modelled dry deposition flux that occurs, which has a pronounced effect

on the integrated mass of NH_4^+ and NH_3 in the air column.

An ideal method would be to use a hybrid scheme for vertical mixing. For the primary emission species of SO_2, NO_x and NH_3, the multi-layer mixing scheme would be employed, with a height dependence of emissions being used where appropriate. For the secondary species of $(NH_4)_2SO_4$, H_2SO_4, HNO_3, NH_4NO_3, NO_3, PAN and H_2O_2, the scheme of instantaneous mixing would be employed. However, due to the complex gaseous and aqueous phase chemistry in the model, it is not certain whether the hybrid mixing scheme would be feasible. Initial testing of this scheme found that instabilities developed in numerical methods used to calculate the cloud chemistry reactions. To overcome this problem, the cloud chemistry scheme would have to be converted to a less unstable method which would retain the basics of the equations, but which would be simpler and more stable. This project would involve a considerable amount of work and is beyond the scope of this study.

5.8 Sensitivity analysis of the amount of cloud cover in the model

For the model results presented so far in this chapter, cloud cover has been set at 6 oktas. This value was chosen as it represents a long-term average over the British Isles, and was based on data in World Survey of Climatology, Volume 5 (1970). It is important to see how sensitive the model is to this parameter and see if variation in the results occur for different cloud cover values. In this section, model results are presented for cloud cover values of 0, 4, 6 and 8 oktas. These represent a range of values, and should give some indication of the model's dependence on the choice of cloud cover.

5.8.1 Reduced nitrogen

Table 5.13 contains comparison data of modelled results using the four chosen cloud cover values. The most obvious feature of the data is that a linear relationship does not exist between cloud cover and the model results. The lowest annual dry deposition occurs with a cloud cover of 4 oktas, with the results for 0, 6 and 8 oktas being greater than this value.

Cloud Cover (oktas)	Annual Dry Deposition (Gg year^{-1})	Annual Wet Deposition (Gg year^{-1})	Annual Export (Gg year^{-1})
0	120.7	52.7	143.7
4	91.8	59.9	165.4
6	94.6	58.7	163.8
8	103.8	55.8	157.5

Table 5.13: A comparison of annual modelled budgets of reduced nitrogen using a range of cloud cover values.

The largest dry deposition occurs with zero cloud cover, which is probably not surprising since this state will generate large daytime NH_3 deposition velocities (section 3.1). Zero cloud cover during the day will mean that the modelled solar radiation will be high (equation 3.12), causing the modelled values of V_d to high. As well as large values of V_d, zero cloud cover will generate large rates of vertical diffusion, due also to the large rate of daytime solar radiation in the model. At nighttime, zero cloud cover will have the opposite effect. It will caused to the model to class the lower atmosphere as being very stable (Pasquill stability classes, section 3.1.2, Table 3.3) and will cause suppression of vertical dispersion and the NH_3 dry deposition velocities. However, the low rate of vertical diffusion will mean that modelled surface concentration of NH_3 will be very large, which could lead to a fairly large dry deposition flux.

The implications for the model of using a cloud cover of 8 oktas means that diurnal variations in both vertical dispersion and deposition velocities will be suppressed, and thus day and nighttime deposition fluxes will be fairly similar. The reduced daytime rate of vertical diffusion will lead to greater surface concentrations and this may offset the effect of the reduced modelled deposition velocities. Similarly, nighttime deposition velocities will be relatively large, as will the rate of vertical diffusion.

The overall effect on NH_3 dry deposition of varying the cloud cover illustrates how both the modelled rate of vertical diffusion and V_d are negative correlated with variations in cloud cover during the daytime, and are both positively correlated with variations in cloud cover at night. Using two values which are at the extreme range of cloud coverage produced an larger rate of dry deposition than

Cloud Cover	Annual Dry Deposition	Annual Wet Deposition	Annual Export
0 oktas	50.0	87.6	772.3
4 oktas	52.4	88.8	768.7
6 oktas	53.8	87.6	768.5
8 oktas	59.0	86.7	764.2

Table 5.14: A comparison of annual modelled budgets of oxidised nitrogen using various values of cloud cover.

compared with using mid-range values of 4 and 6 oktas.

Wet deposition data have an opposite result compared with the dry deposition. Increased dry deposition reduces the amount of reduced nitrogen in the atmosphere, and thus there is less NH_x available to be wet deposited and exported. This is reflected in the data in Table 5.13.

5.8.2 Oxidised nitrogen

The comparison data for oxidised nitrogen shows a more linear relationship between deposition/export and cloud cover. This is because the the majority of the modelled dry deposition is in the form of NO_2 (71%, Table 5.7). The model uses an annually-averaged dry deposition map (section 4.3.8) for NO_2. These values are temporally-invariant and thus the variation of cloud cover does not affect the magnitude of the deposition velocities. The main factors which affect the results are the rate of vertical diffusion and the rate of chemical reactions. The chemical reactions during the day include the two-way reaction between NO and NO_2, and the conversion of NO_2 to HNO_3 and NO_3^- (section 3.3). During the daytime, there will be a quasi-equilibrium between NO and NO_2, and NO_2 will also be converted to HNO_3. At nighttime, there will no dissociation of NO_2 to NO, and thus there is no equilibrium between the two species and so NO_2 concentrations will increase. This increase will be offset by the additional nighttime conversion of NO_2 to NO_3^-.

It is difficult to determine which effect is the dominant one when cloud cover is varied, as the rate of dissociation of NO_2 to NO is dependent on cloud cover (section 3.3, Table 3.10). The overall effect of the competing processes is that the annual flux of dry deposition to Great Britain is a minimum when employing

Cloud Cover	Annual Dry Deposition	Annual Wet Deposition	Annual Export
0 oktas	222.0	173.6	1400.6
4 oktas	249.4	175.8	1373.5
6 oktas	255.8	170.2	1370.4
8 oktas	275.5	154.9	1365.8

Table 5.15: A comparison of annual modelled budgets of sulphur using various values of cloud cover.

zero cloud cover in the model and is largest when complete cloud cover is used in the model.

There is little variation in the annual wet deposition totals. Modelled wet deposition of oxidised nitrogen is exclusively in the form of nitrate, and thus variations in cloud cover will be a combination of the effects of vertical dispersion, and the rate of chemical reactions, specifically the conversion of NO_2 to NO which will limit the creation of HNO_3 and NO_3^-.

5.8.3 Sulphur

The argument used for the deposition of oxidised nitrogen can be applied to sulphur as well, in that modelled dry deposition of SO_2 is responsible for the vast majority of sulphur dry deposition. A map of annually-averaged deposition velocities is used for dry deposition of SO_2. The magnitude of these values are temporally-invariant and are not affected by any variation in cloud cover. In the model, sulphur chemistry is not affected by variations in cloud cover, and thus the main factor is the rate of vertical diffusion.

Zero cloud cover will mean reduced concentrations during the day due to increased vertical mixing. At nighttime, the rate of vertical diffusion will be low, but SO_2 are uniformly spread throughout the lowest 300 m, and the increased stability may actually lead to lower nocturnal concentrations as depletion in the surface layer due to dry deposition may be greater than the rate of replenishment as material is transported down from higher levels in the air column.

Suppression of diurnal variations will occur with complete cloud cover, and the results show that this leads to a large annual rate of dry deposition. Wet deposition shows little variation between the results for 0, 4 and 6 oktas. However,

Cloud Cover	Annual Dry Deposition	Annual Wet Deposition	Annual Export
250 m	94.6	58.7	163.8
500 m	97.3	57.2	162.6
800 m	99.8	55.1	162.2

Table 5.16: A comparison of annual modelled budgets of reduced nitrogen using various values of cloudbase height.

there is a slight reduction in the wet deposition for a cloud cover of 8 oktas.

5.9 Sensitivity analysis of the cloudbase height used in the model

The height of the cloudbase used for previous model results in this chapter was set at 250 m. This value was taken from Hertel *et al.* (1995), where it was used in the ACDEP model to describe the height above which in-cloud process of wet deposition would occur. The ACDEP model is set up to be deterministic, in that it models specific events and periods in time,) and wet deposition would only occur during a rain event. As has been discussed previously, (section 5.2). the fact that FRAME employs a constant drizzle approach meant that as a first order approximation, this value was used to define the base of the cloud. As with the cloud cover in the previous section, it is necessary to assess the implications of the choice of cloudbase height, and conduct various tests to determine the sensitivity of the model to this parameter. The three values to be used in this test are 250 m, 500 m and 800 m.

5.9.1 Reduced nitrogen

Table 5.16 gives information on the modelled data of annual fluxes of dry and wet deposition, and annual export for three different values of the cloudbase height. With an increase in the height of the cloudbase, annual dry deposition fluxes increased slightly, and the annual wet deposition and export showed a corresponding decrease.

The data from Table 5.16 imply that the model is not very sensitive to any change in the cloudbase height, and that a three-fold increase in this value will

Cloudbase height	Wet Deposition		Export	
	% NH_3	% NH_4^+	% NH_3	% NH_4^+
250 m	8	92	6	94
500 m	14	86	12	88
800 m	25	75	29	71

Table 5.17: A comparison of annual modelled budgets of reduced nitrogen using various values of cloudbase height.

Cloud Cover	Annual Dry Deposition	Annual Wet Deposition	Annual Export
250 m	53.8	87.6	768.5
500 m	54.2	87.1	768.6
800 m	54.1	86.7	769.1

Table 5.18: A comparison of annual modelled budgets of oxidised nitrogen using various values of cloudbase height.

only alter the annual dry deposition flux by 5%. However analysis of the data presented in Table 5.17 illustrates more clearly the effect of varying the cloudbase height. Increasing this value leads to a reduction in the amount of NH_4^+ in the modelled air column. This is due to the in-cloud oxidation of SO_2 to H_2SO_4, and subsequent creation of ammonium aerosol. Increased cloudbase height reduces the number of vertical layers in the air column in which in-cloud oxidation can occur, and thus reduces the vertically-averaged rate of SO_2 oxidation. Another effect will be due to the vertical distribution of NH_3. On average, NH_3 will decrease with height, and thus less NH_3 will be present in the modelled layers at a height of 500 m and 800 m, than at 250 m. It was described in section 3.3.3 how NH_3 enhances the rate of in-cloud oxidation, and thus decreased NH_3 concentrations will reduce this effect. The overall effect is that there is less H_2SO_4 available to react with NH_3 and form $(NH_4)_2SO_4$.

5.9.2 Oxidised nitrogen

Oxidised nitrogen shows no observable variation with different cloudbase heights (Table 5.18). This is due to the fact that very little oxidised nitrogen chemistry occurs in the modelled cloud, except an enhanced reaction of NH_3 and HNO_3 to

Cloudbase height	Export			
	% NO	% NO_2	% NO_3	% PAN
250m	7	60	30	3
500m	7	60	30	3
800m	7	60	30	3

Table 5.19: A comparison of annual modelled exports of oxidised nitrogen using various values of cloudbase height.

form NH_4NO_3. Any NH_3 is the modelled cloud will react with HNO_3 and H_2SO_4 instantaneously, and thus increased cloudbase heights will reduce the vertically-averaged rate of formation of NH_4NO_3. This reaction is in addition to the equilibrium reaction described in section 3.3.1. In general there is no variation in the ratios of the oxidised nitrogen species presented in Table 5.19. Modelled wet deposition is only in the form of NO_3, which comprises NO_3^- and HNO_3.

5.9.3 Sulphur

The results in Table 5.21 reflect the argument given in section 5.9.1, in that increased cloudbase height leads to lower rates of SO_2 oxidation, resulting in less SO_4 wet deposition and more SO_2 dry deposition.

The increase in $(NH_4)_2SO_4$ ratio in total sulphur wet deposition is due to the fact that while the vertically integrated mass of H_2SO_4 in the air column is reduced with increasing cloudbase height, it is still reacting with NH_3 to form $(NH_4)_2SO_4$. However it should be noted that overall, a reduced amount of $(NH_4)_2SO_4$ will be wet deposited with a higher cloudbase height, as illustrated by the reduced NH_4^+ wet deposition in Table 5.17. With less SO_2 oxidation, this means that more SO_2 can be exported, as shown in Table 5.20 where the annual export of sulphur has increased slightly with the higher cloudbase heights.

5.10 Discussion

The results in this chapter have illustrated a number of important aspects of atmospheric modelling, and have the shown the varying degrees of sensitivity a model has to the choice of parameterisation used for certain modelled processes.

Cloud Cover	Annual Dry Deposition	Annual Wet Deposition	Annual Export
250 m	255.8	170.2	1370.4
500 m	263.8	150.2	1382.2
800 m	271.4	123.5	1401.3

Table 5.20: A comparison of annual modelled budgets of sulphur using various values of cloudbase height.

Cloudbase height	Wet Deposition		
	% SO_2	% $(NH_4)_2SO_4$	% H_2SO_4
250m	19	30	51
500m	23	31	46
800m	30	33	37

Table 5.21: A comparison of annual modelled wet deposition of sulphur using various values of cloudbase height.

Cloudbase height	Export		
	% SO_2	% $(NH_4)_2SO_4$	% H_2SO_4
250m	73	10	17
500m	77	9	14
800m	85	7	8

Table 5.22: A comparison of annual modelled exports of sulphur using various values of cloudbase height.

The modelled results for SO_2 concentrations over-estimate measured data by a significant factor. This error could be partly due to the choice of windspeed, since there is no vertical wind shear in the modelled air column. Wind speeds were optimised for NH_3, which is a ground-level source, and in higher levels of the air column, use of a ground based wind speed may mean that the air column at these levels spends longer over an emission source than would actually occur and so would have more material emitted into it, resulting in higher concentrations. Also there is no allocation of SO_2 emissions into the atmosphere, dependent on source height. This could lead to an over-estimation of surface concentrations in locations with elevated sources, with the use of the present scheme of a homogeneous distribution of emissions over the lowest 300 m. There is a better agreement between modelled sulphate wet deposition and observed data. The

overall magnitude of the two data sets are in fairly good agreement, as indicated by slope of the regression line (0.90), and there was a significant correlation between the two sets of data. The largest under-estimation of modelled fluxes is in northern Scotland.

Modelled concentrations of NO_2 agreed very well with recorded data. Modelled fluxes of nitrate wet deposition also compare well to observed values, though the agreement between modelled and measurements is not as good as that for NO_2 concentrations.

Modelled concentrations of NH_3 have a significant correlation with measured data. As has already been stated, it is difficult to compare averaged concentrations over a 20 km grid square to measurements taken at a specific site, due to large spatial variability that occurs with NH_3 concentrations. Looking at Figure 5.21, the model under-estimates the measured concentrations over virtually all of Wales and central and southern England. Model over-estimation occurs in a area encompassing northern and western Scotland. The correlation plot (Figure 5.20) has a regression gradient which is close to 1, showing that the model is estimating the overall magnitude of the concentrations to a fair degree of accuracy, and the intercept of 0.99 ppb gives an indication of the average over-estimation of modelled concentrations. The modelled dry deposition of NH_3 has an annual flux to Great Britain of 87.9 Gg NH_3-N $year^{-1}$. This value is slightly less than the official estimate of 94.5 Gg NH_x-N, which was calculated using an interpolated map of observed NH_3 concentration, and an inferential model (section 2.2.1). However the spatial distribution of the two data sets (Figures 2.2 and 5.22) do not agree so well over many areas of Great Britain, especially in northern Scotland, where the FRAME model predicts much less dry deposition than the inferential model. This is due to the large disagreement in surface concentration data, which has already been discussed. The FRAME model under-estimates the magnitude of NH_x wet deposition at most measurements locations. The gradient of the regression line is 0.54, giving an indication of the degree of under-estimation.

The use of an alternative vertical mixing scheme, namely the instantaneous mixing of emissions throughout the boundary layer, showed the sensitivity of the different model species to the type of parameterisation chosen to represent this process.

The choice of vertical dispersion had some effect on the oxidised sulphur and nitrogen species, but these effects were not as pronounced as the change that occurred with the results for reduced nitrogen. The correlation coefficient for NH_x wet deposition increased slightly, and the gradient of the regression increased from 0.54 to 0.83. This was reflected in the overall total wet deposition flux of NH_x-N for Great Britain, which increased from 58.7 Gg NH_x-N $year^{-1}$ to 83.6 NH_x-N. This increase in wet deposition was accompanied by a huge decrease in the surface concentrations of NH_3. Maximum concentrations were just over 1 ppb (Figure 5.29), compared to the results produced using the multi-layer mixing, where concentrations exceeded 8 ppb at a number of locations (Figure 5.19). The modelled budget of NH_x dry deposition to Great Britain decreased from 94.6 Gg NH_x-N to 19.0 Gg NH_x-N, a dramatic reduction of nearly 80% from the multi-layered value.

The FRAME model showed a varying degree of sensitivity to cloud cover, dependent on the species under consideration. Dry deposition fluxes were more sensitive to variation in cloud cover than the corresponding wet deposition. Dry deposition fluxes are dependent on surface concentrations, which are affected by the rate of vertical dispersion. Reduced cloud cover allows for higher daytime rates of dispersion, thus generally reducing surface concentrations and dry deposition fluxes. In the case of NH_3, reduced cloud cover also increases the magnitude of the modelled deposition velocities, thus actually increasing the rate of dry deposition during the day. This means that the relationship between cloud cover and modelled NH_3 dry deposition fluxes is not a linear one. For SO_2 and NO_2 reduced cloud resulted in increased dry deposition. Sulphate and nitrate wet deposition decreased with increased cloud cover, probably due to the reduced amount of material in the air column available to be oxidised, as a result of the increased dry deposition.

The main process in the model that is affected by varying the height of the cloudbase is the oxidation of SO_2 to H_2SO_4. The availability of H_2SO_4 also affects the amount of NH_3 which is converted to $(NH_4)_2SO_4$. Thus the main effect of increasing the height of the cloud base is to reduce the amount of sulphate in the air column, which means that sulphate wet deposition is reduced. There is a resultant increase in amount of SO_2 in the air column, leading to an increase in

the sulphur dry deposition. Oxidised nitrogen is hardly affected by a variation in cloudbase height. Reduced amounts of H_2SO_4 in the air column means that concentrations of NH_4^+ are also reduced. Whilst the annual wet deposition flux of NH_x to Great Britain is only slightly decreased, a increased proportion of the flux is in the form of NH_3, as opposed to NH_4^+.

Chapter 6

Modelled Results on a 5 km Grid

Modelled results on a fine resolution grid of 5 km × 5 km are presented in this chapter. In the first section, changes made to the model are discussed, which are a result of increasing the resolution of the model from a 20 km × 20 km grid. The next section introduces a receptor model, which is based upon FRAME. The purpose of the receptor model is to describe concentration gradients and diurnal variations at a specific location. Results from this model are presented and discussed. Subsequent sections of this chapter contain results from the FRAME model on a country-wide basis. A number of experiments are described and the results from these experiments are analysed. The final part of this chapter looks at the problem of local dry deposition, and modelled estimates are presented on the percentage of emissions that are dry deposited in the same grid square and the amount of dry deposition to grid squares that are due to emissions being dry deposited in the same grid square.

6.1 Adapting the model to run on a 5 km grid

To convert FRAME to run on a 5 km × 5 km grid, a number of modifications to the model code were required. The 5 km × 5 km emissions data for NH_3 were used (Dragosits *et al.*, 1996; Figure 2.5), and the 10 km × 10 km emissions data for SO_2 and NO_x were disaggregated onto a 5 km grid, by assuming that each 10 km grid square contained 4 × 5 km grid squares which have the same emission flux. The same procedure of disaggregation was performed on the 20 km × 20 km landuse database, in order to create a 5 km version. A 5 km × 5 km rainfall dataset was used, which represents an long-term annual average. All other 20

km datasets, including the surface wind data, which are used to model the NH_3 deposition velocities (section 3.1) and the annually-averaged deposition velocities for NO_2 and SO_2 were disaggregated onto a 5 km $\times$ 5 km grid.

The main effect of running the model on the increased resolution is that computational time is increased by a factor of about 4, and takes about 2 days to run on a Sun Sparc 10 workstation. This is because 4 trajectories on the 5 km $\times$ 5 km grid will, on average, cover the same area as 1 trajectory on the 20 km $\times$ 20 km grid.

6.2 The receptor model

In this section, a model is introduced which is based upon the FRAME model. The philosophy behind this model is to describe diurnal and vertical variations in concentrations that occur at specific locations in Great Britain. Straight line trajectories are employed, which arrive at the specified location every hour, for each wind direction. This allows the model to produce detailed data on the diurnal variations of annually-averaged concentrations.

Trajectories originate from 24 equally-spaced wind directions on the compass. The model runs on a 5 km $\times$ 5 km grid, as described in the previous section. The trajectories are initialised at the edge of the model domain using the concentration data described in section 4.3.1. The set of optimised wind speeds for dry deposition (section 4.3.2) are used to advect the air column. All chemical and physical processes in the model are identical to those in FRAME.

The results from the model can be used to analyse diurnal variations in concentrations, and compare modelled concentration data with measured data where possible. The model also produces results on vertical concentration profiles. This allows a detailed assessment of certain aspects of the modelled results, which would not be possible with the full FRAME model due to the extremely large amount of data that would be generated.

In the following section, results from the receptor model are presented and analysed. These results are for a rural site in Scotland, at the Institute of Terrestrial Ecology, which is located in east-central Scotland at GB grid reference NT245635. Ammonia concentrations have been recorded at this site for a number

of years (Burkhardt *et al.*, 1996), and comparisons of modelled data are made with measurements. The model describes the diurnal variations in NH_3 at the surface, and the vertical gradients of NH_3 that occur during a 24-hour period.

As was discussed in section 1.3, the main sources of NH_3 are from volatilisation of livestock waste and fertilisers. The process of volatilisation has been found to be dependent on the temperature and wetness of the soil (section 1.3). Thus daytime conditions are generally more favourable for emissions to occur. Also, emissions from croplands occur via the leaf stomata (Farquhar *et al.*, 1980) and in general plant stomata close at nighttime, and open during the day apart from at high temperature, above 25-35°C (Monteith, 1975).

Two sets of modelled data are presented. The first set of data were created using the standard model assumption of constant emissions, with no diurnal variation. This assumption is investigated with the second set of results, which were created by implementing a simple diurnal variation in the emission rate. This was done by assuming the emissions rate is constant during the night, and during the daytime the emission rate is sinusoidal with the maximum daytime flux being five times the nighttime value (ApSimon *et al.*, 1994). The 24-hour daily average flux is equal to the constant flux, and the ratio of the averaged daytime emission rate to the nighttime emission rate is about 3.5:1, at the Spring equinox. Asman and van Jaarsveld (1992) stated that a diurnal variation in emissions derived from measurements could be explained from diurnal variations in the aerodynamic resistance and temperature. They found that using an diurnal variation in the emission rate in the TREND model, which was very similar to that used by ApSimon *et al.* (1994), resulted in a 20% reduction of the annually-averaged surface concentrations of NH_3 and NH_4^+ aerosol. They performed a comparison with a sample set of measured data, and it was found that the use of a diurnal variation in modelled emission gave a better agreement than with the use of a constant emission rate.

6.2.1 Diurnal variations in ammonia concentrations

Figure 6.1 is a plot showing the dependence of modelled NH_3 surface concentrations on flow direction, and the amount of diurnal variation that occurs. Emissions were assumed to be constant in the model run that produced these data.

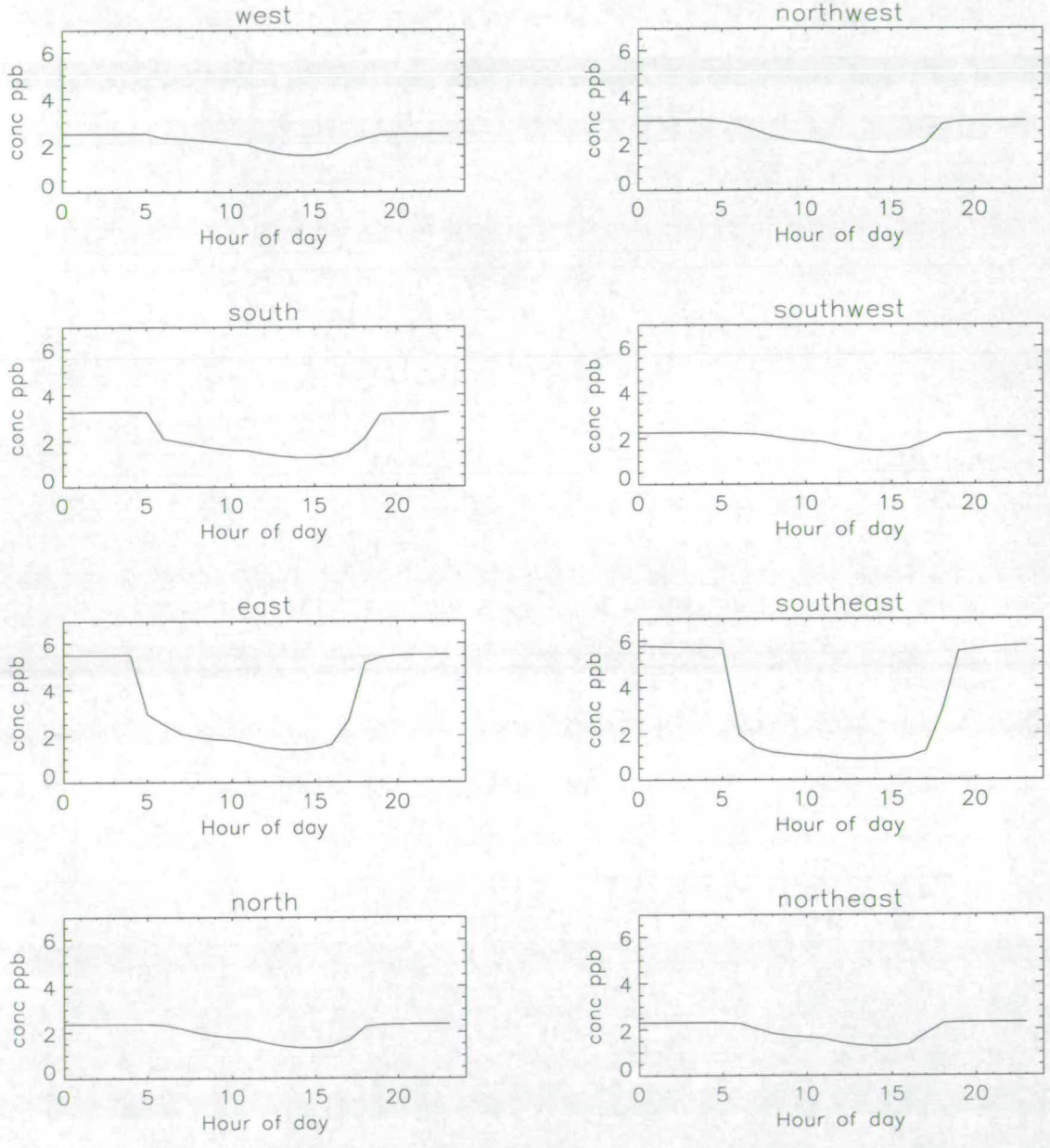

Figure 6.1: Diurnal variations of modelled surface concentrations of NH_3 at ITE, Edinburgh from the receptor model. Each plot represents the diurnal variation at a height of 1.5 m, for different wind directions. Data represent an annual average. Units are ppb.

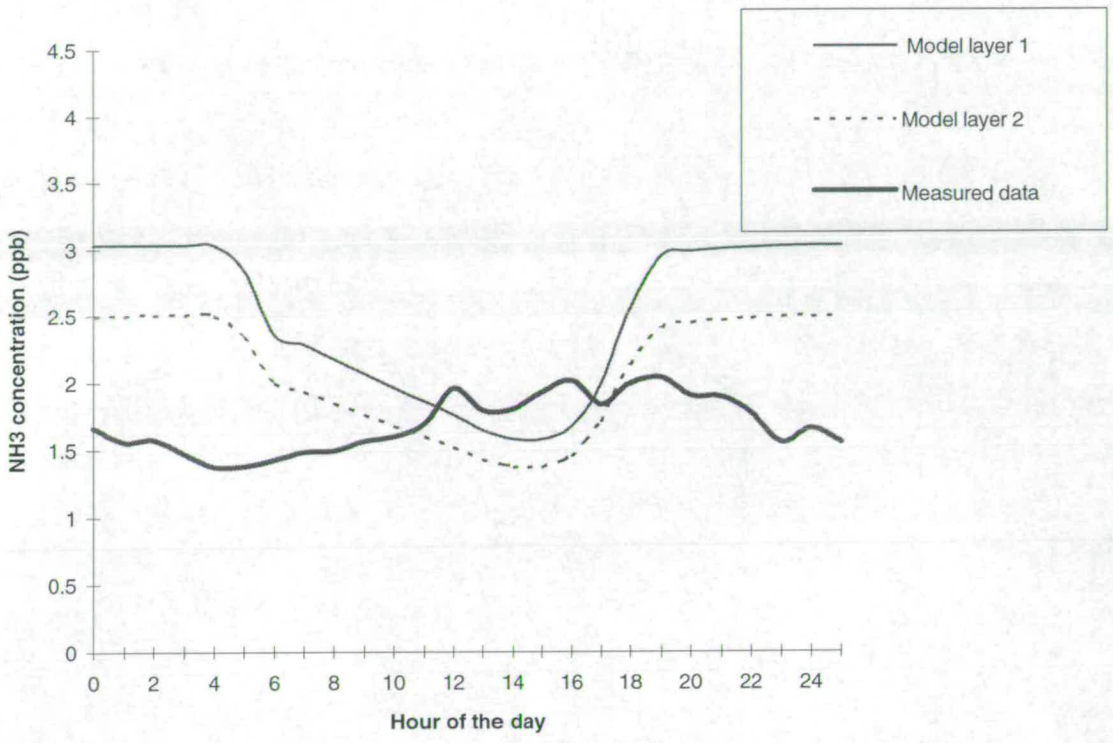

Figure 6.2: A comparison of the diurnal cycle of measured concentrations of NH_3 (Burkhardt *et al.*, 1996) and modelled concentrations of NH_3 at 2 layers (1.5 m and 3 m) produced using constant modelled emissions. The measured data are representative of windspeeds greater than 1 m s^{-1}. Units are ppb.

The units are ppb. All of the plots in this figure have a diurnal cycle, with the maximum concentrations occurring at night due to the increased atmospheric stability and reduced values of V_d. The greatest diurnal variation occurs with trajectories coming from the east and southeast, though trajectories from the south also show a large diurnal cycle. One explanation for this may be the location of the receptor point, which, in this experiment, is located in eastern Scotland, near Edinburgh. At this site, trajectories which arrive from the east and southeast, have spent a small amount of time over Great Britain, and thus very little NH_3 will have been emitted into the air column from British sources. This will mean that surface concentrations may be dominated almost entirely by NH_3 due to local emissions from the surrounding grid squares, since emissions from European sources such as Denmark and the Netherlands will be relatively well mixed in the boundary layer. Diurnal variations range from 4.5 ppb with

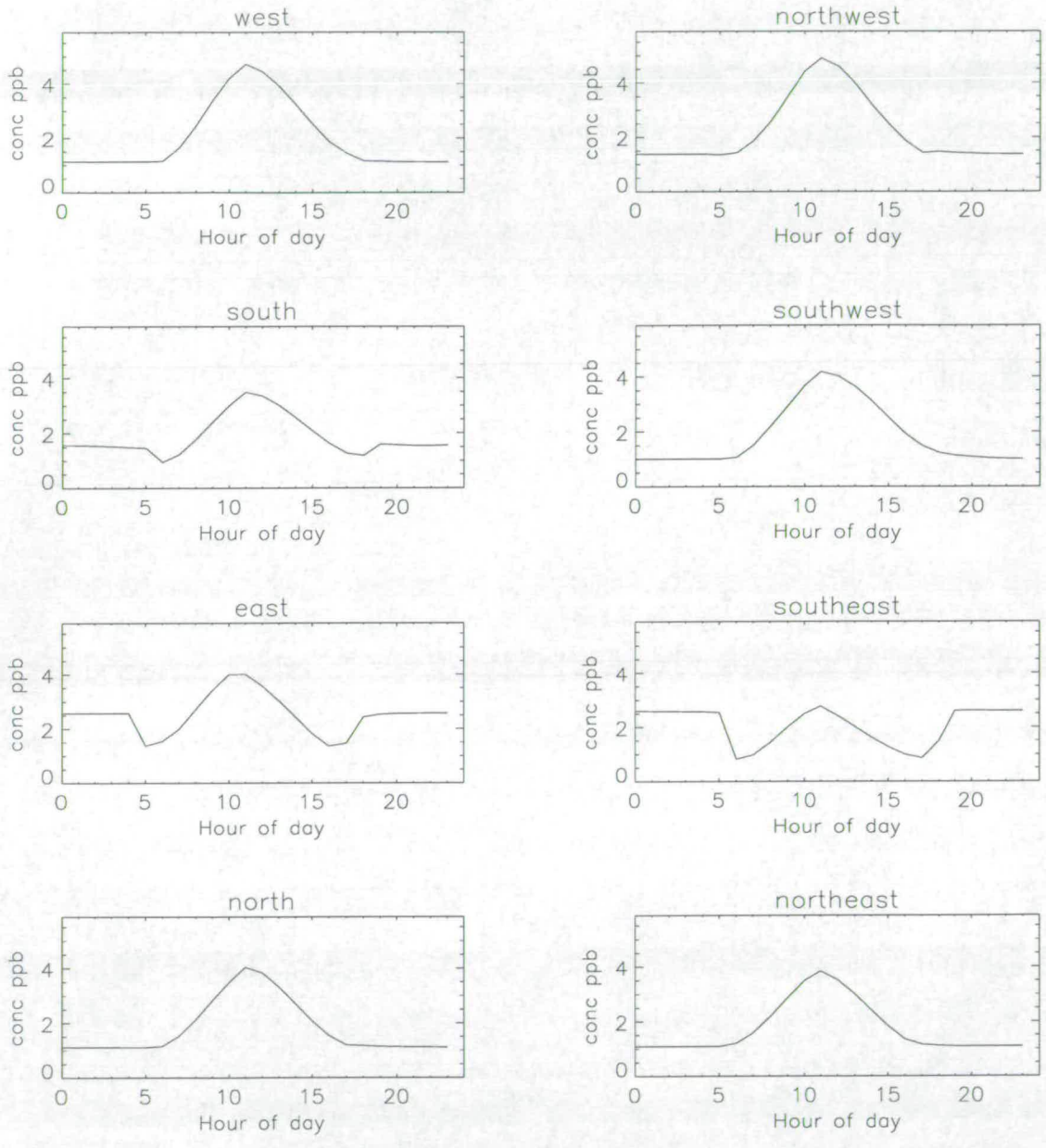

Figure 6.3: Diurnal variations of modelled surface concentrations of NH_3 at ITE, Edinburgh, from the receptor model using a diurnal variation in the emission rate. Each plot represents the diurnal variation at a height of 1.5 m, for different wind directions. Data represent an annual average. Units are ppb.

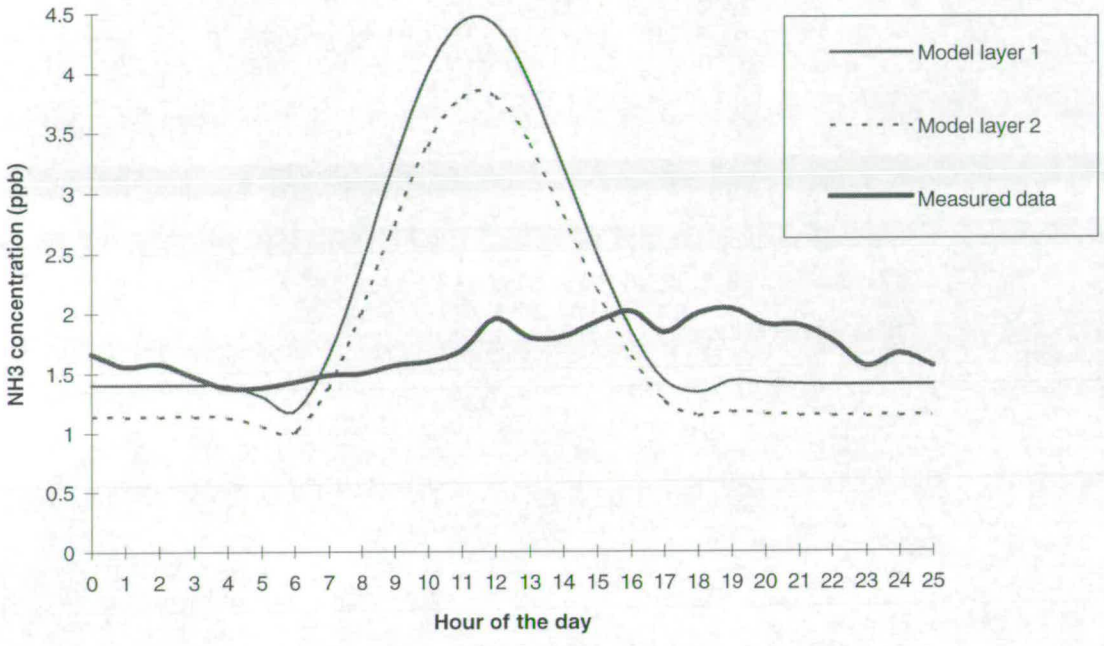

Figure 6.4: A comparison of the diurnal cycle of measured concentrations of NH_3 (Burkhardt *et al.*, 1996) and modelled concentrations of NH_3 at 2 layers (1.5 m and 3 m) produced using a diurnal variation in the modelled emissions. The measured data are representative of windspeeds greater than 1 m s^{-1}. Units are ppb.

southeastern trajectories, to around 1 ppb with trajectories from the north and northeast.

A comparison of the annually-averaged variation NH_3 concentrations, over a 24-hour period, for measured data and modelled data is shown in Figure 6.2. Concentrations of NH_3 have been recorded over a period of 2 years (Burkhardt *et al.*, 1996) at a rural site near Edinburgh, Scotland (Institute of Terrestrial Ecology). The instrumentation used in the study of Burkhardt *et al.* are known as continuous wet rotating denuders, which work by continuously sampling the air to provide concentration data with a resolution of 2 minutes. It is an extremely sensitive system, with a detection limit of 0.02 μg m^{-3} (Wyers *et al.*, 1993). Data of the wind direction and wind speed have also been recorded, and thus the concentration data can be categorised by wind direction and wind speed. These data can be compared with model results, and and be used to perform more

detailed comparisons at a specific location than is possible with the diffusion tube data discussed in section 5.5.1. Since the measurement height of 2 m is the boundary height between the first and second vertical layers in the model (Figure 4.1), the results for both model layers are presented here.

Nocturnal model concentrations, assuming constant emissions, are over twice the measured values, but during the daytime, there is a general trend for the measured data to increase, bringing them into better agreement with the modelled data. While the maximum modelled concentrations occur at night, the maximum measured concentrations occur during the late afternoon.

A plot of the modelled diurnal variations in surface concentrations of NH_3 is shown Figure 6.3. These data have been created by the use of a diurnal variation in emissions. The use of a diurnal variation in the emission rate (a constant nocturnal flux and a sinusoidal daytime variation with a maximum value which is 5 times the nocturnal rate) results in a significant change in the diurnal cycle of concentrations, with the maximum modelled concentrations now occurring during the day. The largest diurnal variation in concentrations occurs with trajectories coming from the west, which have a difference of 3.5 ppb between the minimum nocturnal and the maximum daytime values. The diurnal cycle for trajectories from the east and southeast are substantially different from the data for other wind directions. The increase in surface concentration due to large daytime emissions is offset by the rapid dilution due to mixing with less polluted air from above and also increased dry deposition. This has the effect of reducing the diurnal variation, especially for southeasterly trajectories where the minimum concentrations occur at dawn and dusk, and maximum daytime values being barely greater than the nocturnal concentrations. The parameterisation of the vertical diffusion and NH_3 deposition velocities in the model are not continuous functions, and the change between day and night is discontinuous. However, the diurnal variation in the emission flux is a continuous function, and thus the results in Figure 6.3, especially for the east and southeast, reflect the combination of these continuous and non-continuous functions.

Figure 6.4 shows a comparison between measured and modelled surface concentrations of NH_3. Both sets of data have a maximum concentration during the daytime, but the maximum modelled concentrations are more than twice the

maximum of the measured concentrations. This disagreement may be due to the fact that emissions of NH_3 are assumed to occur throughout a grid square. Thus a large diurnal variation in the emission rate will cause a correspondingly large diurnal variation in surface concentrations across entire grid square. In reality this is not the case, and concentrations that are measured at locations some distance from large emissions source will be less affected by variations in the emission rate, due to mixing with less polluted air by lateral and vertical dispersion, and also due to deposition processes especially dry deposition. The use of a coarser resolution landuse database may mean that the dry deposition velocity on a 20 km grid square may be less than the value for the corresponding 5 km grid square, since the 20 km grid square may contain areas with lower modelled values of V_d, such as urban areas including the nearby city of Edinburgh, Scotland. Nocturnal concentrations are in much better agreement.

6.2.2 Vertical gradients of ammonia concentrations

A plot showing the modelled vertical structure of NH_3 concentrations up to 87.5 m is shown in Figure 6.5, and these data represent a complete diurnal cycle. This plot illustrates the effect of using diurnally varying rates of vertical diffusion and dry deposition on modelled NH_3 concentrations. During the night, large vertical gradients exist near the surface, with maximum surface concentrations of 3 ppb. These decrease rapidly with height, reaching values of around 0.5 ppb, at 87.5 m. The largest vertical gradients exist close to the surface, in the lowest 20 m, with values of about -0.1 ppb m^{-1}. This is due to the increased stability of the modelled air column during the night, which reduces the rate of vertical exchange of material between layers, and also decreases the values of V_d used in the model to describe NH_3 dry deposition (section 3.1.1). During the daytime, the rate of vertical diffusion is much greater, allowing for increased mixing of material. This has the effect of reducing vertical gradients, as shown in the figure. Daytime surface concentrations are reduced to minimum of 1.4 ppb. The diurnal variation in concentration at the surface is 1.6 ppb compared to a variation of just 0.1 ppb at a height of 87.5 m.

The use of a diurnal variation in emissions has a marked affect on the results (Figure 6.6), as was mentioned in the last section. The largest concentrations

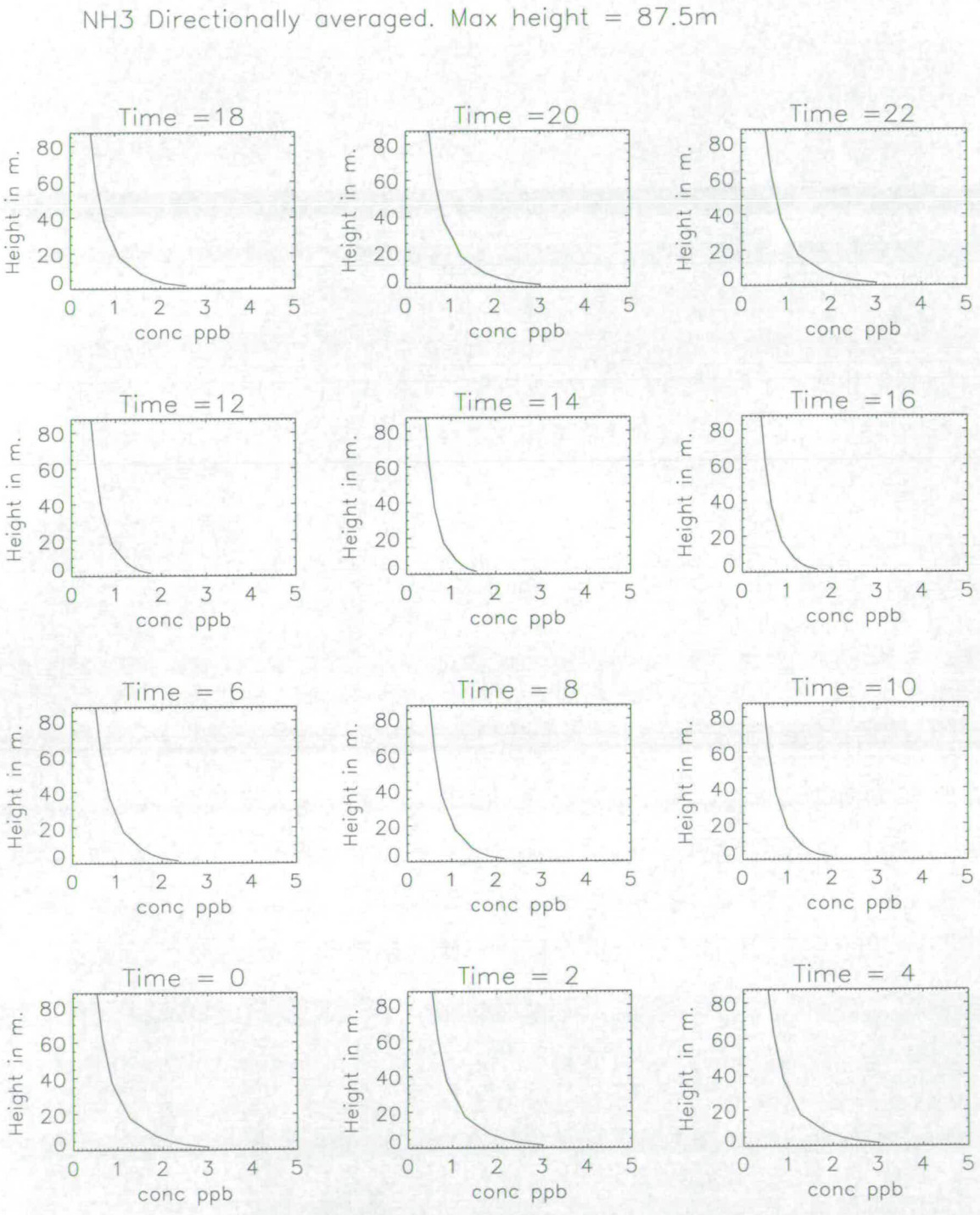

Figure 6.5: Directionally-averaged modelled concentrations of NH_3 at ITE Edinburgh from the receptor model. Each plot represents the vertical concentrations at a specific hour of the day, and the entire sets of plots describes the diurnal cycle. Data represent an annual average. Units are ppb.

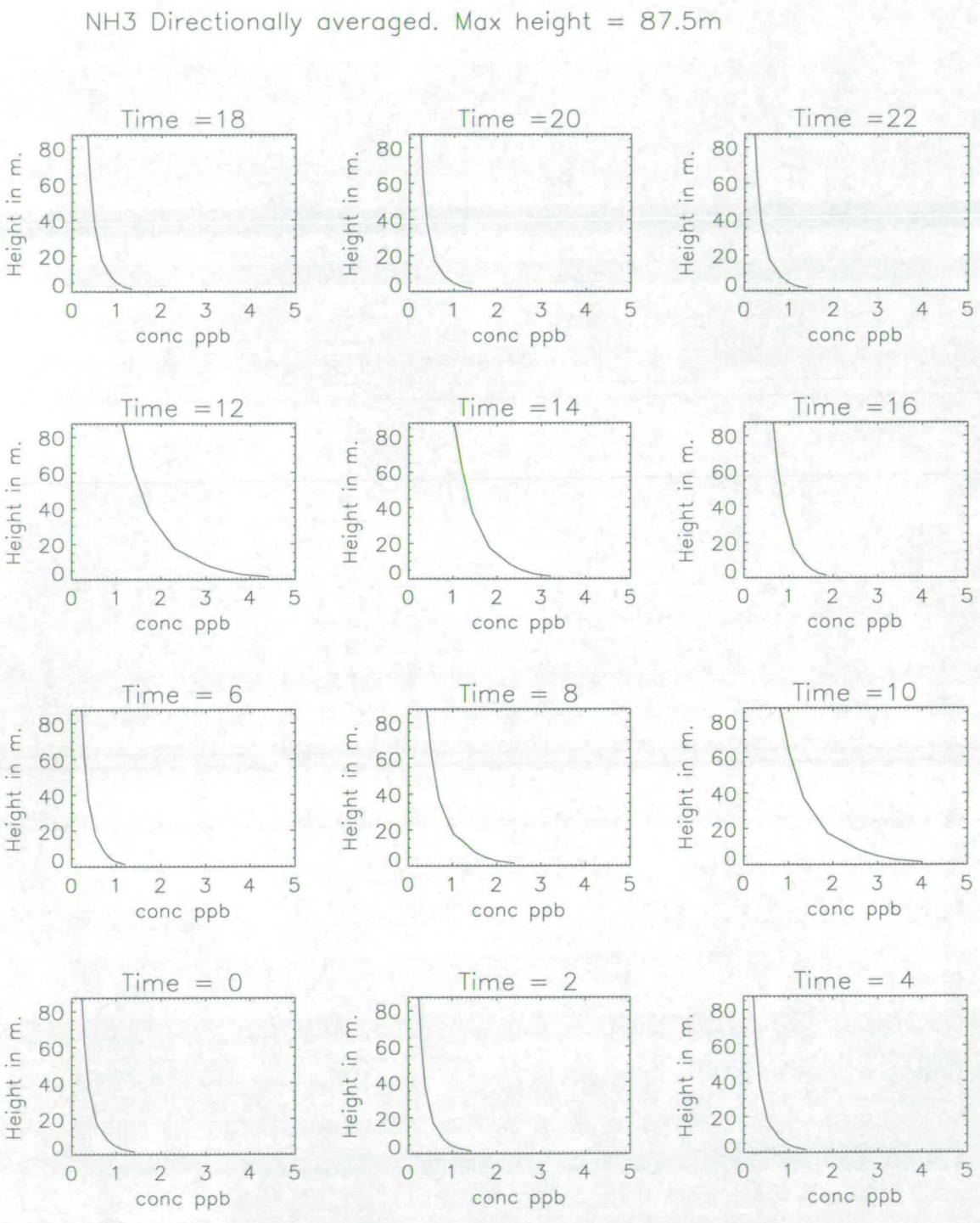

Figure 6.6: Directionally-averaged modelled concentrations of NH_3 at ITE Edinburgh from the receptor model, using a diurnal variation in the emission rate. Each plot represents the vertical concentrations at a specific hour of the day, and the entire sets of plots describes the diurnal cycle. Data represent an annual average. Units are ppb of NH_3.

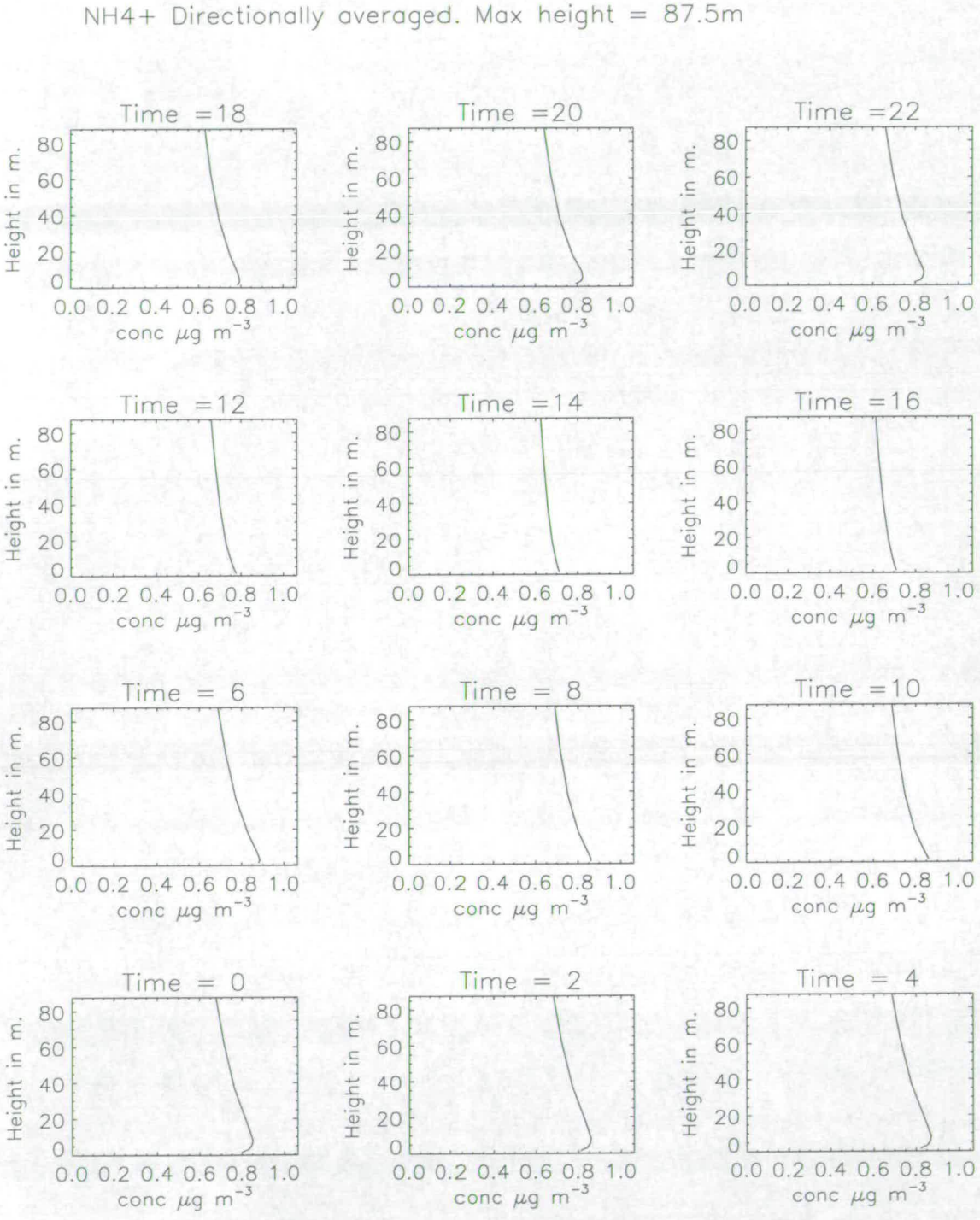

Figure 6.7: Directionally-averaged modelled concentrations of NH_4^+ aerosol at ITE, Edinburgh from the receptor model. Each plot represents the vertical concentrations at a specific hour of the day, and the entire sets of plots describes the diurnal cycle. The data were produced using an assumed constant emission rate. Data represent an annual average. Units are $\mu g\ m^{-3}$ of NH_4^+.

now occur during the middle of the day, with a maximum surface value of 3.9 ppb at 1200 hours. The large daytime emission rate also means that large vertical gradients now exist in the daytime and are actually larger than nocturnal values, though significant surface gradients still exist at night due to the increased stability. Concentrations well above the surface are much greater during the daytime, reaching values of 1.1 ppb at 87.5 m, compared to the corresponding value in Figure 6.5 of 0.4 ppb. This is due to the large emission rate combined with the high rate of daytime vertical mixing, resulting in more material being transported upwards. It should also be mentioned that the increased surface concentrations will combine with the large daytime V_d to produce very large dry deposition fluxes during the day, while correspondingly small emission fluxes at night combine with small modelled deposition velocities to produce very low dry deposition fluxes. The overall effect on the annual dry deposition is not immediately apparent and is investigated later in later in this chapter (section 6.4.3).

A plot of the vertical structure of NH_4^+ concentrations is shown in Figure 6.7. These data were produced using a constant emission rate of NH_3. Vertical gradients are much less than those for NH_3 (Figure 6.5), with the largest gradients occurring during the night, and much reduced daytime gradients of nearly zero occurring during the middle of the day. There is a general negative gradient in concentrations above 5 m, which reflects the fact that NH_4^+ is a secondary product of NH_3, and thus reflects the general vertical structure of NH_3 concentrations shown in Figure 6.5. The diurnal variation in surface concentrations is about 0.2 μg m^{-3}. One interesting feature is that while concentrations generally have a negative vertical gradient, during the night a positive gradient exists close to the surface, showing the effect of removal due to dry deposition.

6.2.3 Comparison of concentration roses for measured and modelled data.

In this section, data in the form of concentration roses of NH_3 are presented, and comparisons are performed between measured concentrations (Burkhardt *et al.*, 1996) and modelled concentrations. Figure 6.8 contains 2 concentration roses. Each concentration rose has both modelled data and measured data. The modelled data in these plots are for an average height of 1.5 m (1st model layer,

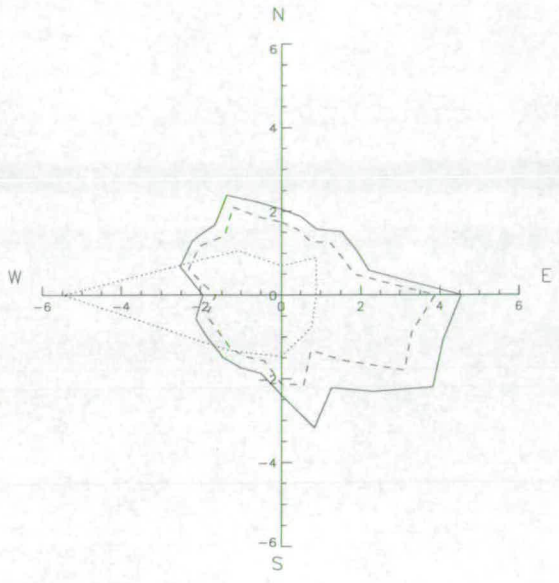

Figure 6.8: A comparison of measured and modelled concentration roses of NH_3, with the use of constant emission rates in the model, for two model layers (1.5 m and 3 m). The measured data (2 m; dotted line) are from ITE, Edinburgh, and are the mean for a two year period (1992-1994) (Burkhardt *et al.*, 1996). The modelled data are for concentrations from the receptor model. 1.5 m is the full line and 3 m is the dashed line. Data represent an annual average. Units are ppb.

1-2 m, full line) and an average height of 3 m (2nd model layer, 2-4 m, dashed line). The modelled results were created assuming a constant emission flux. The measured concentrations (dotted line) are the mean of data which were recorded over a two year period, at a height of 2 m, and thus can be considered a long term average (Burkhardt *et al.*, 1996). Since the measurement height of 2 m is the boundary height between the first and second vertical layers in the model (Figure 4.1), the results for both model layers are presented here.

For the majority of the wind directions, the modelled concentrations shown in Figure 6.8 over-estimate the measured data, especially with wind from the east and southeast. Modelled concentrations in the first model layer are over 4 times greater than the observed concentrations from the east, and over 3 times as large in the second layer. However, measured concentrations from the west are much larger than the model predictions. This is an example of the effect of very local

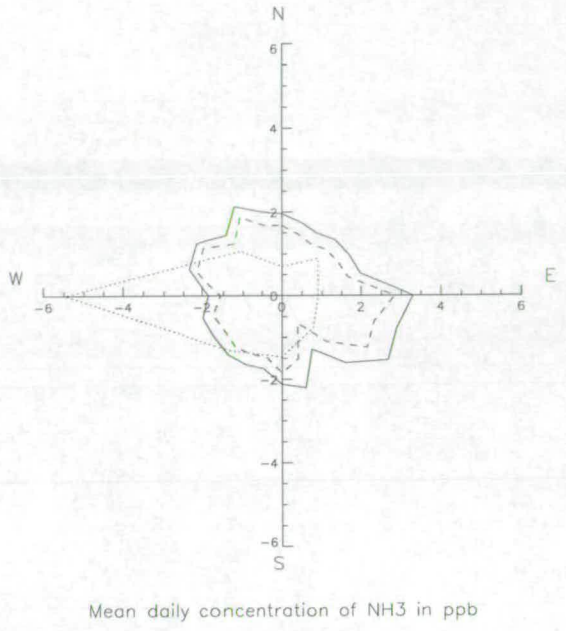

Figure 6.9: A comparison of measured and modelled concentration roses of NH_3, with the use of diurnal variation in the modelled emission rate, for two model layers (1.5 m and 3 m). The measured data (2 m; dotted line) are from ITE, Edinburgh, and are the mean for a two year period (1992-1994) (Burkhardt *et al.*, 1996). The modelled data are for concentrations from the receptor model. 1.5 m is the full line and 3 m is the dashed line. Data represent an annual average. Units are ppb.

emissions, since a mixed farm is located just 250 m to the west of the monitoring site. Even with a fine resolution emission grid of 5 km grid squares, the model is not able to reproduce this feature adequately. Concentration data for the second layer are smaller than those in the first layer, as expected from Figure 6.5, and are a closer fit to the measurements.

Figure 6.9 is a similar plot of a concentration rose of NH_3 containing both modelled concentration data and measured data, but the model data were created using the diurnal variation in the emission rate. The modelled concentrations in this figure are generally less than the concentrations in Figure 6.8, and are a better fit to the measured data. The modelled concentrations in the second model layer are less than the first layer concentrations, and compared with all the data in Figures 6.8 and 6.9, appear to give the best agreement with the observed data. The under-estimation in concentrations from the west has not changed, but the

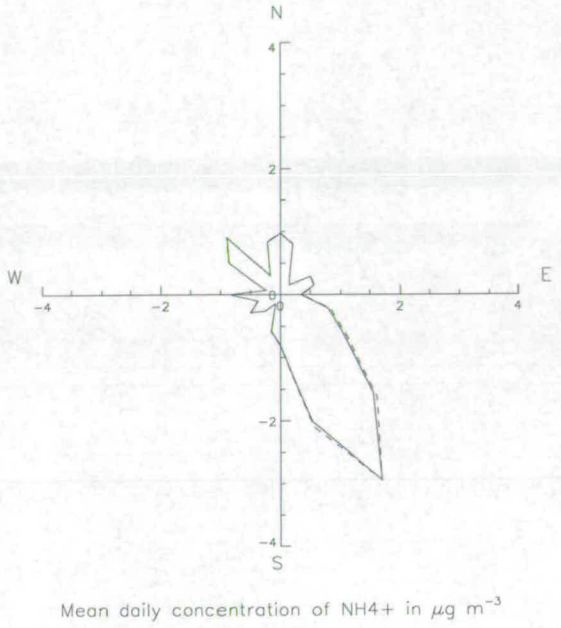

Figure 6.10: A plot of modelled concentration concentration roses of NH_4^+ aerosol, with the use of constant diurnal emission rate of NH_3 in the model. Data from two model layers are presented (1.5 m and 3 m). 1.5 m is the full line and 3 m is the dashed line. Data represent an annual average. Units are μg m^{-3}.

previous over-estimation with winds from the east and southeast has been reduced considerably. These results substantiate the results of Asman and van Jaarsveld (1992) who reported a 20% reduction in the annually-averaged concentrations of NH_3 and NH_4^+ with the use of a diurnal variation in the emission rate. This implies that with decreased surface concentrations, dry deposition might have increased, and there may be more NH_3 at higher levels and thus available for conversion to NH_4^+ aerosol as shown in Figure 6.10. This is investigated later in this chapter (section 6.4.3).

A concentration rose showing the directional-dependence of NH_4^+ surface concentrations is shown in Figure 6.10. Concentrations are generally low for most wind directions, with values less than 1.5 μg m^{-3}, except for trajectories arriving from a south-southeasterly direction. In these cases, concentrations are much larger, with the maximum value of over 3 μg m^{-3}. The significance of the direction of these trajectories can be understood by referring to the emissions data

for SO_2 and NO_x that are used as input for FRAME (Figures 5.7 and 5.8). The major emission sources of SO_2, and to a lesser extent NO_x, are in the north Midlands/south Yorkshire region, and this area lies on a south-southeast bearing from the receptor point. The high concentrations of SO_2 and NO_x emitted into the modelled air means that large quantities of acid (H_2SO_4 and HNO_3) are produced, which react with NH_3 to form NH_4^+ aerosol. There is little difference in the data between the two model layers. There are no measurements available to compare concentration roses of NH_4^+ at ITE, Edinburgh.

6.3 Analysis of results for Great Britain from the FRAME model on a 5 km grid using constant emissions

In this section, country-wide results are presented from the 5 km version of the FRAME model, using a constant emission flux of NH_3. These include maps of NH_3 surface concentrations, dry deposition of NH_3 and wet deposition of NH_x. An annual budget of reduced nitrogen for Great Britain is presented.

6.3.1 Modelled surface concentrations

A plot of modelled surface concentrations of NH_3 is shown in Figure 6.11. Since the emissions data for NH_3 are for 1988, these data represent an annual average for 1988 and the units are ppb. This plot can be compared to the corresponding NH_3 concentration data from the 20 km version of FRAME (Figure 5.19). The areas of maximum concentrations are generally in the same locations as in Figure 5.19, such as East Anglia, south west England and parts of the England/Wales border. However the increased resolution of Figure 6.11 allows the spatial distribution of modelled concentrations to be more clearly defined. It illustrates the large horizontal gradients that occur between areas of high and low emissions, such as East Anglia, and also shows small areas of high emissions near the coast, which are not defined in Figure 5.19. Areas of low concentration (< 1 ppb) have been more clearly distinguished, as in the case of the Pennines in northern England, areas of Cumbria in northwest England, southern Scotland, and in western Wales.

A correlation plot of these data, and the observed surface concentrations of

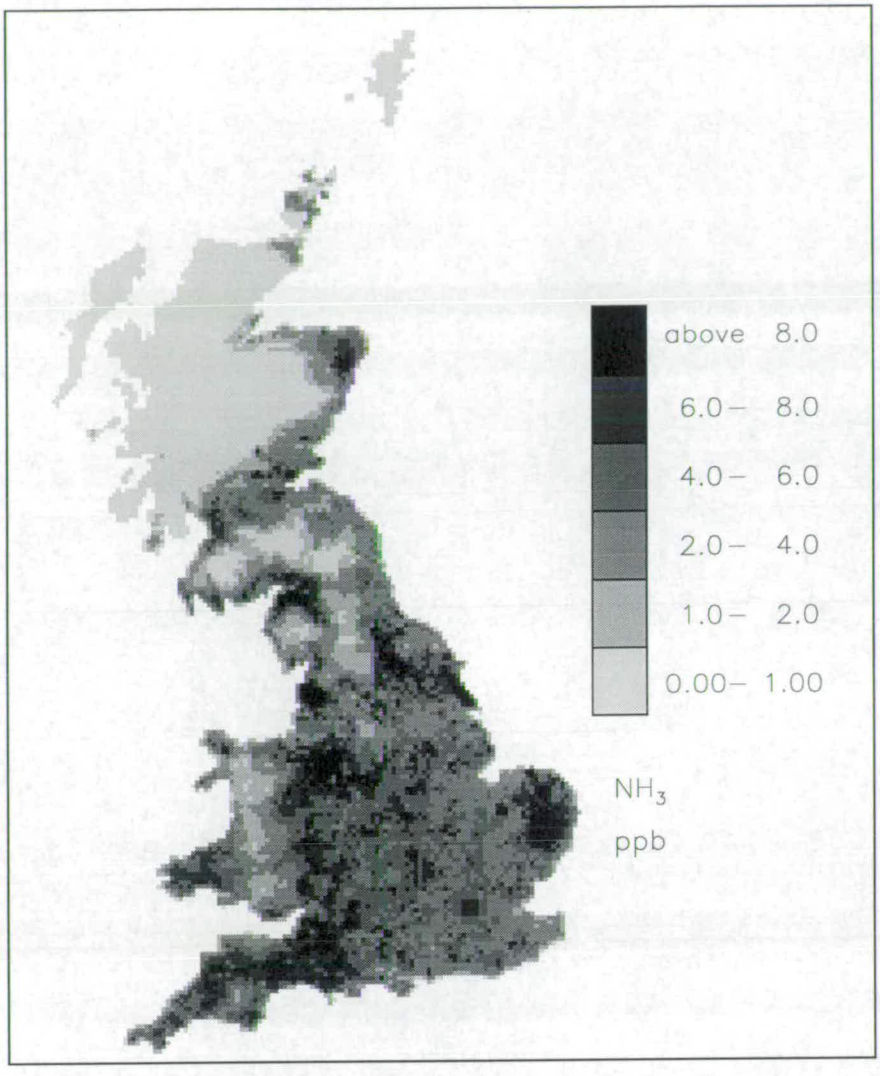

Figure 6.11: Modelled surface concentrations of NH_3 for Great Britain (1988) on a 5 km $\times$ 5 km grid, using a constant emission rate. Data represent an annual average. Units are ppb.

NH_3, which were recorded using diffusion tubes (sections 2.2.1, 5.5.1), is shown in Figure 6.12. The observed data are slightly different from the data presented in Figure 2.1 since these are the mean values for just one year, whereas the data in Figure 2.1 are the mean of the entire 3 year period. The correlation coefficient (R) has a value of 0.7. For the sample size of n = 51, this correlation has a probability (P) of having arisen by chance of 9.96×10^{-9}, which is statistically significant at the P = 0.1% level. The dotted line is the one-to-one agreement and the solid line is the regression line. The slope of the regression line is 1.29 and the intercept is 0.40 ppb. At first glance, it would seem that the increased horizontal

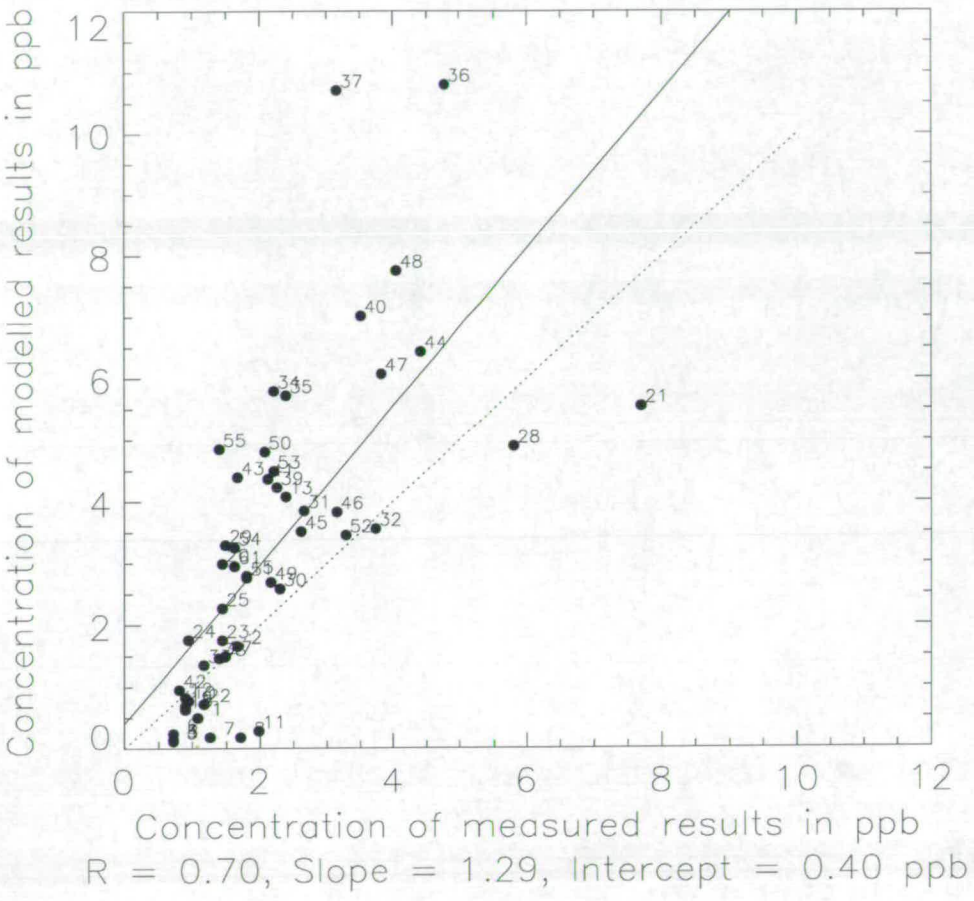

Figure 6.12: Correlation plot of modelled NH_3 surface concentrations from the FRAME model on 5 km grid versus observations from a network of measurements sites (Atkins and Lee, 1992; multiplied by a correction factor of 0.45). Units are ppb. Each point has number assigned, which corresponds to the location of the measurement site shown in Figure 6.13. The full line is the regression line and the dotted line is the one-to-one line.

resolution of the model has not resulted in an improved correlation with measured data, compared with the regression analysis of NH_3 surface concentrations for the 20 km version of FRAME (Figure 5.20). The slope of the regression line has increased (from 1.17 to 1.29), the intercept has decreased and the value of R has remained virtually the same. However, analysis of Figure 6.13, which is the map of the categorised relative differences between modelled and measured data (Figure 6.13), tells a slightly different story.

In this plot, there are 15 locations where the magnitude of relative difference between measured and modelled data is less than 0.25. In comparison, for the

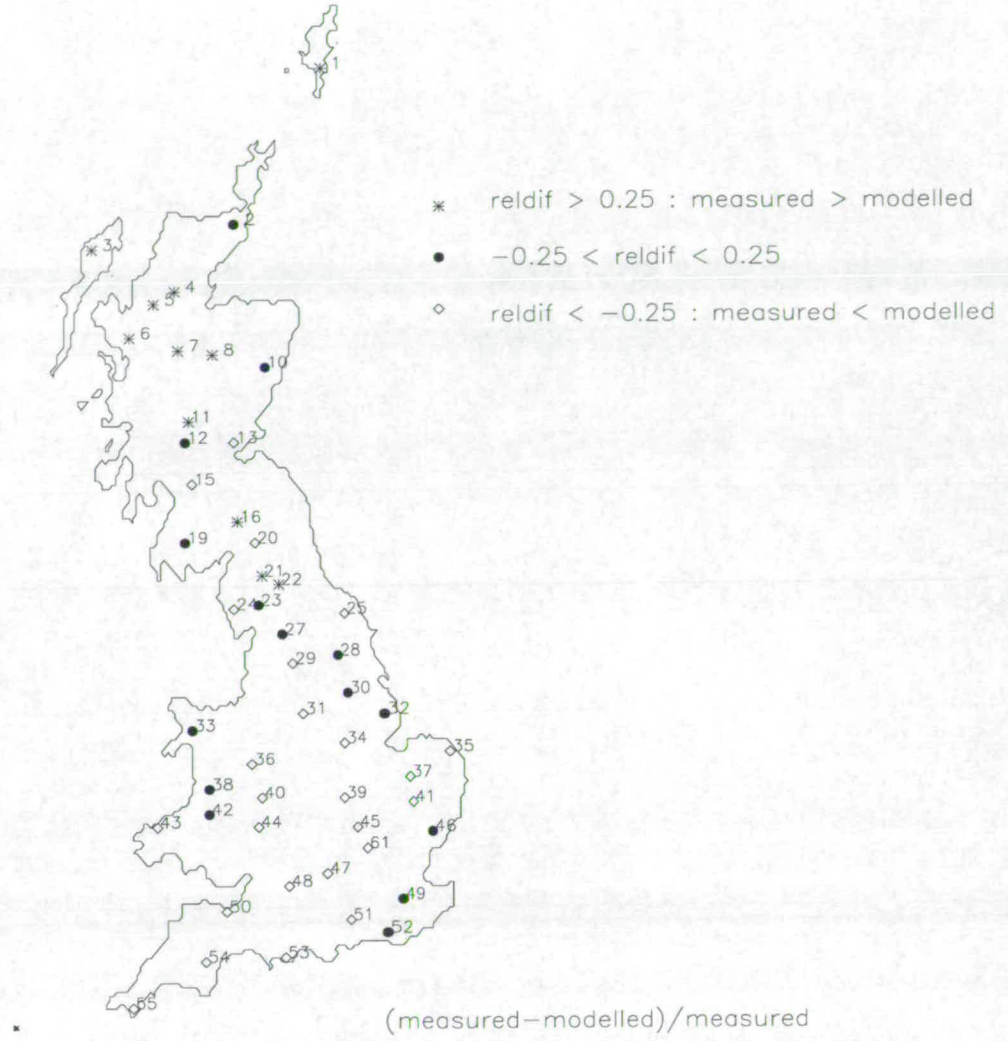

Figure 6.13: A map of categorised relative differences from $\frac{\text{measured}-\text{modelled}}{\text{measured}}$ of NH_3 surface concentration. Measured data are multiplied by a correction factor of 0.45. Modelled data are from the 5 km version of FRAME.

results from the 20 km version of FRAME, there are only 6 locations where the magnitude of the relative difference less than 0.25. Whilst the correlation analysis initially implied that little change had occurred, a more detailed examination shows at many of locations the modelled concentrations have decreased in value and there is less over-estimation of observed values. Modelled concentrations at a few locations have increased dramatically, especially at sites 37 and 36, where the 20 km concentrations of 6.6 ppb and 6.2 ppb respectively have both increased to about 10.7 ppb for the 5 km results. At the same time, the concentration at station 28 has decreased from 7 to 5 ppb, but this decrease has brought the data much closer to the one-to-one line and is advantageous. Thus an increase

in horizontal resolution has generally increased the agreement between measured and modelled data, but has also drastically decreased it at two locations (36 and 37). This can be analysed further by looking at the standard deviation of the two sets of data. For the 20 km data, the standard deviation is 1.71. With stations 36 and 37 removed, this value is virtually unchanged, at 1.72. However, with the 5 km data, the significance of the outliers become apparent. The standard deviation, including stations 36 and 37 is 1.84, which is greater than the 20 km results. However, with the two outliers removed (stations 36 and 37) the standard deviation becomes 1.48, showing that the use of finer resolution emissions database has reduced the standard deviation of most of the data, and with the exception of two locations, there are better agreement between the modelled and the measured surface concentrations of NH_3.

6.3.2 Dry deposition of ammonia

The annual flux of modelled dry deposition, on 5 km × 5 km grid, is shown in Figure 6.14. The total annual flux of NH_3-N for Great Britain is 95.5 Gg year^{-1}, which can be compared with the corresponding 20 km total of 87.9 Gg year^{-1}. Use of the finer horizontal resolution has allowed areas of very high dry deposition flux to be distinguished, in comparison with the corresponding plot of 20 km dry deposition (Figure 5.22). There are some areas of very high grid square averaged dry deposition (> 10 kg ha^{-1} year^{-1}) that are located within 2 grid squares of areas of very low grid square averaged dry deposition (< 2 kg ha^{-1} year^{-1}). This clearly illustrates the large spatial variability of dry deposition that can occur, and why the use of an inferential model with concentration data from just relatively few stations (section 2.2.1) is inadequate to describe the spatial distribution of dry deposition over such a large area as Great Britain. It must be mentioned that these dry deposition data were created with the use of a 20 km landuse database. The large spatial variability in the surface concentrations and dry deposition is a direct result of the high resolution emissions. Ideally it would have been appropriate to employ a landuse database with the same high spatial resolution, but one was not available. The implications of this are discussed in section 6.3.6.

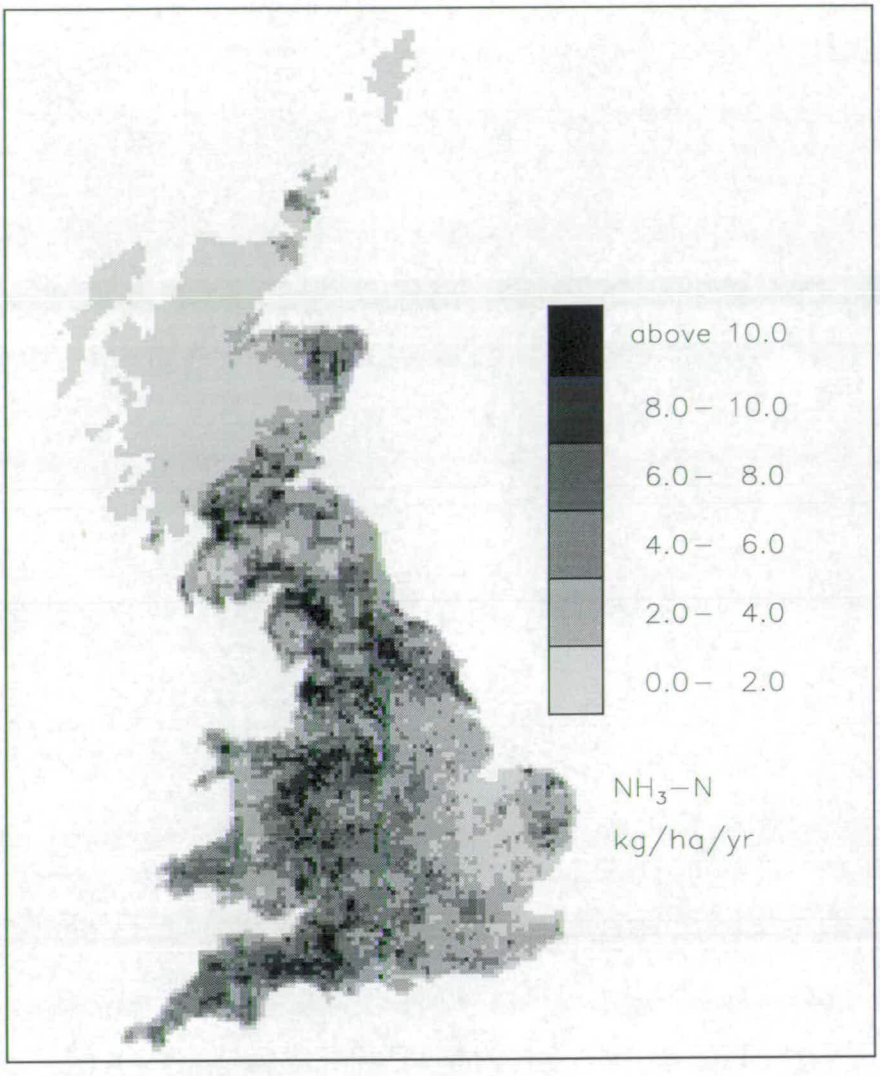

Figure 6.14: Modelled annual flux of NH_3-N dry deposition to Great Britain (1988) on a 5 km grid. Units are kg ha^{-1} $year^{-1}$.

6.3.3 Surface concentrations of ammonium aerosol

Figure 6.15 is a plot of the modelled surface concentrations of NH_4^+ from the 5 km version of the FRAME model. There is little difference between this plot and the corresponding plot from the 20 km version of FRAME (Figure 5.23), apart from the fact that there are fewer areas for the 5 km data where there are concentrations of greater than 2 μg m^{-3}, compared with the 20 km data. The better agreement between modelled surface concentrations of NH_4^+ for different spatial resolutions, compared to the modelled surface concentrations of NH_3, reflects the fact that NH_4^+ aerosol is a secondary reaction product of NH_3, and the longer atmospheric residence time of this species allows greater vertical mixing,

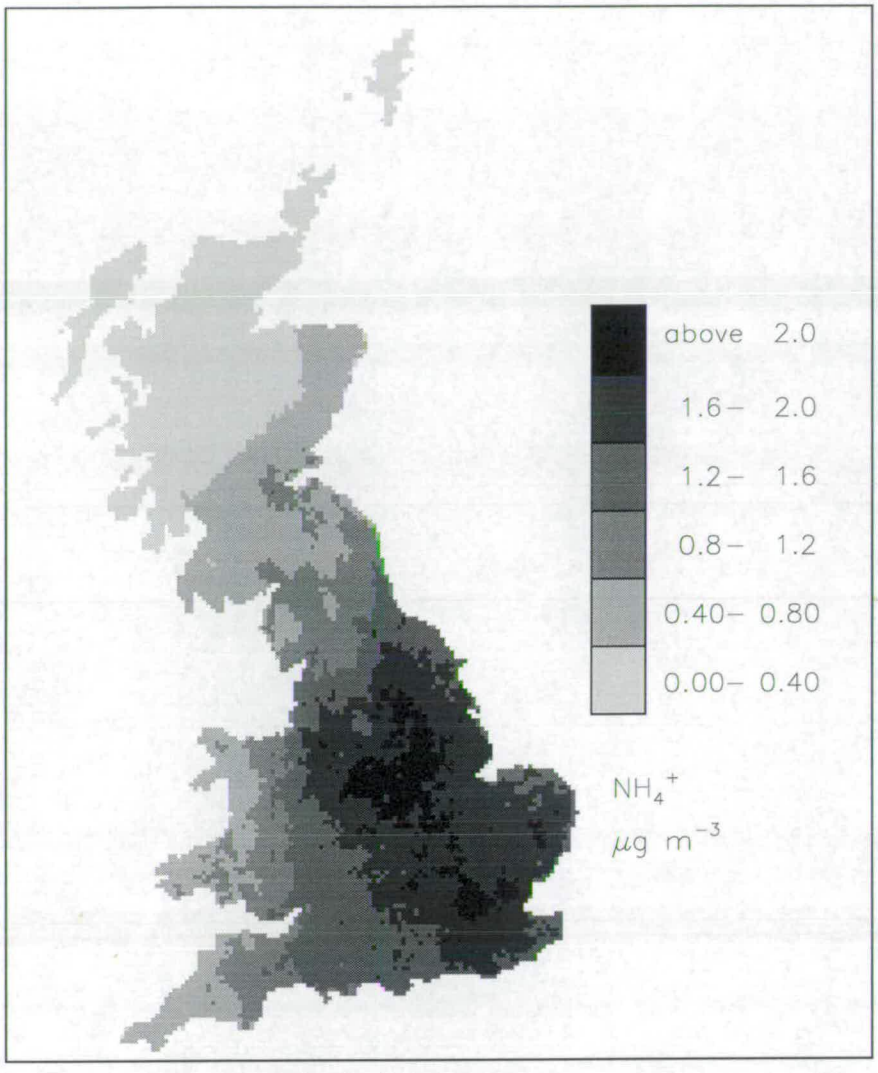

Figure 6.15: Modelled surface concentrations of NH_4^+ for Great Britain (1988) on a 5 km $\times$ 5 km grid. Data represent an annual average. Units are $\mu g\ m^{-3}$.

which reduces the spatial variation in concentrations.

6.3.4 Dry deposition of ammonium aerosol

The total flux of ammonium dry deposition to Great Britain, as calculated by the FRAME model on a 5 km $\times$ 5 km grid, is 6.5 Gg year^{-1} of NH_4^+-N. This value is 6.3% of the annual dry deposition flux of reduced nitrogen to Great Britain which is 102.0 Gg year^{-1} of NH_x-N.

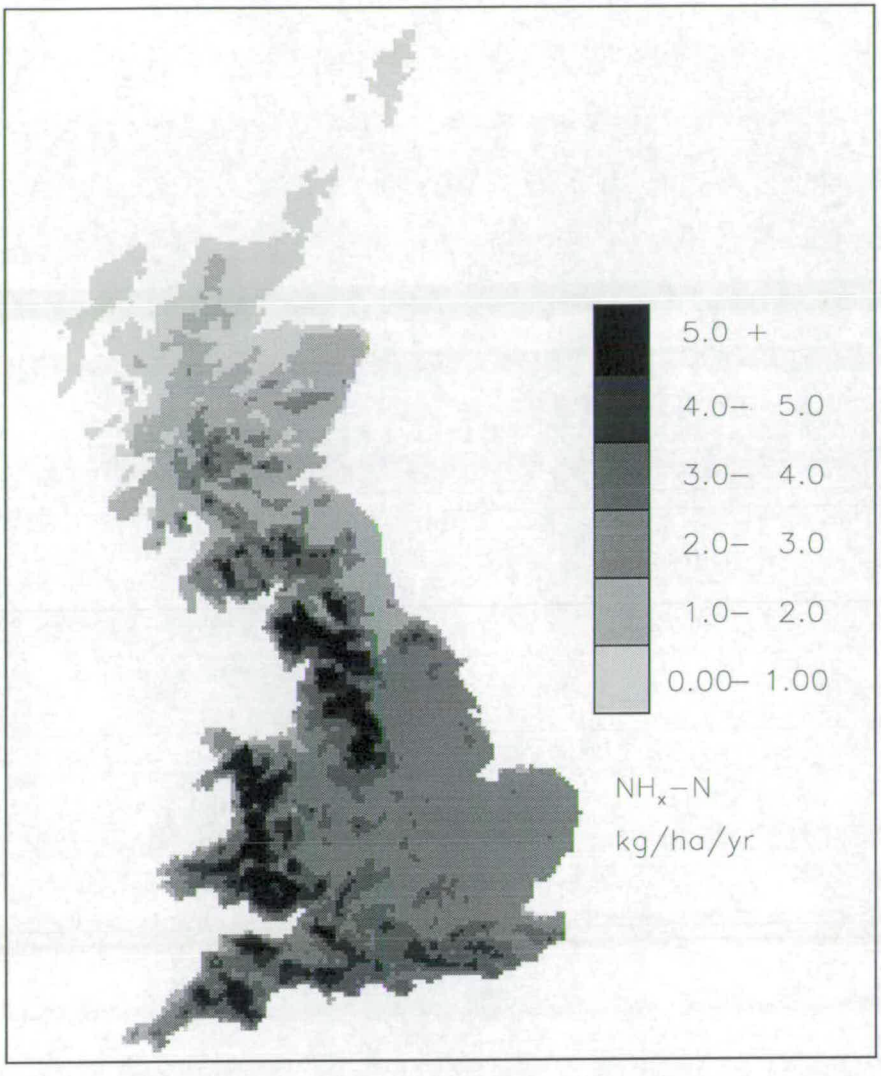

Figure 6.16: Modelled annual flux of NH_x-N wet deposition to Great Britain (1988) on a 5 km grid. Units are kg ha^{-1} $year^{-1}$.

6.3.5 Wet deposition of reduced nitrogen

The main contributor to wet deposition of reduced nitrogen is ammonium aerosol. Section 6.3.3 showed how spatial distributions of surface concentrations of ammonium aerosol had not varied much between the two spatial scale versions of the FRAME model (20 km grid and 5 km grid). This implies that while there is a large difference in the spatial distribution of NH_3 concentrations, there should not be much difference in the overall wet deposition flux of NH_x-N. A plot of the modelled wet deposition of reduced nitrogen is shown in Figure 6.16. The overall shape is similar but the high resolution has more clearly defined areas of high and low wet deposition. The modelled annual flux of NH_x-N wet deposition from the

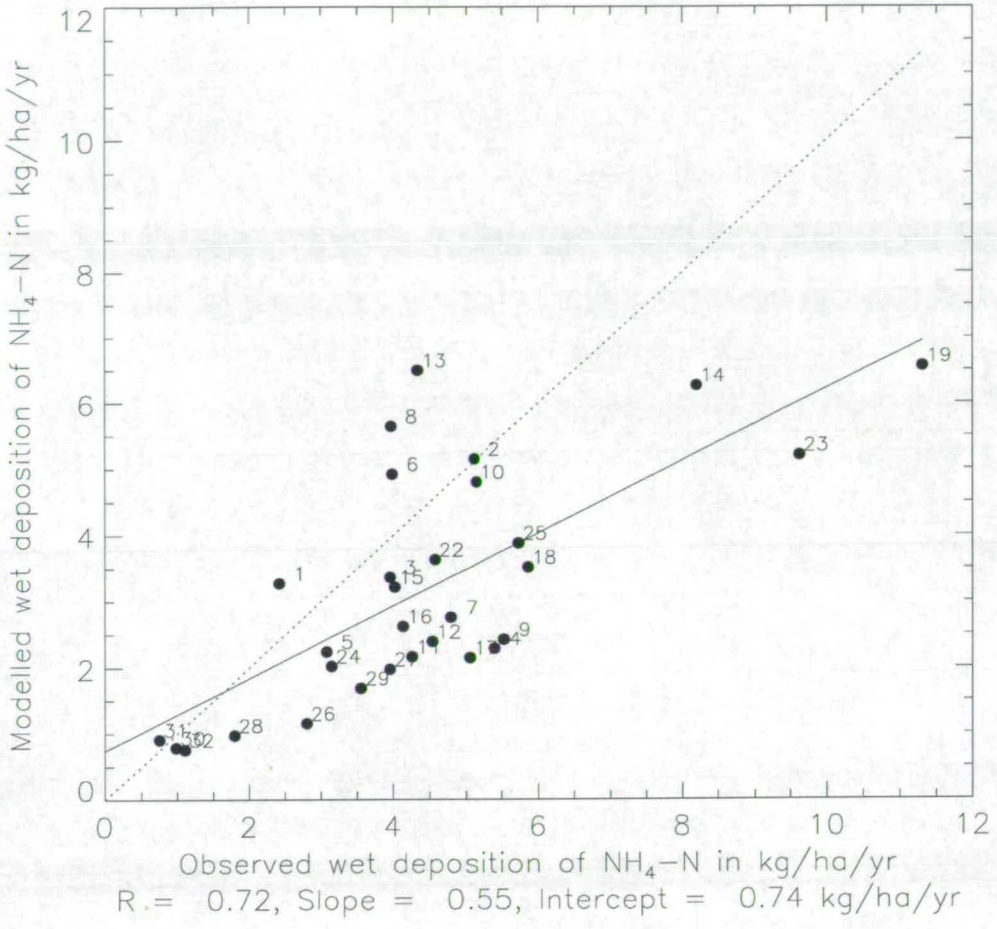

Figure 6.17: Correlation plot of modelled NH_x-N wet deposition fluxes on a 5 km grid, produced using constant emissions, versus observations from a network of measurements sites. Units are kg ha^{-1} $year^{-1}$. Each point has number assigned, which corresponds to the location of the measurement site shown in Figure 6.18. The full line is the regression line and the dotted line is the one-to-one line.

5 km version of the FRAME model is 64.6 Gg $year^{-1}$, of which 55.1 Gg $year^{-1}$ is from NH_4-N and 9.5 Gg $year^{-1}$ is wet deposition of NH_3-N. The ratio of NH_4^+ to NH_3 is 5.8:1. The results from the 20 km version of FRAME give the total wet deposition of NH_x-N to be 58.7 Gg $year^{-1}$ and the ratio of NH_4^+ to NH_3 at nearly 7.54:1. The effect of increasing the spatial resolution has resulted in an increase in the total amount of reduced nitrogen wet deposited, and a reduction in the ratio of NH_4^+ to NH_3.

A correlation plot of modelled wet deposition fluxes of NH_x against observed data from the UK Secondary Acid Deposition Network (section 1.5.3) is shown in

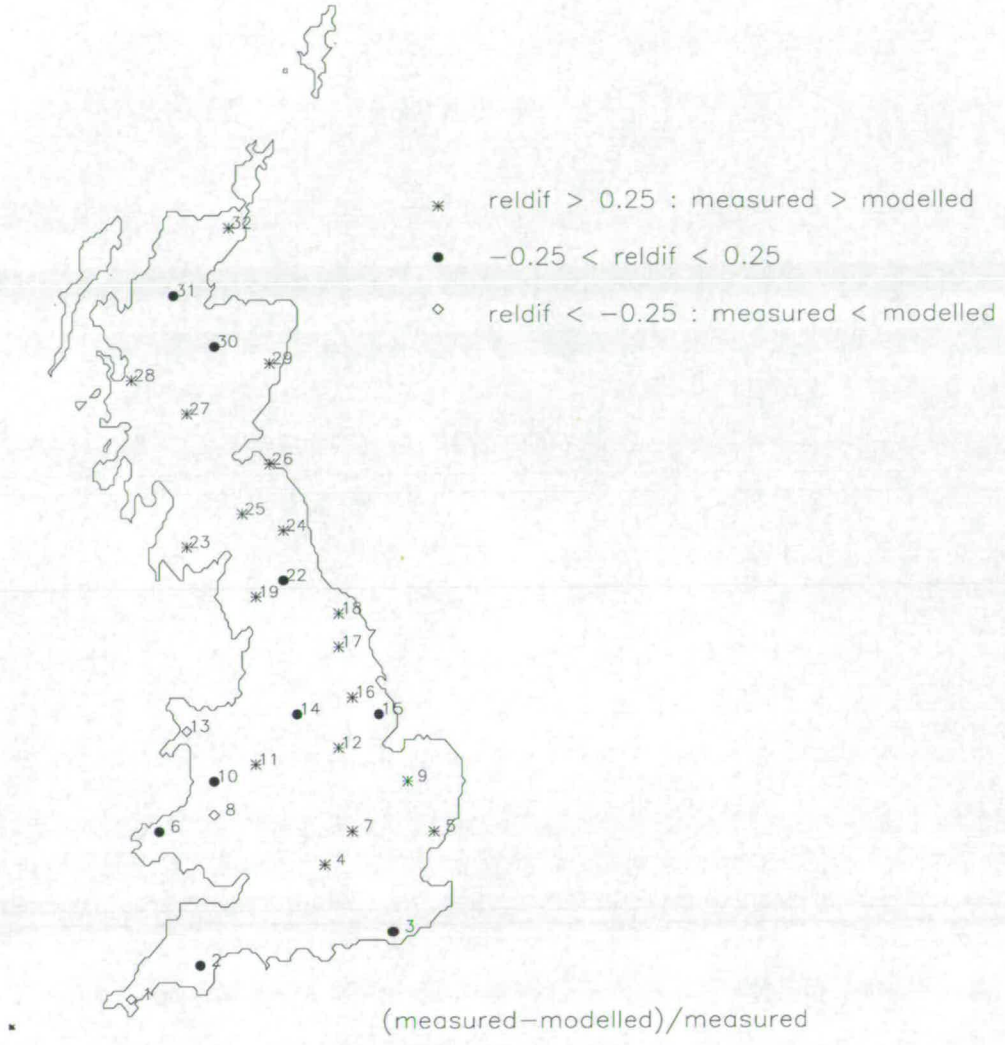

Figure 6.18: A map of categorised relative differences from $\frac{\text{measured}-\text{modelled}}{\text{measured}}$ of NH_x-N wet deposition fluxes. Modelled data are from the 5 km version of FRAME.

Figure 6.17. The correlation coefficient (R) is 0.72. For the sample size of n=30, this correlation has a probability (P) of having arisen by chance of 8.68×10^{-6}, which is statistically significant at the P = 0.1% level. The slope of the regression line is 0.55 and the intercept is 0.74 kg ha^{-1} $year^{-1}$. In comparison with the same set of results on the 20 km scale (section 5.5.5) little change has occurred in the regession results. The value of R has increased sligh;tu frpm 0.71 to 0.72 and the slope of the regression line has also increased by a very small amount (0.54 to 0.55). The location of the measurement stations are shown in Figure 6.18, which is a plot of the categorised relative differences of (modelled - measured)/measured. At 9 of the stations, the magnitude of the relative differences are less than 0.25, showing locations where there is reasonable agreement between the model and

observations. At 3 of the stations, the relative differences are such that the model is over-estimating the observations by more than 25%. At the remaining 18 stations, the model under-estimates the observations by more than 25%.

Fowler (1994) recommended that the use of orographic enhancement function (section 4.3.9, Dore *et al.*, 1992) to produce maps of wet deposition should be restricted in spatial scale to a 20 km × 20 km grid, and should not be used on a finer scale. This may be due to the fact that wind drift of rainfall may mean that a 5 km grid will have some uncertainties in the actually spatial distribution of the wet deposition fluxes, compared to a 20 km grid. Fowler (1994) stated that there was no procedure to apply such a simplification on a finer scale such as a 5 km × 5 km grid. Authors such as Metcalfe *et al.* (1995) have shown the improvements in model results that occur with the use of such an enhancement. Whilst recognising the comments of Fowler (1994) as having merit, the lack of any other simple parameterisation (at the time of writing), which can be applied on a fine spatial scale, means that the parameterisation of Dore *et al.* (1992) is retained in the present version of the model on a 5 km scale.

6.3.6 An annual budget of reduced nitrogen for Great Britain from the 5 km version of the FRAME model

The modelled annual budget for reduced nitrogen from the 5 km version of the FRAME model is given in Table 6.1. The annual import of reduced nitrogen is 36.6 Gg year^{-1} and the annual export is 151.2 Gg year^{-1}. The dry deposition total of NH_x is 102 Gg year^{-1} which compares very well with the official estimate from ITE, used by the UK Department of the Environment, of 94.5 Gg year^{-1} (RGAR, 1996). However, the spatial distribution of these two datasets are very different (Figures 2.2 and 6.14). The annual flux of wet deposition is 64.6 Gg year^{-1}, which is about 50% of the official estimate of 131 Gg year^{-1} (RGAR, 1996).

If it had been possible to include a 5 km landuse dataset in the model, it is possible that more interesting results would have been produced. Using a finer resolution landuse dataset would have meant that the spatial distribution of different landtypes within a 20 km square would become more distinct and an increased spatial variation in the dry deposition patterns could have been

Wind sector origin of trajectories	Emissions of NH_x-N	Import of NH_x-N	Dry deposition of NH_x-N	Wet deposition of NH_x-N	Export of NH_x-N
0 - 45	281.2	2.1 (0.2)	86.8 (9.8)	59.9 (6.4)	136.6 (14.7)
45 - 90	281.2	35.5 (2.8)	102.0 (8.0)	80.3 (6.4)	134.2 (10.6)
90 - 135	281.2	107.7 (7.1)	133.2 (9.1)	112.3 (7.3)	143.5 (9.3)
135 - 180	281.2	79.5 (6.8)	135.7 (12.2)	120.0 (10.0)	105.0 (8.8)
180- 225	281.2	55.8 (6.5)	90.6 (12.2)	82.3 (8.8)	164.2 (18.2)
225 - 270	281.2	33.2 (6.4)	90.4 (17.4)	47.5 (9.2)	176.6 (34.1)
270 - 315	281.2	29.7 (5.3)	87.3 (15.7)	42.2 (7.5)	181.4 (32.2)
315 - 360	281.2	8.3 (1.4)	104.2 (17.6)	52.2 (9.2)	133.1 (23.3)
Averaged annual modelled budget of NH_x-N	281.2	36.6	102.0	64.6	151.2

Table 6.1: Modelled annual budget of reduced nitrogen for eight wind sectors and an averaged annual budget for the country for 1988. These data are from the 5 km version of the FRAME model. Data in brackets are the frequency weighted total for each wind sector. The units are Gg of NH_x-N $year^{-1}$.

observed, compared to the dry deposition data that has already been presented in Figure 6.14. This is important as the largest concentrations occur in the vicinity of the emission source which in the case of the model is the 5 km grid square. A small area of high modelled deposition velocities, such as moorland or forest, surrounded by grassland, and close to a emission source, would have little impact on the overall dry deposition to the aggregated 20 km grid square. However if the landuse data were on a 5 km resolution, dry deposition to this area might be enhanced considerably. This illustrates the need for fine resolution modelling of NH_3 dry deposition, because the susceptible areas to damage may be of a small area and may be located in the vicinity of a large emission source.

6.4 Assessment of modelled results using a diurnal variation in the emission rate of ammonia

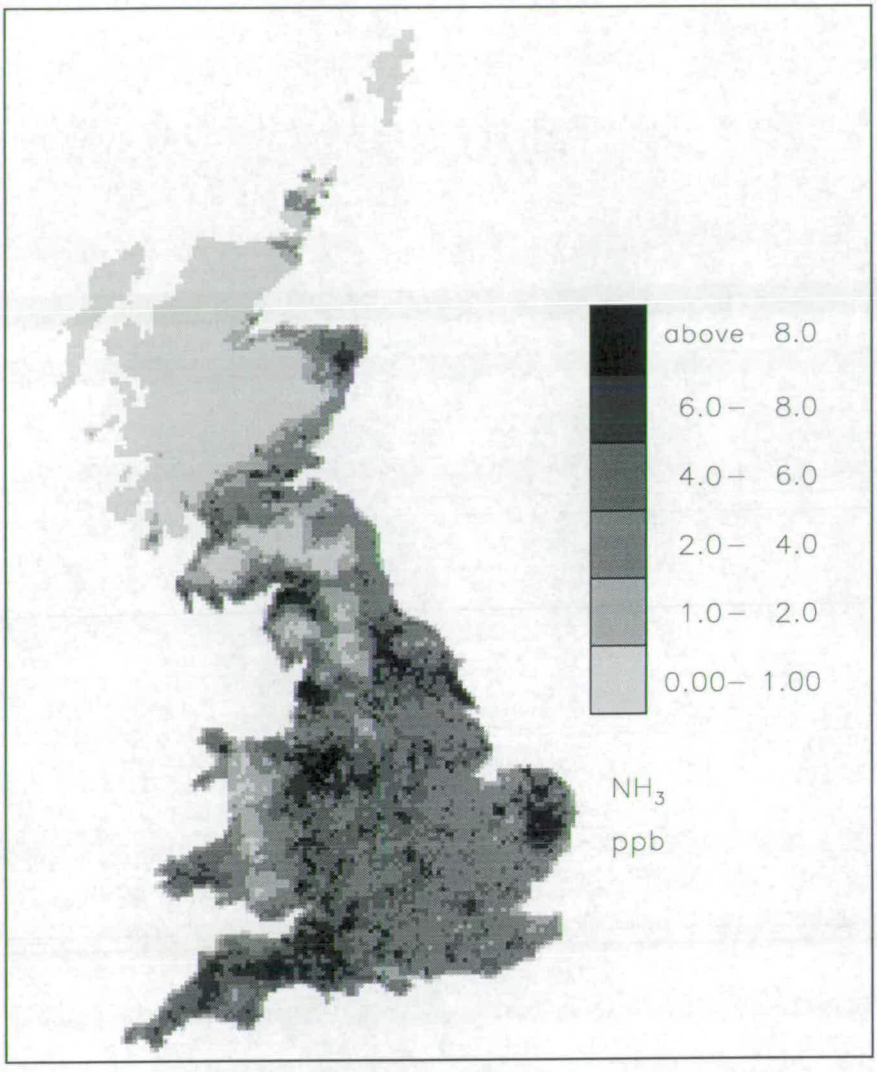

Figure 6.19: Modelled surface concentrations of NH_3 for Great Britain (1988) on a 5 km $\times$ 5 km grid, using a diurnal variation in the emission flux. Data represent an annual average. Units are ppb.

The extent to which a diurnal variation in the emissions flux of NH_3 affects the modelled results is examined in this section. The same diurnal variation described in section 6.2 is used, and data are presented for surface concentrations, deposition fluxes and an annual budget. These data are compared with the data from section 6.3 to assess the effect of a diurnal variation in emissions on model results.

6.4.1 Surface concentrations of ammonia

Figure 6.19 is a plot of the modelled field of NH_3 surface concentrations for 1988, produced using the diurnal variations in emissions. This map is very similar to

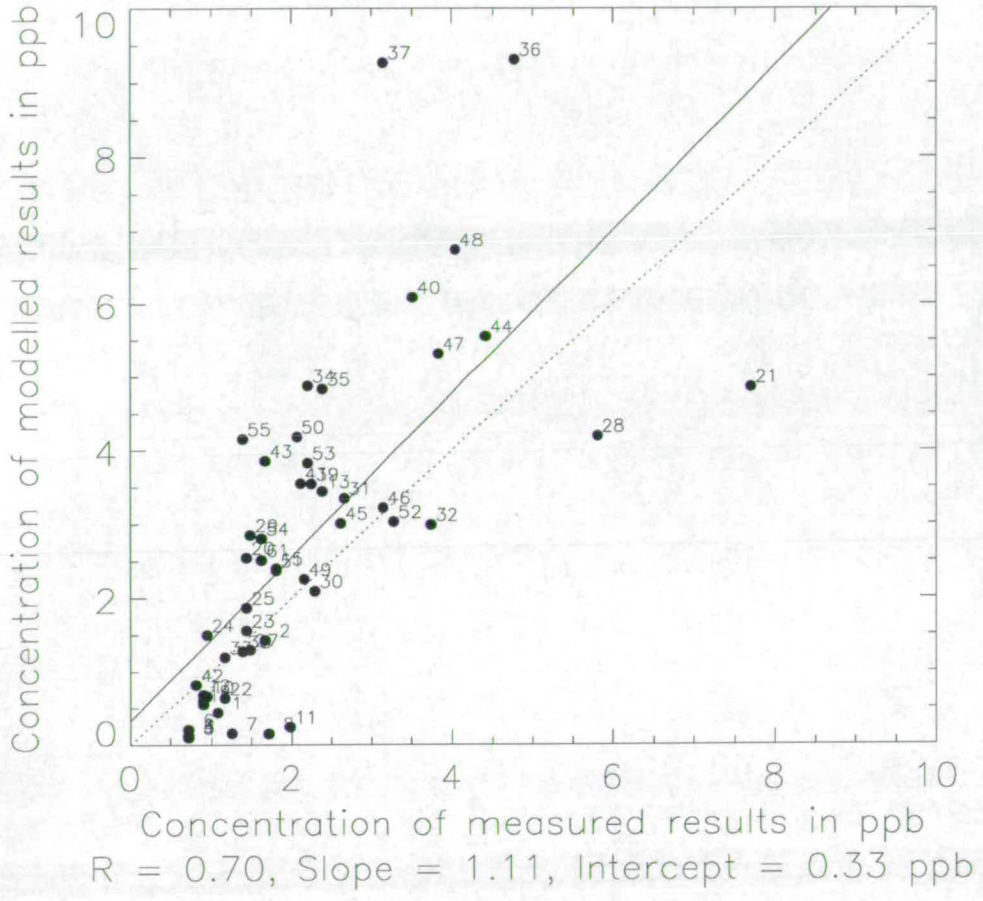

Figure 6.20: Correlation plot of modelled NH_3 surface concentrations on a 5 km grid, produced using the diurnal variation in emissions, versus observations from a network of measurements sites (multiplied by a correction factor of 0.45). Units are ppb. Each point has number assigned, which corresponds to the location of the measurement site shown in Figure 6.18. The full line is the regression line and the dotted line is the one-to-one line.

Figure 6.11, which was produced using the constant emission flux, but careful analysis shows that the mean of the surface concentrations for the entire country in Figure 6.19 is 14% less than the results produced using constant emissions. This is in agreement with the results from the receptor model (section 6.2.3), where the use of the diurnal variation in emissions produced lower surface concentrations.

A correlation plot of these modelled concentration data and measured surface concentrations (multiplied by a correction factor of 0.45, section 2.2.1) is shown in Figure 6.20. The correlation coefficient (R) has a value of 0.7. For the sample

size of n = 51, this correlation has a probability (P) of having arisen by chance of 8.36×10^{-9}, which is statistically significant at the P = 0.1% level. The slope of the regression line is 1.11 and the intercept is 0.33 ppb. In comparison with the correlation plot of modelled concentrations using constant emissions (Figure 6.12), the results in Figure 6.20 show a better agreement with the measured data. Whilst the value of R has remained virtually the same, the gradient of the regression is now much closer to 1. The modelled concentrations at stations 37 and 36, which are outliers on the correlation plots, have been reduced from around 10.5 ppb to about 9.5 ppb. The standard deviation of these data, including stations 37 and 36 is 1.58, which is a large decrease from the 5 km results, using constant emissions of, 1.84. However, with the 2 outliers removed from the data, the standard deviation becomes even smaller, with a value of 1.26. This is less than the corresponding 5 km results using constant emissions of 1.48, and shows that the use of a diurnal variation in emissions has brought a closer agreement between measured and modelled surface concentrations of NH_3.

By using the results from the correlation analysis in Figure 6.20, a relationship can be derived between the modelled data and the uncorrected measurements which is more complex than just a single multiplication factor of 0.45. Using the gradient and intercept data from the regression line, one finds that

$$\chi_{mod} = 0.5\chi_{meas} + 0.33 \tag{6.1}$$

where χ_{mod} are the modelled concentrations and χ_{meas} are the measured data. Whilst this equation gives an approximate correction for measurements, there are some locations, such as the locations in central and northern Scotland, where the large differences between the measurements and the modelled data are not accurately described by this correction function.

6.4.2 A comparison of modelled concentrations of ammonia at a number of vertical levels in the atmosphere

The plots of annually-averaged surface concentrations of NH_3, shown in Figure 6.19, illustrated the large spatial variability that occurred with using a multi-layer scheme of vertical dispersion and a fine resolution map of NH_3 emissions. It is

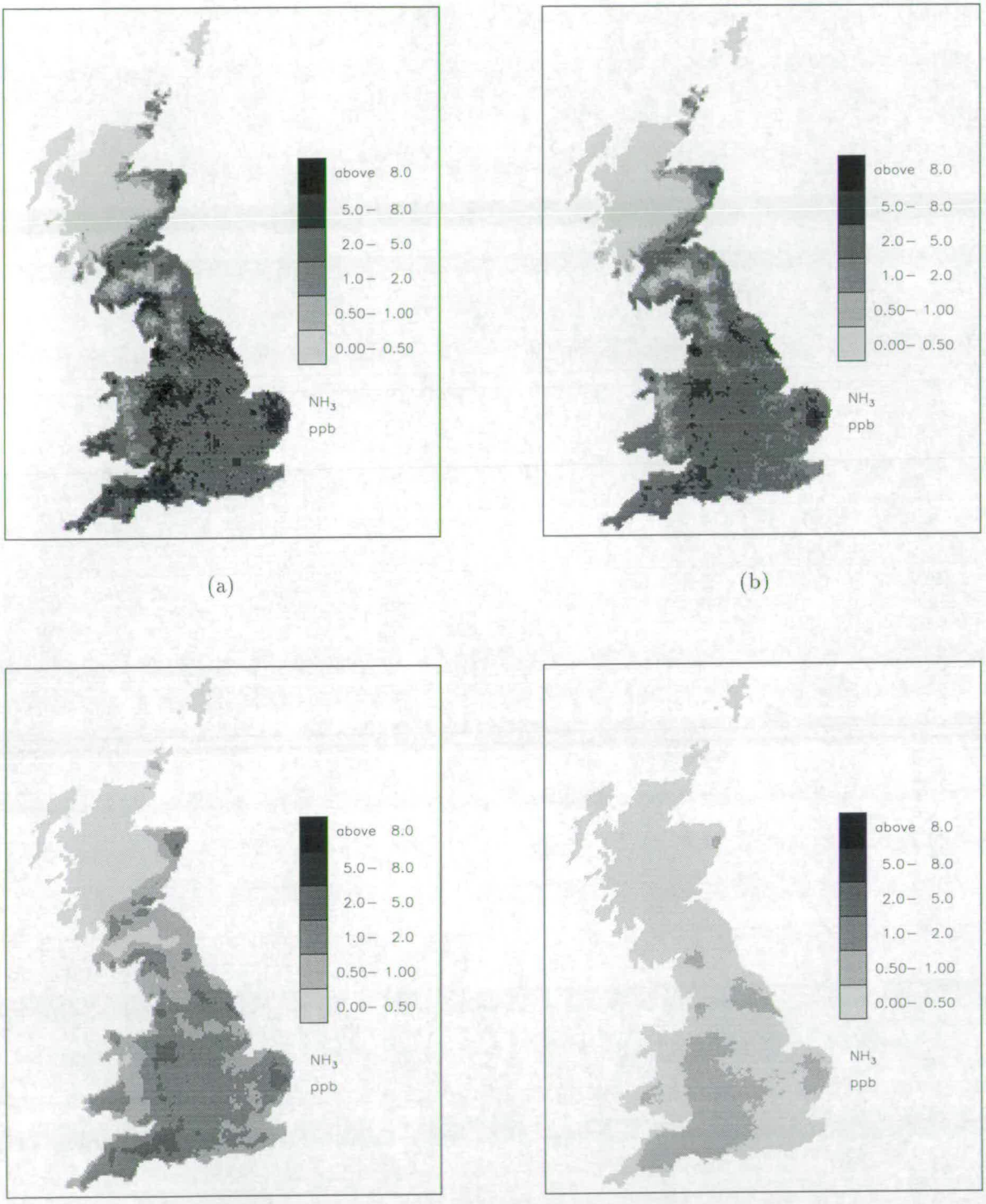

Figure 6.21: Modelled concentrations of NH_3 for Great Britain (1988) on a 5 km × 5 km grid, at 4 different levels in the air column: (a) surface; (b) 5 m ; (c) 37.5 m; (d) 175 m. Data represents an annual average. Units are ppb.

expected that concentrations in higher levels in the air column will be less affected by the large spatial variability of emissions, since the multi-layer vertical mixing scheme will act as a dampening effect on the forcing action of the emissions. This is shown in Figure 6.21, which contain four concentration maps. Each map is a plot of the annually-averaged concentrations at a specified level in the model. Figure 6.21(a) is the surface concentration data displayed in Figure 6.19, but on a revised scale. Figure 6.21(b) is a similar plot, but for the model layer corresponding to an mean height of 5 m above the surface. Figure 6.21(c) is for 37.5 m above the surface, and 6.21(d) is for a height of 175 m.

Even at a height of 5 m, which corresponds to the third layer in the model (Figure 4.1), the concentrations are significantly reduced, compared to the surface values. There is also a reduction in the spatial variability, which is most noticeable in central and southern England. This area has a vary large spatial variability of emissions (Figure 2.5), with a number of 'point source' grid squares surrounded by much lower emissions areas. At a mean height of 37.5 m, which is the sixth vertical layer in the model, the magnitude and spatial distributions of concentrations are very different to the surface layer. The maximum values are between 2 and 5 ppb, and the horizontal gradients between areas of high and low emissions are very small. The concentration peaks occur only in large regions of high emissions (Figure 2.5), as discussed in section 2.3.1. Smaller regions of high emissions seem to have little effect on the spatial distribution of concentrations well above the surface. At 175 m there are a few areas which have concentrations of greater than 0.5 ppb. In fact most of the high concentrations occur in the region encompassing southeast Wales, the southwest of England and the England/Wales border. Interestingly this plot resembles the NH_3 concentration data produced by FRAME using the vertical dispersion scheme of instantaneous mixing (Figure 5.29), and shows how the concentrations well above the surface are well mixed.

6.4.3 Dry deposition of reduced nitrogen

The modelled field of annual dry deposition of NH_3-N to Great Britain,using the diurnal variation in the emission flux, is shown in Figure 6.41. The total annual flux of NH_3-N to Great Britain is 86.4 Gg year^{-1}. This is over 9 Gg year^{-1} less than the corresponding dry deposition total produced using constant emissions

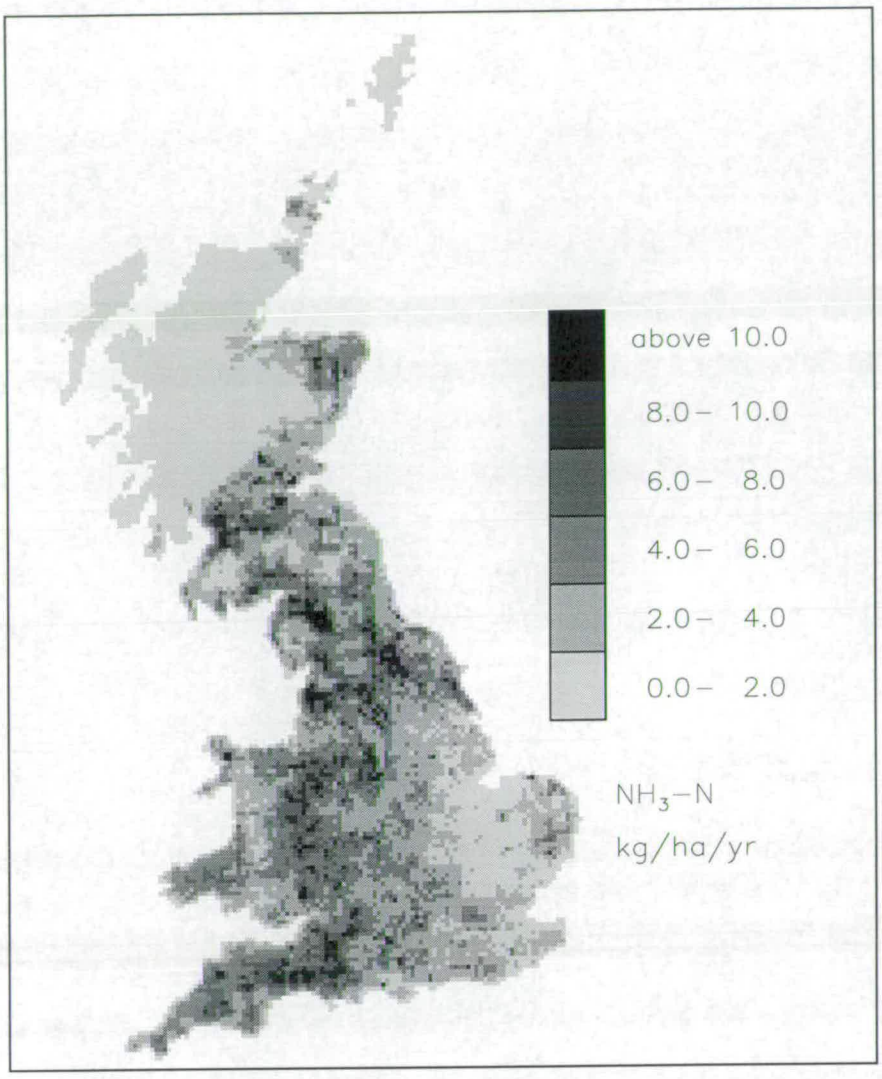

Figure 6.22: Modelled annual flux of NH_3-N dry deposition to Great Britain (1988) on a 5 km × 5 km grid, created using the diurnal variation in the emission flux. Units are kg ha^{-1} $year^{-1}$.

of 95.5 Gg $year^{-1}$ (section 6.3.2) and is a reduction of 9.4%.

The use of a diurnal variation in emissions has had a similar effect on dry deposition as it had on the surface concentration data in the previous section, in that values are generally reduced compared to the data produced using constant emissions. These results disprove the hypothesis in section 6.2.3, which suggested that the use of a diurnal variation in the emissions rate might increase the annual dry deposition flux of NH_3. This information, together with the fact that surface concentrations are less, suggest daytime concentrations of NH_3 in higher levels in the air column may be increased with the use of the diurnal variation in the

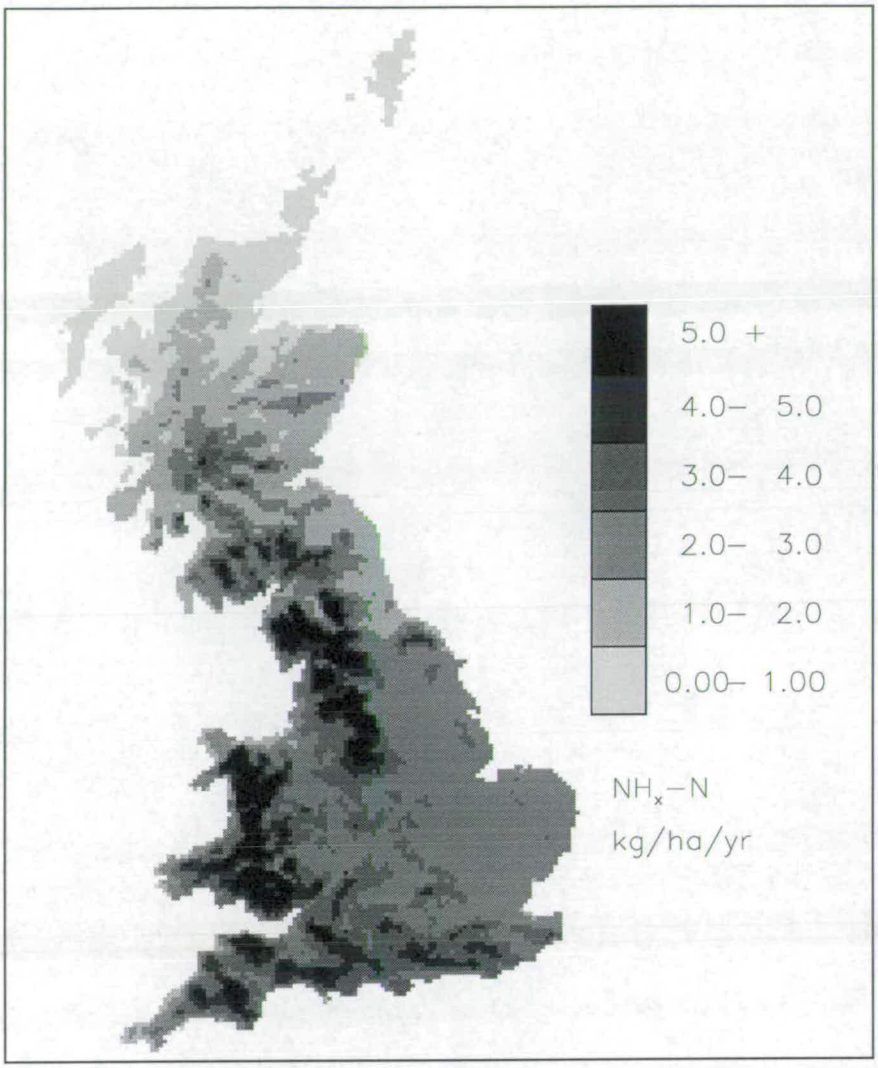

Figure 6.23: Modelled annual flux of NH_x-N wet deposition to Great Britain (1988) on a 5 km × 5 km grid, created using the diurnal variation in the emission flux. Units are kg ha^{-1} $year^{-1}$.

emission flux, as was shown section 6.2.2.

The total annual flux of NH_4^+-N to Great Britain is 6.15 Gg $year^{-1}$, which is only 0.25 Gg $year^{-1}$ less than the total given in section 6.3.4 for constant emissions, and is a reduction of only 4%.

Whilst surface concentrations and dry deposition fluxes of NH_3 have been reduced significantly by the adoption of a diurnal cycle in the emissions flux, the results for NH_4^+ show that it is much less affected by the choice of emissions scheme.

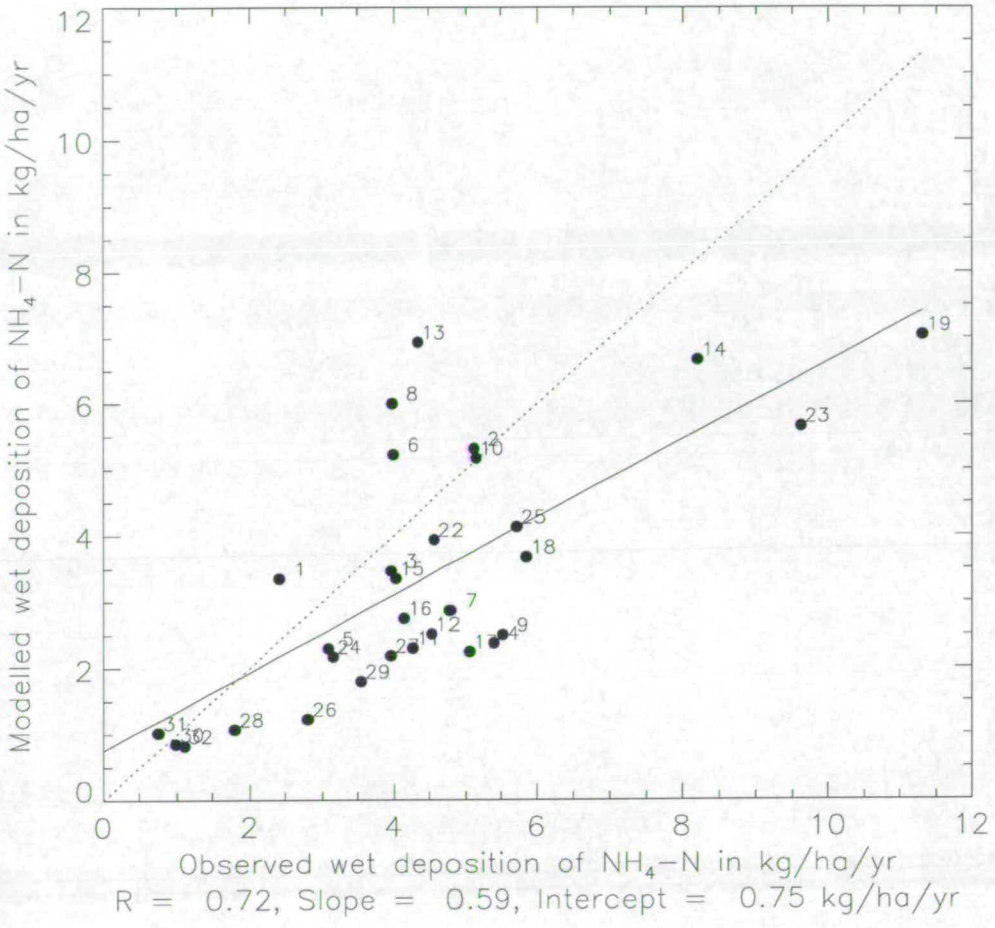

Figure 6.24: Correlation plot of modelled NH_x-N wet deposition fluxes on a 5 km grid, produced using the diurnal variation in emissions, versus observations from a network of measurements sites. Units are kg ha^{-1} $year^{-1}$. Each point has number assigned, which corresponds to the location of the measurement site shown in Figure 6.25. The full line is the regression line and the dotted line is the one-to-one line.

6.4.4 Wet deposition of reduced nitrogen

The modelled field of NH_x-N wet deposition, created using a diurnal variation in the emission flux, is shown in Figure 6.23. The total annual flux of wet deposition of reduced nitrogen to Great Britain is 68.3 Gg $year^{-1}$, which is an increase of 2.4 Gg $year^{-1}$ over the results produced using a constant emission flux (section 6.3.5).

The contribution from NH_4^+ wet deposition to the total wet deposition flux is 58.8 Gg $year^{-1}$, and NH_3 contributes 9.5 Gg $year^{-1}$. The ratio of NH_4^+ to NH_3 is 6.2:1, which shows that using a diurnal variation in emissions has increased the

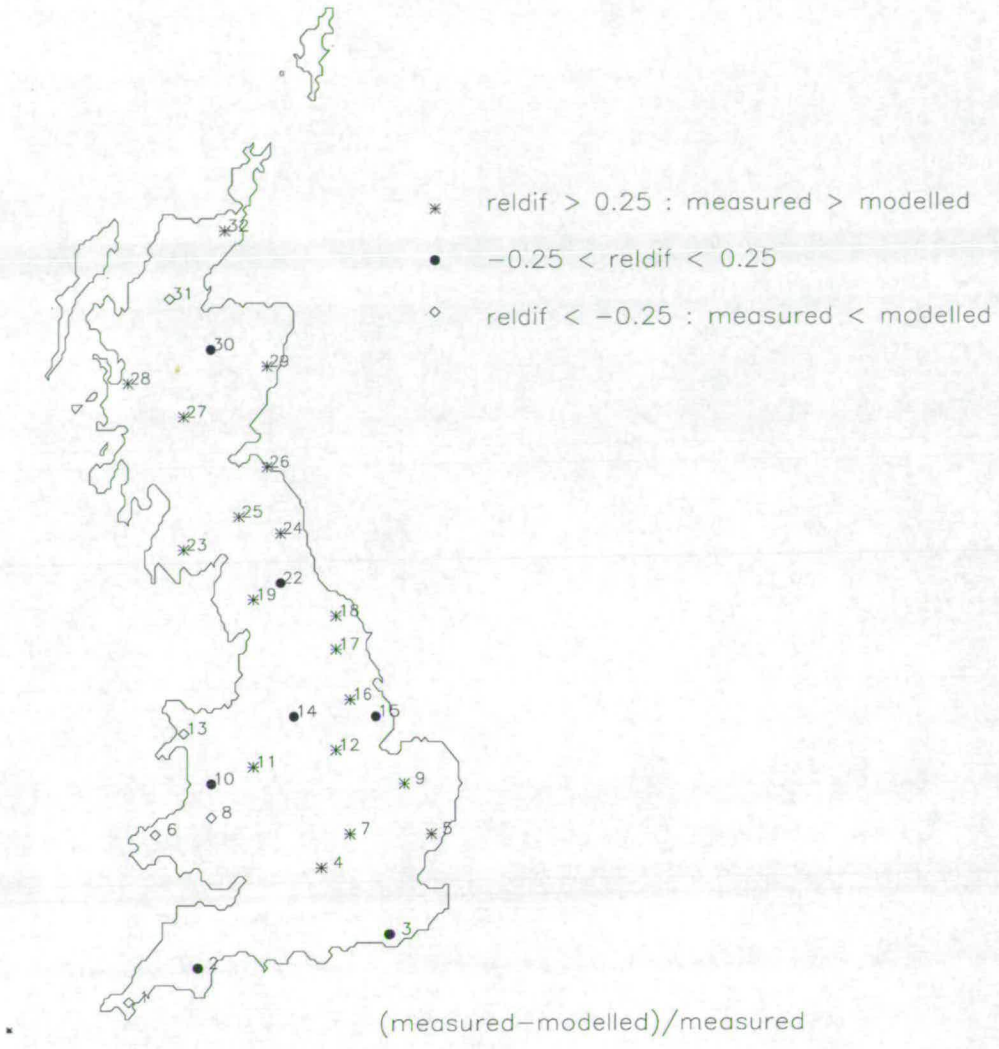

Figure 6.25: A map of categorised relative differences from $\frac{\text{measured}-\text{modelled}}{\text{measured}}$ of NH_x-N wet deposition fluxes. Modelled data is from the 5 km version of FRAME, produced using the diurnal variation in emissions.

total wet deposition flux as a whole to Great Britain, and has also increased the NH_4^+:NH_3 ratio in the wet deposition flux.

A correlation plot of modelled wet deposition fluxes against measured data from the UK Secondary Acid Deposition Network (section 1.5.3) is shown in Figure 6.24. Compared to the correlation plot of results produced using constant emissions (Figure 6.17), the slope of the regression line has increased from 0.56 to 0.59, while the intercept has changed from 0.74 to 0.75. There is no change is the value of R to two decimal places.

The location of the measurement stations are shown in Figure 6.25, which is

Wind sector origin of trajectories	Emissions of NH_x-N	Import of NH_x-N	Dry deposition of NH_x-N	Wet deposition of NH_x-N	Export of NH_x-N
0 - 45	281.3	2.1 (0.2)	86.3 (9.4)	59.9 (6.5)	137.1 (14.9)
45 - 90	281.3	35.3 (2.8)	91.8 (7.3)	84.0 (6.6)	140.7 (11.1)
90 - 135	281.3	107.7 (7.1)	111.0 (7.3)	121.3 (8.0)	156.7 (10.3)
135 - 180	281.3	79.5 (6.8)	116.5 (10.0)	131.3 (11.3)	113.0 (9.7)
180- 225	281.3	55.8 (6.5)	96.6 (11.2)	79.0 (9.2)	161.4 (18.7)
225 - 270	281.3	33.2 (6.4)	86.8 (16.8)	48.1 (9.3)	179.6 (34.7)
270 - 315	281.3	29.7 (5.3)	85.0 (15.1)	42.5 (7.6)	183.6 (32.7)
315 - 360	281.3	8.3 (1.4)	89.7 (15.5)	56.8 (9.8)	143.0 (24.7)
Averaged annual modelled budget of NH_x-N	281.3	36.6	92.6	68.3	156.9

Table 6.2: Modelled annual budget of reduced nitrogen for eight wind sectors and an averaged annual budget for the country for 1988. These data are from the 5 km version of the FRAME model, produced using a diurnal variation in the emission flux. Data in brackets are the frequency weighted total for each wind sector. The units are Gg of NH_x-N $year^{-1}$.

a plot of the categorised relative differences of (modelled - measured)/measured. The number of stations at which the magnitude of the relative difference is less than 0.25 has decreased from 9 in Figure 6.18, to 7 in this plot. The number of stations where the modelled over-estimates measured data by more than 25% has increased by 2, and thus the number of locations where the model under-estimates the observed data by more than 25% has remained the same.

6.4.5 A annual budget of reduced nitrogen for Great Britain from the 5 km version of the FRAME model

There are a number of major differences between the budget data in Table 6.2, and the budget data in Table 6.1, produced using constant emission. In Table 6.2, the dry deposition fluxes from the use of diurnal emissions are always less than the corresponding dry deposition fluxes from constant emissions, but with wind originating from 90-180° the differences are very large. In these wind sectors

the use of a variation in the diurnal emission flux leads to a 19% reduction in the dry deposition fluxes. This decrease in dry deposition is accompanied by an increase in the wet deposition flux of 10% for winds from 90-135° and 13% for winds from 135-180°. In all the other wind sectors, there is the same pattern, with reduced dry deposition and increased wet deposition, though the differences with the data in Table 6.1 are less pronounced. On average, the use of a diurnal cycle in emissions leads to a 10% reduction in the annual dry deposition flux, but an increase of 6% in the annual wet deposition flux. The annual export of reduced nitrogen increases by 4%.

6.4.6 Discussion

The use of a diurnal variation in the emission flux has produced results significantly different to those produced using a constant emission rate. The emission rate during the daytime is sinusoidal, with the maximum daytime flux being five times that of the constant nighttime value. This means that most of the emission occur during the day, and the reduced emissions at night result in lowered surface concentrations and dry deposition. High emission in the daytime will cause large surface concentrations, and combining with the maximum values of the modelled NH_3 deposition velocities implies that dry deposition will be increased during the day. However, the maximum rate of vertical diffusion also occur at these times, and thus there may be a large dispersion of the emissions into higher levels of the modelled atmosphere.

Modelled surface concentrations and dry deposition fluxes of NH_3 are generally reduced with the use of diurnal emissions compared to constant emissions, while the increased amount of NH_x dispersed into the atmosphere results in an increase in the annual wet deposition flux of NH_x. The use of diurnal emissions results in an improved correlation with measured data for wet deposition fluxes, and a closer agreement between the regression line and the 1 to 1 line for both wet deposition and surface concentrations of NH_3. Results for reduced nitrogen from the FRAME model on a 5 km $\times$ 5 km grid are improved by the use of a diurnal variation in emissions, and thus it is adopted into the model formulation as standard.

6.5 Assessment of the effect of changing the parameterisation of the dry deposition of ammonia in the model.

The objective of this section is to assess the effect of the treatment of NH_3 dry deposition in the model on NH_3 surface concentrations fields and dry deposition of NH_3. In previous models, dry deposition of NH_3 has often been modelled with the use of a constant and spatially-invariant value of V_d. The TERN model used a value of 0.01 m s^{-1} as a base option, and in an early transport model for NH_3 (Asman *et al.*, 1987) a value of 0.008 m s^{-1} was used. The TREND model (Asman and van Jaarsveld, 1992) uses a similar resistance analogy to the one used in FRAME (section 3.1) based on a canopy resistance (R_c) value of 30 s m^{-1}, but no distinction was made for different land types.

In this section two runs of the model are compared. The first set of data were created using the scheme of land-dependent and diurnally-varying values of V_d and have already been presented in this chapter (section 6.4.1). The second set of results were created using a constant land-independent value of 0.008 m s^{-1}, which is the average modelled value of V_d from the data shown in Figure 4.17.

Both sets of data were created using the diurnal variation in emissions. Comparisons are performed on surface concentrations of NH_3 and dry deposition fluxes of NH_3 from these two schemes, and the differences in the two sets of results are discussed.

6.5.1 Effect of the treatment of the deposition velocity of on surface concentrations of ammonia

To analyse the differences made using two different parameterisations of V_d, a difference plot of the two surface concentrations fields was created, and is shown in Figure 6.26. It represents the concentrations produced using the land-dependent and diurnally-varying values of V_d minus the modelled surface concentrations of NH_3 produced using the constant V_d of 0.008 m s^{-1}. The difference map can be split into two areas of interest. In eastern, central and southern England there are greater concentrations due to the smaller and diurnally-averaged values of the land-dependent V_d, compared with the constant value of V_d (0.008 ms^{-1}). Over

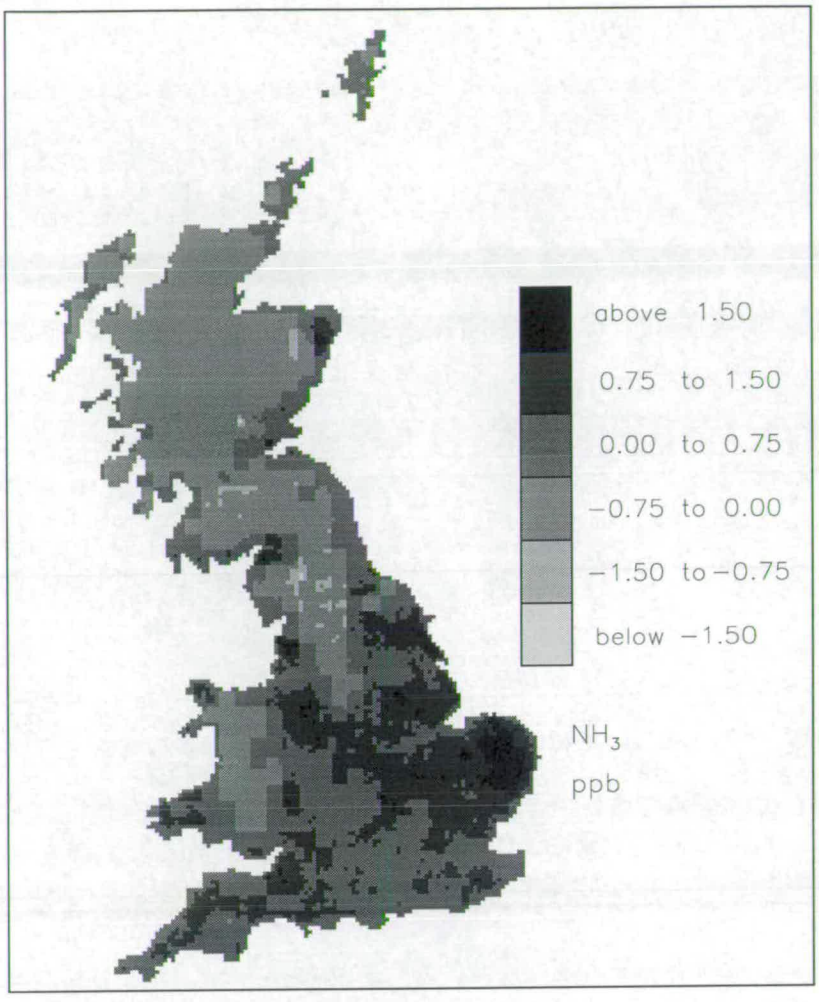

Figure 6.26: Difference plot of modelled surface concentrations of NH_3 produced using the land-dependent and diurnally-varying values of V_d minus the modelled surface concentrations of NH_3 produced using the constant V_d of 0.008 m s^{-1}. Data are for 1988.

Wales, northern England and Scotland, the reverse is true with the more detailed treatment of V_d resulting in lower surface concentrations. These differences can be attributed to the 'type' of land prevalent in these areas. Over most of southern and central England, the land is relatively flat and has a large amount of arable crop cover, grassland and urban areas. Over the rest of the map however, there are regions where more semi-natural land classes dominate, such as moorland and forests. Thus most of southern and central England will on average be assigned a value of V_d less than 0.008 m s^{-1} resulting in less NH_3 being removed from the atmosphere, whereas the rest of the country will have in general a greater value

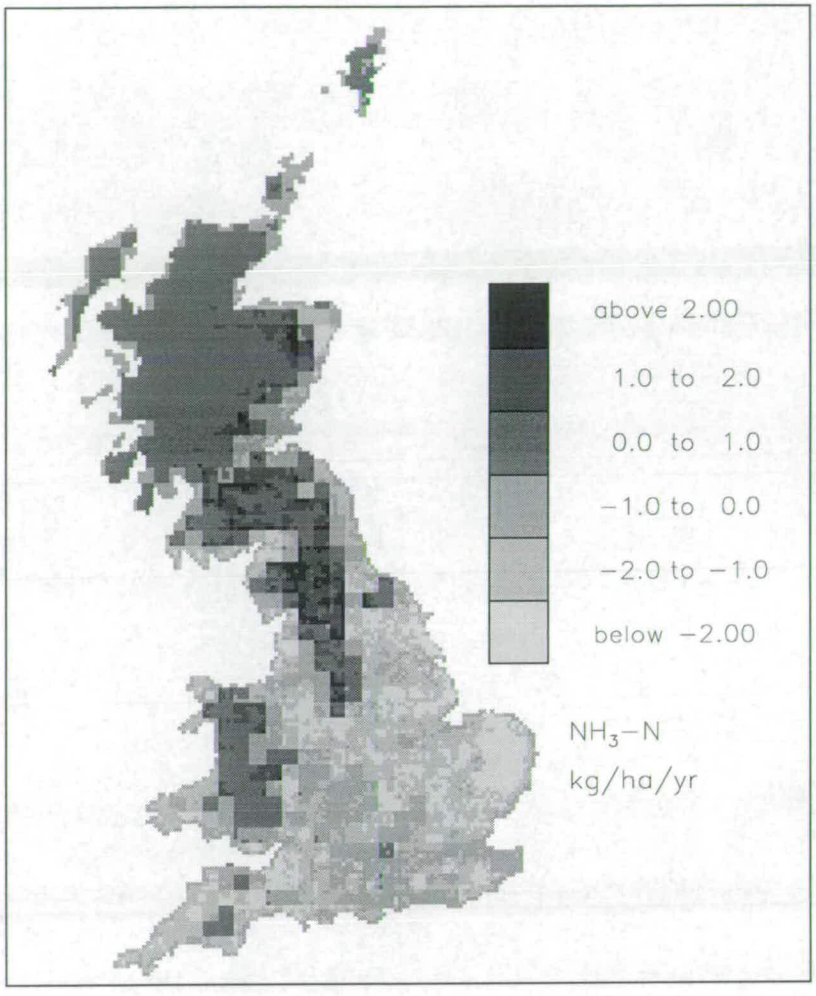

Figure 6.27: Difference plot of modelled dry deposition flux of NH_3 produced using the land-dependent and diurnally-varying values of V_d minus the modelled dry deposition flux of NH_3 produced using the constant V_d of 0.008 m s^{-1}. Data are for 1988.

than this.

6.5.2 Effect of the treatment of the deposition velocity on the dry deposition flux of ammonia

A difference plot of the dry deposition flux of NH_3 produced using the two parameterisations of V_d is shown in Figure 6.27. This plot can be related to the difference plot of surface concentrations in Figure 6.26. In general, the areas which have reduced surface concentrations due to the use of the land-dependent and diurnally varying V_ds, are the same areas which have the greater flux of NH_3 dry deposition. Similarly areas in eastern, central and southern England, where

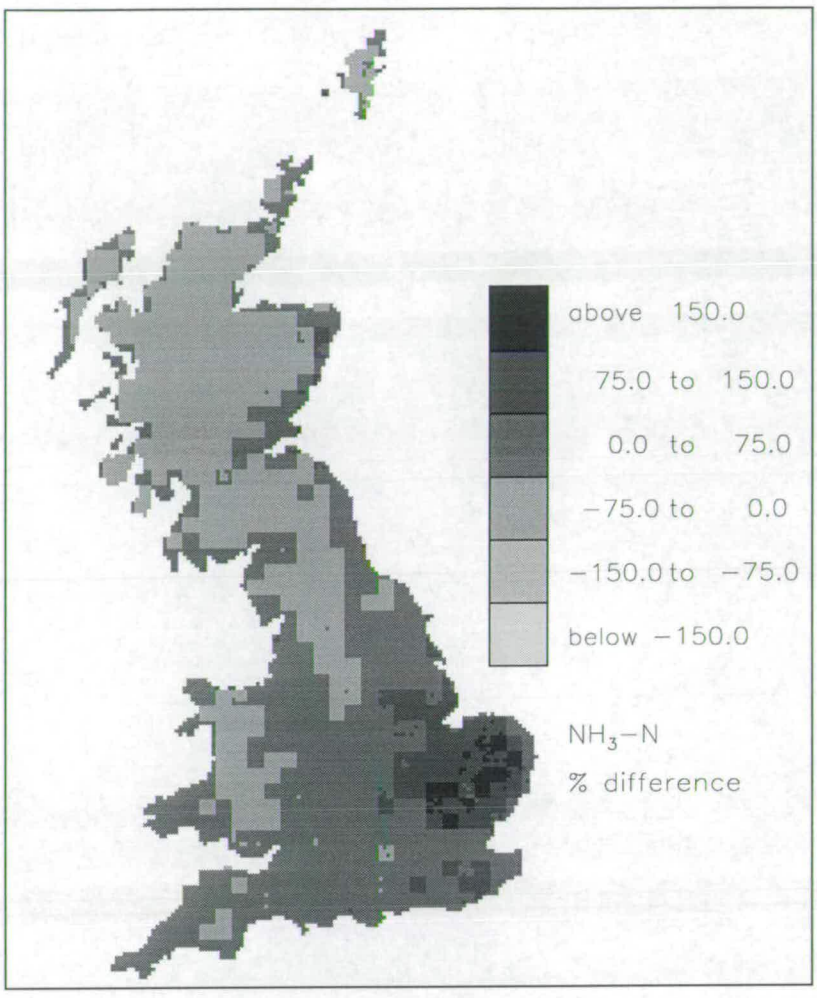

Figure 6.28: Percentage relative difference plot of modelled dry deposition flux of NH_3. The plot is $\frac{\text{ConstantV}_d - \text{landuseV}_d}{\text{landuseV}_d}$, and shows the effect of changing the dry deposition scheme from a land-dependent scheme to one using a constant value.

there were increased surface concentrations due to the use of the more complex parameterisation of V_d, have the lower dry deposition fluxes.

Figure 6.28 is percentage difference plot of the same data in Figure 6.27, and shows the effect of changing the dry deposition scheme to one using a constant value (0.008 m s^{-1}). The most affected area is East Anglia, where dry deposition is dramatically increased. This plot can be used with Figure 6.27, to more fully assess the effect of changing the parameterisation of V_d for ammonia.

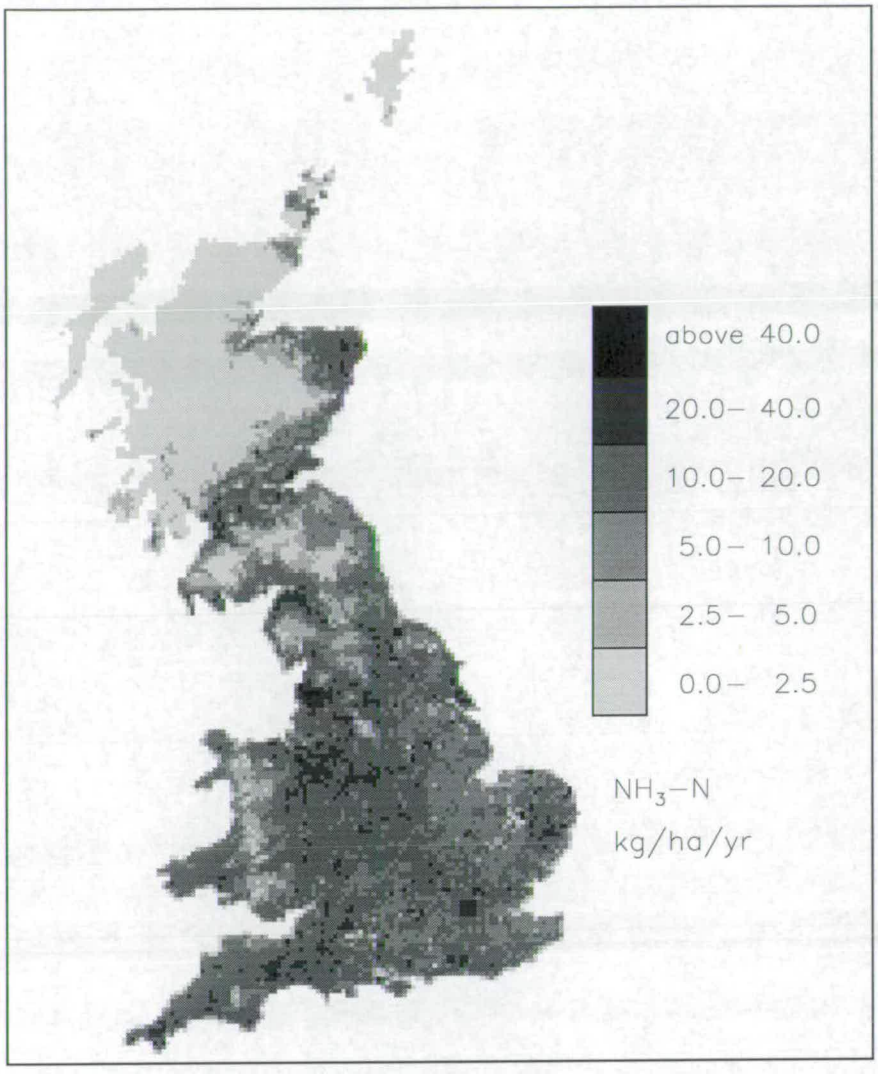

Figure 6.29: 5 km × 5 km map of NH_3-N emissions for Great Britain for 1969 (kg ha^{-1} $year^{-1}$) (Dragosits *et al.*, 1996).

6.6 Estimation of the spatial distribution of ammonia surface concentrations and annual dry deposition in 1969

One of the key input data in the model are the emissions data. The NH_3 emissions data used in the present version of the model are representative for 1988 (Dragosits *et al.*, 1996) and the SO_2/NO_x data are from the from the UK National Atmospheric Emissions Inventory (Eggleston, 1992b) and are annual data for 1992.

During the last 3 decades, emissions of these species have changed, both in

the spatial distribution and magnitude of sources. For SO_2, the general trend has been a decrease, with the estimated annual emissions for 1970 of about 3100 Gg S year^{-1} (RGAR, 1990) decreasing to a value of 1695 Gg S year^{-1} for 1992 (Eggleston, 1992b). This has been due to fuel switching in industry, increased energy efficiency and restructuring of the industrial base (RGAR, 1990). Larger power stations have replaced smaller units which were located in urban areas. The emissions data for 1970 have been spatially disaggregated onto a 20 km × 20 km grid by Smith and Hunt (1979), and these data are used in the model as an approximation of the spatial distribution of sulphur emissions for 1969.

The change in NH_3 emissions over the last few decades have been discussed in Dragosits *et al.* (1996). Since the main source of emissions are agricultural, changes in farming practices over the last few decades would be the main factors influencing NH_3 emissions. Dragosits *et al.*, (1996) stated that the main changes that have occurred in agricultural policy since 1969 are the introduction of the Common Agricultural Policy (CAP) in 1973, and changes in crop production and increased nitrogen inputs to crops. They estimated annual emissions on a 5 km × 5km grid for Great Britain for 1969, and these data are shown in Figure 6.29. The total annual emissions for Great Britain for 1969 was 227.4 Gg N year^{-1}, which means that in 2 decades, the estimated annual emissions has risen by nearly 24%.

To attempt to assess how the spatial distribution of NH_3 surface concentrations and dry deposition fluxes have changed over the two decades, the FRAME model was run using the estimated 1970 emissions of sulphur and the 1969 emissions of NH_3. No emissions maps for NO_x were available, and thus the present day emissions data were used. Since the emission total has had no general trend in the magnitude of the annual flux for the country over the last 2 decades (RGAR, 1990), no scaling factor was applied to the NO_x emissions.

Due to computational restrictions and availability of data, the present day boundary data, used to initialise the model concentrations on the edge of the model domain (see section 4.3.1), were employed. All other data used by the model remained unchanged.

6.6.1 Results

The plot of annual average surface concentrations of NH_3 for 1969 is shown

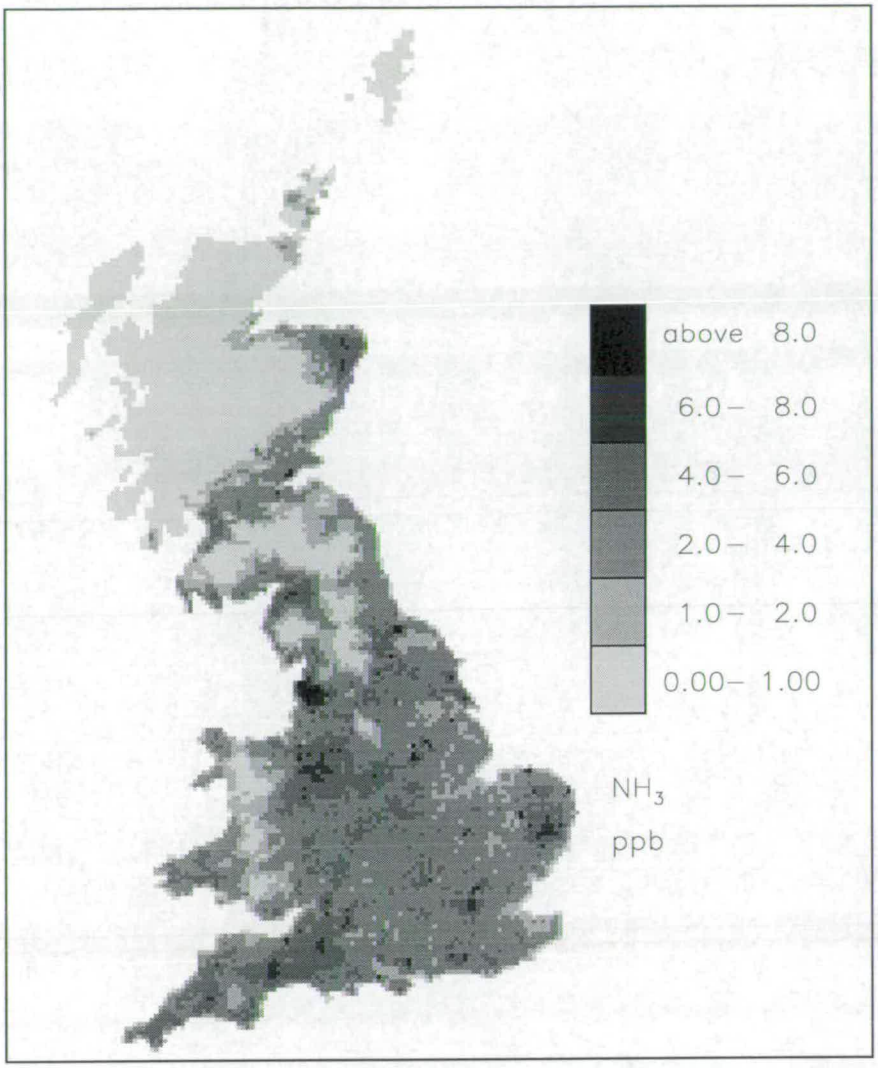

Figure 6.30: Modelled surface concentrations of NH_3 for Great Britain on a 5 km × 5 km grid for 1969, using a diurnal variation in the emission flux. Data represent an annual average. Units are ppb.

in Figure 6.30. Compared to the concentration plot in Figure 6.19, concentrations over a period of about 2 decades have increased over most of the country, especially in areas of high emission, such as East Anglia, the England/Wales border and southwest England. Concentrations in central Scotland seem to be have been affected less than other areas. A mean increase in the NH_3 emission flux of 23.7% between 1969 and 1988 has resulted in a increase in the mean surface concentration of 34% for Great Britain.

The plot of annual dry deposition flux of NH_3-N to Great Britain in 1969 is shown in Figure 6.31. Like the surface concentration data, dry deposition fluxes

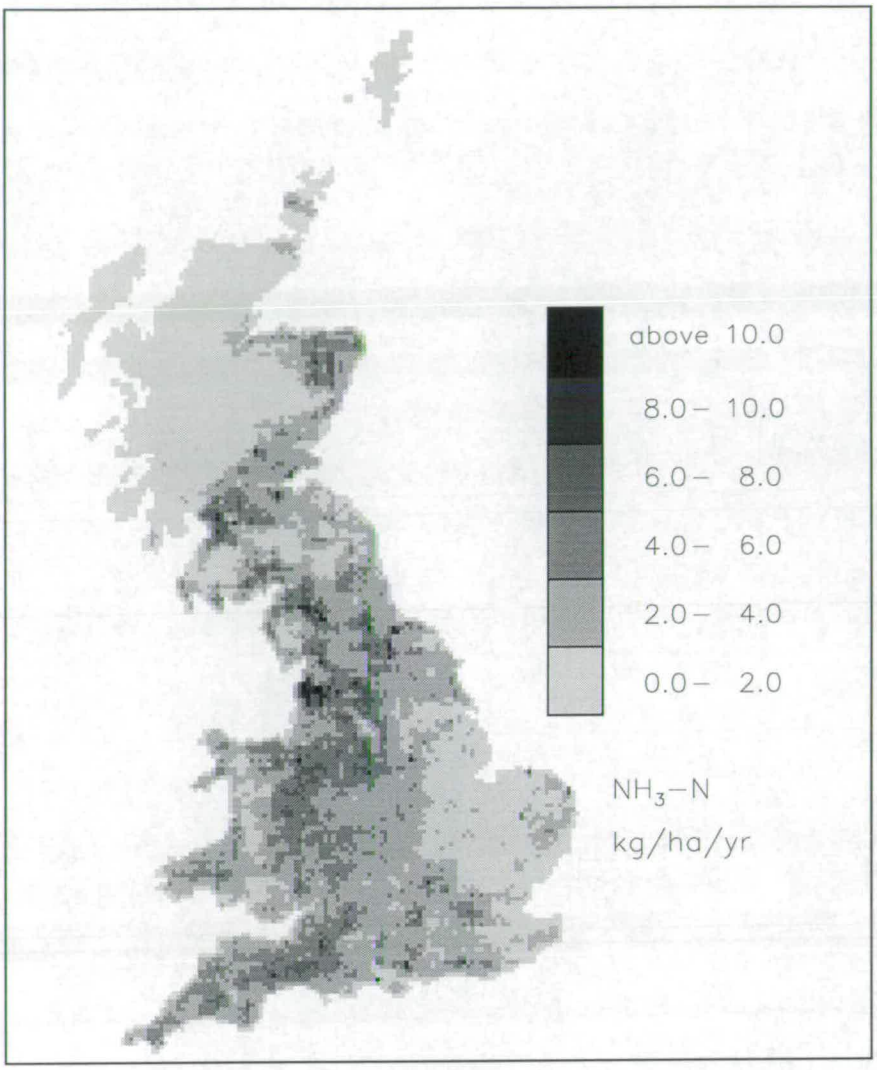

Figure 6.31: Modelled annual flux of NH_3-N dry deposition to Great Britain on a 5 km $\times$ 5 km grid for 1969, created using the diurnal variation the emission flux. Units are kg ha^{-1} $year^{-1}$.

have generally increased over the period from 1969 to 1988.

A summary of the modelled annual budget for that year is shown in Table 6.3. The total dry deposition flux of NH_x-N is estimated to 71.7 Gg $year^{-1}$. The mean increase in the dry deposition flux between 1969 and 1988 is 29%, but this is accompanied by an increase in the wet deposition flux of only 14%. This lower increase of wet deposition is probably due to the 45% decrease in the estimated annual emissions of sulphur for the country, resulting in less H_2SO_4 in the atmosphere to react with the NH_3 in 1988 to form $(NH_4)_2SO_4$.

Wind sector	Emissions of NH_x-N	Import of NH_x-N	Dry deposition of NH_x-N	Wet deposition NH_x-N	Export of NH_x-N
Averaged annual modelled budget of NH_x-N (1969)	227.6	36.6	71.7.6	59.8	132.7
Averaged annual modelled budget of NH_x-N (1988)	281.3	36.6	92.6	68.3	156.9

Table 6.3: Modelled annual budget of reduced nitrogen for Great Britain for 1969 and 1988. These data are from the 5 km version of the FRAME model, produced using a diurnal variation in the emission flux. The units are Gg of NH_x-N $year^{-1}$.

6.7 Dry deposition of ammonia to sensitive areas

To help identify sensitive areas which may be prone to large fluxes of NH_3 dry deposition, a receptor map of the dry deposition to any forest present in a grid square was created by the Institute of Terrestrial Ecology (INDITE, 1994) on a 20 km $\times$ 20 km grid using an inferential model and NH_3 concentration data measured by diffusion tubes (section 2.2.1). The data presented in INDITE (19994) provided estimates of the dry deposition flux to any forest areas within each grid square.

This exercise is repeated here using results from the 5 km version of the FRAME model, together with the diurnal variations in emissions as discussed in the sections 6.2 and 6.4. Two land classes are considered here: moorland and forest. A plot of the estimated annual flux of modelled dry deposition of NH_3 to moorland is given in Figure 6.32. This plot is closely related to the surface concentration plot in Figure 6.19, with the largest estimate of dry deposition occurring in the areas of highest concentration. In these areas, the estimated dry deposition flux is greater than 30 kg N ha^{-1} $year^{-1}$. In most of northern England and Scotland, the flux to moorland is less than 10 kg N ha^{-1} $year^{-1}$. This plot is not a budget map, but provides an estimate of the dry deposition flux to any moorland that may be present in a grid square.

A similar plot of the annual flux of modelled dry deposition of NH_3 to any forest areas that may occur in a grid square is shown in Figure 6.33. The spatial

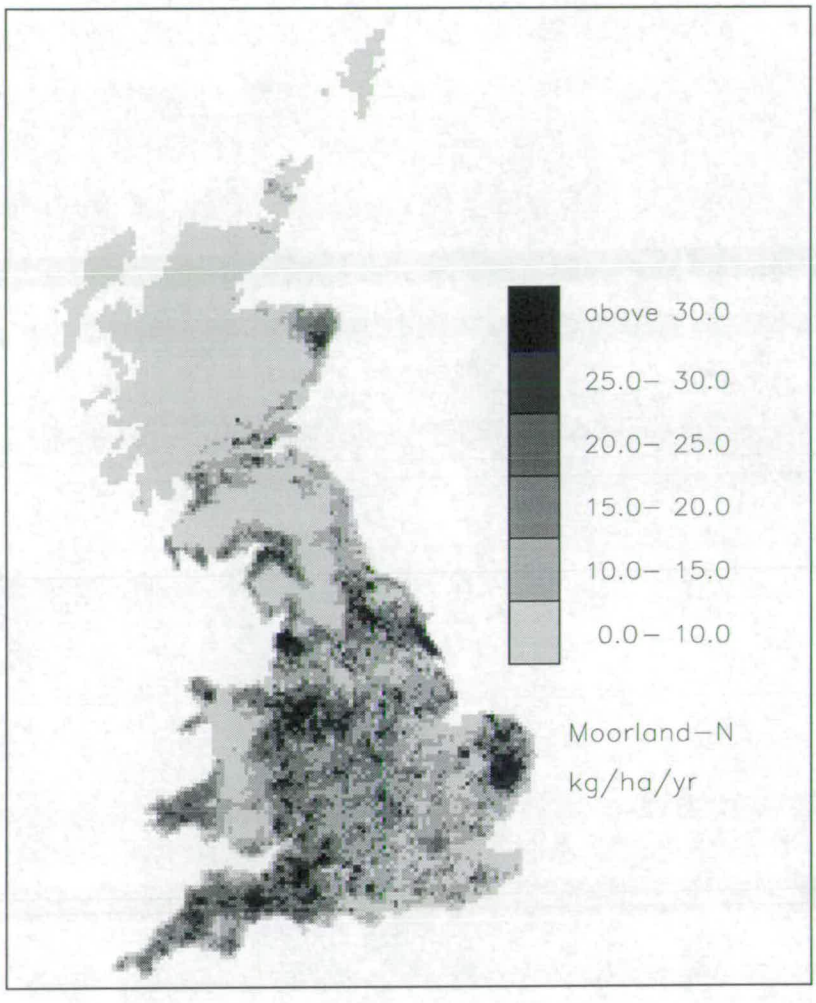

Figure 6.32: Estimated annual flux of modelled dry deposition of ammonia in Great Britain (1988) (kg N ha^{-1} $year^{-1}$) to any areas of moorland which may occur in grid squares. Created by the 5 km version of the FRAME model using a diurnal variation in emissions.

distribution of the data in this plot is very similar to the that in Figure 6.32, but values are larger. This is a consequence of the modelled values of V_d being larger than the value for moorland (section 3.1.3, Figure 3.3). The maximum dry deposition fluxes to forest exceed 40 kg N ha^{-1} $year^{-1}$, which is in good agreement with the data in INDITE (1994), but the spatial patterns are very dissimilar. As with the moorland plots, in areas of low surface concentrations, such as northern England and Scotland, the dry deposition flux to forests is generally less 10 kg N ha^{-1} $year^{-1}$.

In Bobbink and Roelofs (1994), critical loads (section 1.5.4) for various ecosys-

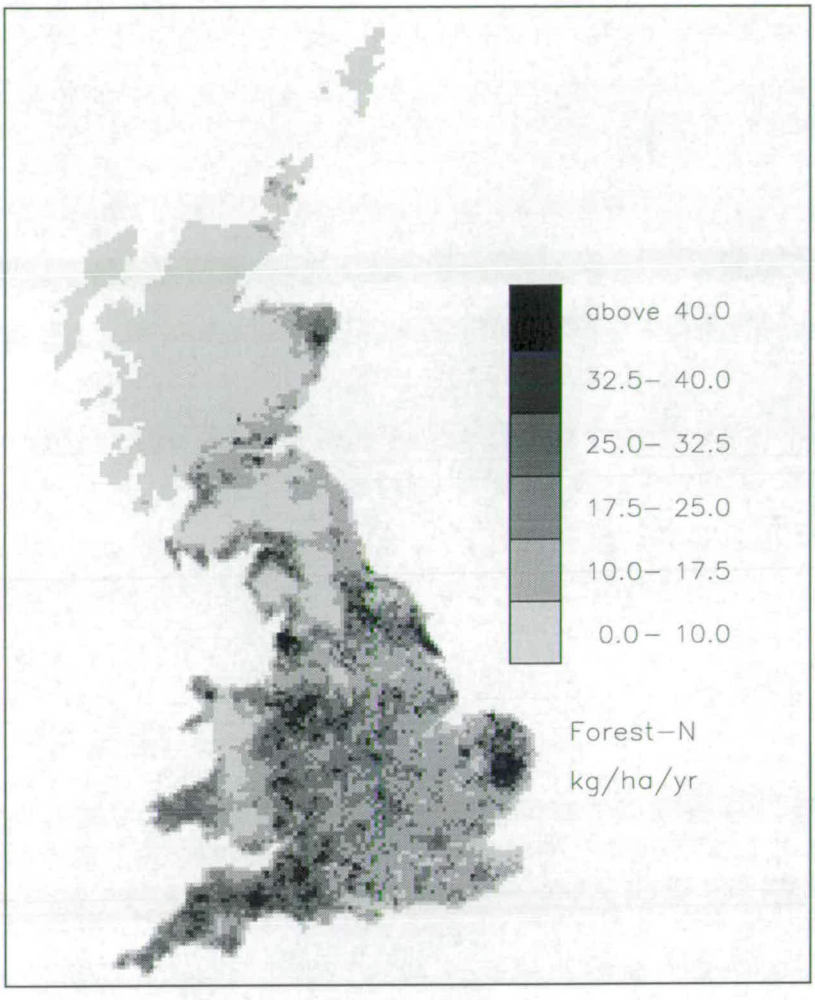

Figure 6.33: Estimated annual flux of modelled dry deposition of ammonia in Great Britain (1988) (kg N ha^{-1} $year^{-1}$) to any areas of forest which may occur in grid squares. Created by the 5 km version of the FRAME model using a diurnal variation in emissions.

tems were given. For heathland/moorland, the authors recommended a critical load of 15-22 kg N ha^{-1} $year^{-1}$. Annual deposition of nitrogen above the critical load may result in the replacement of the heather by grass, as reported for Dutch heathland by Bobbink (1992). Analysis of Figure 6.32 shows that there are a few areas, corresponding to high emission areas (Figure 2.5), where modelled dry deposition to moorland exceeds this value. This is only the input from NH_3 dry deposition, and atmospheric inputs of nitrogen will also occur due to wet deposition of NH_4^+ and NO_3^-, and dry deposition of NO_2 and HNO_3 (INDITE, 1994). For forests, Bobbink and Roelofs (1994) recommend a wide range of critical loads

for various tree species. For most of the species, a value of 20 kg N ha^{-1} $year^{-1}$ seems to define an upper limit for the critical load ranges. Looking at Figure 6.33, this limit is exceeded in areas of high emissions, as with moorlands.

These data for estimated dry deposition to moorland and forests represent grid-averaged values, and due to the high spatial variability that can occur within a few hundred metres of an emission source (section 5.1), there may be a wide spatial variation of both surface concentrations and dry deposition fluxes of NH_3 within a single 5 km $\times$ 5 km grid square.

6.8 Estimation of the in-square dry deposition of ammonia

One of the main uncertainties concerning NH_3 is the estimation of the amount of emissions that are deposited within the vicinity of the emissions source. Asman (1996) employed a multi-layer model similar to FRAME, with vertical mixing performed by K-theory eddy diffusivity, to analyse this problem. Atmospheric conditions were set at neutral stability and meteorological data were set to represent an average over Europe. The author estimated that within 2000 m of an NH_3 source, with a height of 1 m, 60% of the emissions had been dry deposited. In fact within the first 100 m, 40% of the emissions had already been dry deposited.

The FRAME model was adapted so that it could provide estimates of in-square dry deposition over the entire country. In this case, in-square dry deposition refers to the emissions from a grid square that are dry deposited within the same square, and are thus not available for long-range transport. In the normal setup of the model, when the air column is advected along a trajectory, it will pass over a certain grid only once on that trajectory. However, to calculate the in-square dry deposition, the air column was transported across a grid square twice, instead of just once. For the first run, the emissions were set to zero, and thus all deposition was due to material emitted from other grid squares (and also from European emissions). The air column was then run across the grid square again, but this time emissions of NH_3 were allowed into the air column, and thus deposition was due to both 'in-square' and 'other' sources such as other grid squares and continental European emissions. Although the model is non-linear, a first-order

estimation of the in-square dry deposition can be determined by the difference between the results for the second run over a grid square, and the first run.

$$DD_L = DD_T - DD_{NL} \tag{6.2}$$

where DD_L is the 'in-square dry deposition', DD_T is the total dry deposition due to both 'in-square' and 'other' sources, and DD_{NL} is the dry deposition from 'other' sources. The one major drawback with this method of estimating the 'in-square' dry deposition is that moving the air column twice over a grid square means that the running time for the entire model is doubled, and thus calculating in-square dry deposition on a 5 km $\times$ 5 km grid is computationally expensive, taking between 3 to 4 days to calculate.

In this section, estimates of in-square dry deposition from the FRAME model are presented. Maps are provided for the fraction of total dry deposition due to in-square deposition for the country as a whole, the fraction of emissions that are dry deposited within the same emitting grid square and a budget map for in-square dry deposition.

6.8.1 Estimates of the fraction of total dry deposition due to in-square dry deposition

Figure 6.34 is a plot of the modelled fraction of the total dry deposition to 5 km $\times$ 5 km grid squares that are due to in-square dry deposition. This is equivalent to

$$\frac{DD_L}{DD_T} \tag{6.3}$$

where DD_T is the total dry deposition of NH_3-N to a grid square, and DD_L is the in-square dry deposition of NH_3-N. There are large spatial variations in this plot, with much of central, eastern and southern England having values ranging from less than 0.4 to greater than 0.7, though there are a predominance of squares which have values ranging from 0.4-0.6. In Wales, Northern England and Scotland, there are more squares where in-square dry deposition contributes to greater than 60% of the total annual dry deposition, especially in northwest Scotland where this is overwhelmingly the case. The mean fraction for the in-square dry deposition divided by total dry deposition for the whole country is 0.61.

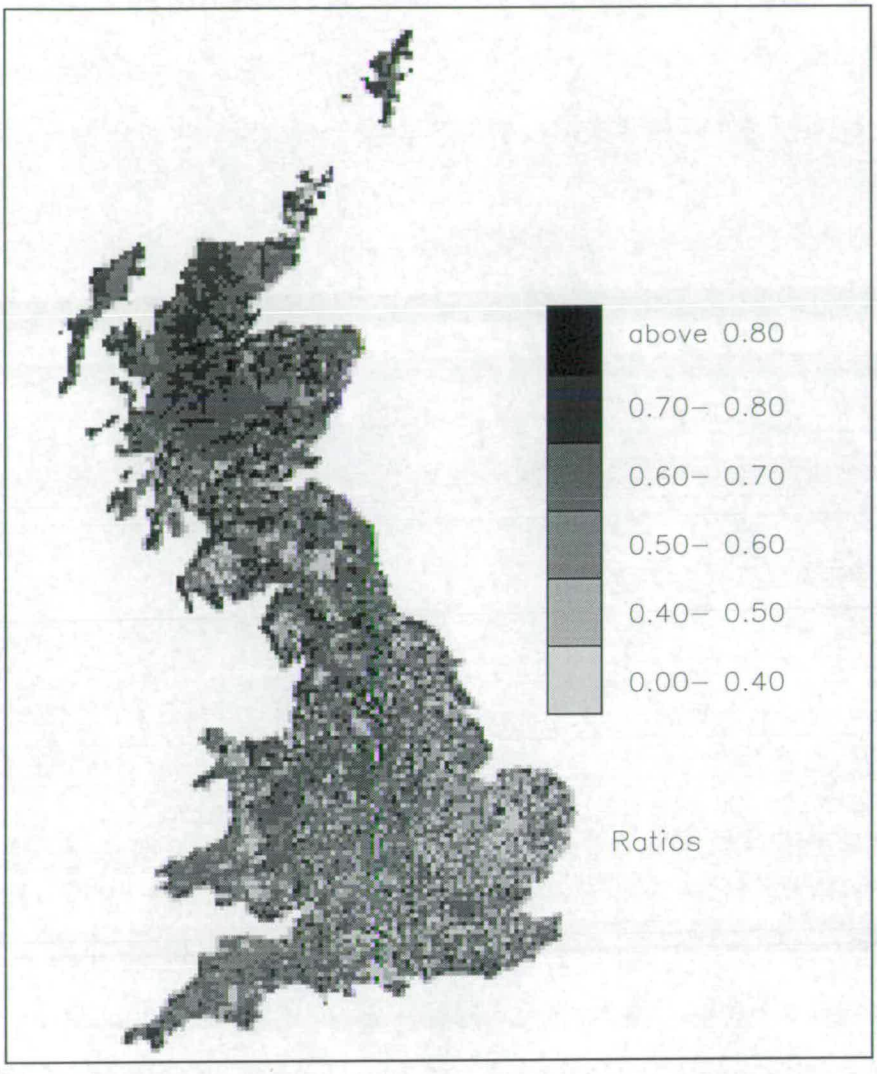

Figure 6.34: Estimate of the fraction of total dry deposition of NH_3 to Great Britain on a 5 km $\times$ 5 km grid, that are due to in-square dry deposition of emissions (1988).

The spatial distribution of the in-square dry deposition fraction seems to be a consequence of a number of factors. These include the the emission flux for a grid square and the air concentrations in surrounding grid squares. In the case of East Anglia, there is a large area which contains grid squares of high emissions (Figure 2.5), and very low modelled values of V_d (Figure 4.17). Air concentrations in this area are large (Figure 6.19). Emissions from a grid square in this area cause large surface concentrations, but also large amounts of NH_3 are advected in from surrounding grid squares. Thus the contributions of grid square emissions to the overall surface concentrations is not as large as if it had been an isolated high emission square surrounded by low emissions squares. In

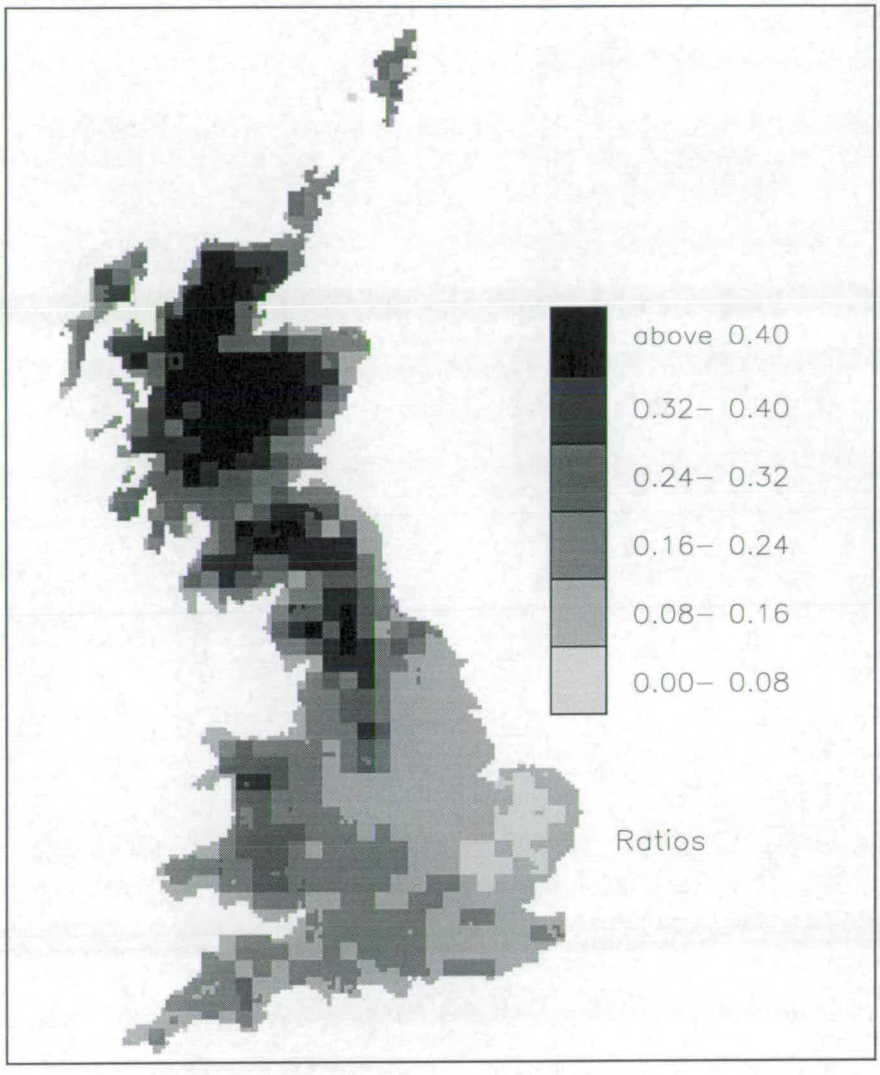

Figure 6.35: Estimate of the fraction of emissions of NH_3 for Great Britain that are dry deposited within the same emitting grid square, on a 5 km × 5 km grid (1988).

northwest Scotland, surface concentrations of NH_3 are very low (Figure 6.19), and thus while the emissions are also very low (Figure 2.5), the results suggest that surface concentrations are more dependent on same grid square emissions in this region, than for many other parts of the country.

6.8.2 Estimates of the fraction of emissions that are dry deposited to the same grid square

Figure 6.35 is a plot showing the fraction of emissions for Great Britain (Figure 2.5) that are dry deposited within the same emitting grid square. The spatial distribution of this plot is extremely similar to the plot of the grid-averaged

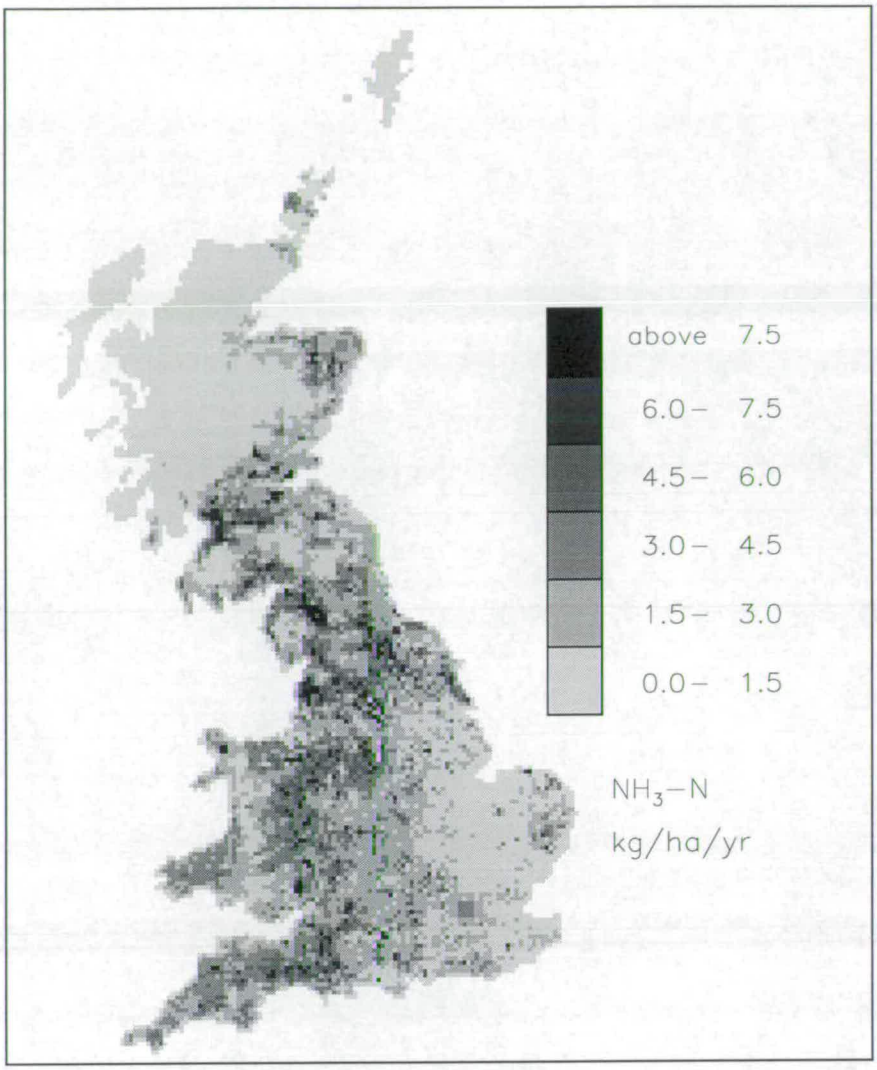

Figure 6.36: Modelled annual flux of NH_3-N dry deposition of emissions to the same grid square, in Great Britain on a 5 km × 5 km grid (1988). These data were created using the diurnal variation in the emission flux. Units are kg N ha^{-1} $year^{-1}$.

values of the modelled V_ds (Figure 4.17) used in FRAME. This implies that the magnitude of the deposition velocites for NH_3 are the main factor which determines how much of the emissions are dry deposited in the same emitting grid square. Another factor is the rate of vertical dispersion, which has some latitudinal variations due to the effect of solar radiation (sections 3.1.2, 4.1).

The area where the maximum fraction of emissions are dry deposited in the same emitting grid square is central and northern Scotland, with values over 40%. In East Anglia, less than 8% of the emission are dry deposited in the same emitting grid square. For the country as a whole, the mean fraction of emissions

which are dry deposited in the same emitting grid square is 0.22. The more coarser resolution of this plot is due to the 20 km landuse database used in the model.

6.8.3 Budget estimates of in-square dry deposition to Great Britain

A plot of the modelled annual flux of NH_3-N in-square dry deposition to Great Britain, on a 5 km × 5 km grid, is shown in Figure 6.36. The total annual flux of in-square dry deposition of NH_3-N is 52.5 Gg N $year^{-1}$. The highest fluxes of in-square dry deposition occur in areas of high emissions (Figure 2.5) and also areas with large modelled deposition velocities of NH_3, as expected. Fluxes are greater than 7.5 kg N ha^{-1} $year^{-1}$ in some of these grid squares. These fluxes are extremely large and they imply that emissions of NH_3 are contributing a significant amount to the total annual nitrogen deposition to that same grid square. The areas of lowest in-square dry deposition are East Anglia, the east Midlands, and northwest Scotland, where in-square dry deposition in these areas is less than 1.5 kg N ha^{-1} $year^{-1}$ in some grid squares.

The estimation of in-square dry deposition of NH_3 is important information as it allows emissions reduction strategies to be formulated. By assuming a linear relationship between in-square dry deposition and emissions, these data can be used to target specific areas of high nitrogen deposition and determine whether emissions of NH_3 in that area contribute significantly to the overall deposition flux of nitrogen. This may be a more cost effective method than using a 'blanket reduction' of a specified % in emissions. This is a short-range strategy, as opposed to a more long-range transport approach which might have to consider methods to reduce wet deposition fluxes of NH_x to certain areas, and thus would have to consider a more wider area reduction strategy.

6.9 Final results from the FRAME model

In this section, the final results from the FRAME model are presented as colour plots. The results include a surface concentration map of NH_3, an annual dry deposition map of NH_3-N, an annual wet deposition map of NH_x-N and a total

annual deposition map of reduced nitrogen to Great Britain. A map of the annual emissions flux for the country is also included for comparison with the results. These data are displayed in Figures 6.37 to 6.41.

6.10 Discussion

In this chapter, the FRAME model was used on a 5 km × 5 km to analyse the atmospheric behaviour of NH_3 and NH_4^+ in detail.

A receptor model was created which allowed detailed investigation of the vertical and diurnal variations of NH_3 and NH_4^+ concentrations. The use of a multi-layer scheme of vertical mixing in the model produced large vertical gradients in concentrations, dependent of the time of day and the choice of NH_3 emission scheme. The use of a diurnal variation in the emission rate significantly affected the diurnal cycle of surface concentrations of NH_3. Diurnal variations in surface concentrations were shown to be directionally-dependent. A comparison with measured data showed the use of a diurnal emission rate generally gave a better agreement between modelled and observed data. The measured concentration rose also illustrated the effects of very in-square emissions sources, which cannot be resolved even with a fine resolution grid of 5 km squares.

There was a large effect on NH_4^+ surface concentrations due to an area of large emissions of SO_2 and NO_x located in central England. Surface concentrations of NH_4^+ aerosol from this wind direction were much greater than for other wind directions, and this illustrated how emissions of SO_2 and NO_x can affect the atmospheric lifetime of reduced nitrogen.

Surface concentration data from the FRAME model on a 5 km × 5 km grid, showed the large spatial variation in results that can occur with the use of fine resolution emission data and a detailed scheme of vertical diffusion. Agreement with observed data showed a improvement with the use of the 5 km data with constant emissions, but the best agreement occurred when the diurnal emissions rate was used in the model. There was an increase in the total flux of dry deposition of NH_3 due to the increase in modelled spatial resolution, and the horizontal variability increased with areas of both very high and very low dry deposition became apparent. This is also true for modelled wet deposition of

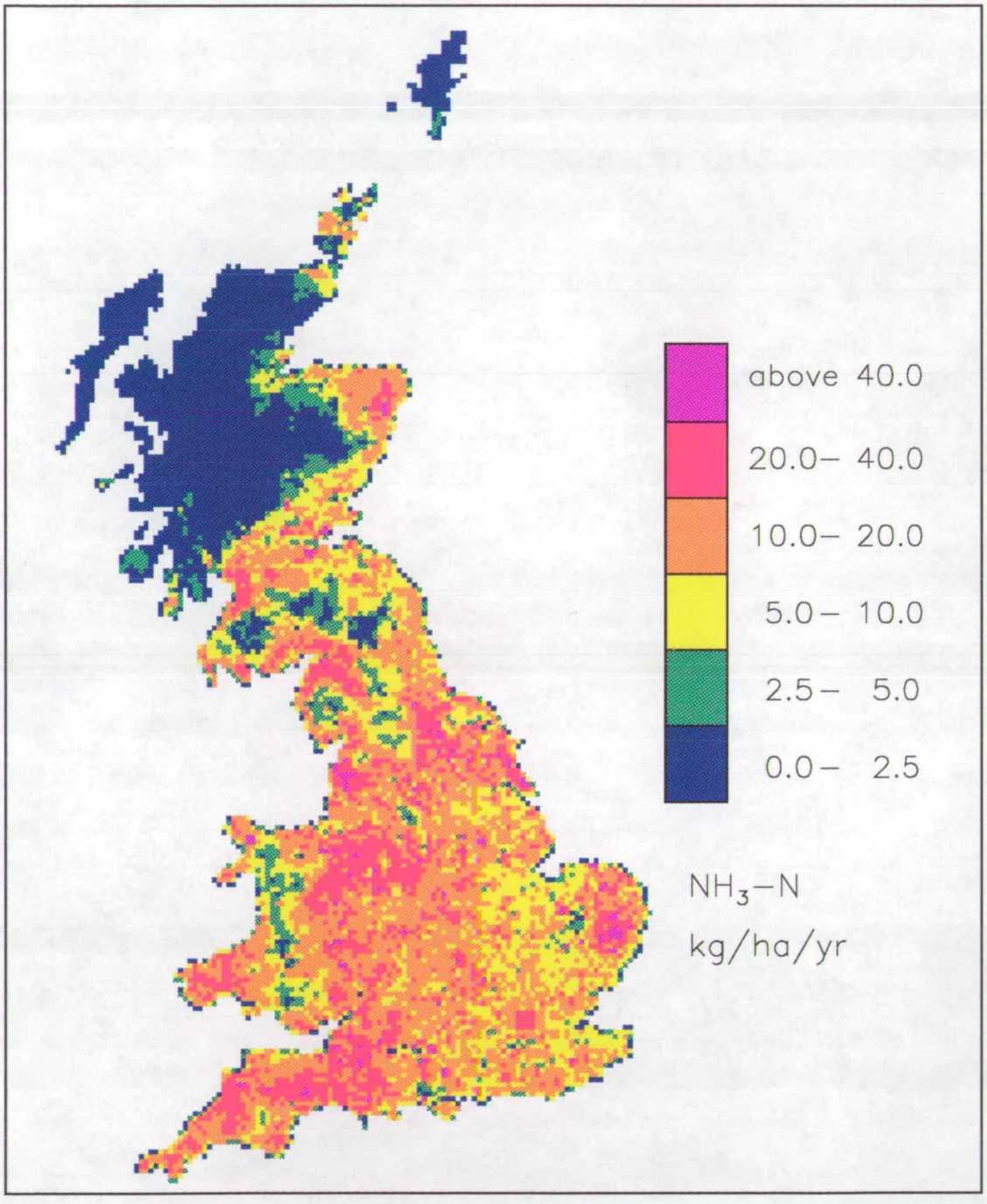

Figure 6.37: 5 km × 5 km NH_3-N emissions map for Great Britain for 1988 (kg ha^{-1} $year^{-1}$) (Dragosits *et al.*, 1996).

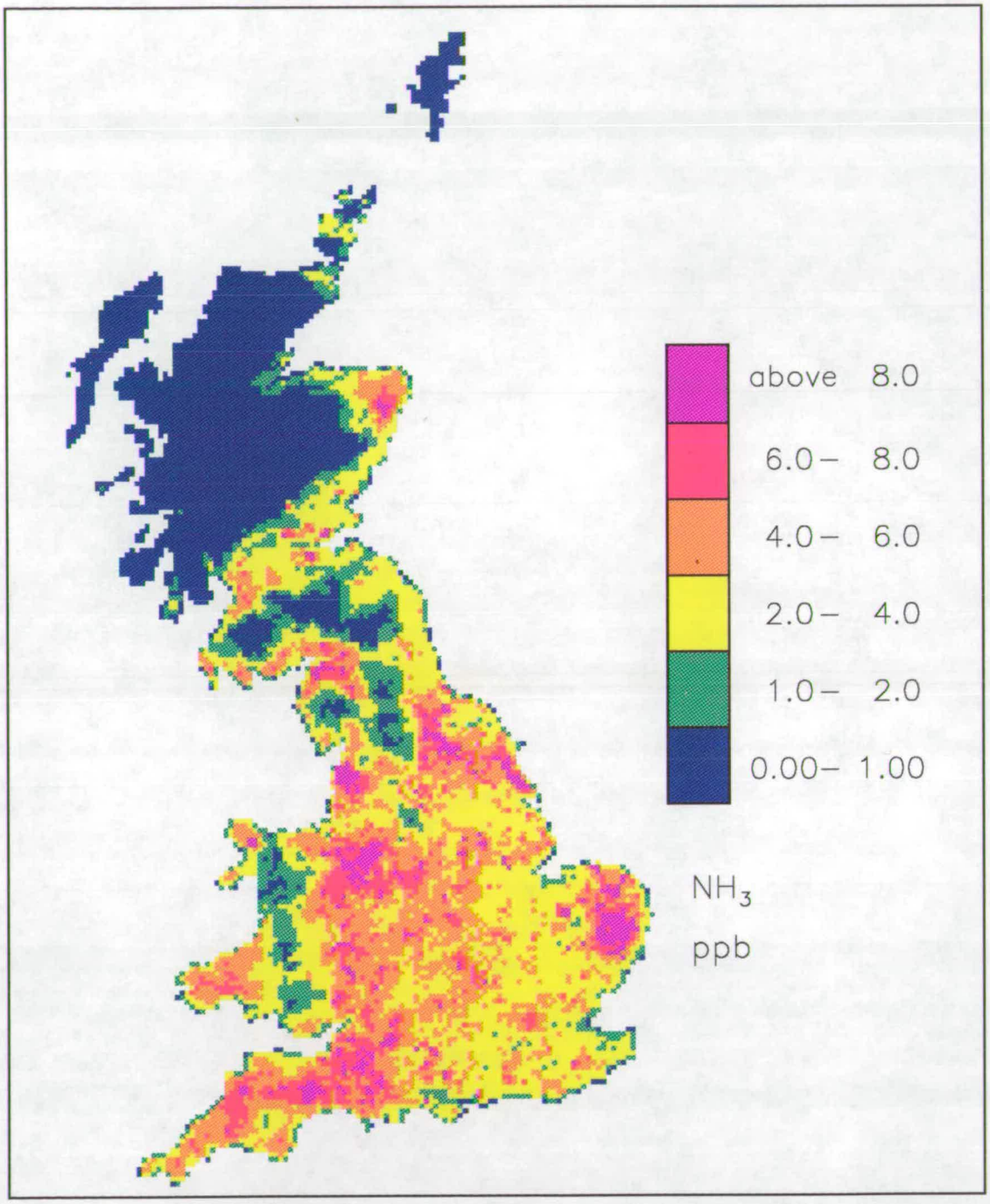

Figure 6.38: Modelled surface concentrations of NH_3 for Great Britain (1988) on a 5 km × 5 km grid, using a diurnal variation in the emission flux. Data represent an annual average. Units are ppb.

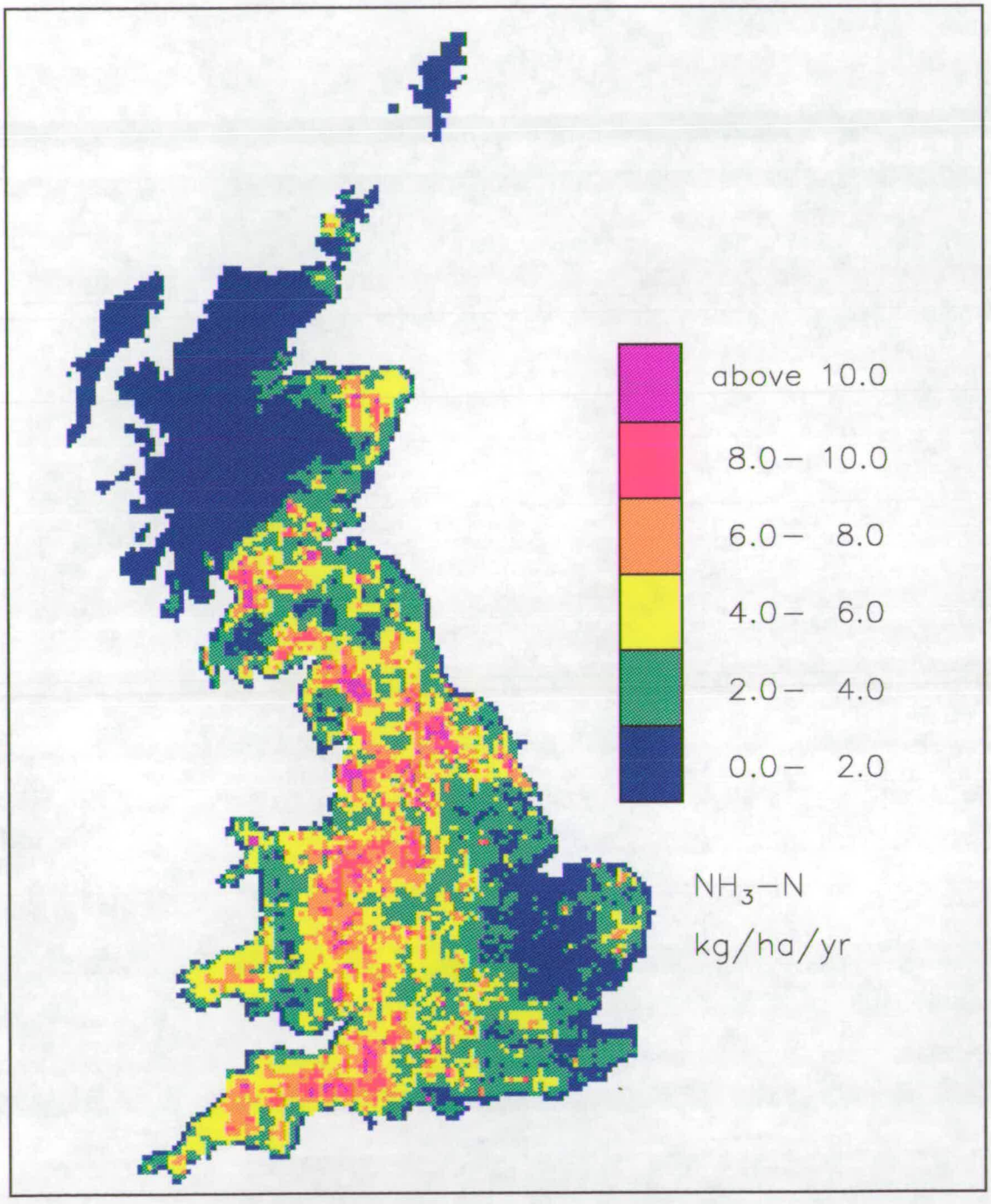

Figure 6.39: Modelled annual flux of NH_3-N dry deposition to Great Britain (1988) on a 5 km × 5 km grid, created using the diurnal variation in the emission flux. Units are kg ha^{-1} $year^{-1}$.

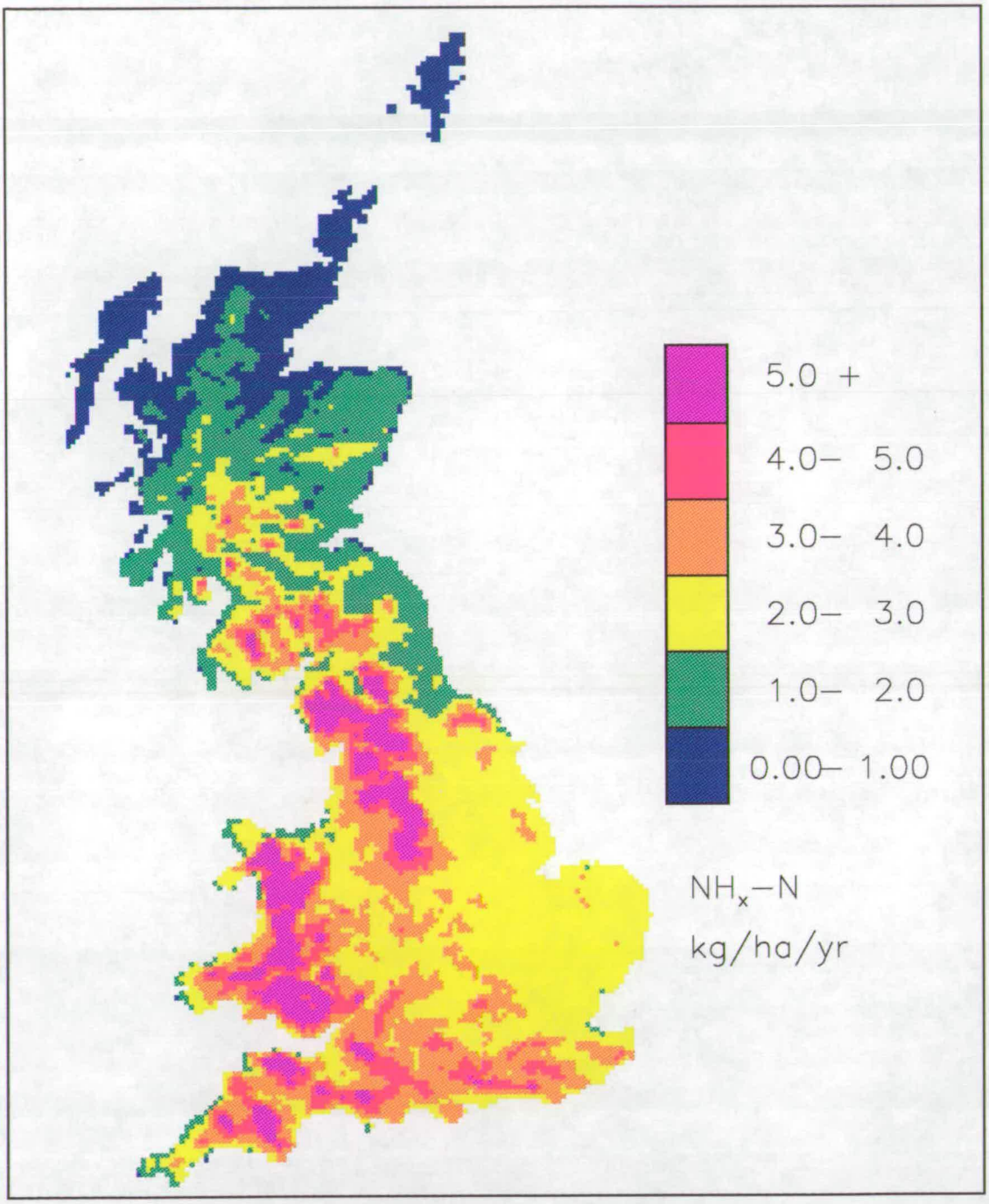

Figure 6.40: Modelled annual flux of NH_x-N wet deposition to Great Britain (1988) on a 5 km × 5 km grid, created using the diurnal variation in the emission flux. Units are kg ha^{-1} $year^{-1}$.

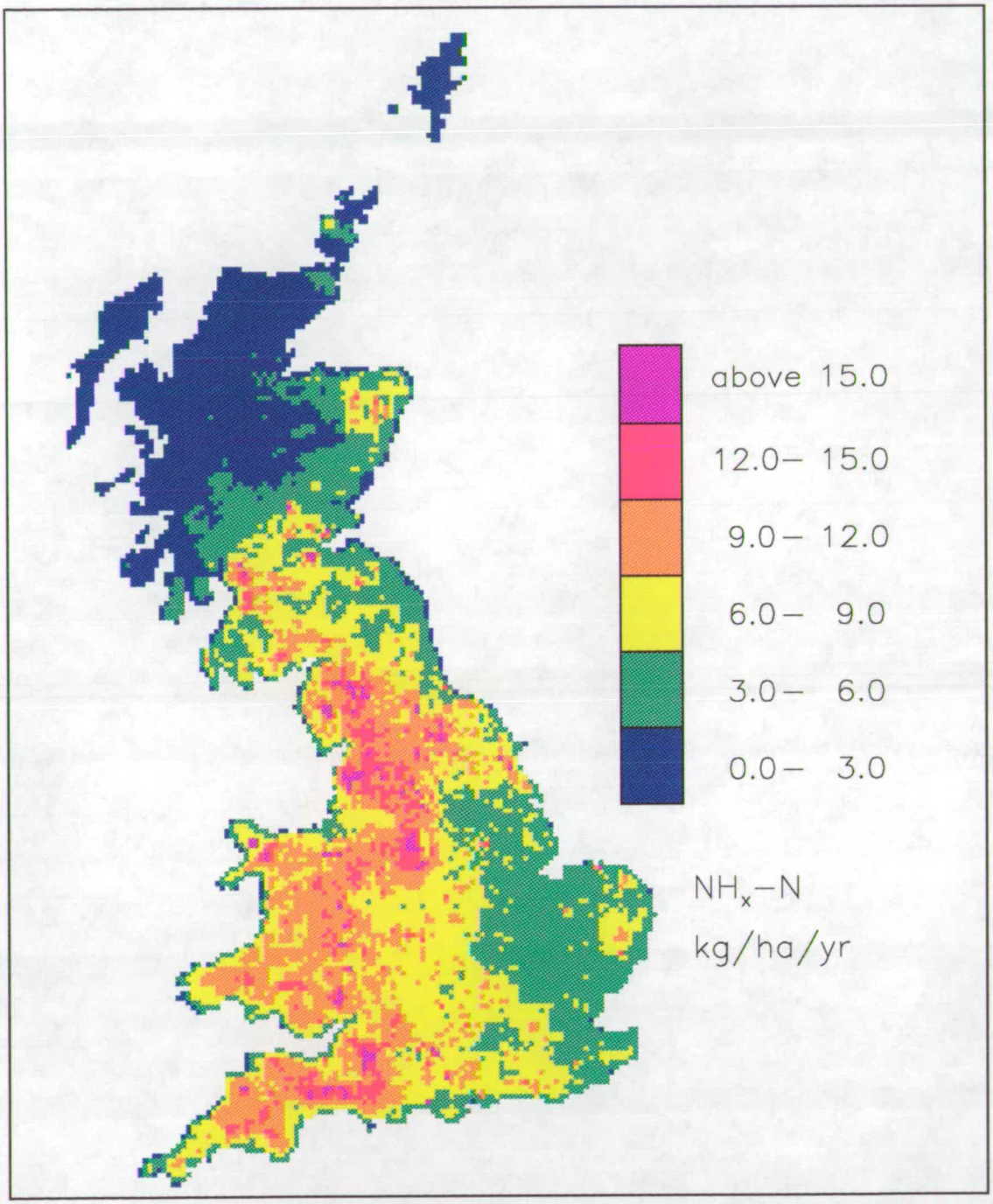

Figure 6.41: Modelled annual flux of total deposition of reduced nitrogen to Great Britain (1988) on a 5 km × 5 km grid, created using the diurnal variation in the emission flux. Units are kg ha^{-1} $year^{-1}$.

reduced nitrogen. The use of a diurnal emissions rate improved the agreement with observed data, and was adopted as a standard parameterisation in the model.

Examination of modelled concentrations over Great Britain at various heights showed how the spatial variability of NH_3 concentrations decreases with increasing height, and that at a height of 175 m concentrations of NH_3 were less than 1.0 ppb.

The effect of using a land-dependent formulation of NH_3 dry deposition, compared with a spatially- and diurnally-invariant value, showed how the spatial distribution of annual dry deposition fluxes of NH_3 to a 5 km $\times$ 5 km grid are changed by at least 2 kg N ha^{-1} $year^{-1}$ at some locations. The surface concentrations of NH_3 were also affected, with a change of at least 1.5 ppb occurring in some locations. This result showed that when a detailed scheme of vertical mixing is also used by the model, the parameterisation of V_d is an important process.

The FRAME model predicted that the dry deposition of NH_3 to areas of moorland may be very spatially variable, and could be as large as 30 kg N ha^{-1} $year^{-1}$ in some areas, and much less than 10 kg N ha^{-1} $year^{-1}$ in other locations. For forest the maximum dry deposition in a grid square may be greater than 40 kg N ha^{-1} $year^{-1}$. This is over twice the estimated critical load for most forest types.

Estimates of the fraction of total dry deposition of NH_3 that are due to in-square dry deposition, over Great Britain, are extremely spatially variable, with values ranging from less than 0.15 to greater than 0.75. Larger values generally occurred in northern and western areas of Great Britain. On average 61% of the total dry deposition to Great Britain is a result of emissions being dry deposited to the same 5 km grid square.

The model calculated that the spatial distribution of the fraction of emissions that are dry deposited within the same emitting grid square is very similar to the map of modelled deposition velocities for NH_3 for NH_3. For Great Britain as a whole, 22% of the emissions are dry deposited to the same 5 km $\times$ 5 km grid square.

The map of the annual flux of in-square dry deposition of NH_3 to Great Britain highlighted grid squares where the in-square dry deposition contributes more than 7.5 kg N ha^{-1} $year^{-1}$ of the total nitrogen input to a grid square. These data can

be used to determine areas where reduction in NH_3 emissions will be an effective measure to reduce the total nitrogen flux below a required limit.

Chapter 7

Conclusions and Recommendations

The main focus of this project was to describe the spatial distribution of NH_3 dry deposition over Great Britain with a more detailed resolution than has been done previously. This has been achieved by the use of an atmospheric transport model which includes a detailed description of the vertical dispersion process, a land-dependent scheme of NH_3 dry deposition and a detailed parameterisation of the main tropospheric reactions of reduced nitrogen, sulphur and oxidised nitrogen.

The use of the FRAME model on a 5 km $\times$ 5 km grid has produced the most detailed estimate of the large spatial variability of NH_3 surface concentrations and annual dry deposition fluxes in Great Britain currently available. Compared to previous estimates, which were created using measurement data from a limited number of locations, the results from FRAME provide greater information on the large spatial variability of dry deposition of NH_3 and illustrate regions where previous estimates may be seriously overestimating the annual dry deposition flux. This information is crucial for the application of the critical loads approach, since regions affected by high deposition may be of limited size, and thus estimates of atmospheric inputs of reduced nitrogen should be on a very fine spatial scale.

The use of a multi-layer mixing scheme and land-dependent deposition velocities were shown to have a significant effect on the spatial variation of modelled surface concentrations and dry deposition fluxes of NH_3. In comparison with other models, which employed instantaneous mixing of emissions, the results from the FRAME model illustrated that that it is better able to model the short-range dispersion of NH_3.

Results have been produced which estimate that, on average, 22% of the emissions were dry deposited within the same 5 km grid square. This was found to be significant in areas where there are high emissions of NH_3, and where there is also a prevalence of land where large values of V_d may occur. This information can be used as part of an overall strategy to reduce deposition of atmospheric pollutants by applying both large-scale (national and continental) and small-scale (local) reductions in emissions.

Results from the model have been used to determine the most effective sites for a new atmospheric monitoring network for ammonia. This will provide a comprehensive testing of the model predictions. By using these results, sensitivity tests can be performed on various model parameters and input data to assess their accuracy.

In addition to these key points, other aspects of the work here have shown:

- The good performance of the model on a 20 km grid and the degree of improvement using the 5 km grid. The effect of a few outliers on the overall model assessment was highlighted.
- Good comparison of modelled ground-level concentrations of NH_3 with the best estimates of NH_3 from measurements, which were adjusted to account for reported overestimation.
- Very good comparison of ground-level concentrations of NO_2 with measurements, but overestimation of SO_2 concentrations.
- The use of a diurnal variation in the emissions of NH_3 with diurnally-varying meteorology gave better agreement with measurements.
- Over 50% of the dry deposition to a 5 km grid square is a result of emissions being dry deposited in the same grid square.
- The underestimation of modelled wet deposition of NH_4^+ may be due to simplified assumptions in the model, and results in an overestimation of the annual export budget.
- The non-linearity of model results with respect to wind speed and cloud cover.

7.1 Future work

One of the main areas of uncertainty in the FRAME model is the parameterisation of wet deposition. The use of height-independent scavenging coefficients may be an over-simplification for FRAME, since it contains a detailed description of in-cloud chemical processes. Also, the absence of wet and dry periods, and directional-dependence of rainfall, may be causing the under-prediction of wet deposition patterns of NH_4^+. More work is needed to determine the best and most cost-effective method of parameterising this in a statistical atmospheric transport model.

Another source of error is the vertical distribution of SO_2 and NO_x emissions. The present scheme of a homogeneous profile through the first 300 m is an approximation, and is possibly one the main reasons why SO_2 surface concentrations are over-predicted in the model. The effect of plume rise could be very important, and be accounted for by effectively increasing the stack height of the emissions source.

Initial testing in Chapter 5 suggested that a hybrid vertical dispersion scheme could be employed, where the primary emissions of NH_3, SO_2 and NO_x were allocated according to source height, while the secondary oxidation products were mixed using instantaneous mixing. The main problem is the complex cloud chemistry scheme, which became unstable. This would have to be simplified and made stable, possible including only linear first order reactions.

To account for the effect of altitude, a simple parameterisation has been included in the wet deposition process. Another enhancement into the model might be to include a reduction in cloudbase height in areas of higher altitude, reflecting the decrease in distance between the surface and the cloudbase.

Throughout this project, it has been assumed that there is no relationship between the magnitude of the emissions, deposition velocities and canopy resistances. Thus no account has been taken of the effects of very high levels of nitrogen deposition to modify the exchange process. The results of Sutton *et al.*, (1992) and Erisman and Wyers (1993a) suggest that large levels of nitrogen deposition may result in a 'nitrogen saturation' effect on the vegetation, possibly leading to some of the 'excess' nitrogen being re-emitted to the atmosphere. This

would imply that the use of a model on a single-run basis may not be sufficient to describe nitrogen fluxes over a long period of time. Results of the model may have to be incorporated into a new emissions database, or that the process of dry deposition be modified to account for the use of a 'compensation point' approach, which could be linked to be dependent on nitrogen input from the atmosphere. A series of model runs would be needed, with each run, using deposition data from the previous run to adjust the model parameterisations as required.

Appendix A

The Trajectory Scanning Routine

Determination of the initial position of the trajectory on the perimeter of the model domain

The number of grid squares in the model domain depends on the horizontal resolution of the model. Using 20 km grid squares provides a domain of 33 by 61 grid cells for Great Britain. A 5 km grid resolution increases this to 132 by 244 elements. For the first trajectory using a given wind direction, the initial position at the edge of the model domain is determined by the following set of procedures.

The model classifies the angle of the trajectory by deciding on whether the trajectory is heading in a predominantly north/south direction or an east/west direction. The angle of the trajectory (θ_i) is adjusted to define it in terms of trajectory heading as opposed to origin, and also converted to radians which are used in the trigonometry calculations (θ).

$$\theta = 450.0 - \theta_i + 180.0 \tag{A.1}$$

$$\theta = \theta * \pi/180.0 \tag{A.2}$$

The next step is to determine the predominant heading of the trajectory, by using the logical indicator *ystep* as follows:

$$ystep = abs(sin(\theta)) > (sin(\pi/4)) \tag{A.3}$$

Thus if the angle of the trajectory is predominantly north/south (the angle of the trajectory θ_i lies between 315° to 45° or 135 ° to 225°) then *ystep* is defined

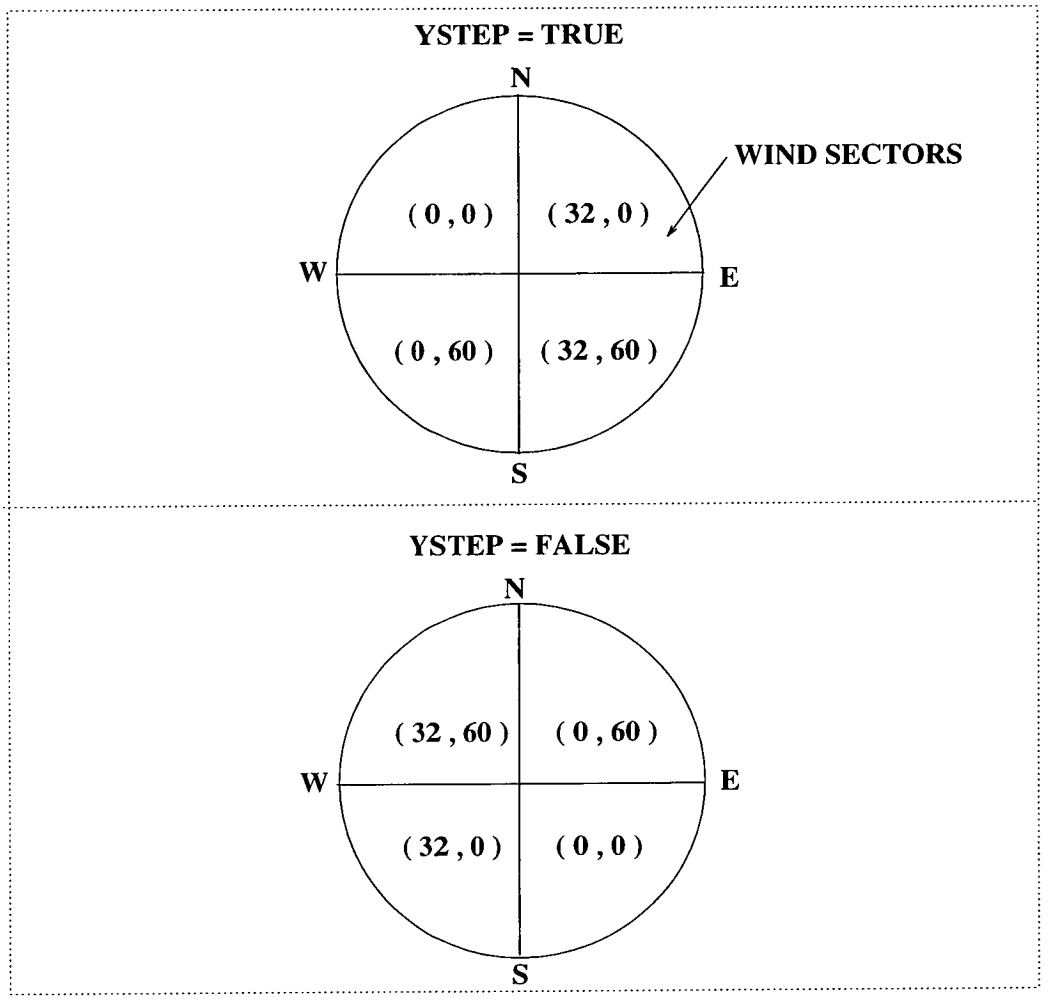

Figure A.1: Determination of the initial position of trajectory, using the definition of the logical indicator *ystep*, and the origin of the trajectory in terms of wind sectors.

to be *true*, otherwise *ystep* is *false*.

The state of the logical indicators *ystep* is then used to define the initial position (X_i,Y_i) of the trajectory on the domain boundary. This is summarised in Figure A.1 (assuming 20 km grid squares). The numbers referred to the array location of the grid squares.

The initial coordinates (x,y) of the trajectory are in the centre of the grid square, and are in km from the southwest corner of the domain. Thus for a grid square (X,Y), the coordinates for a 20 km grid are

(x,y) = (20*X + 10 , 20*Y + 10).

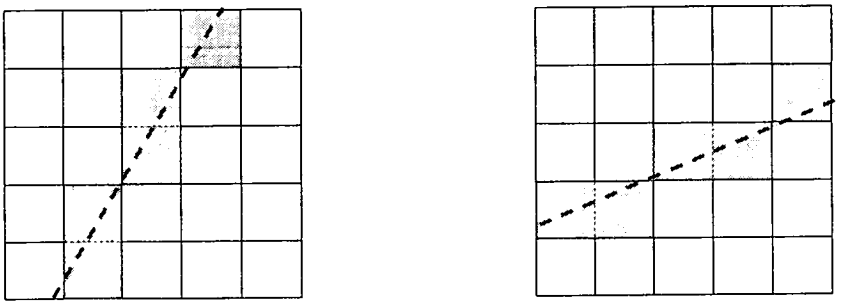

YSTEP=TRUE YSTEP=FALSE

Figure A.2: The path of the trajectory depending on the state of the logical indicator *ystep*.

Movement of the trajectory to the next grid square

When the air column has been determined to have finished traversing a grid square, the column is then moved to the next grid square on the trajectory. The location of this new grid square (x_{i+1},y_{i+1}) is dependent on the trajectory angle, the current grid square coordinates (x,y) and the state of the logical indicator *ystep*. This is illustrated in Figure A.2.

If *ystep* = *true* then the trajectory has been defined to be moving predominantly along a north/south direction. In this case, the y coordinate of the next grid square is defined as

$$y_{i+1} = y + 20 * \frac{sin(\theta)}{\mid sin(\theta) \mid} \tag{A.4}$$

Thus the y coordinate is just moved either north or south by 20 km, and remains at the centre of the grid square. The corresponding x coordinate (x_{i+1}) is defined as being the value on the trajectory corresponding to (y_{i+1}).

If *ystep* = *false* then the trajectory has been defined to be moving predominantly along an east/west direction. In this case, the x coordinate of the next grid square is defined as

$$x_{i+1} = x + 20 * \frac{cos(\theta)}{\mid cos(\theta) \mid} \tag{A.5}$$

The x coordinate is moved either east or west by 20 km, and remains at the centre of the grid square. The corresponding y coordinate (y_{i+1}) is defined as being the value on the trajectory corresponding to (x_{i+1}).

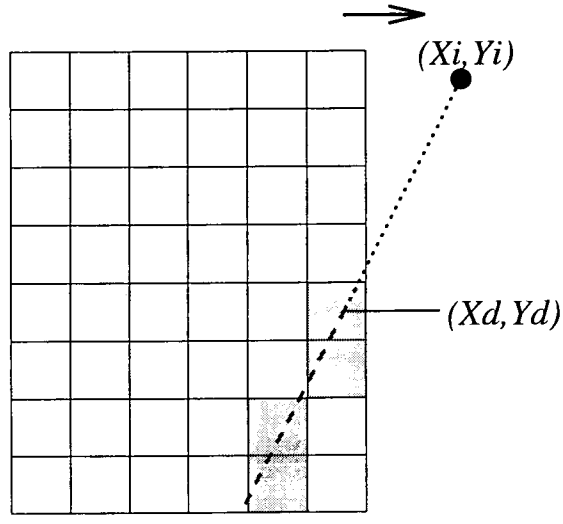

Figure A.3: The determination of the first grid square inside the model domain (X_d,Y_d), when the initial grid square (X_i,Y_i) lies outside the model domain.

Movement of the initial grid square on the boundary

Once a trajectory is finished, a new trajectory commences. The initial grid square of this new trajectory (X_{i+1},Y_{i+1}) is determined from the previous initial position (X_i,Y_i), and the state of the logical indicator *ystep*.

If *ystep* = *true* then the values of (X_i,Y_i) are adjusted by the following equations:

If $(\cos(\theta) \neq 0)$ then

$$X_{i+1} = X_i - INT\frac{cos(\theta)}{\mid cos(\theta) \mid} \tag{A.6}$$

$$Y_{i+1} = Y_i \tag{A.7}$$

If $(\cos(\theta) = 0)$ then

$$X_{i+1} = X_i + 1 \tag{A.8}$$

$$Y_{i+1} = Y_i \tag{A.9}$$

If *ystep* = *false* then the values of (X_i,Y_i) are adjusted by the following equations.

If $(\sin(\theta) \neq 0)$ then

$$Y_{i+1} = Y_i - INT\frac{sin(\theta)}{\mid sin(\theta) \mid} \tag{A.10}$$

$$X_{i+1} = X_i \tag{A.11}$$

If $(\sin(\theta) = 0)$ then

$$Y_{i+1} = Y_i + 1 \tag{A.12}$$

$$X_{i+1} = X_i \tag{A.13}$$

When the initial position reaches the edge of the domain, it is then extends out past the domain, as shown in Figure A.3. An imaginary trajectory is traced out from the imaginary grid square (X_d,Y_d), until the trajectory reaches the domain. The first grid square inside the domain (X_d,Y_d), is then defined as the first grid square on the trajectory.

Appendix B

Structure of the FRAME model

A flow chart showing the main structure of the FRAME model is shown in Figure B.1. When FRAME is run, a number of datasets are read into the program. These data include emissions of SO_2, NH_3 and NO_x, windspeed, data deposition velocity data and rainfall data for Great Britain. An initial angle is assigned to a trajectory and the initial position of the trajectory is calculated using the algorithm in Appendix A. The program then calculates the 24-hour cycle of the depth of the atmospheric boundary layer. The air column is initialised with concentrations for the calculated boundary data (section 4.3.1).

Each trajectory has a number of key routines which are calculated once for each new grid square. These include the chemical conversion rates, the rate of vertical diffusion, the emission flux and dry deposition velocities.

For each timestep there are a core set of routines that are calculated. The main processes are the vertical transfer of material between model layers, the change in concentration of the model species due to chemical reactions and the removal of material from the air column by dry and wet deposition.

When a trajectory has been completed, another trajectory commences with new initialised concentrations. When all the trajectories have been completed for a certain angle, the angle is increased by 15° and the model then starts off new trajectories from this angle. When the angle has gone through a full 360° it is reset to 000 and the initial time of the trajectories is increased by 6 hours. When a 24-hour cycle is completed the model has finished and the results are sent out to external datafiles.

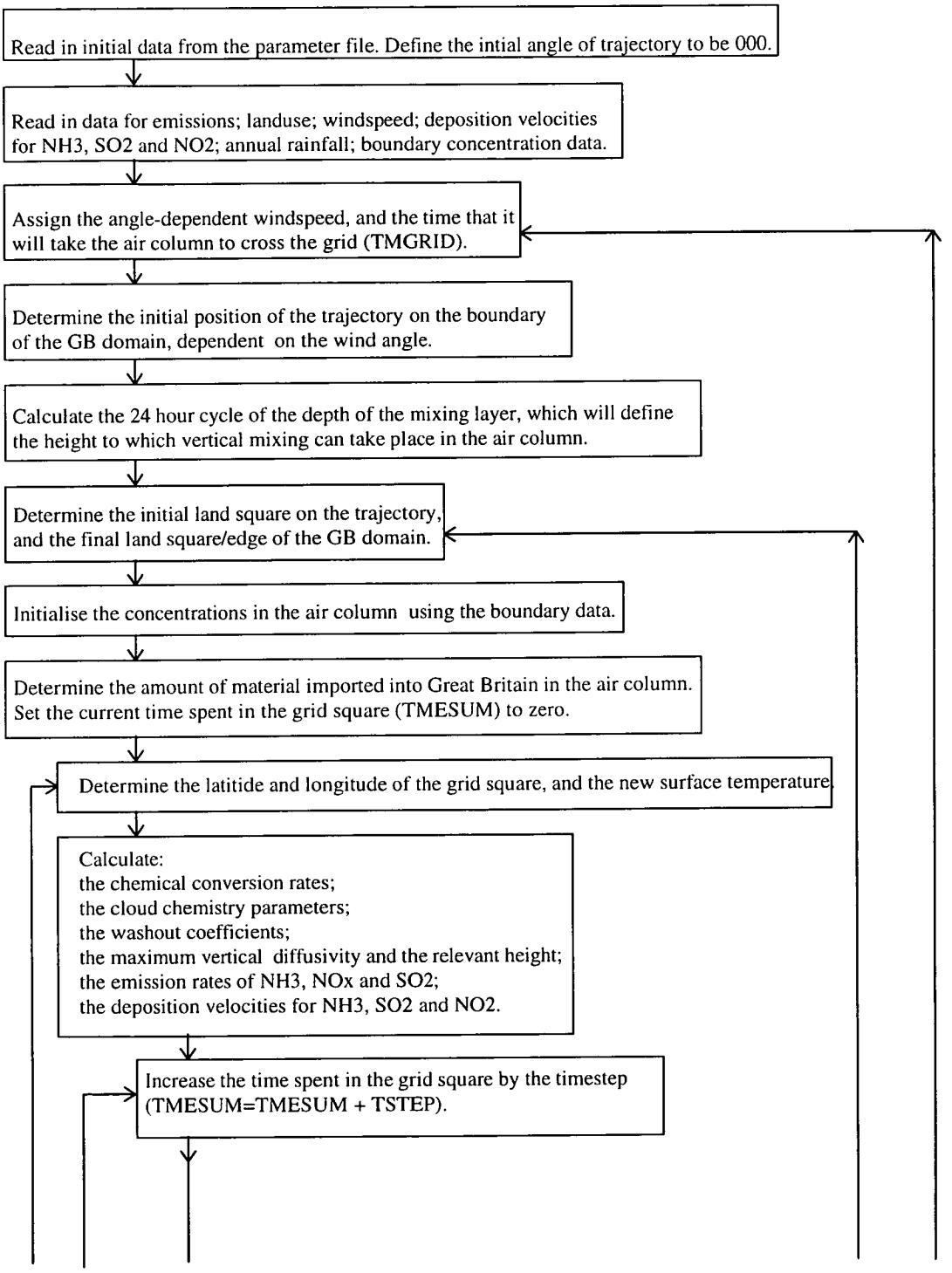
Read in initial data from the parameter file. Define the intial angle of trajectory to be 000.
Read in data for emissions; landuse; windspeed; deposition velocities for NH3, SO2 and NO2; annual rainfall; boundary concentration data.
Assign the angle-dependent windspeed, and the time that it will take the air column to cross the grid (TMGRID).
Determine the initial position of the trajectory on the boundary of the GB domain, dependent on the wind angle.
Calculate the 24 hour cycle of the depth of the mixing layer, which will define the height to which vertical mixing can take place in the air column.
Determine the initial land square on the trajectory, and the final land square/edge of the GB domain.
Initialise the concentrations in the air column using the boundary data.
Determine the amount of material imported into Great Britain in the air column. Set the current time spent in the grid square (TMESUM) to zero.
Determine the latitide and longitude of the grid square, and the new surface temperature
Calculate:
the chemical conversion rates;
the cloud chemistry parameters;
the washout coefficients;
the maximum vertical diffusivity and the relevant height;
the emission rates of NH3, NOx and SO2;
the deposition velocities for NH3, SO2 and NO2.
Increase the time spent in the grid square by the timestep (TMESUM=TMESUM + TSTEP).

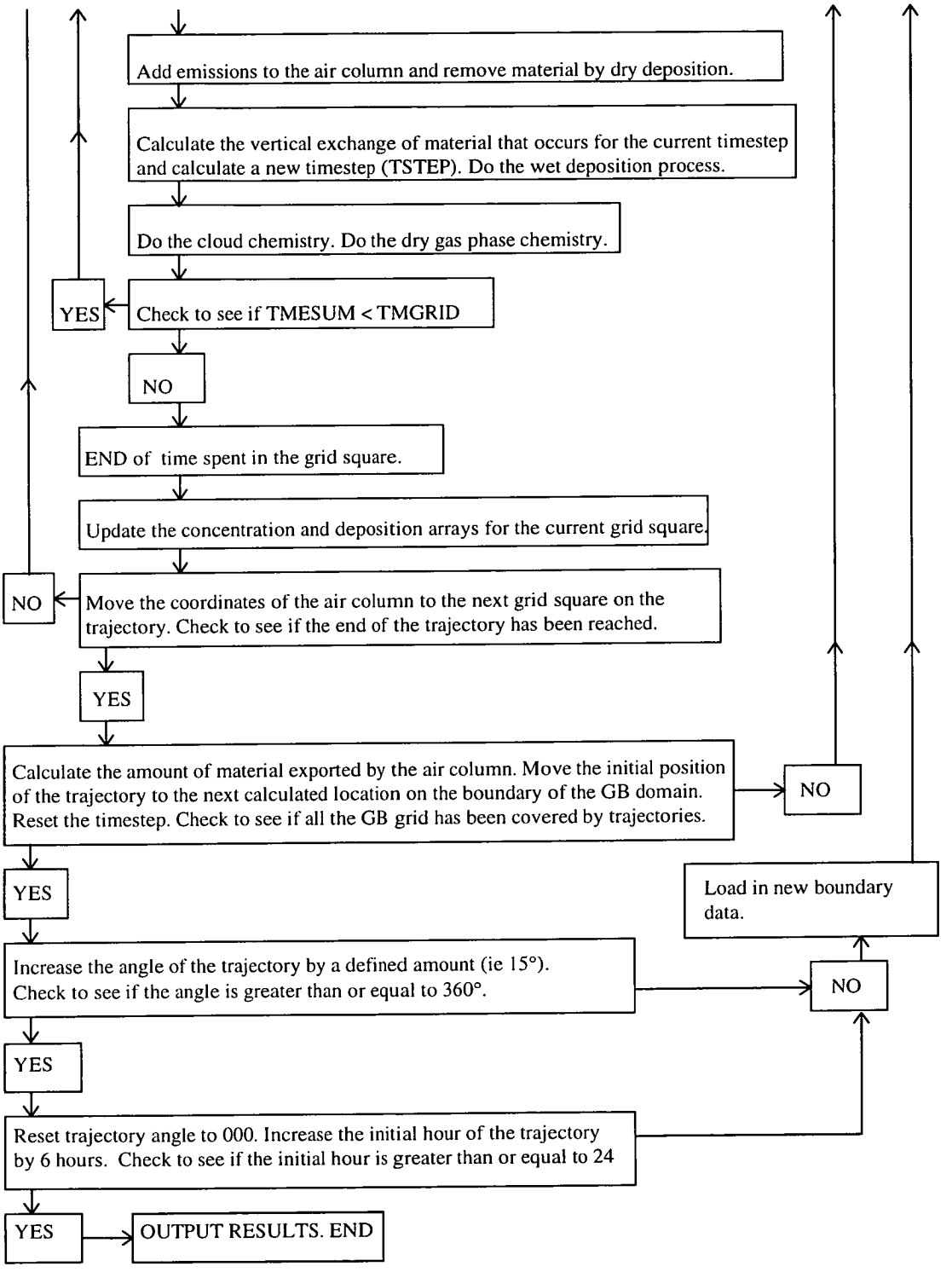

Figure B.1: A flowchart showing the overall structure of the FRAME model, and how the various routines described in chapters 3 and 4 are used in the model.

References

Adema E.H., Heeres P. and Hulskotte J. (1986). On the dry deposition of NH_3, SO_2 and NO_2 on wet surfaces in a small scale wind tunnel. In: *Proc. 7th World Clean Air Congress*, Vol 2. (Ed by Hartmann H.F.) pp 1-8. Clean Air Society of Australia and New Zealand, Eastwood.

Allen A.G., Harrison R.M. and Wake M.T. (1988). A mesoscale study of the behaviour of atmospheric ammonia and ammonium. *Atmospheric Environment* **18** , 1347-1353

Anderson H. (1991). Ammonia monitoring - passive diffusion tube sampling. In 'Nitrogen and Phosphorus in Soil and Air' project abstracts of the Danish NPo Research Programme. Ministry of the Environment Protection, Kobenhavn, Denmark.

ApSimon H.M., Goddard A.J.H., Wrigley J. and Crompton S. (1984). Atmospheric transport of radioisotopes and the assessment of population doses on a European scale. CEC report EUR 9128,EN.

ApSimon H.M., Kruse M. and Bell J.N.B. (1987). Ammonia emissions and their role in acid deposition. *Atmospheric Environment* **18** , 1939-1946.

ApSimon H.M., Barker B.M. and Kayin S. (1994). Modelling studies of the atmospheric release and transport of ammonia - applications of the TERN model to an EMEP site in eastern England in anticyclonic episodes. *Atmospheric Environment* **28**, 665-678.

Asman W.A.H. and Janssen A.J. (1987). A long-range transport model for ammonia and ammonium for Europe. *Atmospheric Environment* **21**, 2099-2119.

Asman W.A.H., Drukker B. and Janssen A.J. (1988). Modelled historical concentrations and depositions of ammonia and ammonium in Europe. *Atmospheric Environment* **22**, 725-735.

Asman W.A.H. (1990). A detailed ammonia emission inventory for Denmark. Report DMU LUFT A-133, National Environmental Research Institute, Roskilde, Denmark.

Asman W.A.H. (1992). Ammonia emission in Europe; updated emission and emission variations. RIVM report. 228471008. RIVM, Bilthoven, The Netherlands.

Asman W.A.H. and van Jaarsveld J.A. (1992). A variable-resolution transport model applied for NHx for Europe. *Atmospheric Environment* **26A**, 445-464.

Asman W.A.H. (1994). Emission and deposition of ammonia and ammonium. *Nova Acta Leopoldina NF 70* **288**, 253-397.

Asman W.A.H. (1996). Factors influencing local dry deposition of gases. *Atmospheric Environment (Ammonia Special Issue)* (Ed by Sutton M.A., Lee D.S., Dollard G.J. and Fowler D.) (submitted).

Atkins D.H.F and Lee D.S. (1992). The distribution of ammonia in the United Kingdom. AEA Technology AEA-EE-0469, Harwell Laboratory, Oxfordshire.

Barrett K., and Seland Ø. (1995). European Transboundary Acidifying Air Pollution - Ten years calculated field and budgets to the end of the first Sulphur Protocol. *EMEP report* **1/95**. Norwegian Meteor. Inst. Oslo, Norway.

Bobbink R., Heil G.W. and Raessen M.B.A.G. (1992). Atmospheric deposition and canopy exchange processes in heathland ecosystems. *Environmental Pollution* **75**, 29-37.

Bobbink R. and Roelofs J.G.M. (1994). Empirical Nitrogen Critical Loads: update since Lökeberg (1992). *Mapping and modelling of critical loads for nitrogen - a workshop report.* (Ed by Hornung M., Sutton M.A. and Wilson R.B.) pp 9-19. Report of an UN-ECE workshop, Grange over Sands, 23-26 October 1994. Institute of Terrestrial Ecology, Edinburgh.

Boermans G.M.F. and van Pul W.A.J. (1992). SLAM, a short-term and local-scale ammonia transport model. In *Objectives for Next Generation of Practical Short-Range Atmospheric Dispersion Models.* (Ed by Helge R. Olesen and Torben Mikkelsen) pp 157-163. May 8-9, 1992 at Risø, Denmark.

Bujisman E., Maas H., and Asman W. (1984). Een geedetailleerde ammmoniak-emisssiekaart van Nederland. (A detailed ammonia map of the Netherlands). report C-84-20. Instituut voor Meteorolgie en Oceanografie, Rijksuniversiteit Utrecht, Netherlands (in Dutch with English summary).

Bujisman E., Maas H.F.M., and Asman W.A.H. (1987). Anthropogenic ammonia emissions in Europe. *Atmospheric Environment* **21**, 1009-1022

Bull K.R., Ashmore M.A., Battarbee R., Bell J.N.B., Campbell G., Colls J., Coote A., Cresser M., Davison A., Fowler D., FreerSmith P., Hall J.R., Harriman R., Hornung M., Irwin J., Jenkins A., Kuylenstierna J., Langan S., Loveland P., Orrmerod S., Reynolds B., Wilson M.J. and Wilson R.B. (1991a). Critical loads maps for the United Kingdom. NERC News, July.

Bull K.R. (1991b). The critical loads/levels approach to gaseous pollution emission control. *Environental Pollution* **69**, 105-123.

Bull K., Dyke H. and Hall J. (1994). Exceedances of Acidity and Nutrient Nitrogen Critical Loads. *Mapping and modelling of critical loads for nitrogen - a workshop report.* (Ed by Hornung M., Sutton M.A. and Wilson R.B.) pp 158-159. Report of an UN-ECE workshop, Grange over Sands, 23-26 October 1994. Institute of Terrestrial Ecology, Edinburgh.

Burkhardt J., Sutton M.A., Milford C., Storeton-West R.L. and Fowler D. (1996). Analysis of ammonia concentrations at a site on southern Scotland from continuous measurements over a period of 2 years. *Atmos. Environ. (Ammonia Special Issue)* (Ed by Sutton M.A., Lee D.S., Dollard G.J. and Fowler D.) (in press).

Carson D.J. (1973). The development of a dry inversion-capped convectively unstable boundary layer . *Quart. J. Roy. Meteor. Soc.* **99**, 450-467.

Chamberlain A.C. and Little P. (1981). Transport and capture of particles by vegetation. In: *Plants and their Atmospheric Environment* (Ed by Grace J., Ford E.D. and Jarvis P.G.) pp 147-173. Blackwell Scientific, Oxford.

Carruthers D.J. and Choularton T.W. (1983). A model of the seeder-feeder mechanism of orographic rain including stratification and wind drift effects. *Quart. J. Roy. Meteor. Soc.* **109**, 575-588.

Dentner F.J. and Crutzen P.J. (1994). A three dimensional model of the global ammonia cycle. *Journal of Atmospheric Chemistry* **19**, 331-369.

Derwent R.G. and Nodop K. (1987). Long-range transport and deposition of acidic nitrogen species in north-west Europe. *Nature* **324**, 356-358.

Derwent R.G., Dollard G.J. and Metcalfe S.E. (1988). On the nitrogen budget for the United Kingdom and north-west Europe. *Quart. J. Roy. Meteor. Soc.* **114**, 1127-1152.

Dore A.J., Choularton T.W., Fowler D. and Storeton-West R.L. (1990). Field measurements of wet deposition in an extended region of complex topography . *Quart. Journ. Roy. Met. Soc.* **116**, 1993-1212.

Dore A.J., Choularton T.W. and Fowler D. (1992). An improved wet deposition map of the United Kingdom incorporating the seeder-feeder effect over mountainous terrain. *Atmospheric Environment* **26A**, 1375-1381.

Draaijers G.P.J., Ivens W.P.M.F. and Bleuten W. (1988). Atmospheric deposition in forest edges measured by monitoring canopy throughfall. *Water, Air and Soil Pollution* **42**, 129-136.

Dragosits U., Sutton M.A. and Place C.J. (1996). The spatial distribution of ammonia emisison in Great Britain for 1969 and 1988 assessed using GIS techniques. In: *Poster Procceding of Atmospheric Ammonia: Emission, Deposition and Environmental Impacts.* (Oxford 1995) (Ed by Sutton M.A., Lee D.S., Dollard G.J. and Fowler D.) (in press).

Duyzer J.H., Bouman A.M.H., Dierderen H.S.M.A. and van Aalst R.M. (1987). Measurement of dry deposition velocities of NH_3 and NH_4^+ over natural terrains. *Report R 87/273.* MT-TNO, Delft.

Dwyer A.J. and Hicks B.B. (1970). Flux-gradient relationships in the constant flux layer. *Quart. J. Roy. Meteor. Soc.* **96**, 715-721.

Eager M. (1992). The development of an ammonia emissions inventory for Great Britain using GIS techniques. MSc Thesis. Department of Geography, The University of Edinburgh.

ECETOC (1994). Ammonia Emissions to Air in Western Europe. Technical Report 62. Avenue E. Van Nieuwenhuyse 4, (Bte. 6) B - 1160 Brussels, Belgium.

Eggleston H.S. (1992a). An improved U.K. ammonia emission inventory. In *Ammonia emissions in Europe: emission coefficients and abatement costs.* Proc. of a workshop 4-6 Feb. 1991. (Ed by Klassen G.) pp 95-107. IIASA, Laxemburg, Austria.

Eggleston H. S. (1992b). Pollution in the atmosphere: future emissions from the U.K. Report for the U.K. Department of Environment. Warren Spring Laboratory, Stevenage, Hertfordshire, SG1 2BX.

Eliassen A. and Saltbones J. (1983). Modelling of long-range transport of sulphur over Europe. A two dimensional model run and some model experiments. *Atmospheric Environment* **17**, 1457-1473.

Erisman J.W., Vermetten W.M. and Asman A.H. (1988). Vertical distribution of gases and aerosols - the behaviour of ammonia and related compounds in the lower atmosphere. *Atmospheric Environment* **22**, 1153-1160.

Erisman J.W. (1989). Ammonia emissions in the Netherlands in 1987 and 1988. RIVM Report 2284710066. National Institute of Public Health and Environmental Hygiene, Bilthoven, Netherlands.

Erisman J.W. and Wyers G.P. (1993a). Continuous measurements of surface exchange of SO_2 and NH_3; implications for their possible interactions in the deposition process. *Atmospheric Environment* **27**, 1937-1949.

Erisman J.W., van Pul A. and Wyers G.P. (1993b). Parameterisation of dry deposition mechanisms for the quantification of atmospheric input to ecosystems. In: *General Assessment of biogenic emissions and deposition of nitrogen compounds, sulphur compounds and oxidants in Europe.* Proceeding of the joint CEC/BIATEX workshop, Aveiro (May 1993). (Ed by Slanina J., Angeletti G., and Beilke S.) pp 223-241. Air Pollut. Res. Report 47, CEC, Brussels.

Farquhar G.D., Firth P.M., Wetselaar R. and Wier B. (1980). On the gaseous exchange of ammonia between leaves and the environment: determination of the ammonia compensation point. *Plant Physiology* **66**, 710-714.

Fekete K.E. (1992). Regional-scale transport model for ammonia and ammonium. *Atmospheric Environment* **27a**, 1099-1104.

Fowler, D. and Cape, J.N. (1984). The contamination of rain samples by dry deposition on rain collectors. *Atmospheric Environment* **18**, 183-189.

Fisher B.E.A. (1984). The long-range transport of air pollutants - some thoughts on the state of modelling. *Atmospheric Environment* **18**, 553-562.

Fisher B.E.A. (1987). Assessing recent ammonia inventories using a statistical long-range transport model. Report TPRD/L/3159/R 87. Central Electricity Research Laboratories, Leatherhead, U.K.

Fowler D., Cape J., Leith I.D., Choularton T.W., Gay M.J. and Jones A. (1988). The influence of altitude on rainfall composition. *Atmospheric Environment* **22**, 1355-1362.

Fowler D. (1994). Atmospheric inputs of Nitrogen. *Mapping and modelling of critical loads for nitrogen - a workshop report.* (Ed by Hornung M., Sutton M.A. and Wilson R.B.) pp 128-141. Report of an UN-ECE workshop, Grange over Sands, 23-26 October 1994. Institute of Terrestrial Ecology, Edinburgh.

Fuhrer K., Neftel A., Anklin M., Steffelbach T. and Legrand M. (1996). High resolution ammonium ice core record covering a complete glacial-interglacial cycle. *Journal of Geophysical Research* **101**, 4147-4164.

Garland J.A. (1977). The dry deposition of sulphur dioxide to land and water surfaces. *Proc. Roy. Soc. London* **A. 345**, 245-268.

Gilham C., Leech P. and Eggleston H. (1992). U.K. emissions of air pollutants 1970-1990. Warren Spring Laboratory, Stevenage Herts. Report LR 887 (AP).

Golder D. (1972). Relations amongst Stability Parameters in the Surface Layer. *Boundary Layer Meteorology* **3**, 47-58.

Grennfelt P. and Thőrnelőf E. (1992). (Eds.) *Critical Loads for nitrogen - a workshop report.* Nord 1992;41. Nordic council of Ministers, Copenhagen.

Grime J.P. (1979). *Plant Strategies and Vegetation Processes.* Wiley, Chichester.

Gunderson P. (1992). Mass balance approaches for establishing critical loads for nitrogen in terrestrial ecosystems. In : *Critical Loads for Nitrogen* (Ed by Grennfelt P. and Thőrnelőf E.). pp 55-110. Nord 1992;41, Nordic Council of Ministers, Copenhaagen.

Harper L.A., Sharpe R.R., Langdale G.W. and Giddens J.E. (1987). Nitrogen cycling in a wheat crop; soil, plant and aerial nitrogen transport. *Agron. J.* **79**, 965-973.

Hertel O., Christensen J., Runge H., Asman W.A.H., Berkowicz R. and Hovmand M.F. (1995). Development and testing of a new variable scale air pollution model - ACDEP. *Atmospheric Environment* **29**, 1267-1290.

Hicks B.B., Baldocchi D.D., Meyers T.P., Hosker Jr. R.P. and Matt D.R. (1987). A preliminary multiple resistance routine for deriving dry

deposition velocities from measured quantities. *Water, Air and Soil Pollution* **36**, 311-330.

Hornung M., Sutton M.A. and Wilson R.B. (1995). *Mapping and modelling of critical loads for nitrogen - a workshop report* (Eds.) (Report of an UN-ECE workshop, Grange over Sands, 23-26 October 1994). Institute of Terrestrial Ecology, Edinburgh.

Hotson J.McG. (1988). Landuse and Agricultural Activity: An areal Approach for Harnessing the Agricultural Census of Scotland. EPRC Regional Laboratory for Scotland, Working Paper No 11.

Hov Ø., and Hjøllo B.A. (1994). Transport distance of ammonia and ammonium in Northern Europe 2. Its relation to emissions of SO_2 and NO_x. Journal of Geophysical Research **99**, 18749-18755.

INDITE (1994). *Inputs of nitrogen deposition in terrestrial ecosystems.* Department of the Environment, London, U.K.

Jarvis S.C. and Pain B.F. (1990). Ammonia volatilisation from agricultural land. *The Fertiliser Society Proceedings.* **298** The Fertiliser Society , Thorpe Wood, Peterborough, U.K.

Jones J.A. (1981). The estimation of long-range dispersion and deposition of continuous releases of radianuclides to atmosphere. National Radiological Protection Board NRPB-R123, Oxfordshire.

Kruse M., ApSimon H.M. and Bell J.N.B. (1989). Validity and uncertainty in the calculation of an emission inventory for ammonia arising from agriculture in Great Britain. *Environmental Pollution* **56**, 237-257.

Kruse-Plass M., ApSimon H.M. and Barker B. (1993). A modelling study of the effect of ammonia on in-cloud oxidation and deposition of sulphur. *Atmospheric Environment* **27A**, 223-234.

Lee D.S., and Dollard G.J. (1994). The potential magnitude of non-animal sources of ammonia and uncertainties in the total emission of ammonia from the United Kingdom. *Environmental Pollution* (in press)

Levine J.S., Augustsson T.R. and Hoell J.M. (1980). The vertical distribution of tropospheric ammonia. *Geophysical Research Letters* **7**, 317-320.

Mass J.F.M. (1988). Optimisation of the reduction of ammonia emission in the Netherlands. Report 228471005, National Institute of Public Health and Environment Protection, Bilthoven, The Netherlands.

Maul P.R. (1978). A prototype time-dependent model for the long-range transport of sulphur dioxide and associated pollutants. CEGB report SSD/MID/R17 78.

McConnell J.C. (1973). Atmospheric ammonia. *Journal of Geophysical Research* **78**, 7812-7821.

Metcalfe S.E., Atkins D.H.F. and Derwent R.G. (1989). Acid deposition modelling and the interpretation of the United Kingdom secondary precipitation network data. *Atmospheric Environment* **23**, 2033-2052.

Metcalfe S.E., Whyatt J.D. and Derwent R.G. (1995). A comparison of model and observed network estimates of sulphur deposition across Great Britain for 1990 and its likely source attribution. *Quart. J. Roy. Meteor. Soc.* **121**, 1387-1411.

Möller D. and Schieferdecker H. (1989). Ammonia emission and deposition of NH_x in the G.D.R. *Atmospheric Environment* **23**, 1187 - 1193.

Montieth J.L. (1973). Principles of Environmental Physics. Edward Arnold, London. pp 291.

NRC (1979). *Ammonia.* Subcommittee on ammonia. Committee on medical and biological effects of environment pollutants. National Research Council. University Park Press, Baltimore, 305 pp.

Nihlgard B. (1985). The ammonium hypothesis- An additional explanation to the forest dieback in Europe. *Ambio.* **14**, 2-8.

Nilsson B. and Grennfelt P. (1988). *Critical Loads for Sulphur and Nitrogen.* (Report from a workshop at Skokloster, Sweden, 19-24 March 1988) (Eds) Nordic Council of Ministers, Copenhagen, Denmark. 418 pp.

Numerical Recipes in Fortran. Press W.H., Teukolsky S.A., Vetterling W.T. and Flannery B.P. (1986). Cambridge University Press, Cambridge, CB@ 1RP, U.K.

Pasquill, F. (1961). The estimation of the dispersion of windborne material. *Meteorological Magazine* **90**, 33-49.

Paulson C.A. (1970). The mathematical representation of wind speed and temperature profiles in the unstable atmospheric surface layer. *Journal of Applied Meteorology* **9**, 857-861.

Pitcairn C.E.R., Fowler D. and Grace J. (1991). Changes in species composition of semi-natural vegetation associated with the increase in

atmospheric inputs of nitrogen. *Report to Nature Conservancy Council.* Institute of Terrestrial Ecology, Edinburgh.

RGAR (1990). *Acid deposition in the United Kingdom 1986-1988* (Third report of the United Kingdom Review Group on Acid Rain), Department of the Environment, London.

RGAR (1996). (Fourth report of the United Kingdom Review Group on Acid Rain), Department of the Environment, London.

Schjørring J.K., Kyllingsbaek A., Mortensen J.V. and Byskov-Nielsen S. (1993). Field investigations of ammonia exchange between barley plants and the atmosphere. I. Concentration profiles and flux densities of ammonia. *Plant, Cell and Environment* **16**, 161-167.

Schlesinger W.H. and Hartley A.E. (1992). A global budget for atmospheric ammonia. *Biogeochenmistry* **15**, 191-211.

Seinfeld J.H. (1986). *Atmospheric Chemistry and Physics of Air Pollution.* Wiley, New York.

Singles R.J., Sutton M.A. and Weston K.J. (1995). A multi-layer model to describe the atmospheric transport and deposition of ammonia in Great Britain. *Atmos. Environ. (Ammonia Special Issue)* (Ed by Sutton M.A., Lee D.S., Dollard G.J. and Fowler D.) (in press).

Smith F.B. (1975). Turbulence in the atmospheric boundary layer. *Sci. Prog. Oxford* **62**, 127-151.

Smith F.B. (1979). The relationship between pasquill stability P and Kazanski-Monin stability u (in neutral and unstable conditions). *Atmospheric Environment* **13**, 879-881.

Smith F.B. and Hunt R.D. (1979). The dispersion of sulphur pollutants over western Europe. *Phil. Trans. Royal. Soc. London* A **290**, 532-542.

Smith F.B. (1980). The significance of wet and dry synoptic regions on long range transport of pollution and its deposition. *Atmospheric Environment* **15**, 863-873.

Sommer S.G., and Jensen C. (1993). Ammonia volatilisation from field applied urea and mineral fertilisers. *Fertiliser Res.* (in press)

Stelson A.W. and Sienfeld J.H. (1982). Relative humidity and temperature dependence of the ammonium nitrate dissociation constant. *Atmospheric Environment* **16**, 983-992.

Stull R.B. (1988). An introduction to boundary layer meteorology. Kluwer Academic Publishers, P.O.Box 17, 3300 AA Dordreccht, The Netherlands.

Sutton M.A. (1990). The surface/atmosphere exchange of ammonia. PhD thesis, University of Edinburgh, U.K.

Sutton M.A. and Fowler D. (1992). Deposition of atmospheric ammonia to moorlands. *Environmental Pollution* **75**, 15-24.

Sutton M.A. and Fowler D. (1993a). A model for inferring bi-directional fluxes of ammonia over plant communities. *Proceedings of the WMO conference on the measurement and modelling of atmospheric composition changes including pollution transport* (Sofia, 2-8 October, 1993) World Meteorological Organisation, Geneva, 1993.

Sutton M.A., Fowler D. and Moncrieff J.B. (1993b). The exchange of atmospheric ammonia with vegetated surfaces. I: Unfertilized vegetation. *Quart. J. Roy. Meteor. Soc.* **119**, 1023-1045.

Sutton M.A., Fowler D., Moncrieff J.B. and Storeton-West R.L. (1993c). The exchange of atmospheric ammonia with vegetated surfaces. II: Fertilized vegetation. *Quart. J. Roy. Meteor. Soc.* **119**, 1047-1070.

Sutton M.A., Fowler D., Hargreaves K.J. and Storeton-West R.L. (1993d). Interactions of NH_3 and SO_2 exchange inferred from simultaneous flux measurements over a wheat canopy. In: *General Assessment of biogenic emissions and deposition of nitrogen compounds, sulphur compounds and oxidants in Europe.* Proceeding of the joint CEC/BIATEX workshop, Aveiro (May 1993). (Ed by Slanina J., Angeletti G., and Beilke S.) pp 165-182. Air Pollut. Res. Report 47, CEC, Brussels.

Sutton M.A., Fowler D., Smith R.I., Eager M., Place C.J. and Asman W.A.H. (1993e). Modelling the net exchange of reduced nitrogen. In: *General Assessment of biogenic emissions and deposition of nitrogen compounds, sulphur compounds and oxidants in Europe.* Proceeding of the joint CEC/BIATEX workshop, Aveiro (May 1993).(Ed by Slanina J., Angeletti G., and Beilke S.) pp 117-131. Air Pollut. Res. Report 47, CEC, Brussels.

Sutton M.A., Asman W.A.H. and Schjørring J.K. (1994). Dry deposition of reduced nitrogen. *Tellus* **46B**, 255-273.

Sutton M.A., Place C.J., Eager M., Fowler D. and Smith R.I. (1995a). Assessment of the magnitude of ammonia emissions in the United Kingdom. *Atmospheric Environment* **29**, 1393-1413.

Sutton M.A., Schjørring J.K. and Wyers G.P. (1995b). Plant-atmosphere exchange of ammonia. *Phil. Trans. Roy. Soc., London. Series* **351**, 261-278.

Sutton M.A., Fowler D., Burkhardt J.K. and Milford C. (1995c). Vegetation atmosphere exchange of ammonia: canopy cycling and the impacts of elevated nitrogen inputs. *Water, Air and Soil Pollution* **85**, 2057-2063.

Sutton M.A., Milford C., Dragosits U., Singles R., Fowler D., Ross C., Hill R., Jarvis S.C., Pain B.F., Harrison R., Moss D., Webb J., Espenhahn S., Halliwell C., Lee D.S., Wyers G.P., Hill J. and ApSimon H.M. (1996). Gradients of atmospheric ammonia concentrations and deposition downwind of ammonia emissions: first results of the ADEPT Burringtom Moor experiment. In: *Proceedings of gaseous nitrogen transfer in agricultural systems.* IGER, North Wyke, Devon. May 1996. (In press).

Svensson B.H. and Söderlund R. (1976). The global nitrogen cycle. In: *Nitrogen and Sulphur - Global cycles (SCOPE report 7)* (Ed by B.H. Svensson and R. Soderlund). Ecol. Bull., Stockholm **22**, 23-73.

Thijsse T.R., Wyers G.P., Duyzer J.H., Verhagen H.L.M., Wayers A. and J.J. Moels. (1996). Measurement of ambient ammonia with diffusion tube samplers. *Atmospheric Environment (Ammonia Special Issue)* (Ed by Sutton M.A., Lee D.S., Dollard G.J. and Fowler D.) (in press).

Thom A.S. (1975). Momentum, mass and heat exchange of plant communities. pp 57-109, in vol. 1, *Vegetation and the atmosphere.* Ed. J.L. Montieth. Academic Press, London.

Thompson N., Barrie I.A. and Ayles M. (1982). The Meteorological Office rainfall and evaporation calculation system: MORECS (July 1981). Bracknell: The Meteorological Office.

van Breeman N., Burrough P.A., Velthorst E.J., van Dobben H.F., DeWit T., Riddler T.B. and Reijinders H.F.R. (1982). Soil acidification from atmospheric ammonium sulphate in forest canopy throughfall. *Nature.* **299**, 548 -550.

van Hove L.W.A., Adema E.H., Vreedenberg W.J. and Pieters G.A. (1989). A study of the adsorbtion of NH_3 and SO_2 on leaf surfaces. *Atmospheric Environment* **23**, 1476-1486.

Wang A. and Zhao D. (1993). Emissions of anthropongenic ammonia in Asia, presented at: GEIA (Global Emissions Inventory Activity) workshop, Amersfoort, The Netherlands, 1993.

Warneck P. (1988). *Chemistry of the Natural Atmosphere.* International Geophysical Series, **41**, Academic Press, San Diego.

Webb E.K. (1970). Profile relationships: The log-linear range and extension to strong stability. *Quart. J. Roy. Meteor. Soc.* **106**, 85-100.

Weston K.J and Roy M.G. (1994). The directional-dependence of the enhancement of rainfall over complex orography. *Meteorological Applications* **1**, 267-275.

Whitehead D.C. and Raistrick N. (1990). Ammonia volatilisation from five compounds used as fertilisers following surface applications to soils. *Journal of Soil Science* **41**, 387-394.

World Survey of Climatology **5**. Climates in Northern and Western Europe (1970). Elsevier Publishing Company, 335 Jan van Galenstraat, P.O. Box 211, Amsterdam, The Netherlands.

Wyers G.P., Otjes R.P. and Slanina J. (1993). A continuous flow denuder for the measurement of ambient concentrations and surface fluxes of ammonia. *Atmospheric Environment* **27A**, 2085-2090.

Personal Communications

M.A. Sutton. Institute of Terrestrial Ecology, Edinburgh Research Sation, Bush Estate, Penicuik, Midlothian, EH26 0QB, U.K.

K.J. Weston. Department of Meteorology, University of Edinburgh, Kings Buildings, West Mains Road, Edinburgh, EH9 3JZ, U.K.

J.D. Whyatt. School of Geography and Earth Resources, University of Hull, Hull, HU6 7RX, U.K.